Abstract

Buildings construction and realization of public infrastructures have always been a primary need in the human society, developing low cost and user-friendly materials which also encounter safety and durability requirements. Portland cement is the most used material in construction industry from the industrial revolution up to date, but the raising concerns related to the climate change are pushing the governments worldwide to replace it with more eco-friendly and greener materials. Geopolymers are considered to be best alternatives to Portland cement in construction industry, but issues related to cost and mechanical properties are still hindering the commercialization of this material. Geopolymer incorporating wastes is one of the solutions. Fly ash, a thermal power plant by-product, and borosilicate glass, a recycled glass from pharmaceutical vials, are suitable candidates in geopolymers activation. NMR and FTIR spectroscopies demonstrated that borates from borosilicate glass are active compounds in geopolymerization, substituting the alumina is its role, composing a B-Al-Si network never observed before. Various fly ash and borosilicate glass weight contents were studied in terms of mechanical properties (compression test, 3-point bending test). It was found that fly ash 55 wt.% and borosilicate 45 wt.% composition activated in 13 M *NaOH* solution holds the best compressive and flexural strength (45 and 4 MPa respectively), 25% stronger than similar counterparts found in literature. Cellulose fibres in different weight contents were dispersed into the geopolymeric paste to produce geopolymer composites, with the aim to render the material more suitable for structural applications. 3-point bending test showed an improvement of the flexural strength of about 165% (12 MPa), while the chevron notch method displayed a fracture toughness of 0.7 $MPa \cdot m^{1/2}$, in line with the results of geopolymer composites found in literature. In this thesis work, fly ash was also successfully densified in 3 M *NaOH* solution and distilled water through a new method based on hydraulic pressure, called hydro-pressure sintering. This innovative technology involves a drastic reduction of *NaOH* utilization in geopolymerization, rendering the material more eco-friendly. XRD spectroscopy conducted on produced samples revealed a higher formation of crystals, most likely induced by the application of hydraulic pressure (450 MPa).

Keywords

Geopolymers, polycondensation, composite materials, mechanical properties, fracture toughness, hydro-pressure sintering, spectroscopy.

Bibliographic citation

TAVERI, G. Geopolymers Incorporating Wastes and Composites Processing. Brno: Vysoké učení technické v Brně, Fakulta strojního inženzrství , 2019. 152 s. Vedoucí disertační práce Prof. Ivo Dlouhý, CSc.

Statement

I hereby declare that I have written the PhD thesis on my own according to advice of my supervisor Prof. Ing. Ivo Dlouhý, CSc, and all the literary sources are quoted correctly and completely. This dissertation is the property of the Faculty of Mechanical Engineering in Brno and it can be used for commercial purposes only with consent of the doctoral thesis supervisor and the dean of the FME.

V Brně 10.5.2019 Ing. Gianmarco Taveri

Acknowledgments

I would like to thank my supervisor Prof. Ing. Ivo Dlouhý, CSc, for giving me the opportunity to work in materials research, for his valuable advice and support throughout the Ph.D. study. I also would like to thank my co-supervisor Ing. Zdeněk Chlup, Ph.D., for his help in the scientific evaluation of the results.

This work has received funding from the European Union's Horizon 2020 research and innovation program under the Marie Sklodowska-Curie grant agreement No 642557.

NMR analysis at CF Josef Dadok National NMR Centre in this work was carried out with the support of CEITEC – Central European Institute of Technology – open access project, No. LM2011020, funded by the Ministry of Education, Youth, and Sports of the Czech Republic.

I thank all my colleagues in the Group of Brittle Fracture (Luca, Martina, Roman, Luděk, Hynek, Filip, Radek, Zdeněk, Pavel, Šarka and Láďa) for being a great collective, and to the Institute of Physics of Materials for providing me the hinterland and instrumental equipment for my work.

The very special thank goes to all my family, especially to my mother, my father, my grandmother, and my sister, for their love and support during the whole period. A share of this success also belongs to all my friends both in the Czech Republic and Italy for their unconditional friendship and especially to Anthony for providing precious inspirations to my work.

Contents

1. Introduction

The construction industry encountered the primary needs and demand of the humankind since ever, not only supporting the realization and maintenance of any infrastructure and building, including safe dwells and living places but also providing new ideas and technology for the future. It is well understood that since the ancient ages, the human was always looking for material aesthetically pleasant and at the same time practically performing and durable.

In addition, nowadays, the world is facing several environmental issues, including the global emergency of the climate change, a constant increase of the season average temperature, with the consecutive modification of the ecosystem, due to extensive emission in the atmosphere of greenhouse gasses, among all the carbon dioxide (CO_2), and the undue exploitation of open-air landfills, as the disposal of trash of any nature is rapidly increasing. For instance, a sizeable share (about 8%) is covered by the production of the Portland cement, the most exploited material in the world for constructions and building engineering application [1,2]. Besides, the steady increase in the industrialization worldwide is yielding to a disposal of a huge annual amount of industrial wastes and slags, which can be rather reutilized for some other purposes [3].

Due to this reason, new materials for construction applications must encounter safety, durability and performance requirements, while its production should include zero greenhouse emissions and incorporation of wastes. One of the possible ways is to introduce in the market durable and eco-friendly materials like geopolymers. The processing of this material is also compliant with the incorporation of recyclable wastes, like fly ash, a power plant by-product, and borosilicate glass, usually used for lab and pharmaceutical purposes [4]. In its applications, geopolymers are also versatile, including [5]:

- Construction and buildings
- Immobilization of toxic metals
- Refractory utilization

The utilization of compatible wastes in geopolymers, like fly ash and borosilicate glass, would adjust the chemistry of production, conferring mechanical performance, while reducing the cost of production. However, its brittleness and low resistance to crack propagation (fracture resistance) prompt the scientific community to look for some better solution. One of the ways is to produce composites made of fibres dispersed in the matrix. The extent of toughening depends on the type of fibres, their interaction with the matrix and their average size. Therefore, depending on what is meant to be obtained, several solutions are equally applicable. Incorporating cellulose fibres and recycled paper fibres in producing geopolymeric composites is one of the compelling solutions to undertake [6,7]. Due to its specific tensile strength, cellulose fibres are expected to sensitively increase the mechanical properties and resistance to crack propagation of a geopolymeric matrix [8].

2. Scientific background

2.1 Reasons for utilization of geopolymers

2.1.1 Ancient materials

One of the most important requirements that are to be fulfilled in the development of materials for construction application is the durability, a property which has always been a weak point of OPC cement, the most consumed construction material in the world in the last two centuries [9]. However, it is not a mystery that ancient civilizations were realizing buildings and general constructions which are still standing, despite the wearing weather conditions through the millennia.

Indeed, several types of research led to the belief that a likewise alkali activation was also used in the remote past, for building and construction applications. The connection between geopolymer (GP) materials and a potential role in the construction of Egyptian pyramids has most prominently been promoted by Davidovits, who has proposed a number of detailed theories whereby the large building blocks comprising the pyramids are suggested to have been poured-in-place, utilizing chemistry resembling that of alkali activation. More detailed scientific analysis of pyramid stone samples, published in the peer-reviewed academic literature [10,11], has not upheld the suggestions of elevated alkali or aluminum contents in pyramid stones but does show the presence of amorphous silica and other components which could potentially be consistent with the reagglomeration of limestone in a poured-in-place manner. The scientific and historical investigation has to date not been able to produce fully complete evidence either in favour of this theory or to entirely refute it [12].

There has also been significant discussion surrounding the potential connections between ancient Roman concrete and modern alkali-activated binders. Roman concrete differs widely in composition, performance, and durability; among them, the one used for the fabrication of marine piers which was based on the activation of pozzolanic materials, i.e. calcium-rich volcanic ash sourced from Italian southern areas including what is now the Pozzuoli (formerly Puteoli), and Brindisi, where the elevated pH of the environment initiates the reaction of the pozzolanic material [13]. The volcanic ashes used in this concrete often included significant contents of alkalis, and the final concrete products, when examined after 2,000 years in service, often evidenced the presence of zeolites compounds, i.e. analcime, often present in volcanic ashes. Indeed, the examination of Roman mortars with unreacted pozzolana have shown elevated analcime concentrations in the mortar regions compared to the unreacted pozzolana, indicating that the alkaline environment in which the concrete operated has led to the formation of additional zeolites, as is known to be the case when volcanic ashes are exposed to alkaline geological conditions, although the difficulties associated with accurate separation of the reacted and unreacted materials for analyses [14].

The interest in the comparison with Roman concrete, and the relevance to the discussion presented here is primarily derived from arguments related to durability and the retention of strength. Over a period of 2,000 years, this concrete has remained in service in environments including immersion in seawater, while others including the Pantheon in Rome have withstood significant seismic activity. Similarly interesting from this point of view are the hydro-engineering structures, concrete-based roads, multi-layered floors, vaults, and domes which remain to this day. Although it is undoubted that some Roman concrete structures have degraded over the centuries, the fact that so many remain intact does provide some potential lessons in terms of construction materials chemistry and design. A further point to mention is that much of the degradation observed in modern concrete is due to the corrosion of embedded steel reinforcing, while the unreinforced Roman structures are not subject to this mode of decay [12].

2.1.2 Ambient issues

What the entire world is nowadays encountering is not a negligible emergency, especially because not only the entire flora but also the fauna present in the earth crust is negatively affected by the constant change of the eco-system induced by the excessive industrialization prompted by the humankind.

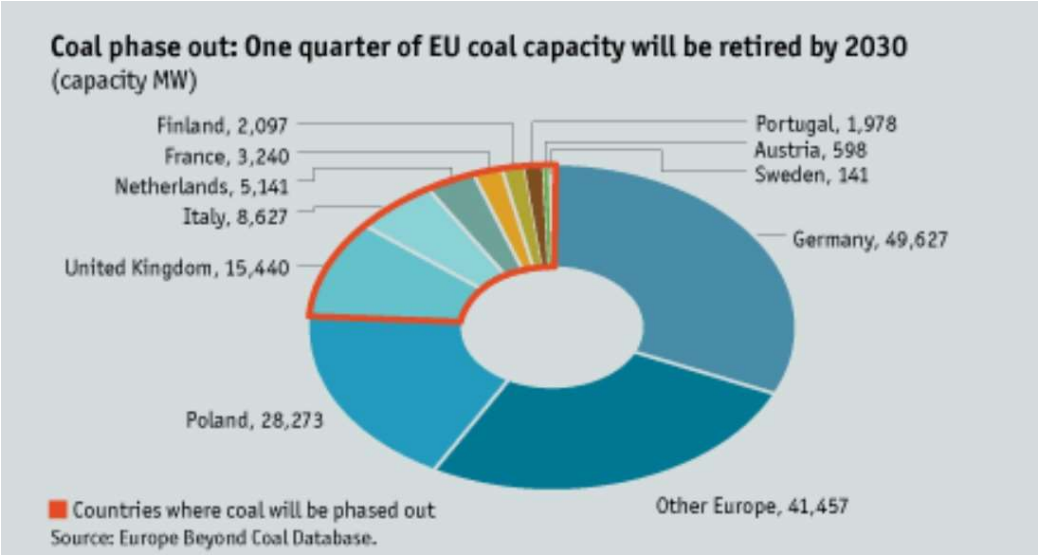

Figure 1: Individual EU countries participation in coal phase-out [15]**.**

One of the major production of electricity in the world is provided by the combustion of coal in a coal-fired power plant, present almost everywhere in the globe. Each continent has its own policy of exploitation of such plants, basing the internal production of electricity on coal combustion with a different percentage. In Europe, during the ’90s, the production of electricity from coal power plants was covering 39% of the utilities. Due to restrictions superimposed by the EU, the countries of the community agreed to diminish the consumption of fossil fuel by the decades, counting a reduction of the share up to 30% in the 2000s. The trend of the EU private electricity producers is to totally phase out the coal-fired plants in favour of green production by the 2020 and 2030 [15]. Figure 1 reports

the individual share of the EU countries which applied to the entire annihilation of the coal combustion by 2030.

Notwithstanding that, the production of by-product from coal ignition is still a tangible emergency. The major by-product of these power plants is not only the excessive greenhouse emission in the atmosphere, contributing to the climate change, but it is also the exhaustion of coal-ash from the combustion chamber (divided in bottom and FA, see Chapter 2.6 Figure 19). According to EU standards, these slags must be gathered, through a specific system, and disposed of safety and controlled landfills. During the years, utilization of coal-ash was an issue, being aluminosilicate scrap, thus the excessive disposal of this material was filling unsustainably the landfills, raising another emergency. In the last decade, the coal-ash, especially the finer form (FA), was sold by the electricity producers to cement producer, the latter utilizing this by-product as aluminosilicate additive or clinker for the production of Portland cement, due to its appreciable pozzolanic characteristic [16]. The pozzolanic properties of the derivatives of coal combustion were known since the begging of the last century, and since then FA has been utilized in cement production, in an amount progressively higher, especially between the '90s and 2000s, when the EU restrictions push the cement producers to utilize more waste materials as feedstock, as reported in Figure 2 [3].

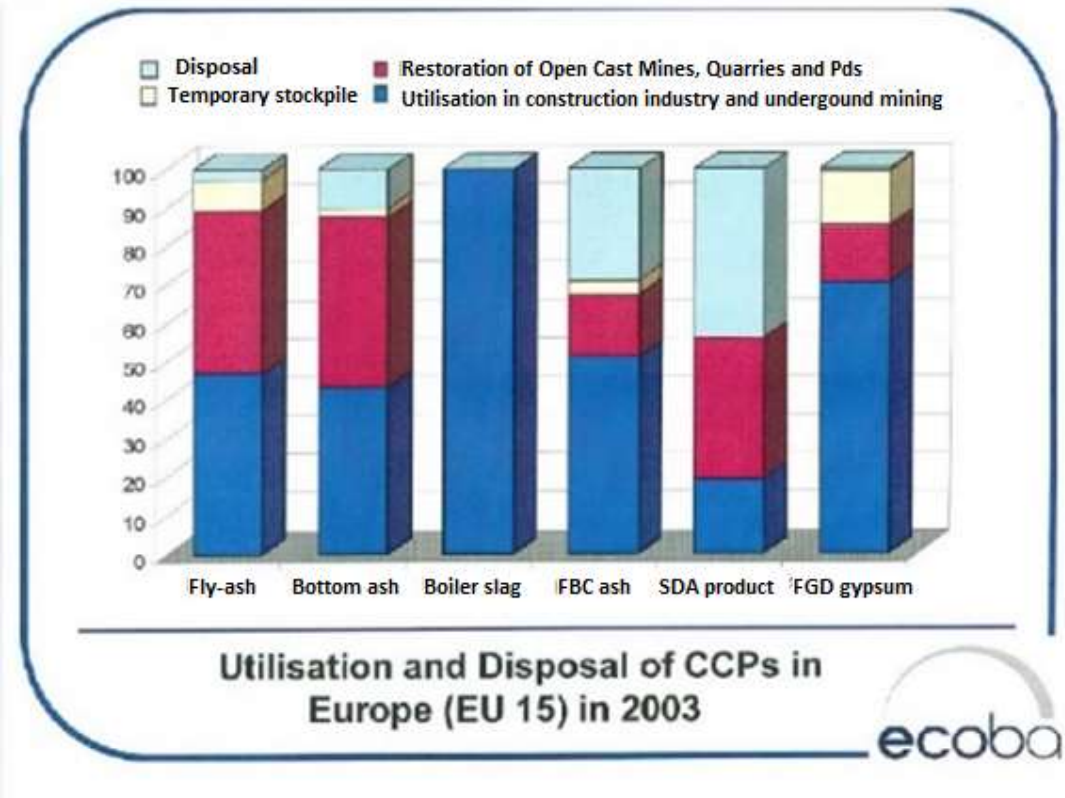

Figure 2: Utilization of coal-ash and derivatives in 2003 [3].

Despite the EU policy in favour of an extensive utilization of the coal ash, the recycling of this waste is still not entirely exploited and, contribution to dispose of in a landfill is still remarkable (see Figure 2). Therefore, new technologies encompassing the utilization of

wastes are necessary to help to empty the landfill, render the waste management more sustainable. FA, being an aluminosilicate-based material, suits very well for the production of GPs and alkali activated materials (AAMs), including FA in an amount as high as 100% of the raw aluminosilicate source, especially for AAMs production.

Another matter of waste management emergency is the re-utilization of urban wastes like for instance can be the glass. Theoretically, the glass is 100% recyclable, and it can be indefinitely recycled without any loss of quality. Among many examples of glass recycling, urban waste glass can be utilized in the production of glass cullet, as a raw material in abrasives, as aggregate in pozzolanic products, in road beds, pavement and parking lots, in the production of fibre-glass, and as fractionators for lighting matches and firing ammunition [17]. Waste glass is also eligible to be reutilized as a raw material in alkali activation of aluminosilicate, being amorphous material based on silica. Recycled glass from many sources can be incorporated in alkali-activation of aluminosilicate, so as to adjust the chemistry of the reaction and replace synthetic materials, like the water glass, normally utilized for the production of GPs [4,18,19].

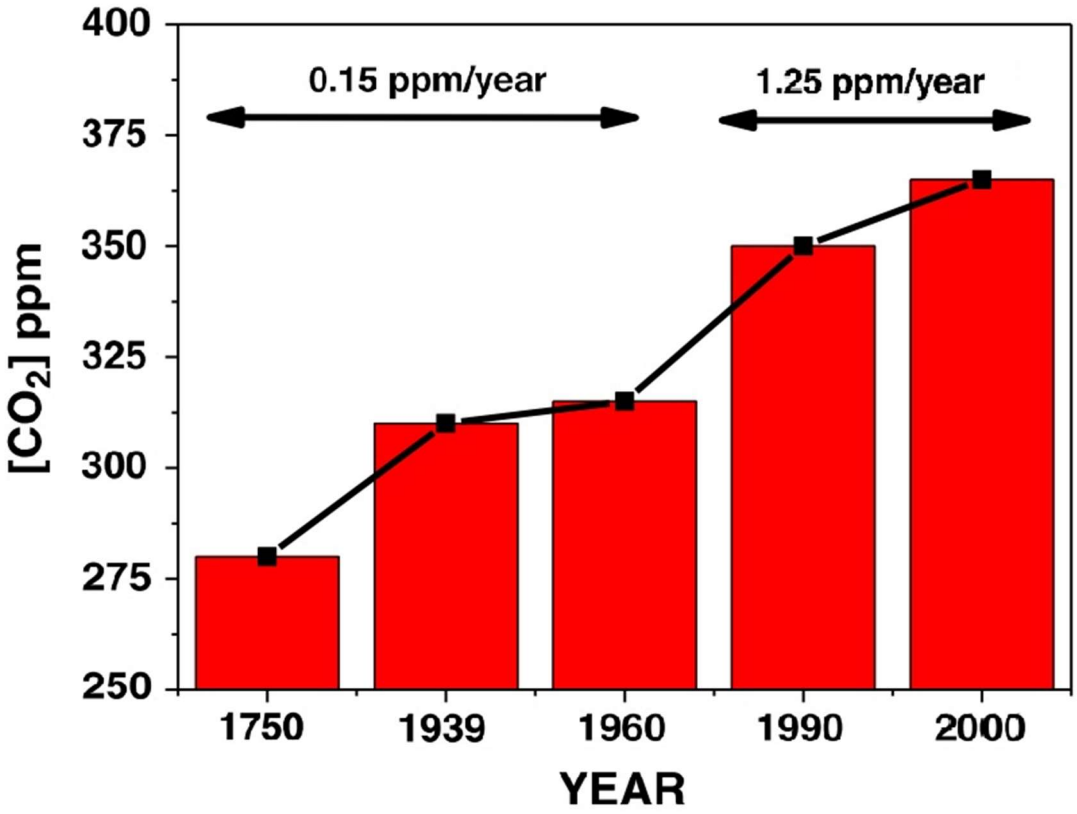

Figure 3: Rate of emission of CO_2 in the atmosphere from the industrialization until today [20].

The last, but not the least, is the worldwide concern regarding the gradual and relentless increase of the average seasonal temperature in the globe, firstly known as global warming, and then named as climate change. This phenomenon is caused by the extensive emission of greenhouse gases in the atmosphere, among all CO_2, which in turn, working as

a mirror, reflects the infrared wavelength emitted by any warm body in the earth (including the earth crust), retaining the heat in the atmosphere, beneath this carbon dioxide layer. Greenhouse gases, and especially CO_2, is daily emitted by natural event and process, like the respiration of any life form in the planet, combustion and Vulcan eruptions, but a big contribution is attributed to the human activities in the last century, characterized by massive industrialization. In particular, burning of fossil fuels, like coal and oil has increased the concentration of carbon dioxide in the atmosphere, even exacerbated by the large deforestation, being the greenery worldwide the only source of oxygen naturally transformed from CO_2 absorption. As corroboration of what just uttered, at the dawn of the industrial revolution in the mid-eighteenth century, the concentration of CO_2 in the air came to about 280 ppm. By the outbreak of World War II 200 years later, CO_2 levels had risen to 310 ppm, i.e., at a rate of 0.15 ppm per year (see Figure 3). But between 1960 and 2000, CO_2 concentration soared from 315 ppm to 365 ppm in just 40 years (1.25 ppm/year), evidencing an irresponsible advance of the technology in the last two decades. Figure 3 depicts the above-described trend [20].

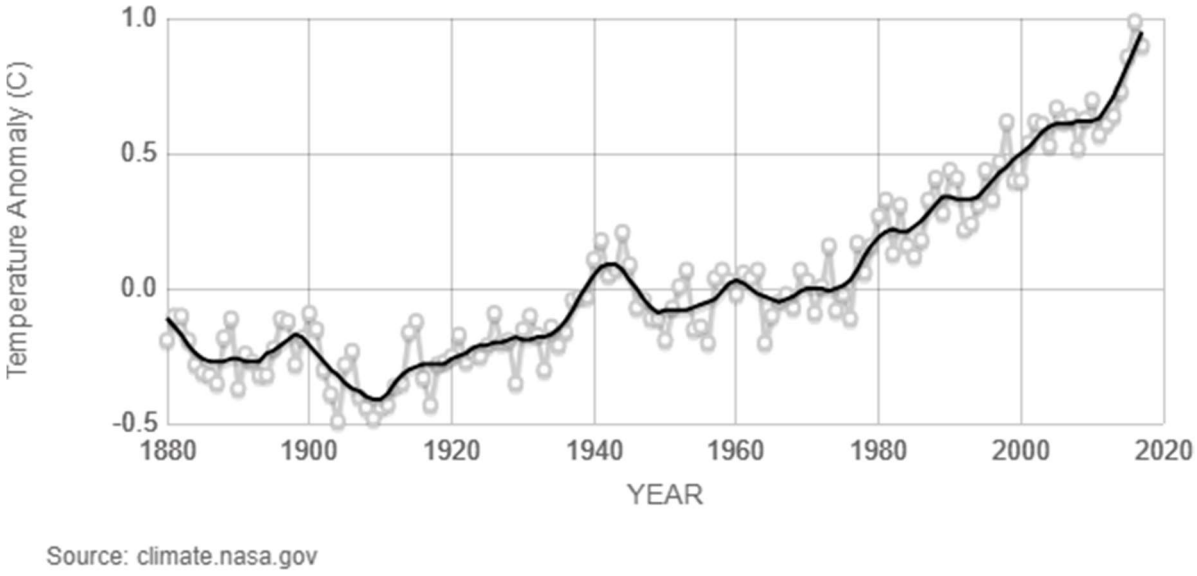

Figure 4: Changing in global surface temperature from the industrial revolution up to today (NASA source) [21]**.**

According to data gathered by NASA stations and provided in the official website [21], this trend is affecting directly the planet's average surface temperature, which has risen about 2.0 degrees Fahrenheit (1.1 degrees Celsius) since the late 19th century, a change driven largely by increased carbon dioxide and other human-made emissions into the atmosphere. Most of the warming occurred in the past 35 years, with 16 of the 17 warmest years on record occurring since 2001. Not only was 2016 the warmest year on record, but eight of the 12 months that make up the year — from January through September, with the exception of June — were the warmest on record for those respective months (Figure 4). The temperature rising is, in turn, affecting the ecosystem, especially causing the shrinkage of the ice sheets in Arctic and Antarctic more rapidly than predicted, glacial retreat in all the mountain chains in the world, decrease of the snow cover, sea level rise, extreme

meteorological events (huge rain falls and hurricanes), oceans warming and acidification. All these events are going against the necessary and clever attitude of prevention of the marine and not a marine ecosystem, as the life cycle of the living forms in the planet is an unstable balance easy to break.

All these reasons motivated the governments worldwide to adopt policies in favour of a reduction of greenhouse emissions, and then direct the technological advances towards greener developments. In this context, many efforts and agreements have been done so far, including the Kyoto Protocol commitments, the first international agreement in which the major developed countries in the world promise to strive to reduce greenhouse gas emissions by establishing measures in the processing stage and implementing clean development mechanisms. Later in December 2009, the Copenhagen summit was attempting to remind and prove the sensitivity of the same and more countries to environmental issues, in some cases with political initiatives point in those directions, and some other cases with scarce results [20]. Among all the policies undertaken by several countries in the world, one comprehends the abatement of the indirect CO_2 emitted for the production of Portland cement, the main construction material, widely used around the world for any kind of architectural structure, which in the last decades experienced an increase in exploitation. Indeed, the processing of Portland cement involves the heating up to 1500 ˚C of lime-alumino-silica sources, said pozzolanic material, whose ability is to produce in such condition calcium-alumino-silicate compounds, in the form of clinker, suitable for the production of the final C-S-H network, typical of Portland Cements [22]. Thus CO_2 is directly liberated during water evaporation and phase transformation of the crystalline compounds, and indirectly during the heating process in kilns. Due to the continuous global increase in demand of Portland cement, currently, cement companies are producing nearly two billion tones/year of their product and emitting nearly two billion tones of CO_2 (or about 6 to 7% of the planet's total CO_2 emissions) in the process. At this pace, by 2025 the cement industry will be emitting CO_2 at a rate of 3.5 billion tones/year, more or less equal to the total emissions in Europe today (including the transport and energy industries).

Merging all these issues, it is evident that replacing OPC with a greener and zero-CO_2 emission products seems to be an important challenge, helping to reduce in a sizeable share the content of greenhouse gases in the atmosphere and then reduce the impact of this gas on the ecosystem. The AAMs and GPs have mechanical, physical and chemical properties which render this material comparable to OPC, and eligible to 100% replace OPC in its applications.

2.2 History of alkali activation

The alkali-activation process is said to be of any chemical reaction in which meanly inorganic element is activated by a highly base solution made of alkali metal elements, such as sodium, potassium, calcium etc., all belonging to the first two columns of the periodic table (alkali and alkaline metals) [19,23,24]. This activation reaction consists of dissolution and rearrangement of species provided by the base material to form a compact bulk made of an interconnected structure of the rearranged species with alkali cations.

The first partial exploitation of alkali activation was dated around 1930 in Germany, where industrial slags were set in dry potash solution, to form hybrid cement. But the first entire alkali activation was carried out in Belgium later in 1940, where still industrial slags were activated and set in caustic soda and base salt solution based on alkali metals, to produce the first clinker free cement, in the first large-scale laboratory study based on alkali activation, led by A.O. Purdon [25]. The first scientific investigation related to the possibility of preparing low-calcium or even calcium-free cementitious materials was carried out by Victor Glukhovsky [12], later in 1957, who investigated the binders used in ancient Roman and Egyptian constructions which he initially called 'soil cement' or 'alkali cement', using clays and alkaline metal solutions. Depending on the composition of the starting materials, Glukhovsky classified these products under two main systems:

$$Me_2O\text{-}Me_2O_3\text{-}SiO_2\text{-}H_2O \quad (1)$$

$$Me_2O\text{-}MeO\text{-}Me_2O_3\text{-}SiO_2\text{-}H_2O \quad (2)$$

These early approaches were followed by numbers of formulations using a wide spectrum of materials, including blast furnace slag, clay, aluminosilicate rocks, and ash. A timeline of highlights in alkaline cement research is summarized in Table 1. In 1981, Davidovits [26–29], a French researcher, published results obtained with blends of metakaolinite, limestone and dolomite, whose products he called geopolymers (on the grounds of their polymeric structure). That term has since been widely accepted for the group of materials associated with the [$Me_2O\text{-}Me_2O_3\text{-}SiO_2\text{-}H_2O$] system defined earlier by Glukhovsky. In 1986 Krivenko [30] published the results of research on the principles governing the physical and mechanical properties of concretes prepared by alkali-activating slag. That same author, in conjunction with professors D. Roy and C. Shi, published the first book on alkaline activation in 2003. Another breakthrough came in 1999 when A. Palomo published the first article addressing the possibility of producing technologically competitive cement by alkali-activating fly ash (FA) from coal-fired steam power plants [31].

Table 1: Main milestones in the history of Geopolymers [31]**.**

Year	Name	Country	Study/Impact
1930	Kühl	Germany	Slag setting in the presence of dry potash [32]
1937	Chassevent	unknown	Slag reactivity measurement using a dry potash and soda solution [12]
1940	Purdon	Belgium	Clinker-free cement consisting of slag and caustic soda or slag and caustic alkalis synthesized with a base and an alkaline salt [25]
1957	Glukhovsky	USSR	Binder synthesis using hydrous and anhydrous aluminosilicates (vitreous rocks, clays, steel mill slag) and alkalis; proposal for a Me_2O-MeO-Me_2O_3-SiO_2-H_2O cementitious system; coining of the term 'soil cement' [12]
1981	Davidovits	France	Alkalis mixed with a blend of burnt kaolinite, limestone and dolomite, and trademarks such as Geopolymer, Pyrament, Geopolycem, Geopolymite [28]
1986	Krivenko	USSR	Principles governing system Me_2O-MeO-Me_2O_3-SiO_2-Al_2O_3 properties; proposal for the generic name 'alkaline cement' and the specific name 'geocement' [30]
1999	Palomo	Spain	Production of hardened cementitious materials from alkali-activated type F fly ashes [24]
2003	Shi & Krivenko & Roy	Ukraine - USA	First book on alkali-activated cements [33]
2014	Provis J., & van Deventer J.S.J	UK & Australia	Alkali-activated Materials State of the art Report. RILEM TC 224-AAM [12]

Early Roman mortars appear to be predominantly based on the development of hardness and strength by carbonation of lime, until it was discovered (either by experimentation or by implementation of knowledge gained from surrounding civilizations) that the formation of aluminosilicate binding phases by the inclusion of volcanic silica-containing ash and/or fired clay gave improvements; that is, changing their mineralogical composition gave an increase in durability. The mineralogical composition of ancient cement is not the same as that of modern PC; the ancient binders tend to be lower in Ca and richer in alkalis, Si and Al. The presence of analcime in various ancient cements supports the idea that such a zeolite is a more stable phase formed as a result of long-term hydrothermal transformation of the initial phases, consistent with the schemes presented in Figure 5, reporting a model built by Krivenko [12], in which among all the information, a high presence of Ca is coincident with less resistance to harsh conditions.

It is also notable that, although modern cement has often been used to repair ancient structures, the modern repairs have only rarely proven to be as durable as the ancient cement under identical exposure conditions. This may indicate that the binder structures formed with lower calcium and higher aluminosilicate content could provide advantages in terms of binder stability over extended time periods or may be related to incompatibility in

material (chemical and mechanical) properties between the existing and new materials if the repair material is not well selected. Although C-S-H gel is a major constituent of both Portland cement paste and many types of ancient cement, it is not quite correct to conclude that its presence is responsible for durability. The resistance to environmental exposure appears to be related to the degree of gel cross-linking, as outlined in Figure 5, and the presence of reduced quantities of calcium and elevated levels of tetrahedral aluminium (often charge- balanced by alkalis, as in the case of zeolites) is strongly advantageous in this area [12]. Therefore, the durability is one of the key factors rendering the GPs and AAMs more attractive than OPC, as demonstrated in the thousands of years by the Pyramids and the Ancient Roman Constructions.

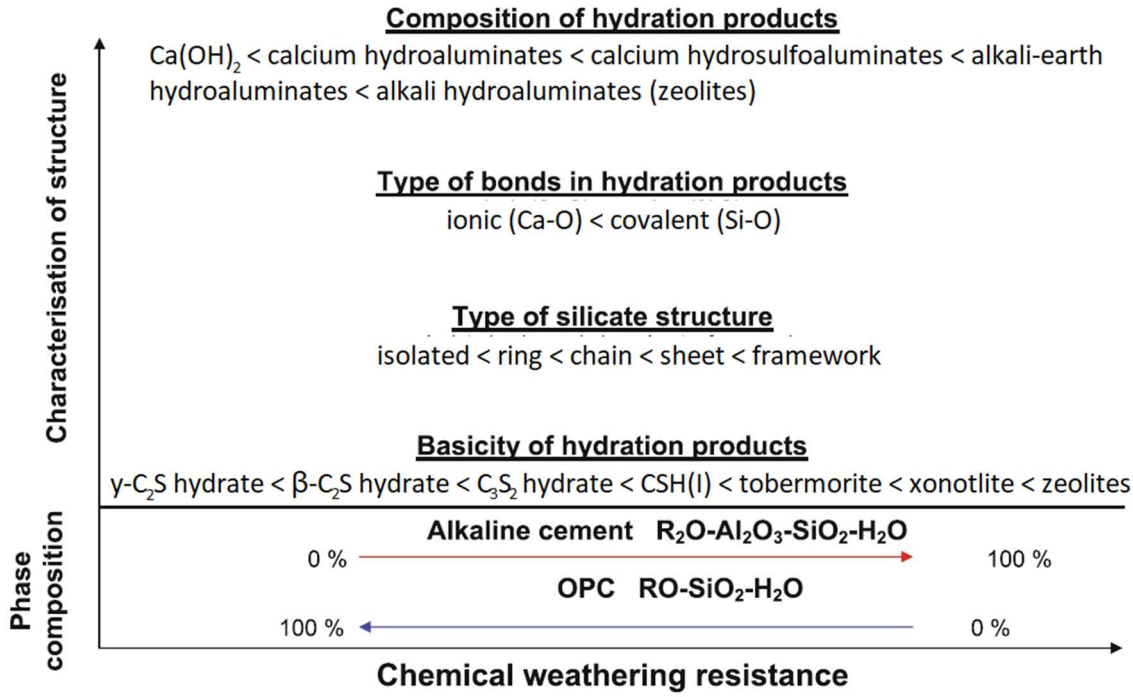

Figure 5: A proposed model putting in relationship mineralogical durability, phase composition and structure (by Krivenko) [12].

2.3 Limitations of alkali-activated materials and geopolymers and discussion on the durability

2.3.1 Obstacles in the commercialization of AMMs and GPs

This paragraph is devoted to clarifying the limitations of AAMs and GP displayed up to date, including cost and durability, and what the scientific research has done and could do to render these materials still more appealing than OPC. The main point of strength so far exhibited by AAMs and GP over OPC was the drastic abatement of CO_2 emission in the entire production cycle of the material, a convincing reason to justify the upscale of these materials.

Nevertheless, concern over Greenhouse gas emissions will obviously not be sufficient in itself to drive AAM uptake in all parts of the world, in particular in many developing nations where cement is relatively inexpensive, margins are low, and cost-effectiveness is paramount. In these regions, supply chains and economies of scale will need to be developed for AAM concrete to compete with cement producers for a share of a rapidly growing market. The ability to utilize local naturally occurring raw materials (pozzolanic soils and clays) as AAM precursors will be highly desirable in these regions, with the main challenge being the sourcing of appropriate activators. The supply of raw materials is also likely to be an issue in some developed nations, where fuse silica and FAs are extensively utilized in blending with OPC and are thus not available in sufficient quantities to launch a large industry sector dedicated to the alkaline activation of such materials. Again in these parts of the world, the development of alkali-activated binders based on materials which would not otherwise be utilized, and in particular materials derived from naturally-occurring soils, appears to be a potentially profitable way forward [12].

The reason hindering the utilization of AAMs and GP, especially in the developed countries, is related to a strict standardization of the mechanical performance for a cementitious binder. These have been developed over many years with benchmarks often set with the chemistry and behaviour of OPC, but despite this, standards containing constraints such as minimum cement content are beginning to be seen as excessively prohibitive, even for OPC-based systems [34]. Products such as AAM concrete or other alternative binders, and even some high-performance cement-based systems, may not simply be an evolution of existing OPC technology but also may require a different chemical and engineering viewpoint to understand their behaviour, and may perform acceptably but without conforming exactly to the established OPC-based benchmarks, particularly with regard to rheology and chemical composition. This has long been believed by cement producers and potential AAM market entrants to be a significant hindrance to the acceptance of AAM technology in the developed world. The main commercial reasons hindering the AAMs and GPs to be up-scaled in industrial production can be synthetized as follows [35,36]:

1. Vested interests and established practices in the construction materials industry;

2. The huge technological gap between laboratory and industrial scale concrete in terms of the handling of powders and wet concrete, and the engineering behaviour of wet and hardened concrete;
3. A lack of industrial and commercial experience of many researchers;
4. A lack of understanding of supply chain dynamics and control;
5. Limited experience of a small selection of source materials, instead of the extensive experience of a wide variety of source materials used under different operating conditions in different climates and countries.

However, the developing world does not have the same entrenched standards and is generally more willing to accept an innovative solution to a problem such as the use of alternative binders in concrete, as market demand is projected to markedly exceed the currently available supply in the next several decades. This was the original driver for the development of alkali-activated binders in the former Soviet Union, as cement demand outstripped supply, and the increasing problems being faced by developing regions in terms of 'counterfeit' cement products in recent years speak to a similar additional driver for the development of alternative, low-cost technologies in the current economic climate. Developing markets, particularly China and India where FA is widely available due to coal-fired electricity generation, and where CO_2 emission is likely to become an increasingly significant political issue, may prove to be the primary areas in which alkali-activation technology becomes increasingly accepted on a regulatory level [12].

Another issue comprehending also the OPC market regards the durability of the material. It is known that AAMs undergoes some problems of durability and corrosion in harsh environments and chemical degradation in time. GPs, being chemically speaking more stable, does not suffer from durability as much as AAMs. Thus, in the upcoming discussion, we will only refer to AAMs and OPC. In terms of durability, there is an urge of replacing OPC in the market, as this material largely suffers disintegration problems due to high permeability which allows water and other highly corrosive media to enter the microstructure and to cause extensive carbonation and corrosion problems. The early deterioration of reinforced concrete structures based on OPC is a current phenomenon with significant consequences both in terms of the cost for the rehabilitation of these structures, or even in terms of environmental impacts associated with these operations [37]. AAMs do not present these severe limitations in durability, but many other weak points have been displayed, in terms of acid corrosion, efflorescence and so forth, especially if compared with GPs. Hereafter, a brief overview of the durability limitations and qualities of AAMs is reported.

2.3.2 Resistance to acid attack

In an acid environment, the network of AAMs seems to be affected in the long term, involving a decrease of the mechanical strength (compressive and flexural), mass loss and change of the microstructure. Palomo et al. [38] investigated the influence of different solution on Metakaolin (MK)-based AAM samples, soaking them for different time frames in sulfuric acid (pH=3), sea-water (pH=7) and sodium sulphate (pH=6). Results show a

decrease of the flexural strength after 90 days of exposure in all the solutions, and with an initial drop of the properties between 28 and 56 days prior increase of the performance again. According to the authors, this first drop of the flexural strength is attributed to a loss of the mass due to degradation of the bulk material, followed by a change of the microstructure, with the formation of faujasite, increasing the actual density of the material, and then the flexural strength. These results, however, demonstrated a general increase of the mechanical properties of the AAM samples, suggesting that the reaction of gelation continues even in aggressive environments. This tendency was previously advertised by Glukhovsky et al. [37], whose studies managed to demonstrate that the tensile strength of alkali-activated slags was anyway increasing in the first week through the material was immersed in the lattice and hydrochloric acid solutions (pH = 3). AAMs and GP experience also a mass loss if exposed to acid environments. Davidovits detected a mass loss of geopolymeric concrete samples of up to 6-7% in 5 vol% hydrochloric acid solution after 4 weeks [37], whereas Pacheco-Torgal et al. [39] reported a mass loss of slag-based AAM samples of 2.6% in a hydrochloric acid solution (5 vol%) after 28 days. Notwithstanding that, the same author was able to demonstrate that the rate mass loss for OPC is higher than AAM and GP, evidencing a mass loss up to 95% in the same period, involving a more drastic loss of the strength. Bakharev et al. [40] compared the loss of OPC and alkali-activated slag materials in term of loss of strength after exposure to the acetic acid solution (pH = 4) within one year of continuous immersion. They reported a 33% strength loss for the alkali-activated slags and 47% for OPC concrete. They claim that the strength loss is influenced by Ca content, 64% for OPC concretes and just 39% or alkali-activated slag concrete. Besides slag compounds have lower Ca/Si molar ratio and are more stable in acid medium. As for OPC concrete calcium compounds, they possess high Ca/Si molar ratios and react with acetic acid forming acetic calcium compounds which are very soluble. They concluded that concrete with less free calcium has a higher performance in acid medium, in agreement with the model constructed by Krivenko in Figure 5.

2.3.3 Alkali-silica reaction

The alkali-silica reaction is a chemical process occurring between an alkali cation and silica after absorption of water, inducing a formation of a new phase and the expansion of the material, and therefore the formation of internal cracks. The condition to be satisfied to have this reaction is the simultaneous presence of amorphous silica, alkali ions and water [37], even though many other authors claim that a big contribution to this reaction is carried by the presence of Ca^{++} cations [41]. AAMs and GPs were not investigated in this problem as much as OPC, but first results from Fernandez-Jimenez et al. [41], showed that in some AAMs, the alkali-silica reaction effects are very less as compared to OPC expansions, as depicted in Figure 6. The study conducted according to the ASTM standards, showed almost no expansion in alkali-activated FA in caustic soda (only 0.1%) after 180 days of testing, whereas OPC evidenced an expansion of up to 1.8% in the same time frame, in line with the literature evidence.

2.3.4 Resistance to high temperature and to fire

Fire and heat-resistance properties are among all, one of the key characteristic that makes AAMs and GP more appealing than OPC. Indeed, traditional Portland cement-based concrete is not structurally stable when exposed to high temperatures, even when other factors affecting concrete's behaviour at high temperatures are chosen appropriately (i.e., size, load, humidity, reinforcement, type of aggregate, etc.). The main reason for OPC-based materials to fail after firing is instability of microstructural elements during heating caused by dehydration and destruction of CSH-gel and other crystalline hydrates. Crystallo-chemically speaking, microstructure phases after firing have nothing to do with initial hydrated products. The most dangerous phase in this respect is calcium hydroxide: during firing, it converts to calcium oxide, and the latter re-hydrates after subsequent cooling with the atmosphere's humidity, resulting in serious volume expansion and almost complete destruction of a matrix. This leads to a collapse of the OPC strength after firing at 800–1000°C up to 20–30% of the initial ultimate compressive strength [42].

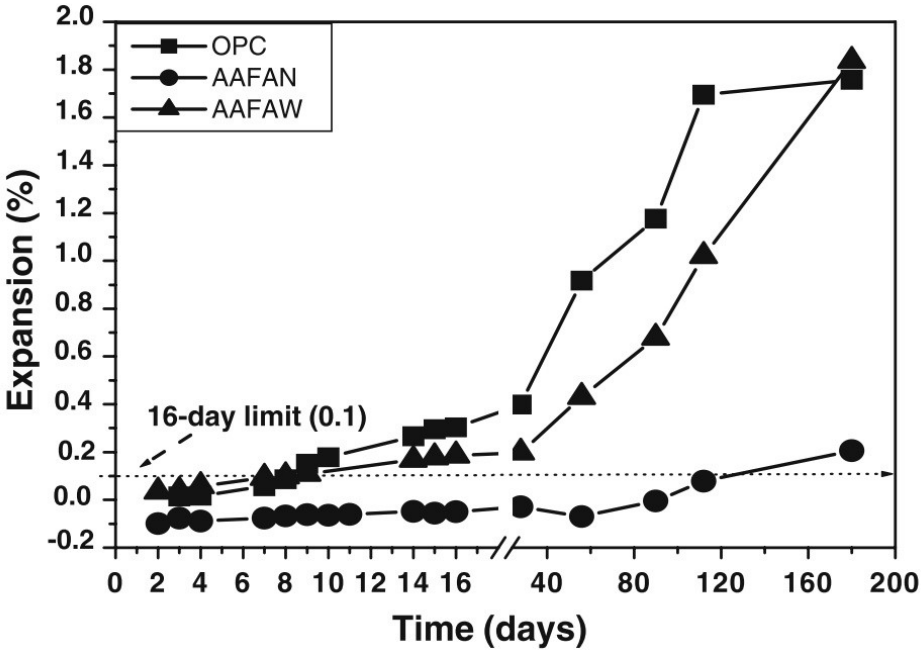

Figure 6: Alkali-silica reaction-induced expansion determined by the accelerated test based on ASTM standard C1260-94 [41].

The possibility to introduce AAMs in the market presented during the '70s, when in the aftermath of a catastrophic fire in France in 1973, the government required to seek for materials resistant to heat and fire [43]. This opened a new additional application for AAMs beside mere construction and gave rise to a broad investigation in heat resistance and fire properties throughout the scientific community between years 80's and '90s. Davidovits in 1991 came up with a new formulation of AAMs based on metakaolin with specific chemistry, who personally renamed it as 'Geopolymer cement'. According to Davidovits, this new alkali activated compound not only is more stable than any other AAMs but it is also resistant to sudden heat and fire stream [43]. The same author tested

the fire resistance of GPs composite based on carbon fabric laminates and compared them to other composite materials commonly used in the fire applications, included fibre-reinforced concrete. He successfully demonstrated that GP composites work at temperatures higher than 800 °C, retaining up to 67% of the flexural strength even if exposed to a heat flux comparable to fire for a long time [44].

Afterward, other authors extended the investigation on these properties to AAMs and GPs made of other aluminosilicate precursors, such as FA and other slags [45]. Firing properties related to the amount of crystallinity in microstructure must be weighted according to the mechanical properties at low-temperature operation. The majority of these authors agreed on the importance of glassy phase amount either in precursors or in reaction products over the efficiency of reaction [26,46,47]. In their work, they inferred that fire and heat-resistance properties are intimately connected to the nature of the crystalline structure, as crystals formed in OPC are compounds not having analogies to natural minerals, resulting in problems connected with OPC durability. In particular, the formation of zeolite-like phases, such as sodalite network (hydroxysodalite), analcime, chabazite structures (zeolite R, herschelite), faujasite family (zeolites Na-X and Na-Y), mordenite, seems to give great benefits on the durability and resistance to acid and heat/fire [45,48].

In AAMs and GPs, the quantitative and qualitative formation of these crystalline phases, if produced (especially in case of GPs), are strictly related to several parameters connected to the beginning of the alkali activation (chemistry of the reaction) and the curing stage, as well as the nature of the aluminosilicate precursors. For instance, Krivenko et al. [45] stated that there is a principal similarity of the phase composition of the hydration products of the metakaolin and FA based AAMs, but more zeolite is produced if FA is used instead of metakaolin as the main source. The phase composition of the autoclave-cured alkali-activated FA is represented mainly by the analcime, zeolite – and zeolite R (chabazite/ herschelite family). Being dependent on the high content of the caustic soda due to peculiarities of the mix formulations, a synthesis of hydroxysodalite in steam cured and dry cured FA-based compositions with SiO_2/Al_2O_3 = 4 correlates well with the results obtained on similar systems with high alkali concentrations and normal pressure of treatment. When using the low-alkali compositions with SiO_2/Al_2O_3 = 6–8 simultaneously with a low-intensity treatment such as steam or dry curing, standard exposition time is not enough for the zeolite crystallization.

Other authors [47] supported the thesis that the amount of alkali (Na_2O/Al_2O_3 ratio) influences that crystalline presence in the microstructure and thus the thermal resistance of the material. The temperature of crystallization of the anhydrous aluminosilicates depends on the initial composition, and first of all, on the alkali content. In the alkali-rich systems (Na_2O/Al_2O_3 = 1.0, SiO_2/Al_2O_3 = 3.6) they appear in limited amounts at 600 °C, in the slightly less alkaline mix (Na_2O/Al_2O_3 = 1.0, SiO_2/ Al_2O_3 = 4.0) they arrear at 800 °C, whereas in the low-alkaline compositions (Na_2O/Al_2O_3 = 0.5, SiO_2/Al_2O_3 = 4.0) the crystallization begins only at 1000 °C. Correspondingly, the higher amount of anhydrous phases crystallized due to temperature growth, the lower amount of initial hydrated products (in this case, hydroxysodalite) remained. That is to say, that theoretically, the

lower the amount of initial alkalinity, the higher the thermal resistance. However, initial alkalinity should warrant a sufficient mechanical strength of conglomerate before firing, since it is known that initial alkalinity in AAMs regulates a velocity of alkaline activation and, subsequently, it regulates strength growth. That's why a mix design of AAMs for high-temperature application should be a compromise between sufficient initial mechanical strength and target properties after firing.

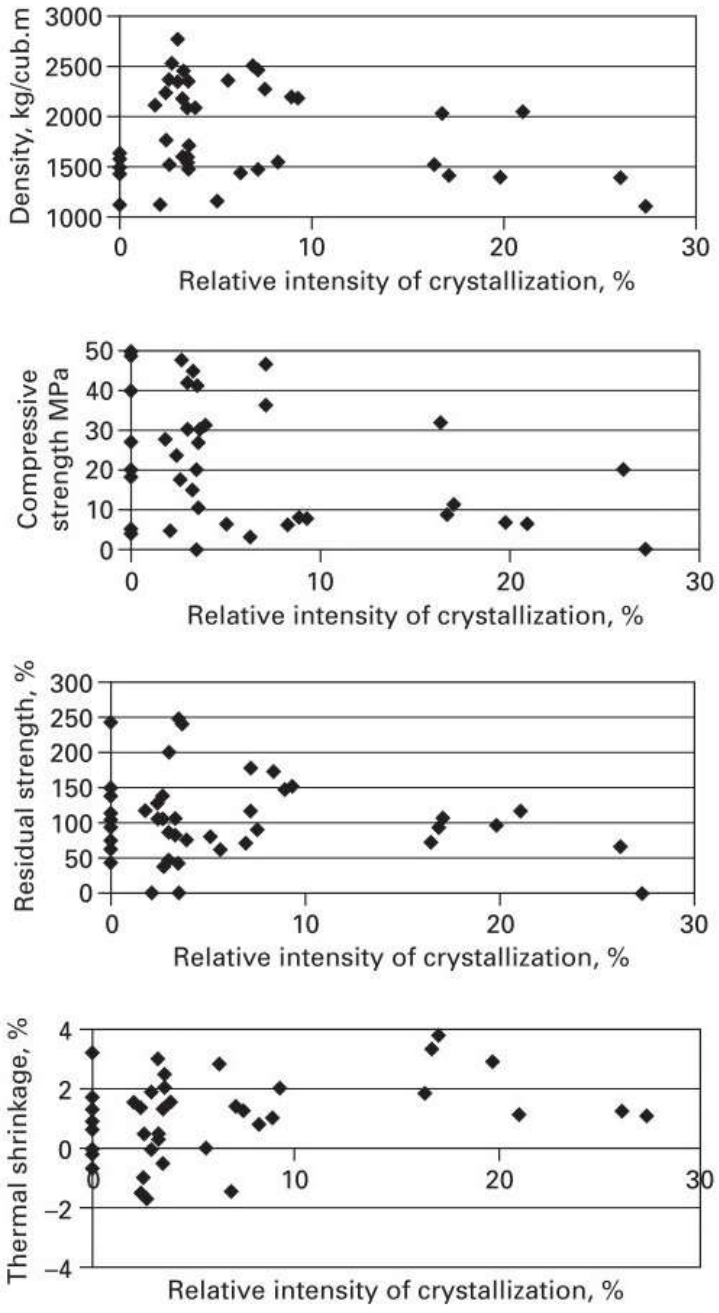

Figure 7: Correlation between relative intensity of crystallization and properties of 'chamotte' geopolymers composition: density, compressive strength after low-temperature treatment, and residual strength and contraction after firing at 800 °C [45].

Therefore, it is clear that in the formation of zeolite crystals in alkali-activation many parameters are influencing the reaction simultaneously, including the type of cation and the direction of phase transformation, never reported above. Thus controlling the crystallization of the AMMs and GPs is not so trivial and requires a good knowledge of the chemistry of the reaction to tailor the parameters accordingly. Because of this, Krivenko et al. [45] carried out a quite complex study focused on the influence of the number of crystals of milled chamotte FA-based GP over several properties, such as density and compressive strength after low-temperature treatment, and residual strength and thermal shrinkage after firing at 800 °C, (see Figure 7). It was revealed that optimal thermo-mechanical properties such as high density and mechanical strength along with low contraction after firing was achieved in the mixes with a microstructure composition presented by an average amount (from 2.5 to 10%) of the thermo-stable zeolite-like products such as analcime, hydroxysodalite and zeolite R. These phases, quantitatively determined through XRD Rietveld refinement method, are characterized by a smooth dehydration and subsequent recrystallization into stable anhydrous alkaline aluminosilicates (such as nepheline and albite) without destruction of the aluminosilicate framework. The high intensity of the crystal formation (higher than 10%) in the autoclave-cured compositions, as well as the insufficient rate of crystallization of the high-silica GPs (from 0 to 2.5%), was found to result in a sharp deterioration of service properties. In case of a high-crystalline structure, it may be caused by the increase in stresses in the already hardened cement stone during intensive recrystallization taking place at high temperature. At the same time, in case of low-crystalline structure, it is caused by the absence of a hard crystalline framework. It was concluded also that heat resistance of the FA-based GPs is higher than that of the metakaolin-based ones.

2.3.5 Resistance to freeze-taw

It is known that OPC concrete mortars and cement can suffer a mechanical decay if exposed to an elevated temperature excursion and gradient in freezing condition, depending on the pore system of the hardened paste. No risk of freezing-thawing deterioration is present if the concrete is saturated, however, when as a consequence of freezing the dilation of the concrete exceeds its tensile strength, damage occurs. The extent of the damage varies from surface scaling to complete disintegration as ice is formed, starting at the exposed surface of the concrete and progressing through its depth. Also in some cases, the salts used for de-icing road or bridge surfaces become absorbed by the upper part of the concrete. This produces high osmotic pressure, with a consequent movement of water toward the coldest zone where freezing takes place, which aggravates the scaling condition of concrete [45].

In the case of GPs and AAMs, freezing-thawing investigations gave controversial results. Puertas et al. [49] investigated the general durability of OPC cement and GPs composites based on slags, FA and a mixture of both wastes, and a relative composite of each material based on dispersed polypropylene fibres. Among the durability testing, freezing-thawing experiments were included, evaluated in term of flexural and compressive strength before and after the treatments at -20 °C, for a total of 50 cycles. The authors found that the slag

based GPs and the FA/slag system did not suffer the freeze-thaw cycles, experiencing an increase of the mechanical properties after the treatment, whereas a general decrease of the flexural strength was detected for the rest of the materials. OPC concrete (both plain material and composite) did not undergo a huge drop of the compressive strength, while the formulation based on FA underwent an abrupt fall of both flexural and compressive strength after freeze-thaw cycles. An opposite result was achieved in the study of Brooks et al. [50], who tested the loss of weight of the OPC and a set of a different formulation of AAMs as a function of the freezing-thawing cycles. The highest mass loss was revealed by the OPC concrete, resulting in a loss of 25% after 300 cycles at 0 °F (-18 °C), loss of weight in AAMs materials is negligible. Similar results were attained by Fu et al. [51] if alkali-activated slags concrete were exposed to a series of freeze-thaw cycles, up to 300 reiterations. In this case, the resistance to freeze-thaw was evaluated in terms of relative dynamic elastic modulus and mass loss. In all the materials a decrease of the controlled parameters was detected, but still in an extent comparable to the study of Brooks.

It is probable that the different results are related to differences in the microstructures of the materials. The porosity and pore size has a significant influence on the resistance to frost, the concentration, and type of activator and the time and temperature of curing have a great influence on the microstructure of the materials. In any case, more studies of GP frost resistance are necessary for the future to enable the mechanisms to be better understood.

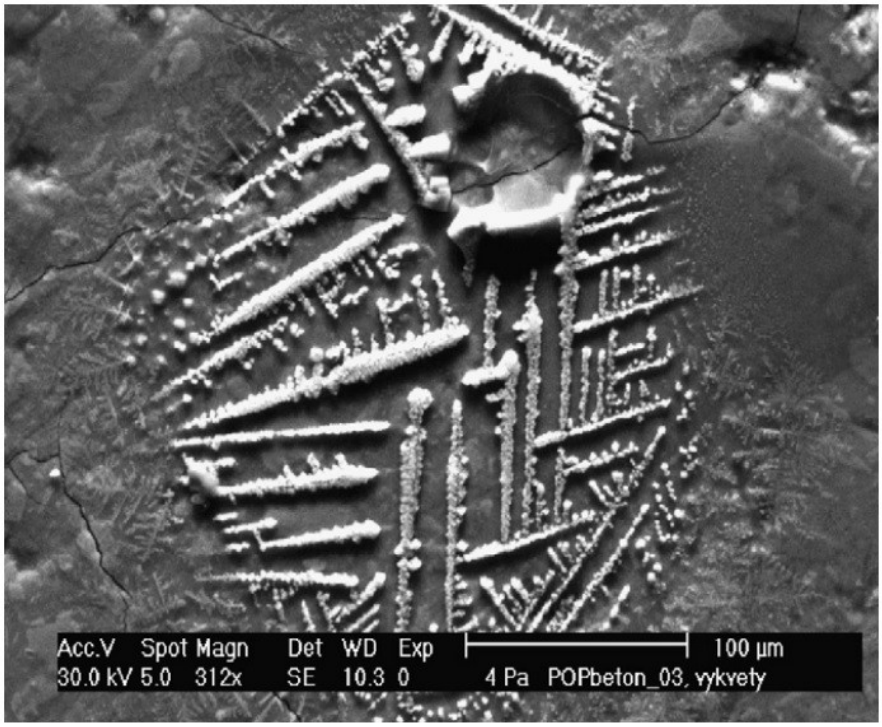

Figure 8: Typical efflorescence in alkali-activated coal fly ash activated in NaOH [52].

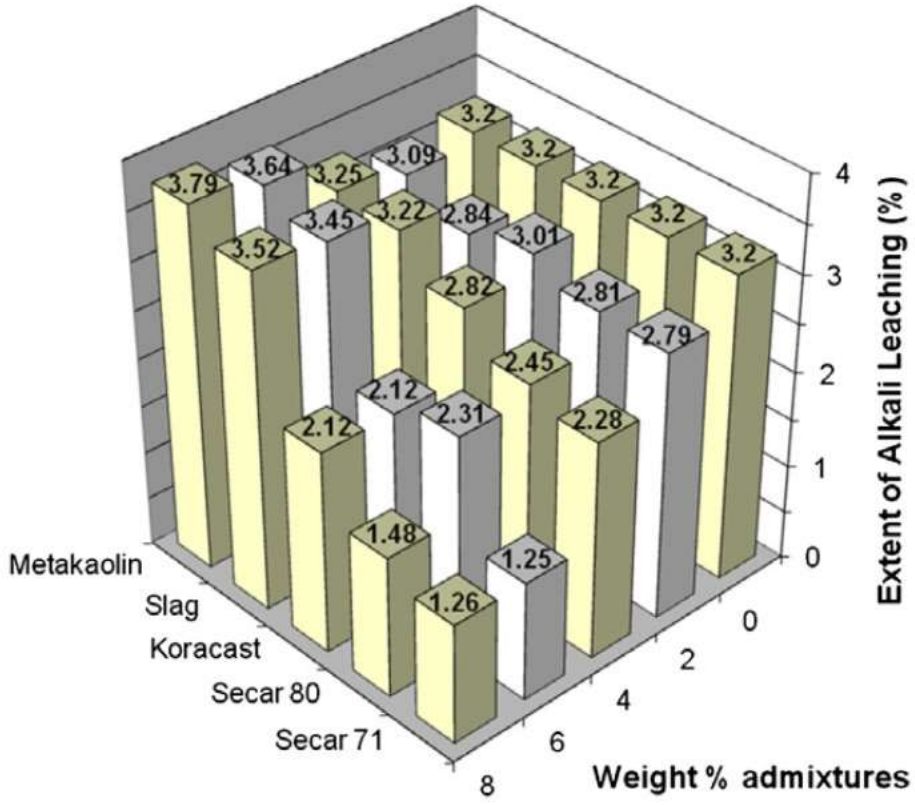

Figure 9: Effect of admixtures on alkali leaching (as a proxy for efflorescence extent) [53].

2.3.6 Efflorescence

The efflorescence is material corrosion of all the alkali-aluminosilicate based materials consisting of a formation of sodium carbonate/sulfates of the following types:

1. $Na_2CO_3 \cdot nH_2O$
2. $Na_6(SO_4)(CO_3, SO_4) \cdot nH_2O$

The formation of these compounds is mostly attributed to an excess of alkali cations in microstructure after activation reaction leading to bonding with carbonates (CO_2) in the air and/or sulfates, especially if caustic soda ($NaOH$) activator is used, yielding to the formation of crystals, also visible at naked-eye. In Figure 8 is depicted as a typical morphology of the efflorescence. Differently to the other cases, this corrosion seems to be not harmful to the chemical-physical-mechanical properties of the materials, but it is only unsightly.

The efflorescence is thought to happen in high wet condition (high relative humidity), as the Na is not present in a cation configuration (Na^+) but rather in $Na(H_2O)_n$ bond, thus promoting the formation of sodium carbonates/sulfate crystals and causing an extreme leaching of the sodium, as the presence of water weakens the sodium bond to the aluminosilicate microstructure [52,54]. It will be explained later that the presence of

moisture is rather, in turn, helping the chemical process of polycondensation of aluminosilicates precursors. Without an excess of alkali after the alkali activation reaction and the hardening of the material, no efflorescence is expected, meaning that the optimization of the reaction and the quantity of sodium in the chemistry is an important factor to decrease the amount of efflorescence formation. This is evidenced in the study of Temuujin et al. [55], whose results showed that high temperature of curing, coinciding with a higher reaction efficiency, leads to a decrease of the efflorescence. Indeed, also additions of aluminates and/or calcium oxides help the uptake of unreacted sodium in the microstructure and then reducing the efflorescence. According to Kani et al. [53], the addition of 8% of calcium aluminate cements (28 wt.% of lime) highly hinders the mobility of the alkali cations and leading to a minimization of the efflorescence, defined in terms of sodium leaching (see Figure 9, the formulation designated with Secar 71 and Secar 80). Nevertheless, it is not safe that efflorescence can be completely annihilated, given that total consumption of alkali elements is considered to be hard to accomplish, and thus always, even in a short extent, alkali excess occurs.

2.4 Alkali-activation and geopolymerization

This chapter is devoted to defining the chemistry of the reactions behind the whole process of alkali-activation and geopolymerization, and define the parameters influencing them. It is opportune, though, to clarify the formal designation of AAMs and GPs. The literature is quite confusing regarding the difference between the two over-mentioned materials if any, and several names have been attributed to this material and the chemistry of reactions, with a reason behind. Nevertheless, the large terminology related to this field is a matter of confusion in the scientific community, especially for those students approaching for the first time to the argument. Recently, due to this complication, the most representative people of the scientific community is trying to put some order, but still, a huge debate is ongoing and different parties supporting different ideologies are formed and still much confusion is induced.

Therefore, the aim of this chapter is to initially report all the terminology related to Alkali-Activated Materials and Geopolymers, and eventually to determine possible differences in terms of chemistry, microstructure, and properties.

2.4.1 AAMs and GPs: two different branches or the same things?

First of all, it is opportune to distinguish between the two terms cement and binder. Cement is considered to be a bulk material uniquely made of silica-calcium-aluminum; when the term binder is used, it refers to the utilization of the same material as the main matrix to 'bind' or 'glue' other macroscopic grains, by addition of aggregates in the viscous paste. Most of the cases, these aggregates are stones or sands. When concrete is used as a binder, then the word 'mortars' is usually adopted [56].

The terminology connected to alkali based materials is strictly related to the individual research work conducted by each of the parties involved in the field during the time. Due to slight discrepancies in chemistry and processing, each individual attributed a customized terminology to the material. As explained in the previous chapters, the cement materials considered in this thesis work are all those solid and stable aluminosilicate material formed by alkali hydroxide or alkali silicate activation of a precursor that is usually (but not always) supplied as a solid powder. This could be taken as a general definition for all the materials treated from now on [45]. Following a chronological progression of the events, the first one who set a low-temperature cement was Kuhl et al., in the 1930s, based on activation of furnace slags in a solution of dry potash, as mentioned in Table 1. This author patent the invention under the name 'slag cement' [32]. Glukhovsky was the first one in the middle of the last century to study in details the chemical activation of the furnace slags and to determine the stages of the process. He was also the first to name this type of material as 'soil cement', as he realized that this is effective on aluminosilicate precursors [31,45]. Glukhovsky also classified two different natures of binders based on the chemical composition of the precursors and then of the network:

$Me_2O–Al_2O_3–SiO_2–H_2O$ (Alkaline binding system) (3)

$Me_2O–MO–Al_2O_3–SiO_2–H_2O$ ('Alkali-Alkaline-Earth' binding system) (4)

Where *Me = Na, K,* etc. and *M = Mg, Ca*, etc. [20]. The first system (3) is characterized by alkali activation of the aluminosilicate precursors with alkali metals belonging on the first column of the periodic table. The second system (4) is characterized by the presence of heavier alkali metals either as an activator or as precursors. Later the first system was studied and developed by most of the authors belonging to the field.

Later in 1980's, Davidovits developed both Glukhovsky's systems with the attempt to produce synthetic zeolite starting from a blend of metakaolin, limestone and dolomite, for several application, and later patented the method of production under the name 'Mineral Polymers', as he defined that these materials are a product of polycondensation reaction between aluminosilicate dissolved sources [28,29]. Besides, this author also defined an alternative chemical designation of the product chemistry as follows:

$M_n\{-(SiO_2)_z-AlO_2\}_n*wH_2O$ (5)

Where *M* ascribes the alkali cation such as sodium, potassium, and calcium, compensating the negative charge of aluminum, *n* stands for the degree of polycondensation, and *z* is 1, 2, 3. In later patents, Davidovits used the Nuclear Magnetic Resonance spectroscopy NMR method applied on silicon (^{29}Si MAS NMR) and aluminium (^{27}Al MAS NMR) to define chemically the bonding and the structure of the product and inferred that this was a semi-amorphous phase based on reorganization of silica and alumina species in a 3-D framework, and renamed it as 'Geopolymer' [57,58]. According to the chemistry of silica and alumina condensation, this phase must have a specific framework depending on the chemistry of reaction (i.e. the chemical composition of sources), which gives rise to several possible silica-alumina compounds [27,59,60]. A Si/Al ratio equal to 1:1 produces a so-called poly(sialate) compound, a ratio of 2:1 corresponds to a poly(sialate-siloxo) compound and when the ratio is 3:1, then the produced compound is called poly(sialate-disiloxo). The chemical compounds and the produce crystalline part of the phase are reported in Figure 10, reproduced from Davidovits's work [26,59,61]. Nevertheless, the term 'sialate' was already in use (since the 1950's) to describe any of the salts of sialic acid, a nine-carbon monosaccharide and an important component of several biochemical systems within the human body. Also, this system of nomenclature implies certain aspects of the GP gel structure which does not correspond to reality; firstly, it describes the only integer Si/Al ratios, and secondly, it provides a one-dimensional description of a three-dimensional network, which will almost invariably prove inadequate. For this reason, Davidovits proposed a series of names and commercial brands, such as Pyrament, Geopolycem, and Geopolymite, and eventually named it as 'Geopolymer'. During his studies, this author affirmed that the highest performance is attained for specific chemistries, falling in the following ranges:

$0.2 < Na_2O/SiO_2 < 0.48; \quad 3.3 < SiO_2/Al_2O_3 < 4.5; \quad 10 < H_2O/Na_2O < 25.$ (6)

Davidovits asserted that the chemistry falling in stoichiometric composition like those above mentioned is a material comparable to the so-called 'Geopolymers'. More specifically, other authors said that among this chemical formulation, the optimum composition took place for Na_2O/SiO_2 = 0.25; H_2O/Na_2O = 10 and SiO_2/Al_2O_3 = 3.3. They also noticed that when using mixtures with a molar ratio H_2O/Na_2O = 25 extremely low mechanical strength specimens were obtained, concluding that the water content is also an important parameter in geopolymerization [1,62].

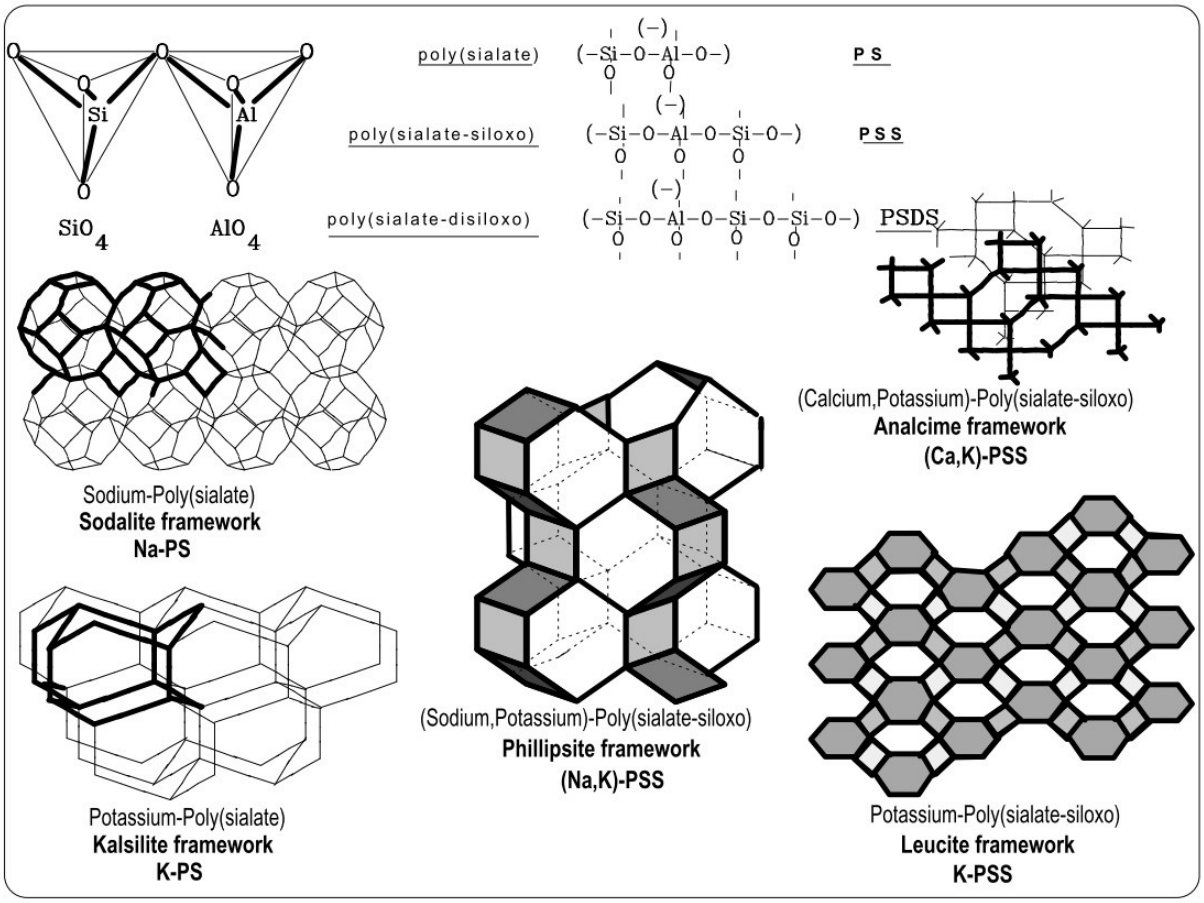

Figure 10: Computer simulations of aluminosilicate compounds and relative frameworks [59].

This differentiation brought by Davidovits's studies was a matter of initial confusion, many people started to use two terminologies interchangeably in the publications or even introduce other terminologies, with the result to complicate even more the situation. Among them, one good example is given by Rahier et al. in studies [63–65] in the late 90's, who studied the setting behaviour of aluminosilicate minerals at low temperature using metakaolinite close to the Davidovits's formulation, and eventually call them 'low-temperature inorganic polymers' or simply 'inorganic polymers', term still largely adopted by the scientific community. Earlier in 1997, Krivenko [30] called these binders 'geocement', to highlight the presence of natural mineral analogues in their hydration products and the similarities in the mechanisms governing the formation of these binders and natural geological materials The introduction of this new terminology was

immediately negatively criticized by Davidovits. During the early 2000s, other authors moved their attention towards the utilization of other aluminosilicate precursors, falling predominately in the first Glukhovsky's system of materials or in the second one with the low calcium content. More specifically, Palomo et al. investigated the proclivity of coal-ash to be alkali-activated with caustic soda or potassium hydroxide, and compared the physical, mechanical and microstructural properties of the FA-based binders with those made of metakaolin as raw precursor [24,66,67]. These authors envisaged the suitability of this waste material to be utilized in alkali-activation due to the high concentration of silica and alumina in the chemical composition. They, moreover, introduced a new description of the semi-amorphous product of the alkali-activation process, calling it as N-A-S-H gel [20,31]. The same authors investigated spectroscopically also the crystalline part of the product by selective chemical attack, asserting that the process of alkali-activation of silica sources produce also zeolite-like phase [68]. Because of this, GPs were also named under the terminology 'zeolite precursors' [68,69]. Van Deventer et al. was investigating the relationship between mechanical and microstructural characteristics of a Glukhovsky's first system materials, based on activation of metakaolin, with Si/Al ratio between 1 and 3 [70]. According to Davidovits's terminology, this material is not a GP. Concurrently to Palomo et al., these authors were also investigating the properties and performance of cement materials process through alkali activation of coal-ash [71]. In their work, all these authors agreed to name it as 'alkali-activated material' or 'alkali-activated cement'. More precisely, Shi et al. extended the classification of many materials under the term 'alkali-activated cement' or 'alkali activated slags', including alkali activated slag-based cement, alkali-activated pozzolan cement, alkali-activated lime-pozzolan/slag cement, alkali-activated calcium aluminate blended cement, alkali-activated Portland blended cement (hybrid cement). In the first family of materials are included alkali activation of blast furnace slags, phosphorus slags, blast furnace slag/FA, blast furnace slag/steel slag, blast furnace slag/MGO, blast furnace slag-based multiple component cement [20]. Other adopted terminologies attributed to alkali-activation of aluminosilicate sources are 'inorganic polymer glass', 'alkali-bonded ceramic', 'alkali-ash material' and 'hydro-ceramic' [45].

In conclusion, the first accepted terminology for materials produced through alkali-activation was provided by Glukhovsky under the name 'soil cement' after activation of furnaces slags. Later in the 1980s, Davidovits conducted a study on alkali processing of a blend of aluminosilicate precursors, including metakaolinite. After NMR spectroscopy of the microstructure, he initially coined the material as 'mineral polymers', and renamed it as 'geopolymers', satisfying restriction in chemical composition. Between the late '90s and the beginning of 2000, Rahier introduced the name 'inorganic polymer' to define a formulation close to Davidovits's one. In the 2000s, Palomo and Van Deventer carried out almost simultaneously the study of the activation of FA, calling them 'alkali-activated materials'. A summary of the timeline of the alkali-activation of aluminosilicate in history is reported in Table 2. From now on, in this thesis work, for a matter of consistency, will be refered as geopolymers (GP) those materials satisfying the Davidovits's stoichiometric restriction, and as alkali-activated materials (AAMs) all the rest.

Table 2: Timeline of different terminologies adopted in alkali-activation of aluminosilicate.

Author	Year	Terminology	Study
Glukhovsky	1967	Soil Cement	Alkali activation of low and high calcium furnace slags [12]
Davidovits	1974	Mineral Polymer	Activation with *NaOH* of metakaolinite [72]
Davidovits	1982	Geopolymer	NMR spectroscopy of the same material [28]
Krivenko	1997	Geocement	Similarities with natural geological materials [30]
Rahier	1999	Inorganic Polymer	Geopolymer like formulation [73]
Palomo and Van Deventer	2003	Alkali-Activated Material	Activation of coal ash in *NaOH/KOH* [71]

2.4.2 Stages of alkali-activation and relative models

The alkali-activation is a process consisting of mixing a suitable liquid, normally an alkali metal base solution, with an aluminosilicate precursor, in the form of powder, so as to accelerate the chemical activation of the aluminosilicate part of the raw material. The procedure of mixing is totally mechanical, occurring under different liquid to solid ratio (l/s), depending on the fineness of the powder (the finer the higher the ratio). The process of activation is purely chemically driven, and controlled only by tailoring of chemical and physical parameters (later on exposed one-by-one).

Several models were developed and have been proposed by different key-note authors of the field, explaining the latter process of activation, eventually, all of them equivalent. Still following a chronological order, the first to propose a model for alkali activation process was Glukhovsky in the 1960s, who was the first one to observe that the alkali metal ions have an active component in the cementitious system, with a fairly high uptake (from 2 to 30%). The same author, then, idealized the process in three stages [20]:

1. Destruction-coagulation
2. Coagulation-condensation
3. Condensation-crystallization

'Destruction-coagulation': according to Glukhovsky [12], the first stage entails the separation of the Me-O, Al-O-Al, Al-O-Si and Si-O-Si species due to a change of the electronic strength of the formed compounds and consecutively an accumulation of the metallic cations (Me^{+}) around silicon atoms and inducing a weakening of the chemical bond, prompting in such a way the dissolution of species. In the case of silica, the rupture of the chemical bond induces a partial negative charge, rendering this compound an anion, promptly neutralized by the metallic cation, in a Si-O-Na^{+} configuration, if the base solution is caustic soda (*NaOH*). Due to this charge concentration around the anions, Weng

et al. [74] conducted a study focusing on the partial charge modelling of the possible anion formation in a process of geopolymerization. According to this model, the resulting possible anion configurations of silicon after dissolution (or destruction) are $[SiO_2(OH)_2]^{2-}$ and $[SiO(OH)_3]^-$ according to the following reactions:

$$SiO_2 + H_2O + OH^- \rightarrow [SiO(OH)_3]^- \quad (7)$$

$$SiO_2 + 2\,OH^- \rightarrow [SiO_2(OH)_2]^{2-} \quad (8)$$

with a higher content of the former for a higher pH of the solution [75,76]. In the same way, aluminates dissolve in the solution, with a partial transformation of the aluminium coordination from trivalent to tetravalent (as the aluminium allows both configurations), forming tetrahedral complexes $Al(OH)^{4-}$ or $Al(OH)_6^{3-}$, still in a ratio depending on the pH [74–77]. The basic reaction for aluminates formation through hydrolysis reaction in an alkali solution is reported below:

$$Al_2O_3 + 3\,H_2O + 2\,OH^- \rightarrow 2\,[Al(OH)^{4-}] \quad (9)$$

'Coagulation-condensation': This is the stage in which the dissolved species come all together and form a unique matrix. According to Glukhovsky, the aluminates and silicates condensate each other, forming again an aluminosilicate compound with the different structure as compared to the base material. The product of the alkali-activation is a semi-amorphous material mainly composed by silica-alumina-sodium-hydrates. Davidovits described the product of geopolymerization according to the chemical formula reported in Equation 5. Other authors, including Shi et al., Palomo et al., Duxson et al. [20,23,71,78,79], called it as N-A-S-H gel. The meaning of this notation will be provided later on. At this point, it is appropriate to clarify what is an alkali-activation, geopolymerization and poly-condensation, and how they do work. Alkali-activation and geopolymerization are essentially the same chemical reactions based on multiple condensations (poly-condensation) of hydrolyzed chemical compound with a partial negative charge (anions), i.e. aluminates and silicates. The difference between both terminologies lies on the fact that alkali-activation normally refers to the AAMs product and geopolymerization refers to a GPs one. A condensation of species is a reaction in which two different or identical monomers come together and form a unique larger chemical compound (oligomers, long chains), by chemical conjunction (condensation) of two or more hydroxyl groups surrounding the anions, with the release of water [80,81]. This is the basic process of any polymerization reaction (for polymer production), e.g. nylon-6, a common polymer is produced according to the scheme reported in Figure 11.

Poly-condensation reaction is very usual among silicic acid compounds. This reaction occurs nearly everywhere there is an excess of dissolution of silica in water. Silica (either crystalline or amorphous) is very stable in water, with a solubility limit typically about 100 ppm (~ 1 mM) [82]. When the condition of the water solution changes (temperature, pH, pressure), this limit is modified, and any excess of silicic acid (that is the product of dissolution of silica in water) in water, immediately yields a condensation of silicic acid

monomers, so as to re-establish the solubility limit again. The condensation of these monomers, then, from a bigger chemical compound based on silica, which can be linear (oligomers) or circular (cyclic members) [82,83]. The formation of the latter is described in the scheme reported in Figure 12.

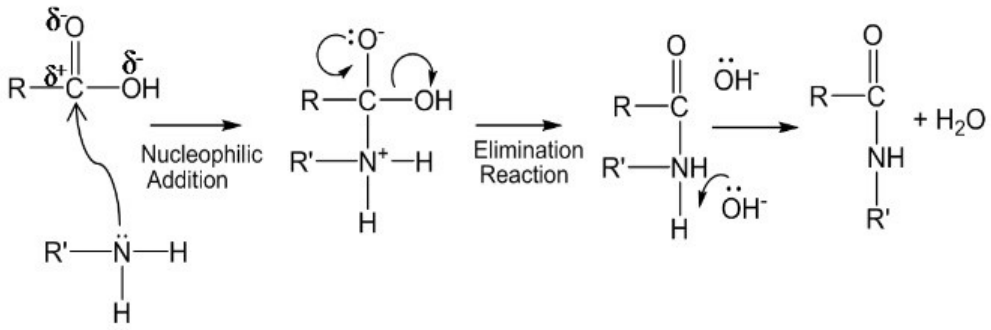

Figure 11: Nylon-6 synthesis reaction [80].

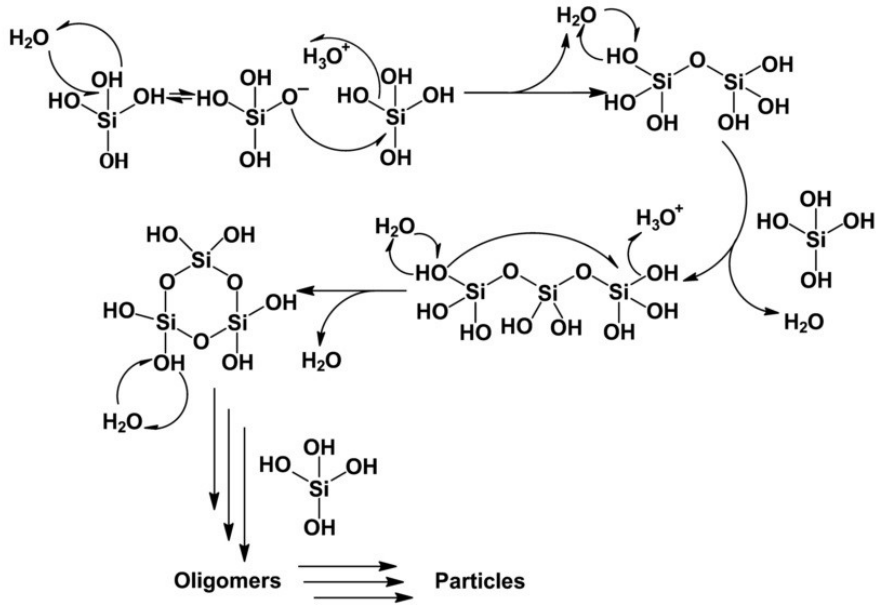

Figure 12: Mechanism of poly-condensation of silicic acid to form cyclic species [82].

This mechanism is the basis of formation of many silica-based materials and structure easily found in nature, such as the formation of the silica skeleton of diatoms and sea sponges, as well as silica structure vegetables. This consists of deposition of nanoparticles formed by condensed silica oligomers, previously formed by condensation of silicic acid species. This process is known as bio-silicification [82,84–86].

In the case of AAMs and GPs, the condensation occurs between hydroxyl groups belonging to aluminates and silicates monomers reported above (equations 5, 6 and 7). The combinations of condensation between this species depend on the pH of the solution and stability of the oligomer compound, and still the partial charge model (PCM) from Weng et al. gives useful insights. First of all, it must be specified that aluminates cannot

condensate each other to form alumina-based oligomers, as the sialate compounds avoid Al-O-Al links, according to the Lowenstein's rule, imposing a chemical modulus (SiO_2/Al_2O_3 ratio) always higher than 1 [45,74–76,87]. Weng's studies, PCM and NMR carried out on the metakaolin-*NaOH* geopolymeric system, inferred no free silicates (of any configuration) detection, suggesting that silicate and aluminates readily react to form condensed dimers, in a way described in the following reactions:

$$[Al(OH)_4]^- + [SiO_2(OH)_2]^{2-} \rightarrow [(OH)_3Al - O - SiO_2(OH)]^{3-} + H_2O \quad (10)$$

$$[Al(OH)_4]^- + [SiO(OH)_3]^- \rightarrow [(OH)_3Al - O - SiO(OH)_2]^{2-} + H_2O \quad (11)$$

At this point, all the silicates are depleted, given that aluminates initially are in surplus compared to silicates, as aluminates are readily dissolved [20,69,76,88]. This formed dimer reacts subsequently with other monomers to form longer chains. The possible combination can be the reaction with either the first configuration of silicate or the second configuration or with aluminates. The PCM model identifies which molecules after condensation is more chemically stable. According to this model, the chemical compound in Equation 8 gives stable subsequent compounds only if reacts with aluminates, but not with silicates, meaning that the molecule in Equation 8 is not favouring the poly-condensation. The chemical compound in Equation 9 is giving stability in any case, especially with both types of silicates, thus favourable to the poly-condensation [75,76]. Due to the dependency of these species on the alkalinity of the solution and the chemical modulus of the raw materials, the extent of poly-condensation is intimately correlated to the chemical reaction conditions. According to the same authors, the alkalinity should be comprised between 5 and 10 M.

'Condensation-crystallization': Glukhovsky, in his model, included a final stage in which nano and micro-particles are formed as a product of poly-condensation, and precipitate to form a bulk material, like happening in the silicification of the silicic acid species. The deposited product (partially) crystallize, as a consequence of the alkalinity of the aqueous medium. Simultaneously, the poly-condensation, either of the chemical compounds or of the nano and micro-particles, continuous [20,45].

Davidovits [27], after his NMR spectroscopy studies of the GPs, introduced an equivalent model, including also three stages like Glukhovsky:

1. Dissolution
2. Transportation
3. Poly-condensation

All the stages are comparable to Glukhovsky's model. Davidovits admitted only a second stage in which dissolved species diffuse in the liquid medium to preferentially condensate each other, a sort of preparation for the third stage [26].

Other authors, like Palomo et al. [20,23,69], Provis et al. [45,89] and Duxson et al. [71], agreed on the Glukhovsky's model, ascribing to the product of alkali-activation a new

notation, the N-A-S-H gel, as they inferred the formation of an aluminosilicate-based semi-amorphous phase, comparable to the process of sol-gel, therefore admitting a gelation in the process. The same authors demonstrated through x-ray spectroscopy (XRD) that the crystalline part is a zeolite-like compound, giving them the input to call the product as a 'zeolitic precursors'. The designation of the product was made to emphasize the similarities with the C-S-H bonds occurring in the OPC. Indeed, the same authors extended the terminology to C-A-S-H or N-(C)-A-S-H gel, depending on the chemistry of the alkali-activation. This was consistent with the breadth of materials they were covering in their study on alkali-activation of materials. The N-(C)-A-S-H gel, being based on calcium hydroxide activation, or anyway characterized by a relevant content of lime, goes beyond the aims of this thesis, thus it won't be treated in details.

Few words, instead, are worthy of being spent for the N-A-S-H gel compound. The same authors, through simultaneous FTIR and NMR spectroscopy analysis, managed to define a more specific model of alkali-activation and production of the N-A-S-H gel, reported schematically in Figure 13. In their model, the authors, similarly to Glukhovsky's model, admitted a dissolution of aluminosilicates for pH higher than 10 in a form of monomers, readily connecting each other forming dimers and oligomers (first two steps in Figure 13). Further condensation of more intricate aluminosilicate compounds forms long chains, even in a 3D configuration (cross-link network), defined by the connectivity of the silicon with four Si and/or Al atoms, and linked with an oxygen bridging (Al-O-Si or Si-O-Si). This aluminosilicate product of alkali activation is defined as gelation of the N-A-S-H gel (gel 1 or gel 2 in Figure 13).

The term gelation is regarded to be a chemical process usually occurring in sol-gel reaction. This is not a case, as the authors wanted to address the process of alkali-activation to the more common and well-known sol-gel. Indeed, the sol-gel process is technique devoted to especially produce metal oxides, like silica and alumina using a suspension (sol) which gradually decomposes and forms a homogenous agglomerate of condensate species in the liquid solution, the process known as gelation (gel), normally in a polymeric structure. The process of monomers condensation in the case of silica, for instance, is the condensation of silanol and siloxane species, like advertised by Davidovits [90,91]. This is why the authors of this model felt confident in assuming this comparison with the sol-gel technique. In particular, according to the FTIR and NMR spectroscopy analysis carried out by Palomo et al. [69], they hypothesized two different steps in which firstly Al-rich N-A-S-H gel (Si/Al $\approx$ 1) is formed, due to the higher reactivity of aluminates in alkali solution, in accordance with the PCM model proposed by Weng et al. [74–76], whose chemical ambient was detected through the NMR and reported in the third stage in Figure 13. As the reaction proceeds, more silicates are dissolved, taking part in the alkali activation and substituting the aluminates in the microstructure. This substitution is also predicted by the PCM model as silicates in Equation 10-11 forms only chemically stable molecules if they connect with another silicate of any configuration. This process induces a transformation of the Al-rich N-A-S-H gel (gel 1) to a more stable Si-rich N-A-S-H gel (gel 2), as depicted in Figure 13, stage 4. This was demonstrated spectroscopically by Palomo et al. [69] through detection of a shift towards higher wavelength of the canonic

Si-O-Si bending vibration peak in FTIR spectra, as the Al-O-Si bond is weaker than Si-O-Si bond, and the prevalent amount of D6R and D8R-type structures in the mid-infrared region of the FTIR. These structures are particular aluminosilicate oligomers in a ring-like configuration, with 6 or 8 Si or Al elements, which form only if Si is much higher in content than Al. The appearance of new peaks in higher ppm regions of the ^{29}Si NMR spectra, corresponding to higher connected Si ambient ($Q^4(nAl)$) with a low value of *n*, is a proof of what just uttered in the FTIR deductions [75].

The participation of more silicates than aluminates in poly-condensation, favours the polymerization of longer and more intricate chains (stage 5 Figure 13), as condensation reaction in a Si/Al ratio higher than 2 is a chemically stable process as explained by the PCM model as well. Further poly-condensation of aluminosilicate chains can either form pure amorphous structure or nano-micro crystals, always attributed to the zeolite-like structure in XRD spectroscopy, justifying these authors to denominate this material also as 'zeolitic precursors' [92], as also explained in details in the Chapter 2.3.3 of this work. The formation of N-A-S-H gel is anyway typical for cement, due to the presence of hydrates groups and less interconnected structure. This results in lower durability of the material. On the contrary, the GP formulation exposed by Davidovits is more concerned to a highly structured network (3D cross-linked), characterized by the higher presence of $Q^4(nAl)$ ambient in the ^{27}Si NMR, giving rise to higher chemical stability [26,93].

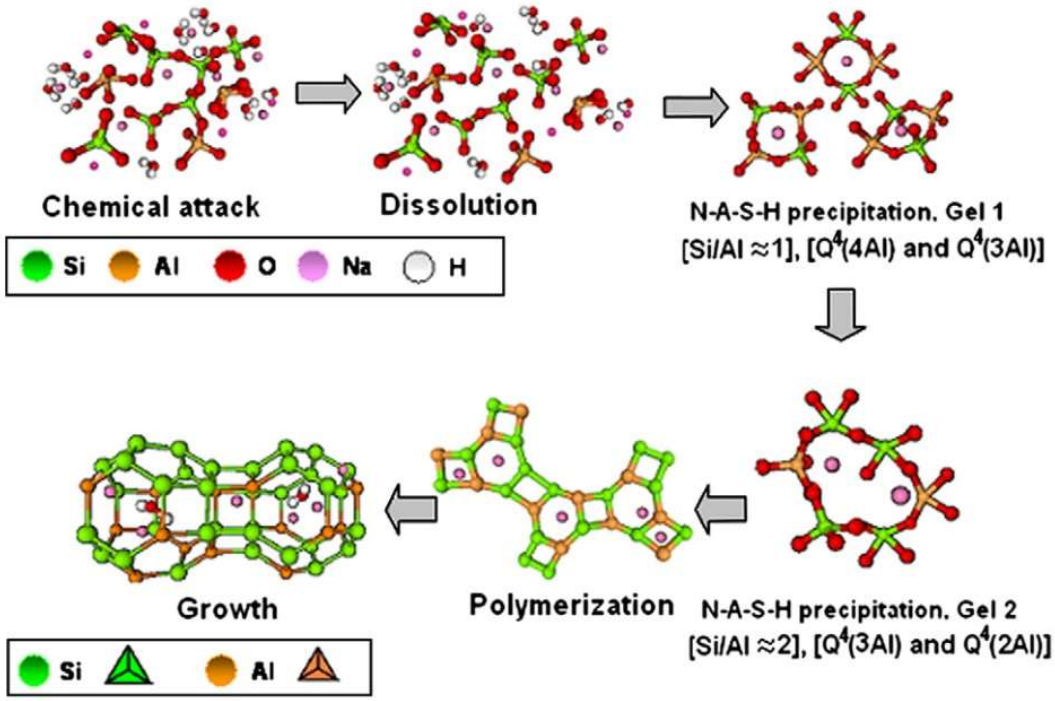

Figure 13: Descriptive model for alkali activation of aluminosilicate [20]**.**

In the upcoming paragraphs, it will be reported the chemical and physical parameters influencing the alkali-activation process, and how all these parameters contribute

positively and/or negatively to geopolymerization in terms of final setting and performance, bearing in mind that all the parameters could concurrently operate in the process. Due to the high number of parameters, the process of geopolymerization is not so trivial and easy to control.

2.4.3 The role of the alkali activators

Regardless the different model used to describe the geopolymerization, one of the most important steps in the process is the first one, comprehending the dissolution of the silicates and aluminates, which are the main bricks of the geopolymeric structure. The extent of dissolution depends in turn on many variables, but the most influencing one is definitely the alkali activator, i.e. the nature of the base solution, the molarity and the pH. The efficiency of the activators will be assessed in terms of microstructural and mechanical properties.

The types of activators giving dissolution of aluminosilicate species so far used in the literature are *NaOH*, *KOH*, sodium silicate (Na_2SiO_3 also known as water glass), potassium or sodium carbonates (Na_2CO_3 and K_2CO_3).

Sodium hydroxide is widely employed, as all the scientific community agrees on the high dissolution rate of silicates and aluminates if this activator is used. Several studies have been conducted by Palomo et al. trying to couple the nature of the alkali solution with the dissolution rate and the given microstructure of FA-based GPs, using essentially *NaOH*, *KOH* and carbonate derivatives or a mixture of the same activators with sodium silicate [24,94]. These authors found that when *NaOH* and mixtures of the same with waterglass are employed, the resulting microstructure in terms of crystalline formation, detected through XRD spectroscopy, is mainly zeolite-like structures, such as hydroxysodalite and herschelite (Na-chabazite type). When *NaOH* is mixed with Na_2CO_3, a lower content of crystalline production was detected, in particular, a lower amount of herschelite, and higher content of carbonates, as this activator moves the chemistry towards more acidic regimes.

In the case of *KOH* and its mixtures, what stands out is the lower amount of zeolitic phases produced by the alkali-activation. Besides this, the authors managed also to demonstrate qualitatively that the activators based on *NaOH* and sodium silicate involve a better dissolution and then a higher quantity of the product of the reaction. The same authors also determined the influence of the alkali concentration on the activation of FA, finding that slightly higher dissolution might be attributed to a solution 10 M *NaOH* over the 8 M *NaOH*, due to the beneficial effect of OH^- anions acting like as catalysts of the reaction. What substantially they quantitatively detected is a higher content of alkali cations in the product of FA activation, explaining a higher glassy state in microstructure: indeed, the higher the content of alkali the lower the chains and the lower the possibility to close ordered crystalline structures, say zeolitic-like structure, as the alkali cations (Na^+ or K^+) act like structure-forming elements, positioning in the empty site left by the aluminosilicate network.

Furthermore, utilization of sodium silicate in the activator solution was found to have a beneficial effect on the microstructure of the alkali activation product, as the morphology do no present much porosity as in the case in which other activators were used. Sodium silicate diffuses in the microstructure, giving rise to a denser product of condensation with higher mechanical performance as the microstructure is modified by the higher content of silicates, i.e. higher SiO_2/Al_2O_3 ratio, demonstrating the concurring effect of various parameters [88].

An equally interesting study on the activation of FA in *NaOH* solution at a different level of concentrations (from 4 M to 18 M *NaOH*) was conducted by Hamidi et al. [95], who coupled the effect of the activators with the mechanical properties of the obtained geopolymeric samples in terms of flexural strength. In this study, it was determined that the mechanical performance of the samples increases as the molarity of the caustic soda solution is increased until a value comprised between 12 and 13 M *NaOH*, in which the trend experiences a deflection and a decrease of the compressive strength. The plot is reported in Figure 14 for a better close up of the trend.

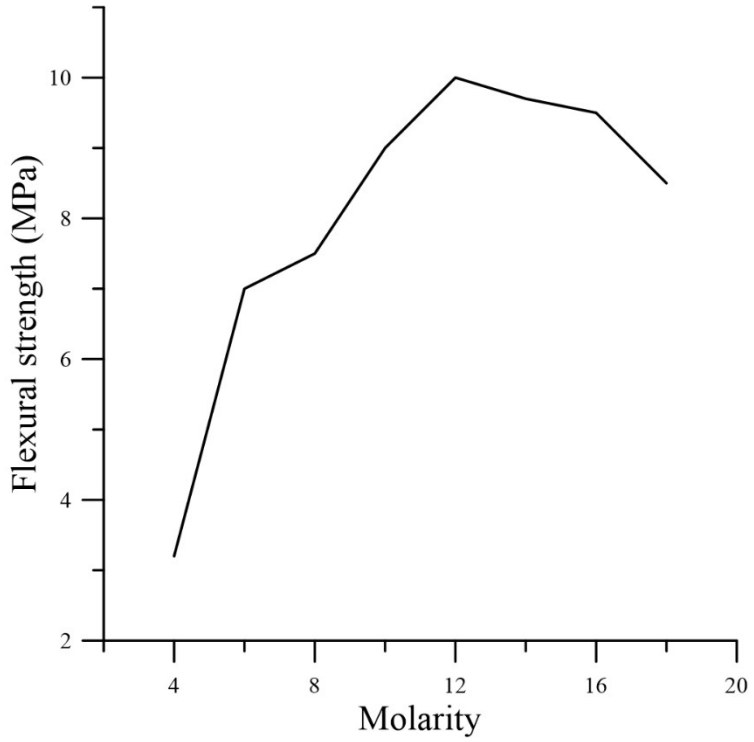

Figure 14: Flexural strength of GP prepared in NaOH solution ranging from 4 M to 18 M [95].

This result goes in contrast with what uttered by Weng et al. [74–76], saying that the optimal alkali concentration for aluminosilicate dissolution and activation must be comprised within 5 M and 10 M. The mentioned discrepancy lies on the different nature of the raw materials, as these authors were using metakaolin. In this context, Van Deventer et al. [96] studied the dissolution rate of several aluminosilicate minerals activated either in *NaOH* or in *KOH* with a concentration within 2 M and 10 M. It was demonstrated that

irrespective of the nature of the raw material, and the concentration of the alkali solution, *NaOH* solution guarantees higher dissolution than *KOH* solution. The content of Si and Al in the chemical composition of the natural sources is also playing an important role, influencing the chemical modulus of the geopolymerization. Interestingly, it was also reported that a higher compressive strength was associated with AAMs activated with a *KOH*-based solution. This was discussed in a way that Na^+ cations tend to pair with small polymer chains (monomers), whereas K^+ cations couples more with longer aluminosilicate chains, forming in turns a more intricate and stable network, all going in favour of higher strength of the product of dissolution. In particular, as the aluminates readily dissolved in the solution, are not prone to bind with all the silicate species, as explained by the PCM model, but this is not true in case *KOH* is used as activator, as the *K*+ cations favours the formation of large silicate oligomers with which aluminates prefer to bind, optimizing then the uptake of all the dissolved species.

2.4.4 The effect of the silica to alumina ratio (SiO_2/Al_2O_3)

Q_n	-δ (ppm)	$Q_n(1Al)$	-δ (ppm)	$Q_n(2Al)$	-δ (ppm)	$Q_n(3Al)$	-δ (ppm)	$Q_n(4Al)$	-δ (ppm)
Q_0	66 to 73								
Q_1	76 to 83	$Q_1(1Al)$ 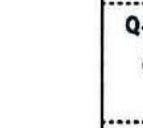	75						
Q_2	86 to 91	$Q_2(1Al)$ 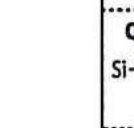	85	$Q_2(2Al)$ 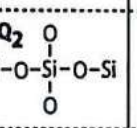	80				
Q_3	95 to 101	$Q_3(1Al)$ 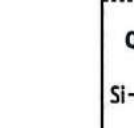	95	$Q_3(2Al)$ 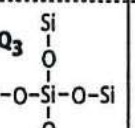	90	$Q_3(3Al)$ 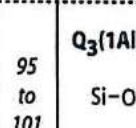	85		
Q_4	103 to 120	$Q_4(1Al)$ 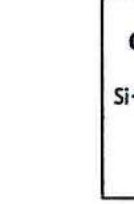	97 to 105	$Q_4(2Al)$ 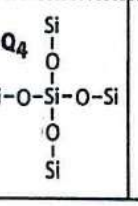	92 to 99	$Q_4(3Al)$ 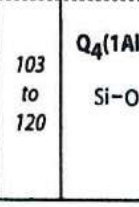	88 to 94	$Q_4(4Al)$ 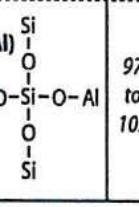	83 to 87

Figure 15: Characteristic resonance signals in the ^{29}Si NMR of aluminosilicate units. The 'n' at superscript or subscript position is interchangeable [26].

The silica to alumina ratio (SiO_2/Al_2O_3) is one of the most important parameters in geopolymerization/alkali-activation, defining the chemistry of the final product. The ratio is strictly dependent on the chemistry of the aluminosilicate source, and different ratios can induce different microstructures. This is the discriminant factor differentiating the GP products from AAMs. As previously mentioned, part of the scientific community is

discordant to admit whether GPs and AAMs are the same material or not, but this ratio can be really helpful to clarify better this concept. This paragraph aims to elucidate not only the role of this ratio but also the differences between these two kinds of materials.

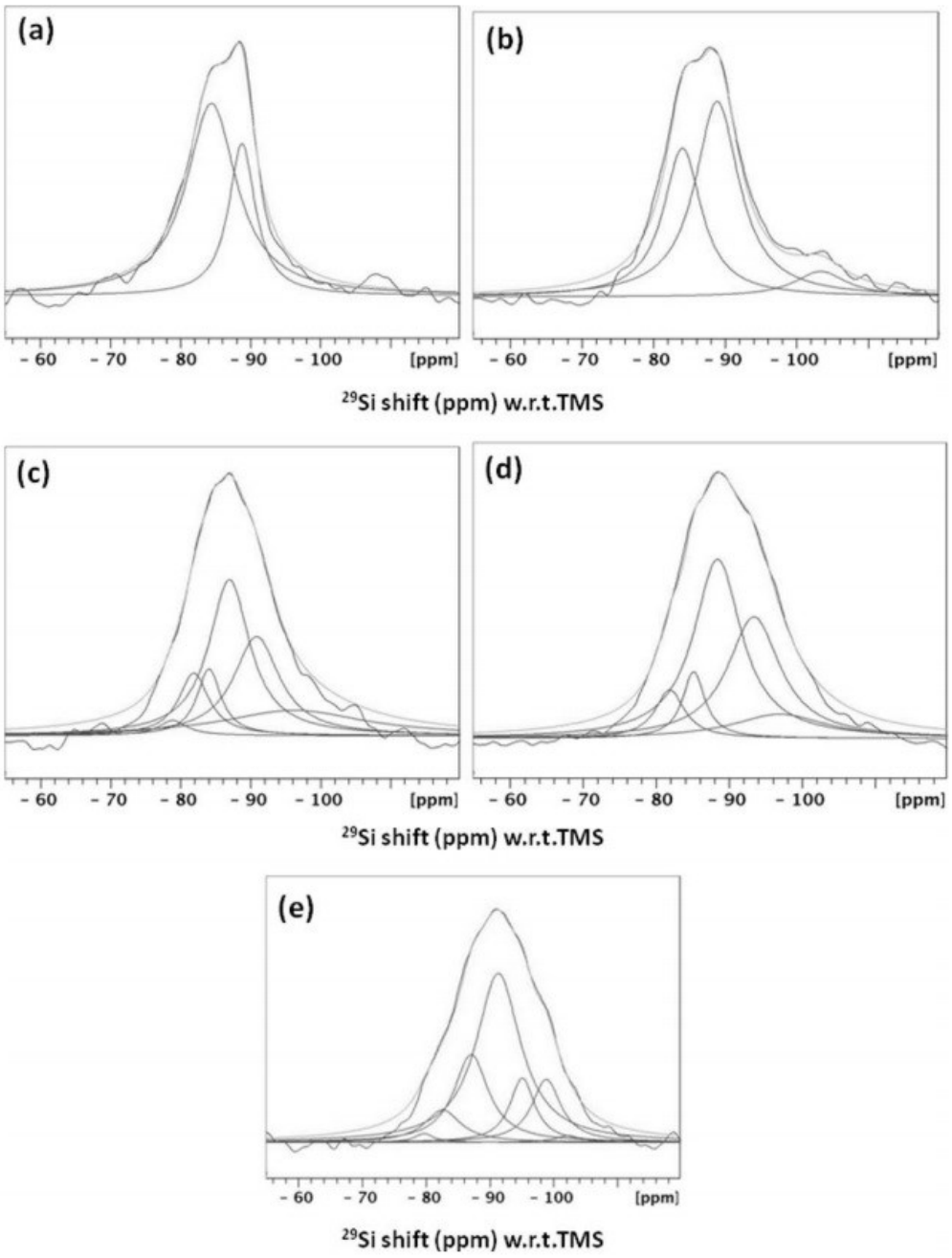

Figure 16: ^{29}Si NMR of geopolymers synthesized with different SiO_2/Al_2O_3 ratio; a) 2.25, b) 2.50, c) 3.00, d) 3.50, e) 4.00 [97].

Equation 6 in Chapter 2.4.1 defines the chemistry (chemical ratios) at the basis of the processing of a GP according to Davidovits's experiments. The silica to alumina ratio was set between 3.5 and 4, if an amorphous highly structured (3D cross-linked) network of Si and Al, interconnected with oxygen bridge-bonds is to be achieved. These results were

deduced through the ^{29}Si MAS NMR spectroscopy, whose spectra is giving some direct information about the type of Si ambient (what Si is connected with).

Before analyzing in details the NMR spectra for GPs and AAMs, it is opportune to introduce a specific $Q^n(mAl)$ notation useful for detection of Si signals in NMR spectroscopy. In this notation, Q defines a unit in a 4-fold configuration (4-valent), n=0,…,4 stands for the number of Q units attached to the reference one, m=0,…,4 is the number of Al units connected with the reference Q unit. Thus, if n=4 (Q^4), it means that Si is surrounded by 4 Q units (Si or Al) and the network is highly structured. In a Q^4 ambient, if m=4, it means that each Si atom is surrounded by 4 Al atoms, whereas if m=0, then only Si elements surround each Si atom [98,99].

According to many authors, a resonance at lower ppm signal (between -100 ppm and -120 ppm) is attributed to Q^4 units with low content of aluminium, whereas for higher m numbers (m=3 or 4), the signal resonates at -80 ppm and -90 ppm [26,99,100]. The detection of the single resonance signal from the whole spectra is carried out through algorithmic-based software, which performs a deconvolution of the entire signal. A brief scheme of each signal is reported in Figure 15. Under this notation, recently, MacKenzie et al. [97] conducted a spectroscopic study on metakaolin based GPs with variable SiO_2/Al_2O_3 ratio. This study clearly demonstrated that an increase in silica content (an increase of the ratio) induces a shift of the whole spectra towards smaller ppm (hence higher presence of $Q^4(0\text{-}1Al)$), as depicted in Figure 16. These results are chemically consistent, as a higher content of reactive alumina yields a higher presence of Al units around the reference Q unit.

A detailed analysis of ^{29}Si NMR spectra was carried out by Palomo et al. [68,101] on AAMs based on alkali-activation of FA in different alkali solutions, maintaining the same SiO_2/Al_2O_3 ratio. From the spectroscopically analysis, they found a higher presence of $Q^4(4,3,2Al)$ units, due to the high content of reactive alumina (SiO_2/Al_2O_3 ratio of about 2) employed in AAMs processing. In many other studies, besides the microstructural analysis, the same authors investigated the crystallinity of GPs and AAMs varying the content of reactive alumina in the formulation [45]. What the latter authors never considered was the probable presence of less structured units, with n=0, 1, 2, 3. As depicted in Figure 15, these units fall in higher ppm, roughly coincident with $Q^4(3,4Al)$ units. This means that the spectra of AAMs characterized by a hump centred in higher ppm, could not only be affected by the higher presence of $Q^4(3,4Al)$, but also by a higher content of Q^2 or Q^3 units, indicating less cross-linked network. For this reason, AAMs are expected to have lower silicon connectivity, whose remaining chemical valence is occupied by hydroxyl groups (-OH). This deduction is confirmed by a lower intensity of the –OH stretching vibration of GPs FTIR spectra when a higher SiO_2/Al_2O_3 ratio is employed [102]. The higher presence of hydroxyl groups in AAMs justifies the notation of an N-A-S-H product of alkali reaction and makes this material more similar to cement-like materials. The Q^1 and Q^0 units are not taken into consideration as they cannot exist after polycondensation, as these units readily form dimers or cyclic species [103,104].

The different microstructure of AAMs renders this material more mechanically resistant than GPs, as demonstrated by Timakul et al. [105] and Chindaprasirt et al. [106], who separately tested class-C FA-based AAMs/GPs in compressive strength, using different silica to alumina ratios. They both observed a pick in the compressive strength of ~60 MPa for a SiO_2/Al_2O_3 ratio of 2.5, and a gradual decrease until 30 MPa when the SiO_2/Al_2O_3 ratio is 3.00. The higher mechanical properties find an explanation in the higher presence of hydroxyl groups, which are more resistant than T-O-T groups (where T=Si or Al), but in turns, undergoes lower durability, as the –OH bonds are chemically less stable and more exposed to higher environmental degradation. On the contrary, the T-O-T bonds are chemically more stable, with undefined durability in mild environments. In the FTIR spectra, the T-O-T asymmetric vibration is susceptible to change of the silica to alumina ratios. The T-O-T bond vibration produces a huge and intensive band in FTIR spectra between 800 and 1200 cm^{-1}, which encompasses all the Q^n silica units. It was observed that a higher content of alumina provokes a shift of the band towards higher wavelengths, due to the more intensive contributions of $Q^4(3,4Al)$ vibrations, located at higher wavelengths [105]. This also contributes to a more resistant microstructure, since the vibration to higher wavelengths means a stiffer type of chemical bonds.

2.4.5 The role of the soda content (SiO_2/Na_2O)

The chemical activation of aluminosilicate sources is carried out by means of a strong base aqueous solution, and in some cases, strong acid solution, as already described in Chapter 2.4.3. Different chemical activator gives rises to different microstructure, and then properties. It was also emphasized that among all, alkali activators were highly used, in turns, caustic soda solution ($NaOH$) and a mix of this with waterglass seemed to be the best compromise in terms of microstructure and final consolidation. If the sodium hydroxide solution and/or waterglass are used as the alkali activator, the silica to soda ratio (SiO_2/Na_2O) becomes a useful indicator of the reaction efficiency, either for AAMs or for GPs.

Criado et al. [92,101,107] carried out a detailed spectroscopic inspection of alkali-activated FA, in terms of XRD, FTIR and NMR spectroscopies, activated with sodium hydroxide and a mix with water glass. Various silica to soda ratios of the activators was considered to analyse the effect of this parameter on the final microstructure and properties of the material. These authors found out that the formation of crystalline phase types is highly dependent on the amount of soda content in the solution: if solely caustic soda was used ($SiO_2/Na_2O = 0$), the XRD pattern revealed the presence of hydrated sodalite and Na-chabazite only. A similar spectrum was detected if the ratio was increased to 0.19. When the ratio of the solution was increased up to 0.69, new Zeolite Y phase started to appear. For ratios around 1.17, Zeolite P phase was visible in the diffraction spectra too. The appearance of new crystalline phases with the increase of the silica to soda ratio concurs with a higher content of the amorphous phase of the final product. This experimental insight may coincide with a more structured microstructure (3-D cross-linked), which is consistent with what said in the previous paragraphs (higher Si content means higher interconnectivity). Better insight can be provided by FTIR and NMR spectroscopies

carried out by these authors on the same experimental materials. They have found a higher presence of less interconnected units (Q^1 and Q^2) if the content of soda is high. When the silica to soda ratio was increased, the above-mentioned units decrease in content in favor of a higher content of Q^3 and Q^4. The authors reasonably stated that higher content of alkali cations in solution hinders the formation of long chains and highly interconnected structure. A similar spectroscopic evidence was found by other authors [97]. Finally, compression test performed on hardened samples revealed the highest compressive strength in samples activated with silica to soda ratio of about 0.69, demonstrating that this material is an AAMs under this chemistry, whereas if the content of silica is increased to have ratio of 1.17, the compressive strength decreases, due to a change in the microstructure, more attributable to GPs compounds. The plot in Figure 17 depicts this trend of mechanical properties.

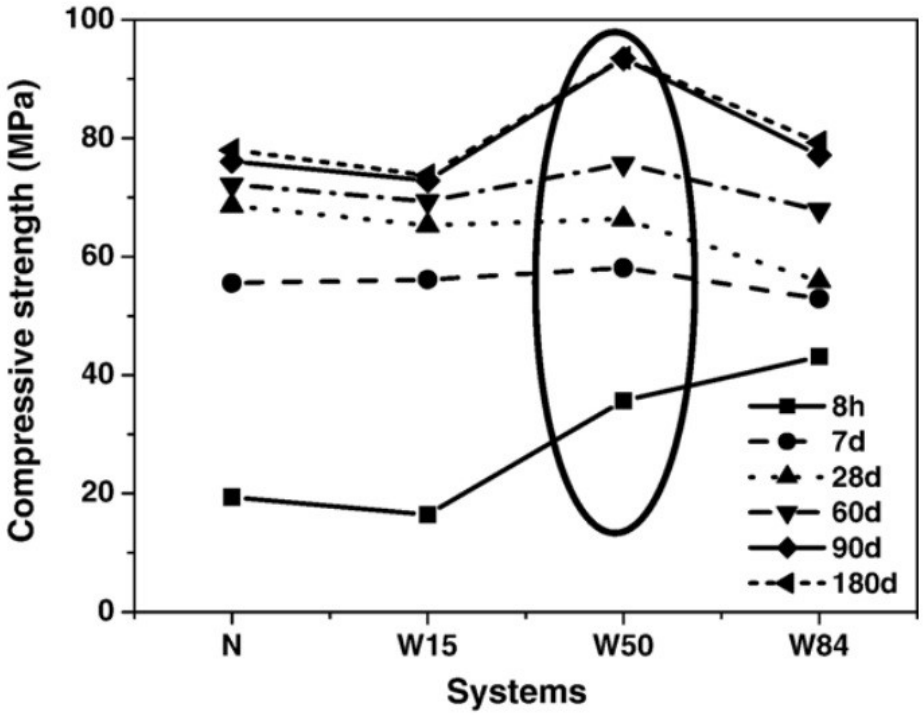

Figure 17: Compressive strength values of GPs sample versus silica to soda ratio [92].

A similar result was found by Trochez et al. [102], who analyzed the effect of soda to silica ratio (Na_2O/SiO_2) on compressive strength of FA-based GPs. The highest value of the mechanical properties coincided with an intermediate value of this ratio (0.25), where the ultimate compressive strength of the material started to decrease when the content of silica increased (lower ratio). In the same way, other research works focusing on the effect of the silica to soda ratio on mechanical properties of GPs and AAMs. All the works agree on the fact that intermediate values of SiO_2/Na_2O ratio, about 2.5, gives rise to higher mechanical properties [108–110]. The power of this result relies more on the fact that this

tendency is not dependent on the type of raw material activated to geopolymerization/alkali-activation.

The modification of the microstructure to a more interconnected network and an amorphous phase, characteristic of a geopolymeric product, is associated with a higher content of reactive silica. This transition is also evidenced by a visible change in the microstructure, detected by SEM observation in the Nasab et al. study [97]. SEM images of samples of SiO_2/Na_2O ratios 2.25, 2.5, 3, 3.5 and 4 show a change in microstructure and homogeneity of the samples as the SiO_2/Na_2O ratio increases. The microstructures of GPs of composition $SiO_2/Na_2O \geq 3.00$ do not change significantly with increasing SiO_2/Na_2O ratio, but the fineness of the texture and the density of the GPs increase markedly from $SiO_2/Na_2O = 2.50$ to 3.00. For the value of the ratio $SiO_2/Na_2O \leq 2.5$, the microstructure is more crystalline, which is consistent with what found by Criado et al. in their XRD study of FA-based AAMs. Similar results were attained also in other research works [111].

2.4.6 The influence of the curing conditions

The poly-condensation reaction happening either in geopolymerization or in alkali-activation is a thermally-assisted chemical reaction, in which the presence of a temperature slightly higher than the room conditions helps to optimize the diffusion and the aggregation of the aluminosilicate species through the liquid phase of the initial slurry [82]. The diffusion of aluminates and silicates to form long-chains structure is guaranteed kinetically by the temperature and effectively by the time: longer soaking times means higher time for the species to diffuse. Besides these two parameters, which are going hand to hand, a humid environment leads to an optimization of the reaction of poly-condensation. The extensive presence of water molecule in the environment prompts the hydrolysis of the hydroxide groups of the diffusing aluminosilicate species during poly-condensation, supplying with molecular water the process of long-chains formation by condensation of monomers and dimers (see the scheme in Figure 12).

It was observed that the mechanical properties (compressive strength and/or flexural strength) of GPs and AAMs are optimal if the curing temperature falls between 60 °C and 90 °C. In alkali-activation of metakaolin, Garcia-Mejia et al. [112] and Muniz et al. [113] in two recent research works, found that the optimal temperature, inducing the highest mechanical strength, is 60 °C. Other authors also found that the highest compressive strength is associated with a temperature ranging from 80 °C even up to 120 °C [114,115]. All these authors employed a curing time no shorter than 24 h, observing a drop of the mechanical properties for a limited soaking time in the above-mentioned temperature of curing.

Recently, it is often reported the significance of the relative humidity in the final set of the samples, for chemical reasons previously reported. Garcia-Mejia et al. [112], in the same work, also analyzed, in more detail, the effect of other reaction parameters, by making a comparative study. Among all, they analyzed also the effect of the humidity, inferring that a relative humidity of 85% associated with a curing temperature of 60 °C, is the optimum

condition for the final setting. Oderji et al. [116], in a recent work, came up with similar results in studying the effect of the temperature and the relative humidity on compressive and flexural strength of FA-based AAMs. They found that the highest compressive and flexural strength coincide with a temperature of 75 °C and relative humidity of 70%. Other authors studied the effect of different methodologies of sample packing during the curing procedure. Kovalchuk et al. [117] were the first authors to analyse the mechanical properties of FA-based AAMs cured in dry air (95 °C, no relative humidity), in a steam oven (95 °C, 100% of relative humidity) or in closed and air-tightened plastic bags (95 °C). The latter yielded the highest compressive strength, even higher than 100 MPa. The curing in the steam oven was giving intermediate results (70 MPa), whereas the lowest compressive strength was associated with dry air conditions. A few years later, Criado et al. [118] conducted the same study, supporting these results with microstructural and spectroscopic analysis, in the attempts to describe the chemistry happening if different methods of curing are used, especially in terms of relative humidity effects. These authors also calculated the degree of reaction by using a selective chemical method to dissolve the unreacted raw material; eventually, they observed that the highest degree of reaction is provided by the closed plastic bag method.

The employment of relative humidity in curing condition is also beneficial for the prevention of the carbonation phenomena during chemical setting of the sample. The carbonation is the formation and precipitation of crystalline sodium carbonate ($NaHCO_3$), due to chemical attack of atmospheric CO_2 to Na^+ cations dissolved in the aluminosilicate paste, sucking away precious sodium to the process of alkali-activation or geopolymerization. Higher content of water in the curing atmosphere decreases the percentage content of CO_2, helping to prevent the formation and precipitation of this crystalline compound [66].

2.5 Utilization of recycled glass in geopolymerization

The management of urban and industrial glass wastes is as significant as the management of FA and similar wastes. To date, the recycling of glass is quite extensive, accounting the 73% of the collected waste glass in the European Union in 2015 [119]. So far, the waste glass was reused to vitrify other glass or as an additive in cementitious materials. Indeed, waste glass was extensively utilized, up to 70% of the entire content of utilized aggregate for preparation of OPC mortars [120].

Only recently, research studies began to utilize waste glass in alkali-activation or geopolymerization. Being the glassy-phase the dissolvable part of an aluminosilicate, waste glass lends itself suitably to chemical activation under alkali-solution, like demonstrated by Rincon et al. [121], who successfully activated grounded urban recycled glass in *NaOH* and then fired at 700 °C for final setting and foaming, using the chemical reduction of iron oxide , and the change of rheology of the glass at elevated temperature. The first step of this process is an alkali-activation of waste glass, whose chemical reactions, similar to those of AAMs, confer hardness to the initial paste. This was previously done using water, *NaOH* or $NaOH/Na_2CO_3$ as alkali activators [122].

The waste glass was utilized, for the first time, uniquely in geopolymerization of FA no later than 2013, in a patent published by Puertas-Maroto et al. [123], in which it is explained the procedure of how to produce GPs materials using coal residues and waste glass, as a first attempt to make this material more sustainable, but also to adjust the chemistry for GPs production. After this invention, the same and other authors focused their attention on the development of GPs entirely from wastes, without using waterglass as silica additive in the formulation. The waterglass, being a sodium silicate produced by dissolution of silica gel in *NaOH* is not entirely user-friendly, as the production of *NaOH* involves high temperatures, and then CO_2 emission. Initially, the attention was drawn to the preparation and the characterization of GPs, by mixing blast furnaces slags (BFS) and urban waste glass with different percentages. The mechanical results, in terms of the ultimate compressive strength, were compared with results coming from samples prepared using water glass instead of urban glass. The mechanical testing revealed that the highest compressive strength is associated with the latter formulation, followed by the formulation including only BFS and no waste glass. Therefore, when BFS is used, the addition of waste glass is detrimental to the mechanical properties [19,124]. It must be pointed out that BFS slags are rich in lime (*CaO*), which rather prompts the formation of (C-)N-A-S-H gel instead of geopolymerizaiton products, thus micro-structurally speaking, a mix of these two compounds is expected, afterward confirmed by spectroscopic analysis [19,125]. Everything changes if FA is used instead of AAS. FA was activated in *NaOH* (8 – 10 M) with different contents of waste glass (0 g, 10 g, 15 g, 20 g, 25 g), and compared with the formulation including water glass instead of waste glass. Mechanical results showed that the highest compressive strength (38 MPa) coincides with the formulation of FA+*NaOH*+25g glass cured at 85 °C for 20 h (99% relative humidity). The formulation including waterglass shown slightly lower compression strength of 36 MPa (see Figure 18). Spectroscopic analysis (FTIR, NMR, and XRD) revealed a chemical

composition attributable to GPs [87]. Similar results were attained by the same authors is waterglass made from the dissolution of urban waste glass in *NaOH* was used in the same previous formulation using normal water glass [126].

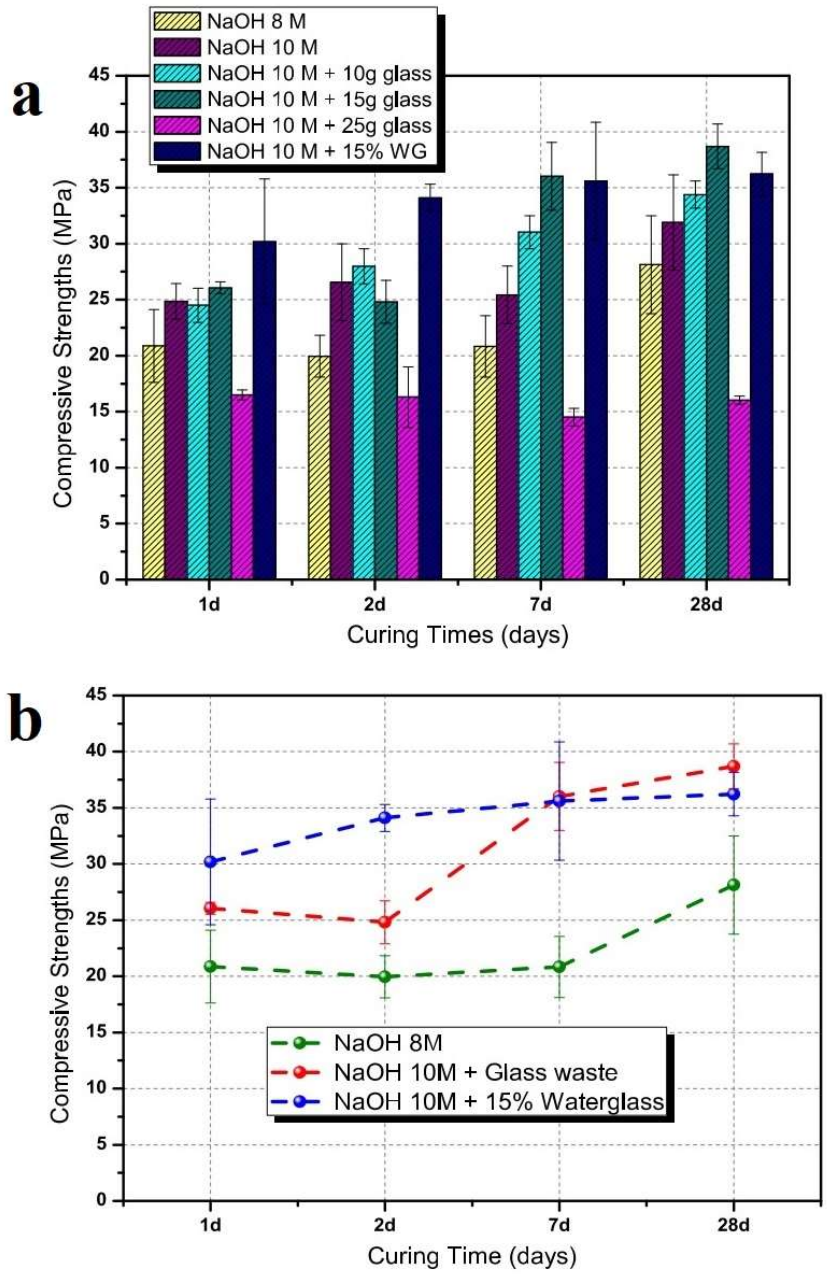

Figure 18: ***a) Compressive strength of FA pastes activated with different formulations and b) comparative compressive strength plot depicting results from FA+NaOH (8 M), FA+NaOH (10 M) + 15g (glass) and FA+NaOH (10 M) + 15%waterglass*** [87].

In this work, as already mentioned in the first chapter, GPs were processed in a formulation which includes only wastes, composed of FA and recycled borosilicate (BSG) glass, so as to adjust the chemistry of reaction. Up to now, BSG was never used at all as silica additive in geopolymerization, thus this gives the innovative imprint to this thesis

work. BSG was rather used in many procedures for ceramic processing, e.g. by sintering of a green body mix made of rejected pharmaceutical BSG with plasma vitrified wastes, to eventually process a porous glass-ceramic material [127]. The same processing methodology was applied for the fabrication of a glass-ceramic composite made of a mix of valoxy, an alumina-rich waste and again rejected pharmaceutical BSG powder, in a variable percentage (10%, 20%, 30%) [128]. In another investigation [129], a composition of coal ash (43.5% Fe_2O_3) and BSG was investigated at different temperature and conditions of sintering, though no alkali-activation was used in this process. The only case in which class C FA based GPs were processed in presence of borates, supplied by the addition of inorganic borate salts in the activator (*NaOH*), is reported in a study conducted by Nicholson et al. [130]. These authors also carried out an ^{11}B NMR spectroscopic analysis on the borate salts and GPs, in which they successfully demonstrated partial incorporation of boron in the microstructure.

2.6 The utilization of fly ash

GP patent by Davidovits was carried out by supplying to the initial paste a mix of powder including metakaolin, which is a refined aluminosilicate source, synthesized from the firing of the kaolinite by means of a dehydroxylation process of the Al-Si chains. This heat treatment, hence, increases sensitively the cost of production, which can be reduced by introducing industrial residues in the formulation. They were used even before the utilization of metakaolin, e.g. as clinker for production of cement, back to 1939 (see Table 1). These solid residues of industrial processes comprehend a huge variety of slags, from FA to metallurgical slags and mining wastes. FA, in particular, was initially utilized by Palomo et al. in geopolymerization technology in the mid '90s, identified as FA-based alkali-activated cement [131]. FA is considered a by-product of coal power plants, deriving from the combustion of pulverized coal in suspension fired furnaces [132,133]. In this chamber, various types of residues are released after combustion, such as FA, bottom ash and gases and/or vapours. FA is the finest part of the ash which is entrained in the flue gases, whereas the bottom ash is a residue consisting of coarser discrete or fused particles heavy enough to drop out of the combustion zone (furnace chamber) onto the bottom of the furnace [133]. All the steps of combustion are reported in Figure 19.

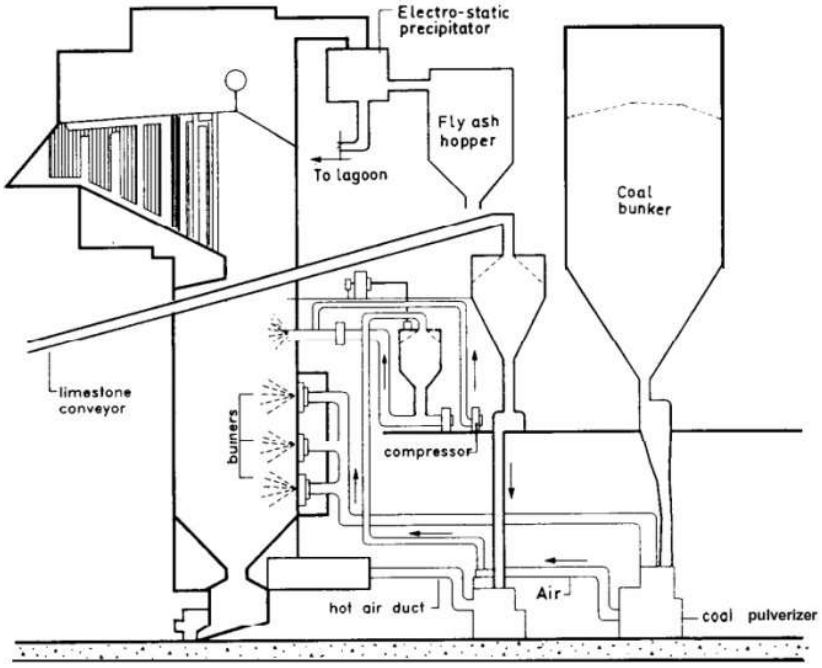

Figure 19: ***Schematic showing the combustion steps and fly ash collectors*** [133].

The classification of FA is based on a subdivision in class C and class F associated with the chemistry of the material: class F fly ash, available in larger quantities, is generally low in lime (*CaO*) content (< 15%), with a percentage of silica and alumina in the range of 40-50% and 20-30% respectively, derived from burning of anthracite and bituminous coal. Class C refers to FAs derived from burning of lignite (brown coal with a defined woody texture) and sub-bituminous coal, with a lime content higher than 15%, and a lower content of silica [132–134].

The utilization of FA as a pozzolanic additive in the preparation of cementitious binders brings many benefits, such as [45]:

- Improved workability imparted by the spherical ash particles and the associated water reduction that minimizes separation of water from the cement mixture.
- Improved compressive strength and other mechanical properties as a result of the reduced water demand.
- Reduced concrete cost as the value of coal FA is lower than that of cement.
- Reduced CO_2 emission as less cement is required.
- Improved durability, and in some cases improved strength, in hardened concrete due to the pozzolanic reaction with calcium hydroxide generated during cement hydration increasing the volume of calcium silicate hydrate binder, which helps fill the reduced water voids and thus creates a more durable and less permeable concrete.

It is necessary to clarify the meaning of the wording 'pozzolan': a pozzolan is said to be any material showing a tendency for pozzolanic reaction, i.e. the capacity to react with calcium (or $Ca(OH)_2$) in the presence of water, forming a C-S-H product. Due to these above-mentioned benefits, FA was then employed as a primary material in the production of GPs in many of the previous studies. Despite the wasteful nature of this material, FA-based GP presents mechanical properties comparable to geopolymeric compounds based on metakaolin or any other refined aluminosilicate sources [46,70,135]. The composition of FA is one of the main parameters affecting the final microstructure and mechanical properties of the GPs. Fernandez-Jimenz et al. spectroscopically examined (NMR, FTIR, XRD, etc…) 4 different types of FAs from different power plants in Spain, and demonstrated that chemistry of the FA is directly affecting the microstructure of the GP samples. More specifically, FA with a lower percentage of silica, a higher percentage of alumina (so a higher SiO_2/Al_2O_3 ratio) and a higher percentage of network modifiers (among all Fe_2O_3) draws lower compressive strength [135]. Palomo et al. [131] developed a mathematical model based on various parameters of alkali-activation/geopolymerization, such as the type of alkali activator, temperature and time of curing and liquid to solid (l/s) ratio, aiming to define the extent of influence of these parameters on alkali-activation of FA from a Pennsylvania power plant, by compressive strength assessment. Four activators (*NaOH* 12 M, *KOH* 18 M, $NaOH+Na_2SiO_3$ and $KOH+K_2SiO_3$), two curing temperatures (65 °C, 85 °C), three soaking times (2 h, 5 h, 24 h) and two l/s ratios (0.25 and 0.30) were simultaneously considered in the study. It was concluded that higher temperature of curing is leading to the better setting of AAM samples, *NaOH* more effectively alkali-activates than *KOH*, and an l/s ratio equal to 0.3 yields slightly higher compressive strength. The addition of sodium silicate to *NaOH* and longer soaking times improved the efficiency of the reaction, as it requires time to set. Finally, it was found that the highest compressive strength was 68.7 MPa, associated with the sample made with *NaOH* and waterglass kept under 85 °C for 24 h with an l/s ratio of 0.3. Criado et al. [136] demonstrated that appreciable modifications in the FTIR and XRD spectra were detected for samples cured up to 1 month, but in terms of compressive strength, the detected improvement given by

raising soaking time from one week to one month of curing does not overcome 3 MPa. In the same study, it was demonstrated that a mould sealing and the humidity retention is a beneficial practice to the final setting, as the geopolymerization reaction needs water to complete.

Since, in most of the cases, the chemical composition of FA does not guarantee the best chemical modulus, as reported by Davidovits in his investigations [59,60], it is a good practice to implement the chemistry of coal-ash with mainly silica sources. This is the reason why FA-based GPs have different properties depending on the FA origin, and the activation with a mixture of sodium hydroxide and waterglass yields higher mechanical performance(increasing the chemical modulus) [66]. Instead of using waterglass as silica precursor in geopolymerization, Puertas et al. [124] reported in 2009 a study in which urban recycled glass was used in geopolymerization of FA. Later in 2015, the same authors managed to demonstrate that utilization of 15g of waste glass in a 100 mL solution of *NaOH*, brings the same benefits as adding 15 wt.% of waterglass in *NaOH* [87]. The urban waste glass was also reused in preparation for general alkali activation, as well as in aggregation for concrete production [17,120,137].

2.7 Geopolymer-matrix composites

Due to the versatility of geopolymerization and the low operating temperature in the curing stage, geopolymeric compounds were widely used as a matrix in composites preparation. One of the main issues encountered in developing concrete-like materials is the enhancement of the fracture toughness [138]. This property is governed by many parameters and conditions, but one can say that it goes hand to hand with the brittleness of the material, and except for specific cases, the ductility is synonymous of higher fracture toughness [139]. For this reason, ceramics, and especially heterogeneous and porous materials, suffer considerably external stresses, favoring the propagation of a crack. A lack of continuity in matrix and presence of preexistent defects are preferential sites for crack nucleation and propagation in a material, leading to failure. The production of composites is one of the possible ways to increment the fracture toughness of a brittle material [139,140].

Yet in literature, many contributions were carried out in geopolymeric composites (GC) development, dispersing different types of particles and fibres or layering with fabrics. The selection of the fibres, in terms of material and size, should be weighted to the natural porosity of the GP matrix.

In their study, Yan et al. reported a sophisticated method to produce metakaolin-based GC, dispersing reduced graphene oxide particles [141]. Despite the creative idea, from the mechanical standpoint, improvement in fracture toughness was not as high as in the case when carbon fibres were used.

Carbon fibres were dispersed in a study conducted by He et al., in which the GP matrix was prepared with kaolinite. A fibre concentration of 10 wt.% entailed an improvement in fracture toughness of up to 4 fold, and in flexural strength of more than 3 fold, as compared to plain GP compound, showing an average flexural strength of 52 MPa. In the same study, visible pieces of evidence of fibre pull-out and crack-bridging were reported [142].

Also other inorganic materials, like basalt fibres, i.e. a common extrusive igneous rock, were used to produce GP reinforced composites. Thaumaturgo et al. [143], conducted a comparative study of fracture toughness in which various content of basalt fibres (0.5% and 1% in the volumetric fraction) were added separately in concrete and GP matrices, showing the influence of basalt percentage in the formulation and the differences between these two composites. They reported that while the highest value of the critical stress intensity factor (2.8 $MPa \cdot m^{1/2}$) for GCs coincides with the addition of 1% in volume of basalt fibres, concrete composites experienced a drop in the crack propagation resistance when addition of fibres exceeded 0.5% in volume and for equal content of basalt fibres in matrix, and the values of fracture toughness of concrete-based composites are from 13% to 50% lower than those ones detected when GPs were used.

Scientific contributions were also reported in polyvinyl alcohol (PVA) and cellulose-like fibers. Interesting is the effort carried out by Alomayri et al., who used cotton fibers in different concentration from 0% to 1% in production of FA-based GC [7]. They found that the maximum flexural strength (equal to 11.5 MPa), starting from 10 MPa (0% fibers content), is given when 0.5 wt.% of cotton fibres were added to the paste. More interestingly, the same authors processed cotton fabric based composites by layering fabrics with GP paste [144], and the achieved flexural strength after addition of 8.3 wt.% of cotton fabric was more than 3 times higher than the flexural strength of the base geopolymeric compound, and improvement of fracture toughness was 2.5 times higher. These authors also carried out mechanical testing to the same formulation under elevated temperatures (200-1000 °C), showing a drop of the mechanical performance at 300 °C, as cellulose decades at that temperature [145].

Attention must be paid to the chemical interaction between cellulose chains and activators in preparation of GC, especially if the solution has an alkali-activated origin. When cellulose gets in contact with *NaOH*, the polymeric chains undergoes an absorption of Na^+ cations, inducing a physical and chemical modification of the network, process known as mercerization. In Figure 20a is reported a sketch of a cellulose monomer. In highly alkali solution, the *–OH* groups of the monomers undergo hydrolysis, with the liberation of water, and leaving behind a negative charge on the oxygen (Figure 20b). The sodium cations, contained in the alkali solution after hydrolysis of the *NaOH*, externally activate the cellulose network, surrounding the negatively charged oxygen of the polymeric chains (Figure 20c); this provokes a disentanglement and physical swelling of the cellulose fibres [146].

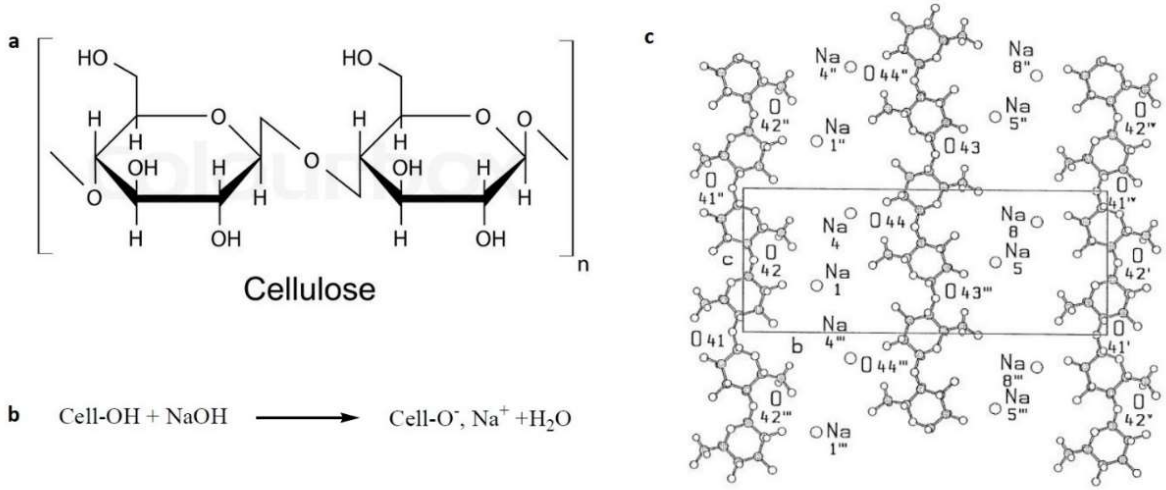

Figure 20: ***Mercerization of cellulose a) cellulose monomer, b) reaction of –OH hydrolysis c) arrangement of the Na^+ around the mercerized cellulose network*** [146].

Nevertheless, this chemical modification of the carbohydrate chains of the cellulose is not associated with a drop of the mechanical properties of the GCs. A deterioration of the cellulose compound is expected in the long term period, especially if the cellulose-based

composite is continuously exposed to a variable wet environment. It was observed that OPC-sisal composites suffer a quite fast degradation of the cellulose fibres even after 10 to 30 wetting and drying cycles of the samples. A flexural strength loss of up to 83% was detected in OPC-cellulose composites [147]. This behaviour is mainly associated with absorption and desorption of water by the cellulose fibres which induces, on the one hand, continuous local hydration of the cement, thus a chemical deterioration of the C-S-H chains, and from the other hand a decomposition and mineralization of the fibres due to migration of hydration products, especially calcium hydroxide, to the fibre lumen and spaces, provoking embrittlement of the fibres. This mechanism seems to happen at a higher rate for short fibres [148]. Several treatments to enhance the durability performance of the composites were studied by the author. The treatments included: (a) modifications to the matrix through the replacement of Portland cement by undensified silica fume and by blast-furnace slag; (b) carbonation of the cementitious matrix and (c) immersion of the fibres in slurry silica fume prior to being incorporated into the Portland cement matrix. The results obtained indicated that the embrittlement of the composites can be avoided almost completely by immersing sisal fibre in a silica fume slurry before adding them to the mix [148]. Another way to decrease the rate of degradation of cementitious-cellulose fibres composites is to mix the binder with a consistent (30 wt.%) aluminate source, e.g. metakaolin. It was observed an increase of the total wet/dry cycles yielding the same degradation of up to 300% [147].

2.8 Applications

Ever since the finding of the AAMs and GPs, these materials have found application in building and construction applications, holding great similarities with the OPC. Despite the potentiality of these products and the innumerable attempts of marketability, the AAMs and GPs encountered many issues of up-scaling, repeatedly failing in the initial ambition of replacing the OPC. The reasons behind this failure are many, either technical or political, already exposed in Chapter 2.3. In this chapter, some examples of applications, and the proposed new technologies attributable to GPs and AAMs are presented, opening new perspective in their exploitation, which could be a breath of fresh air for the stagnant scientific investigation around these materials.

2.8.1 Past applications

When AAMs were, for the first time, developed in USSR in the 1950s by Glukhovsky, as a result of the alkali-activation of BFS raw wastes, the eastern European countries experienced primary exploitation of the potentialities of these materials in buildings and civil infrastructure. Yet in the 1960s, the commercial production of alkali hydroxide-activated BFS concrete in Mariupol was started in the Stroydetal mill of the association Azovshelezobeton. This concrete, in the form of precast blocks, has been used for the construction of houses, garages, and other structures including 2-storey and 15-storeis apartment buildings (Figure 21a). Later, between 1986 and 1984, the similar tall 24 stories building was built in Lipestk, using again pre-cast blocks of alkali-activated BFS [33]. Concurrently, also other eastern countries started to look for a new solution in the construction and retrofitting of buildings. A 6-storeis office and retail building (8.6 m x 31.5 m) and a workshop with an area of 3,500 m^2 were built in China in the 1980s, using an *OPC*-AAS based AAMs (Figure 21b). In 1974 a storehouse was built in Krakow using precast steel-reinforced alkali-carbonate activated BFS concrete for the floor slabs and wall panels [149].

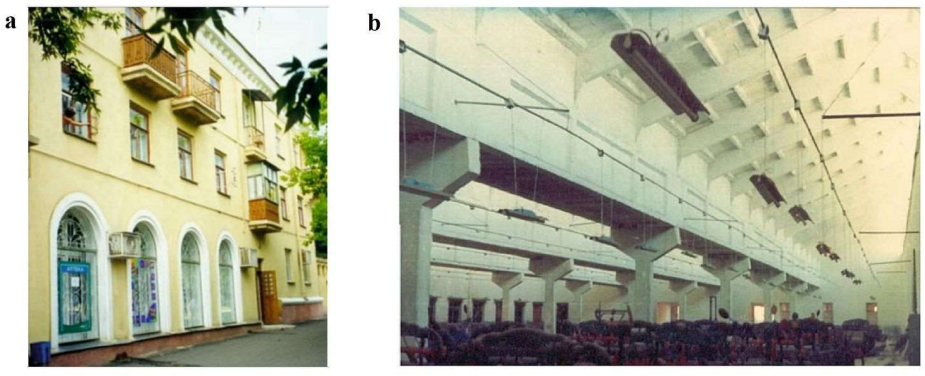

Figure 21: a) Residential building in Mariupol and b) a Na_2SO_4-activated Portland-alkali-activated steel slag cement concrete based workshop in China [12].

Besides these conventional industrial and residential constructions, in the same period, many other specific civil infrastructures were built in Eastern Europe. Among all, a heavy-

duty road to the Magnitnaya Mountain Quarry, in 1984, in Magnitogorsk, using alkali-activated BFS concrete. Many public construction projects were finalized in USSR between the 1960s and the 1980s, including a basin fountain, a drainage collector and silage trenches, using BFS based AAMs [12,33]. In particular, it was found that the utilization of this material prevents excessive corrosion of the concrete in silage trenches [9,150].

In the USA, the usage of AAMs started around the late 1980s, followed by developments related to construction materials applications commenced in the early 1980s through a joint venture involving the US Company Lone Star Industries [151]. This company worked side by side with Davidovits, whose French and US patents formulated between the early 1970s and the 1980s, were instrumental for the commercialization of a BFS-clay based AAMs, known in its commercial name as Pyrament [28,29,58,72]. The Pyrament product range was met with strong interest, and found application in test projects and full-scale application via the U.S. Army Corps of Engineers, state and federal transportation agencies in several jurisdictions in the USA and Canada [152–156], particularly as a material for bridge deck overlays or as a repair material for damaged pavements. The performance of Pyrament sections used in airport runways has also been classified as very good after 25 years in service [157].

EU was the first continent in the world which came to know the innovative process of alkali-activation, due to the first patent settled in Belgium and covering several countries of the old continent, following the scientific work made by Purdon in the early 1950s (see Table 1 in Chapter 2.2) [25]. This invention, based on alkali-activation of BFS slags, was followed by the settlement of a company 'Le Purdocement' in the 1950s, based in Brussels. This company operated a production facility in Brussels from 1952 to 1958, supported by a number of commercial partners, but did not prove to be profitable, either because of the relatively small scale of its production capabilities or from a low interest in the market (the available archive documentation does not provide clear information). The production of Purdocement ceased at the end of 1958, but an inspection operated in 2010 still showed a good condition of the building, constructed with the same patented material, with only some damages due to erosion and carbonation [158].

This first failure to commercialize an AAMs demotivated the scientific community and the enterprises to invest time and money on the development of this material. The hibernation of this material ceased concurrently to Davidovits's work, who had certainly the merit to bring light and optimism on the field. Immediately after the Davidovits's findings, Finland was the first country which tried to exploit this material, early in the 1980s, focused on the development of precast concrete items, under the name F-cement binder [159,160]. During the years 1980 to 1994 a very comprehensive study on alkali-activated BFS concrete took place at Partek (Finland), leading to full-scale pilot production of pre-stressed hollow core slabs, low height high strength beams, waste water system products, pressurized pipes, railway sleepers and pavement stones. Starting from 1994, some AAMs have successfully been applied, including applications as fireproofing adhesives in composites, fire and gas-

tight layers in insulating composites on board large cruise ships and production of tiles for house roofs construction (see Figure 22) [12].

Figure 22: House close to Finland, roofed with tiles made of alkali-activated blast furnace slags [12].

In the same decade, a cementitious material partly based on alkali-activation of slags was developed in the Netherlands, under the copyright ASCEM®. Although it is derived from a high-temperature process, operated at about 1450 °C, this material embodies less CO_2 than OPC and can compete in terms of technical properties. The idea is based on re-use strategies of different waste materials such as FAs and municipal wastes. The technology was already successfully tested in the late 1980s, but not commercialized at that time. Nowadays, other drivers such as CO_2-reduced cement led to the reanimation of that research direction within ASCEM B.V. as a successor of the original development company. The heart of the ASCEM® cement technology is the melting process of the secondary resource mix, meeting a certain composition in the CaO-Al_2O_3-SiO_2 ternary system, to obtain a reactive glass. [161]. The material/process was up-scaled no earlier than 2009 for the production of industrial terrain and pipes.

Important developments were attained in the last decade in Australia, aiming to overcome the obstacles which hinder the AMMs and GPs to be fully commercialized (see sub-Chapter 2.3.1). The scientific efforts endeavoured by the Australian company Zeobond Group in 2006 yielded to the development of the E-Crete™ cement binder, which is generally produced from blends of FAs, slag, and alkaline activators. This is mixed with sand and aggregates in similar proportions to traditional cement binders to form concrete. E-Crete may use standard alkali activators and whatever source materials, such as FAs and

slag, are available [162–164]. The E-Crete^{TM} product was extensively employed, also by second companies, such as VicRoads for the construction of the Salomon Street Bridge in Melbourne in 2009, through the production of E-Crete pre-cast footpath, according to the standards in the VicRoads technical specification [164]. Figure 23 reports some picture of the panels and the bridge in Melbourne. In the same year, still in Melbourne, E-Crete was again selected by VicRoads for the reinstatement of the retaining walls at the Swan Street Bridge, and in the following year, several pathways were realized on Brady Street in Port of Melbourne.

Figure 23: Salmon Bridge in Melbourne (Australia), made of E-Crete precast footpath [12].

Other works in the past, related to the utilization of FA-based AAMs, includes the construction of several railway sleepers meeting the national standards of Japan [165]. For instance, in the 1980s, BFS based AAMs railway sleepers were produced in Poland, matching the requirement of 70 MPa strength through the use of finely ground slag. A pilot-scale research project was conducted in Spain for the development of new pre-stressed steam-cured railway sleepers based on AAMs using FAs [166,167].

2.8.2 Potential applications of the future

AAMs and GPs were also utilized in several examples of non-traditional and niche constructions, due to their stability, wide versatility of production and high-temperature resistance (non-glass based GPs). Many attempts have been done in commercializing GPs and AAMs for application in which lightweight properties are required. The most usual process for light-weighting is the production of foams, a solution widely undertaken in OPC cements yet, through autoclave aerated method, i.e. a hydrothermal method, and applied to AAMs and GPs foaming in USA, Europe, and the former Soviet Union

[33,168,169]. The most applied method of GPs and AAMs foaming regard the production of bubbles through the emission of hydrogen or oxygen while the binder is still in the slurry, using different reagents and compounds. Finely divided metallic aluminum [50,170–172], metallic silicon, either added directly [172] or as a component of silica fume [173–176], hydrogen peroxide [26,177], sodium peroxide [178], and sodium perborate [26] have been used as foaming agents. Chlorine gas generation through the decomposition of calcium hypochlorite has also been proposed [179], although it is unclear what would be the effect of the generated chlorine on the durability of the material in the long term. It is also possible to achieve foaming through the use of suitable surfactants [180,181], and this method has been applied in practice to the production of lightweight alkali-activated BFS panels containing fibrous additions for use as acoustic insulation [12]. A number of authors have also made use of the foaming tendencies of partially-polymerized aluminosilicate gels at elevated temperature to develop AAMs which expand into foam at elevated temperature [182–184]. This property has been noted to be of value in passive fire prevention applications [26,185].

Alkali-activated slags were also employed in Europe for underground applications, including boreholes sealing in salt, sulfur mines and hydro-technical sealing [186]. AAMs have also been developed for down-well cementing in CO_2 storage and sequestration [187]. Drilling fluid and mud can also be mixed with alkali-activated BFS to form a cementitious slurry for cementing operations [188,189], and there has also been work based around the use of alkali silicate-activated FA/BFS blends for similar purposes [190]. Alkali-activated BFS formulations for this application were initially developed by Shell Oil Co. in 1991 for use in the Gulf of Mexico [191], and similar mixes have also been successfully used in China [192] and Brazil [193]. Work reported from the laboratories of some other oil companies [194] did show that under some circumstances, alkali-activated BFS slurries were prone to cracking. However, interest is increasing, as evidenced by the filing of patents by Schlumberger related to the use of alkali-activated cement in oil wells [195] and CO_2 sequestration wells [196].

Interestingly, AAMs and GPs are also applied to the construction of containers for stabilization/solidification (S/S), disposal and/or immobilization of hazardous wastes in the environment. The properties required for AAMs and GPs in this context are dependent on the chemistry of the contained wastes and the sources material in AAMs and GPs processing [12,197–201]. To date, the most used material for these purposes is the OPC cement [202], and there is no practical example of utilization of AAMs and GPs in this application, although they have been extensively studied in the last years both in the treatment of toxic [203–205] and radioactive [45,206] wastes. Due to this reason, we below report only an exhaustive description of the state of the art concerning BFS, Metakaolin, FA-based AAMs and GPs. In general, cationic species are far more effectively immobilized in alkali-activated binders than are anions; transition metals which form oxy-anionic species, in particular, tend to be troublesome. A summary of the elements which have been treated through S/S in AAM binders is given in Figure 24; the elements classified as ‘bound’ are those whose total mobility has been reduced by the treatment.

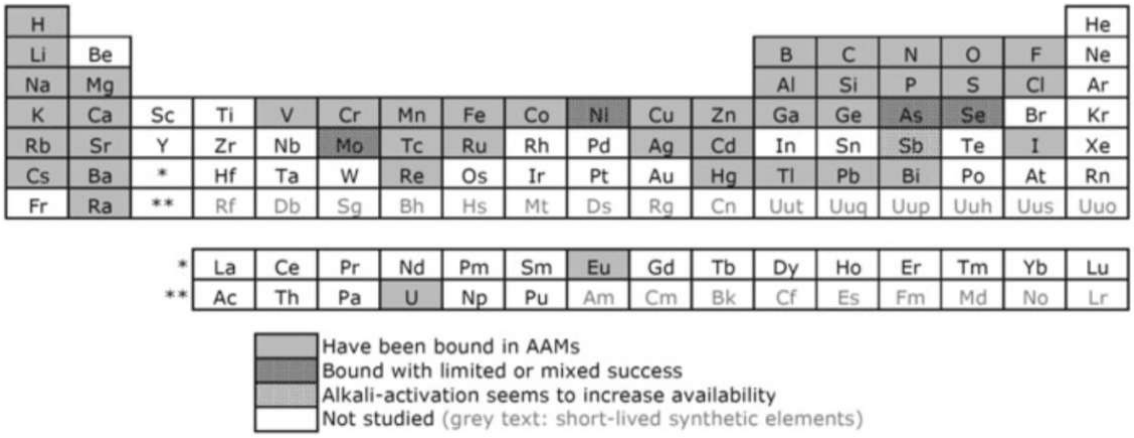

Figure 24: Elements which have been bound (and/or treated through stabilization/solidification) based on a survey of the available literature up to date [45].

In BFS based AAMs, the immobilization of hazardous materials, such as *Pb*, *As* and *Cd*, is dependent on the leachability of these elements entrapped in the alkali-activated network, and it is optimized using alkali-activators like Na_2CO_3 [207–209]. It has been reported that, in general, heavy metals show less interference with the setting and strength development of BFS AAMs than with Portland cement [33,203]. This is potentially due to the enhanced availability of Si in most alkali-activated binder systems (particularly those with waterglass activators), as demonstrated experimentally by Shi et al. [210], who used calorimetry to investigate the early-age reactions involved in S/S of an electrical arc furnace (EAF) dust (containing a mixture of toxic metal species) with OPC and alkali-activated BFS binders. However, there was a notable difference in performance between laboratory-cured and field-cured specimens, which was attributed to the differences in curing regimes applied under the two conditions [211,212].

FA and metakaolin based AAMs have been extensively investigated especially in the stabilization of lead (*Pb*), albeit the understanding of the immobilization mechanisms is not clear yet. Van Jaarsveld et al. [96,204,213] found a chemical affinity in the stabilization of lead with the aluminosilicate matrix, although it is not clear in which chemical compound. Other authors [214,215] supposed the formation of an insoluble Pb_3SiO_5, whose identification was tentatively supported by the results of Zhang et al. [216], though only based on a single XRD peak. The immobilization of arsenic has always been a great challenge in OPC cement, as the cement was implemented only in a case-by-case approach [217]. The S/S treatment of arsenic was found to be effective in AAMs and GPs [206,218,219]. Fernández-Jiménez et al. [220,221] observed by transmission electron microscopy that arsenic is associated with iron-rich FA particles. This correlates to some extent with the known sorption of arsenic onto iron hydroxide surfaces [222]. A much lower immobilization efficiency was found for low-Ca AAMs and GPs in case of cadmium (Cd^{2+}) leaching [221,223]. On the contrary, this element is successfully immobilized in OPC cement, due to the high presence of Ca^{2+} cations, replaced by Cd^{2+} in case of cadmium contaminants [224,225].

Much more practical uses AMMs and GPs have found in the last decades in S/S of low/intermediate level waste (L/ILW), i.e. radioactive wastes, whose key radioactive components are ^{137}Cs and ^{90}Sr. The latter element is efficiently immobilized even in OPC cement, as the C-S-H network provides Ca^{2+} cations readily substituted by the Sr^{2+} cations [226]. Much more problems in immobilization are induced by ^{137}Cs, which is more efficiently immobilized in BFS based AAMs and GPs, as reported in Figure 25, evidencing lower leachability of Cs if retained in the aluminosilicate network, rather than in a C-S-H structure [203,227,228]. For reasons related to the binding of Cs^{+} in gels with pseudo-zeolitic (or proto-zeolitic) structures, metakaolin and FA-based AAMs have been studied extensively for waste immobilization purposes [45,229–234]. Chervonnyi and Chervonnaya [235] studied the combination of ^{137}Cs and ^{90}Sr as present in wood ash from the region surrounding the damaged Chernobyl reactor complex and found that geopolymerization of the wood ash together with thermally activated bentonite provided a factor of 20 improvements in leaching performance compared to OPC. A binder system named EKOR, developed in the Kurchatov Institute, Russia, commercialized by Eurotech was applied as a sealing and dust-reduction agent as a part of the construction of the sarcophagus protecting the damaged reactor core [236,237]. Alkali-activated clay-based binders have also been developed and applied in S/S of radioactive wastes in the Czech and Slovak Republics by the company ALLDECO [12], and also in Germany in collaboration with Cordi-Géopolymère in France [206].

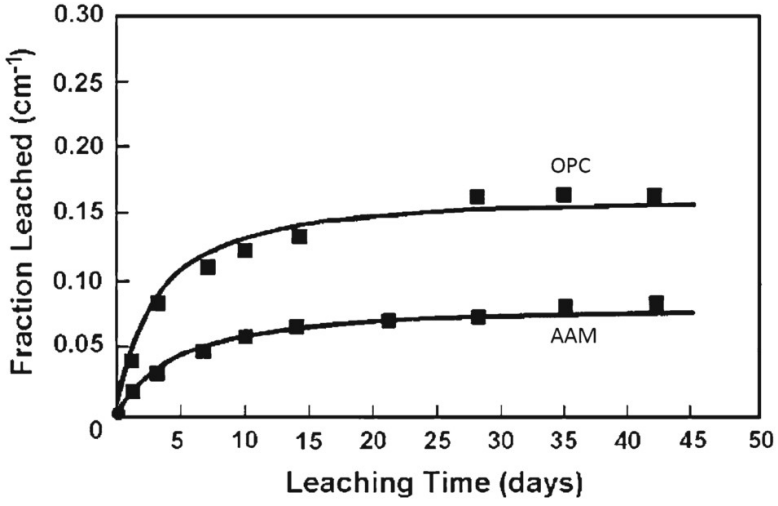

Figure 25: Leachability of Cs^{+} from Portland cement and blast furnace slags based alkali-activated pastes at 25 °C [12].

GPs exhibit good performance at the high-temperature exposition, as the latter involves a chemical transformation in such conditions (see Chapter 2.3.1) [238]. GP composites have been tested for use in aircraft due to their fire resistance and comparatively low density [239]. This technology is still in its infancy, however, it has shown the potential for wider utilization. GP composites have also been used as thermal insulation on the exhaust pipes of Formula 1 race cars [151].

3. Scopes and aims of the thesis

In the last decades, the uncontrolled contamination of the eco-system, partially generated by an unsustainable exploitation of landfills, and the progressive rise of the annual average temperature, due to the extensive emission of greenhouse gases in the atmosphere, like CO_2, drew the attention of the of the scientific community and the governments worldwide, pushing them to adopt a more eco-friendly and sustainable technology policy. The extensive production of CO_2 gas in the atmosphere during OPC clinker synthesis (8% of the annual greenhouse emission) prompts the industry to replace this material.

GPs incorporating silica and aluminosilicate based on wastes is one of these candidates, as the production of this material is an alkali-activated reaction of industrial wastes under a temperature lower than 100 ˚C, and more importantly, it does not draw any greenhouse release. The utilization of FA, a power plant by-product, and borosilicate glass, recycled glass from pharmaceutical vials, makes this material cheaper and more sustainable, preventing, in turn, the undue filling of landfills. The main drawback is the inhomogeneity of the matrix and the amount of porosity (near to 20%), inducing a very low resistance to crack propagation as compared to the cementitious materials. The modulation of the chemical synthesis (e.g. improving the efficiency of some physical and chemical parameter) and the production of GP matrix composites based on the dispersion fibres, e.g. cellulose and recycled paper ones could be possible solutions to the problem.

Therefore, the main aim of this work is to develop and produce an eco-friendly material, with no greenhouse emission, worth of replacing the Portland cement in building and infrastructural and structural applications, while conferring to the material high strength and fracture resistance by dispersing cellulose and waste paper fibres in the matrix.

According to the overall aim, the following subtasks have been formulated giving a baseline for the research work to be conducted on GPs and geopolymeric composites:

- Processing of BSG/FA-based GP from waste materials;
- Physical, chemical and mechanical characterization of different formulations of BSG/FA-based GP;
- Optimization of some chemical-physic parameter influencing the reaction;
- Improvement of the reaction efficiency by applying a hydrostatic pressure (HyPS consolidation);
- Processing of cellulose and paper fibres GC by ultra-sonication dispersion of the fibres in geopolymeric matrix;
- Chemical characterization of the interphase between cellulose and GP matrix;
- Mechanical characterization of GC samples and comparison of the properties with the data from GP characterization.

4. Methodology

4.1 Materials and processing methods

4.1.1 Experimental materials

FA, a coal combustion by-product, from a Bohemian thermal power plant (Počerady power plant, North Bohemia, Czech Republic) was used as a primary aluminosilicate source. The as-received FA powder was thermally treated at 800 °C prior to characterization and alkali activation, in order to burn all the organic impurities out. The loss of ignition was also measured in terms of weight loss percentage of FA.

Borosilicate glass from recycled pharmaceutical vial cullet (Kimble/Kontes, Vineland, NJ, USA) was mixed in different percentage to FA in GP processing. The recycled stock of raw borosilicate glass was collected by 'Nuova Ompi S.r.l.' company (Piombino Dese – Padua, Italy). The as-received glass was ball-milled at 350 rpm and 400 rpm for 15 minutes in an alumina jar with alumina balls (diameter 10 mm) prior mixing with FA and alkali activation, using a Pulverisette 6 line planetary ball mill (Fritsch, Germany). The 400 rpm x 15 minutes BSG powder was eventually used in all the samples production.

The caustic soda (*NaOH*) was purchased from Sigma Aldrich (Saint Louis, MO, USA). The solid anhydrous compound was provided as pellets with a purity exceeding 97% (in a form compliant to American Ceramic Society reagent standards).

The cellulose fibres, for GP matrix composite processing, were provided by CIUR a.s. (Brandýs nad Labem, Czech Republic), in a form of dried macrometric fiber. The average length is ca 1.1 mm, the fibre diameter falls in the range of 35 µm and 45 µm. The density was reported by the supplier to be 470 kg/m^3, holding a humidity amount less than 5.5 wt.%. The as-received cellulose fibres were directly mixed with the aluminosilicate suspension, undertaking no other treatments.

The production of the HyPS samples was based on FA and silica gel consolidation. The silica gel powder was obtained by high energy ball milling of silica gel ball for desiccation (350 rpm for 15 minutes). Fused silica microbeads (average diameter of 1.8 µm) were purchased from Cospheric LLC (Goleta, CA, USA) for the basic construction of a consolidation model of HyPS process.

4.1.2 Manufacturing of geopolymer samples

The FA was dry-mixed with borosilicate glass from recycled pharmaceutical vial cullet and activated with a caustic soda solution, prepared by dissolving *NaOH* pellets in distilled water, as described in Figure 26. Before activation, the BSG was ball-milled at 350 rpm for 15 minutes, in alumina jar/balls, so as to reach the desired grain size. The GP samples were manufactured following 6 different formulations, in which the powder mixture (SiO_2/Al_2O_3 ratio), the molarity of the activator, and the curing time were modulated in order to investigate the influence of these parameters on geopolymerization. A schematic

summary of the methodology used is reported in Table 3. In batches from 'Mix-1' to 'Mix-4', samples were prepared by activating dry mixtures of FA from 70 wt.% to 30 wt.% and BSG from 30 wt.% to 70 wt.% in a 13 M *NaOH* solution and cured for 1 day. The samples processed through the 'Mix-5' batch were based on the 'Mix-2' formulation and cured for 3 days, and finally, 'Mix-6' samples were activated using a 10 M *NaOH* solution (see Table 3 and Figure 26). The alkali solution was added in a sufficient amount to ensure workability to the slurry. In all the mixes, the liquid-to-solid ratio ranged between 0.4 and 0.5. The obtained slurry was cast in rubber moulds and cured in the air at 85 °C.

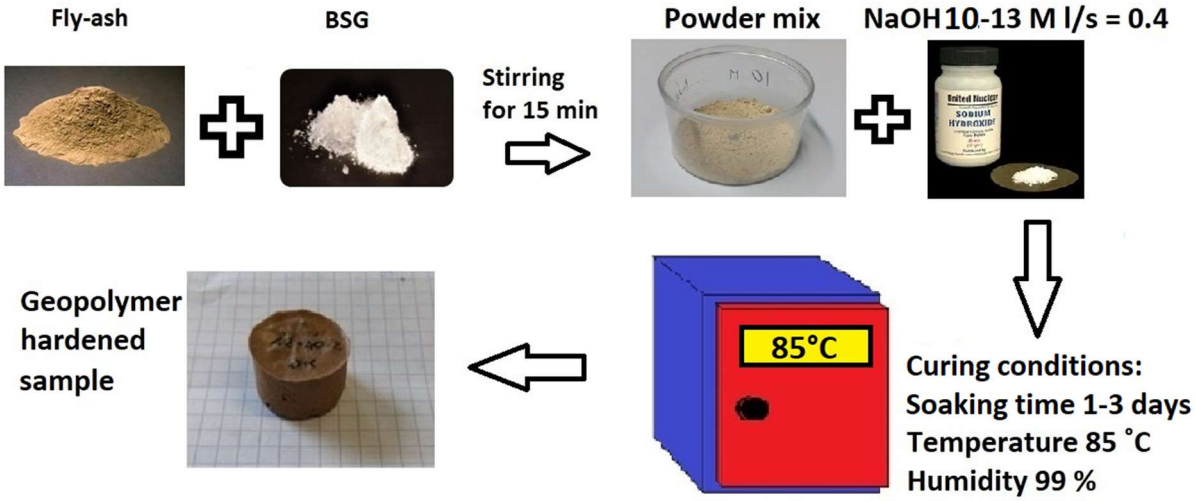

Figure 26: Description of the methodology of the geopolymer samples manufacturing.

Table 3: Resume of different adopted terminologies associated with the formulation and curing conditions.

Sample	Fly ash (wt.%)	BSG (wt.%)	Molarity (M)	Curing Time (day)
Mix-1	70	30	13	1
Mix-2	55	45	13	1
Mix-3	40	60	13	1
Mix-4	30	70	13	1
Mix-5	55	45	13	3
Mix-6	55	45	10	1

Samples casting in rubber moulds were done in such a way to retain the evaporated water in the curing chamber (i.e. chamber was tightly sealed), as the humidity grade influences the geopolymerization process. For this reason, the samples were taken airtight through two methodologies [136]:

- Method 1: Moulds were sealed in latex bags.
- Method 2: Moulds were closed in an air-tightened jar with some water.

Irrespective of the methodologies of processing, after curing, the samples were demoulded and exposed to the lab air for one week prior to testing in order to complete the

geopolymerization. This methodology of preparation was also reported in previous publications [4,240].

4.1.3 Manufacturing of geopolymer composite samples

Mix-1 was properly modified in order to combine the dry mix with cellulose fibres in various percentages (from 1 to 3 wt.%), substituting the FA content (from 69 wt.% to 67 wt.%). The reduction of the FA was not considered sufficient to a cause significant change in the properties of the material. The dry mix was then diluted in distilled water and sonicated for one hour to guarantee homogenization of the mixture and to unravel the bundles of cellulose fibres. The suspension was dried for 12 hours and the dry mixture was activated in a 13 M *NaOH* solution, forming a slurry whose liquid-to-solid ratio was between 0.8 and 0.9, due to mercerization of the cellulose fibres (see Chapter 2.7 and Figure 20). The slurry was cast according to method 1 (see the previous section) and cured at 85 °C for 24 hours (one day), as described in the schematic reported in Figure 27. As above-mentioned, the samples were demolded after curing and kept in air for one week prior to testing.

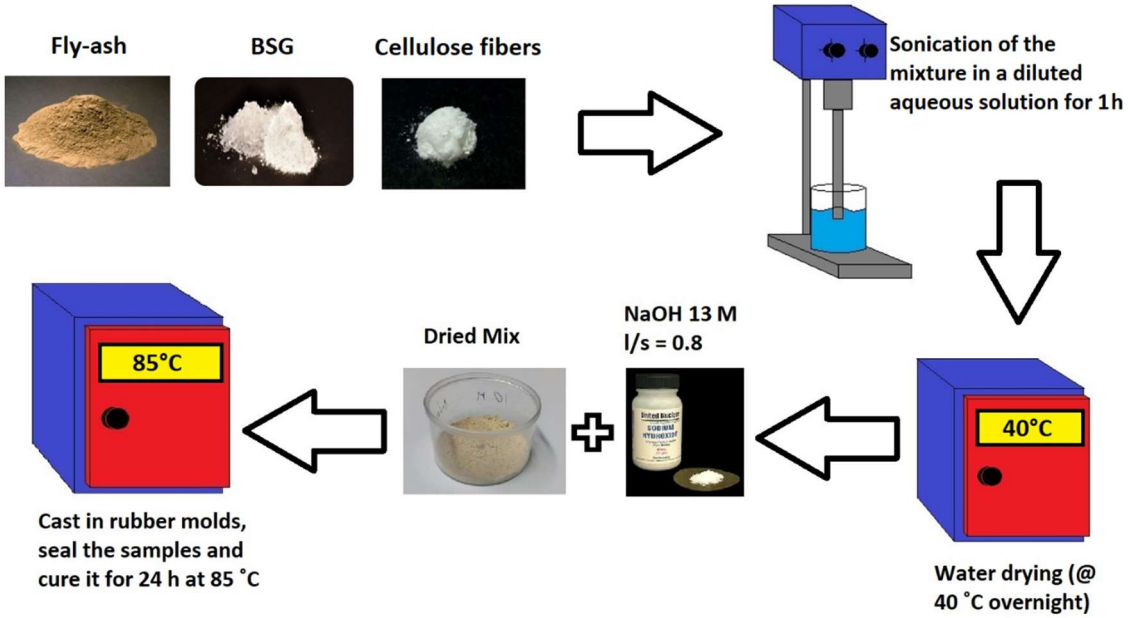

Figure 27: Description of the methodology of the cellulose fibre-reinforced geopolymeric composite manufacturing.

4.1.4 HyPS process

The same FA from the bohemian power plant was mixed with either water or *NaOH* solution (*NaOH* pellets dissolved in distilled water) with variable concentrations (3 M and 5 M). Silica gel powder was also densified in distilled water in order to prove the versatility of the method. The liquid to solid ratio (l/s) was chosen to obtain the desired rheology of the slurry, normally falling in the range of 0.3 and 0.4 in case of FA

densification and 0.5 for fused silica, both powder and microbeads (this parameter is strictly related to the material and the grain size of the powder).

The densification of the slurry was carried out in a compression configuration using an evacuable die for FTIR pellets manufacturing and installed onto a screw-driven testing machine Zwick Z250 (Ulm, Germany), in a compression test setup. The evacuable pellets die used in all the experimental cases was purchased from Specac Company (Orpington, UK), including one die body and base, one plunger and one stainless steel high tolerance cylinder, with a nominal hole diameter of 13 mm (Figure 28a). A picture of the die is in Figure 28b. Once the mixture of powder and solution is put in the die chamber, the system is then sealed to leak-proof, loaded into the compression testing machine and kept under uniaxial load (P = 60 kN) for the holding time of 5 minutes. Equivalent pressure stress (σ) is given by geometrical considerations, according to the following equation:

$$\sigma\ (MPa) = \frac{\mathrm{P}}{\pi \cdot r^2} \tag{12}$$

Where P is the maximum load in compression (N) and r is the hole-radius of the die chamber (mm). The operating temperature was kept at 25 °C (room temperature).

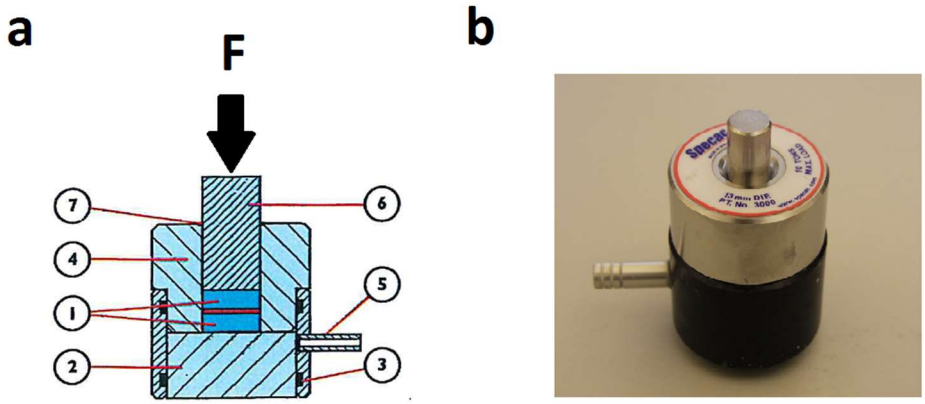

Figure 28: a) Schematic of the die: 1- cylinders 2- base 3- O-rings 4- cylinder body 5- evacuation port 6-plunger and b) photo of the die.

For the demonstration of the Ostwald ripening mechanisms in HyPS process (Appendix A), fused silica microbeads were mixed with water (l/s ratio 100:1) kept under a pressure of 300 MPa for 10 minutes.

The comparative study between this process and the cold sintering process (CSP) (Appendix B) was conducted on fused silica nanoparticles mixed with water and kept under 450 and 600 MPa for 5 minutes. For the production of CSP samples, the same material and conditions were utilized, changing the setup of the experiment – a similar die was uniaxially pressed in a sealing-less configuration in a hot chamber at 200 °C for 2 hours.

The BSG was densified in water (l/s = 0.5) under 500 MPa for 5 minutes to corroborate that the HyPS process can be effectively extended to the processing of many other materials (Appendix C).

4.2 Microstructural investigations

4.2.1 Microscopic observations

Observations of raw materials microstructure (FA and BSG) and the fracture surface of both GP and GC samples were carried out through Scanning Electron Microscopy (SEM), model Tescan LYRA 3 XMH FEG/SEM equipped with X-Max80 EDS detector for X-ray microanalysis. Inorganic samples were carbon coated to ensure the sample conductivity.

The SEM observation of the HyPS samples and the Ostwald ripening mechanisms was performed. Raw fused silica microbeads were observed at the SEM microscope and a series of 200 beads were measured by image analysis (using Image-J software). The same procedure was repeated for the fused silica microbeads after application of hydrostatic pressure. Also, necking observation was carried out.

4.2.2 Spectroscopic characterization

The chemical composition of the primary materials (FA and BSG) was determined through X-ray fluorescence (XRF) using a RIGAKU (Rigaku Corporation, Tokio, Japan) ZSX100e model operating at 60 kV and 150 mA and equipped with Wavelength-dispersion X-ray spectroscopy (WDS), an X-ray Rh tube working at 3 kW, a scintillation counter for heavy element detection, and a gas-flow proportional counter (Ar–methane 10%) for the detection of light elements.

The chemistry and the degree of networking of the polymeric structure were evaluated through a simultaneous interpretation of the spectra from FTIR and NMR. FTIR spectra were collected at the Institute of Biomaterials (Erlangen, Germany) by using a Nicolet 6700 FTIR (Walthan, Massachusetts, USA) spectrometer in the range between 4000 and 400 cm^{-1}. The analyses were conducted on pellets composed of 0.2 g of potassium bromide (KBr) and 0.002 g of GP.

^{11}B, ^{27}Al, and ^{29}Si NMR spectra were obtained using a Bruker Avance-500 spectrometer (Billerica, Massachusetts, USA), belonging to CEITEC institute (Brno, Czechia). The rotation frequency of 10 kHz was used for ^{27}Al and ^{29}Si, 14 kHz was used for ^{11}B. Recycle delay of 5 s was used for ^{11}B, 2 s for ^{27}Al and 20 s for ^{29}Si. ^{29}Si NMR spectra were deconvoluted in the sum of the single chemical shifts, using the DMfit software [87]. The admitted error was calculated to be about ±1 ppm. The functioning principles of the Nuclear Magnetic Resonance (NMR) spectroscopy is based on the interaction between the magnetic field produced by a chemical element when it is spinning around (in the machine rotor) and a crossing determined-a-priori variable magnetic field. The type of resonance tells the particular electrical ambient in which the element is immersed [241]. It must be noticed that the response is anisotropic, that means it depends on the mutual orientation of the magnetic fields. The situation changed when it was shown by E.R. Andrew and I.J. Lowe that anisotropic dipolar interactions could be suppressed by introducing artificial motions on the solid - this technique involved rotating the sample about an axis oriented at

54.74° with respect to the external magnetic field. This became known as magic-angle spinning (MAS) [242–244].

XRD spectroscopy was instrumental to qualitatively and quantitatively inspect the crystalline part of the FA and GP samples. XRD patterns were collected using X´Pert Pro (PANanalytical, Netherlands) powder diffractometer with Bragg-Brentano (theta-theta) geometry, operating with Co Kα 1.2 radiation. It is equipped with a 1-D linear detector and β -filter. The fitting of the XRD peaks was carried out using HighScorePlus software (PANanalytical, Netherlands) and the ICSD database with crystalline models (2017). The Rietveld method was used to quantify the amorphous phase content and the crystalline size (based on the Sherrer's equation).

4.3 Determination of the physical and fracture parameters

4.3.1 Powders characterization and relative density calculation

The evaluation of the grain size of the FA and BSG powders was carried out by means of laser diffraction particle sizing technique, using a Malvern Hydro2000MU (United Kingdom), and located in SASIL S.P.A. facilities (Italy).

The relative density (ρ_{rel}) of each sample was calculated by measuring the actual density of the samples, through volumetric evaluation of the samples, and assessing the theoretical density of the GP samples. The theoretical density was weighted according to the GPs formulations (Table 3). The theoretical densities of FA (d_{FA}) were calculated starting from the density of the single source (i.e. FA and BSG), which were measured by means of an automatic pycnometer PYCNOMATIC ATC (VŠB-TUO, Ostrava, Czech Republic). The proportion of open and closed porosity was deduced by means of the Archimedes method, using high purity distilled water as buoyant. The weighting of the specimens was carried out using a Denver analytical balance (±0.0001 g resolution) [245].

4.3.2 Compression test

The determination of the compressive strength of the GP samples was performed through compression test carried out on 5 mm x 5 mm x 10 mm prismatic specimens, appropriately cut from demoulded Mix-1 and Mix-2 type GP samples (see Table 3). The specimens were tested not earlier than one week after demoulding, in order to complete the geopolymerization. The setup on compression test was mounted on a universal test system INSTRON 8862 testing machine (Norwood, Massachusetts, USA), carrying a system load cell capacity up to ± 100 kN with optional load cells with smaller capacity down to 200 N. The speed rate of the cross-head was set to 0.5 mm/min. The prismatic 5 mm x 5 mm x 10 mm specimens were tested in the height direction, which might be at least twice the length of the other two dimensions, so as to eliminate the local stress induced by the interference of the compressive cones [246].

4.3.3 Flexural strength

The demoulded cylindrical samples obtained after the curing stage were appropriately machined to specimens in a prismatic-like shape, whose measures fell approximately within 4 mm x 3 mm, and a length not shorter than 16 mm, being the span of the setup. A set of at least 10 specimens were tested in a three-point bend configuration (3PB) so as to assess the flexural strength, according to the standards ASTM D790-17 [247]. The data scatter was based on the interquartile range (IQR), with a factor of 1.5. The configuration of the 3PB test comprehends three rollers (5 mm in diameter), mounted two below and one above the sample, as depicted in Figure 29. The tests were carried out on a screw-driven testing Zwick Z50 machine (Ulm, Germany) with load cell capacity up to ± 50 kN with optional load cells with smaller capacity down to 200 N. The speed rate of the cross-head

was set to 10 µm/min. The deflection was measured by inductive transducer incorporated directly into the loading axis.

4.3.4 Fracture toughness

For the evaluation of the fracture toughness (K_{IC}), a chevron notch was cut on a set of 10 specimens with equal size of 3PB specimens, according to the methodology reported in the literature [248]. The marked specimens were then tested in a 3PB mode with a span of 16 mm, with the cross-head speed rate of 10 µm/min, for the evaluation of the fracture load. The calculation of the K_{IC} is therefore performed using the following formula [248]:

$$K_{IC} = \frac{F_{max} Y^*_{min}}{B * W^{\frac{1}{2}}} \quad (13)$$

where F_{max} is the maximum load in bending, B and W are the thickness (3 mm) and the height (4 mm) of the specimen, and Y^*_{min} is the minimum value of the geometric function, dependent on the geometry of the chevron notch (determined by optical measurements of chevron notch depths and angle on fracture surface). The data scatter was based on the interquartile range (IQR), with a factor of 1.5.

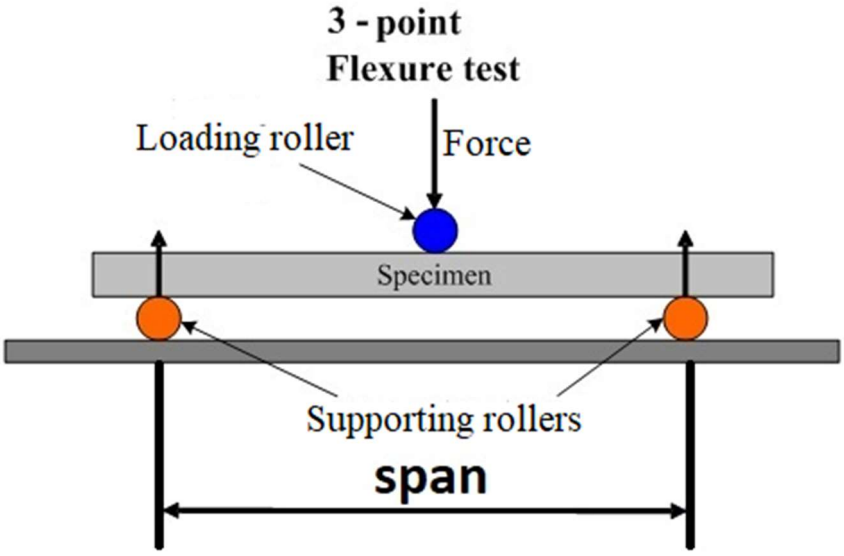

Figure 29: Schematic description of the configuration of a three-point bending test setup.

4.3.5 Vickers micro-hardness

The instrumented micro-indentation experiments were performed on produced Mix-1 and Mix-2 GP samples after one month of curing in the air (room temperature) using a screw-driven ZWICK Z2.5 testing machine (Ulm, Germany) equipped with micro-hardness head ZHU0.2 with optics. The Vickers hardness values were calculated using the following equation [249]:

$$HV = 1.8544 \frac{P}{d^2} \quad (14)$$

Where P is the applied load (N) and d is the diagonal length of the Vickers indentation mark (mm). The average value of microhardness was calculated from a series of 10 indentations.

The differences between HyPS and CPS processes were evaluated in terms of Vickers hardness and indentation fracture toughness (IFT) after the micro-indentation test. The Vickers hardness values were calculated through the Equation 14, commonly used for GP samples [249].

The IFT values were deduced by measuring the characteristic cracks (median cracks) lengths and using the following formula provided by the theory of Anstis et al. [250]:

$$K_{IC} = 0.016 \cdot (\frac{E}{H})^{1/2} \cdot \frac{P}{c^{3/2}} \quad (15)$$

Where E is the Young's Modulus, H is the Vickers hardness value, P is the maximum load of the indentation test and c is the crack length of the indentation. The Young's Modulus was calculated from the reduced one (E_r), deduced from geometrical considerations of the unloading part of the indentation curve [251,252]. The median nature of the cracks was ensured by multiple polishing of the surface sample.

5. Results and discussions

5.1 Characterization of the raw materials

As often stressed throughout the introductory chapter of this thesis work, the GPs are aluminosilicate based materials, manufactured by means of chemical activation of aluminosilicate sources. The composition and microstructure of the primary resources are fundamental characteristics governing the final composition and microstructure of GPs, which in turns affects the physical and mechanical characteristics of the material. Therefore, the selection of the raw aluminosilicate sources and their dosage in the formulation is playing the role of primary importance in the determination of the properties and mechanical performance of this inorganic polymer.

The scope of this chapter is to address the reader a full investigation and description of the raw materials, i.e. FA and BSG, both in term of microstructure and chemical composition.

5.1.1 Chemical composition and microstructure of the powders

FA is a renowned and cheap aluminosilicate compound, being a by-product of an industrial process, due to the high amount of reactive silica and alumina in its composition. The chemical composition was determined through fluorescence X-ray (XRF) spectroscopy and the results are reported in Table 4. The content of calcium oxide (lime) was lower than 15 wt.%, render this FA classifiable under the notation class F, according to the international standards related to coal derivatives (see Chapter 2.6) [133,134]. The content of reactive silica and reactive alumina is 46.3 wt.% and 26 wt.% respectively, both in the average standards for this class of coal ash, what stands out is the content of iron oxide (~ 14 wt.%) beyond the average content in FA, which could negatively influence the geopolymerization reaction.

Table 4: Chemical composition of raw fly ash and borosilicate glass.

	SiO_2	Al_2O_3	B_2O_3	Fe_2O_3	CaO	K_2O	Na_2O	L.O.I [1]	Residues
Fly ash (wt.%)	46.3	26	-	13.9	3.5	3.9	0.2	0.7	5.5
BSG (wt.%)	72	7	12	-	1	2	6	-	-

[1]Loss of ignition (L.O.I.) – calculated through weight loss after fly ash firing.

The silica-alumina content of FA is not enough to guarantee a stoichiometric formulation of the GPs, therefore the addition of recycled silica-based glass to the formulation is a cheap solution to adjust the chemistry of the GP to a more precise recipe. Among all, BSG from recycled pharmaceutical vial cullet was selected as a reactive silica filler. The evaluation of the chemical composition of BSG was also performed through XRF spectroscopy and the results are reported in Table 4. The content of reactive silica (72 wt.%), almost double than the FA, ensures an easiness in chemistry adjustment with less consumption of material. Moreover, the presence of a low amount of alumina (7 wt.%) does not influence negatively this aspect. More interestingly, the high presence of borates

in the chemical composition (12 wt.%), conferring suitable properties for health & science, electronic and lighting applications, can provide, in dissolution stage, borate species which eventually take part into the geopolymerization, replacing the reactive alumina in its role [4].

The reactive silica/alumina phases are considered as such, mainly due to its partial glassy nature: indeed, it was demonstrated that the glassy phase is more readily dissolved in the alkali activator and thus it provides more ionic species to the system [253]. This means that the crystalline part contained in the raw materials contributes less efficiently to the geopolymerization than the amorphous phase. Notwithstanding that, it is worth of determining the crystalline microstructure of the FA (BSG is totally glassy), whose phases could transform into other crystalline phases at the end of the geopolymerization reaction, especially if *NaOH* is utilized as alkali activator. The crystalline phases of the tested material are readily determined by XRD spectroscopy, and Figure 30 reports the spectra of the FA. Compositionally, the FA has a relevant glassy phase content due to a severe exposition to high temperatures during ignition of the coal and sudden quench that the powder undergoes in the combustion chamber of the power plant (see Figure 19). This glassy phase, highly reactive in an alkali solution, is identified in the XRD spectra by a large hump comprehended between 20° and 40° (°2theta): the more intense the hump, the larger the amount of the amorphous phase. The quantitative determination of the content of each phase (including the amorphous phase) is carried out through the internal standard method, using an amount of crystalline alumina known a priori, and then calculate all the other phases knowing the crystalline alumina phase contribution [254]. The internal standard method revealed that almost half of the FA consists of an amorphous phase (44 wt.%, see Figure 30). The crystalline part of the FA is mainly composed by mullite ($Al_6Si_2O_{13}$) for the 21.5 wt.% of the crystalline portion of the FA, the sillimanite ($Al_2(SiO_4)O$) covering the 18.5 wt.% and the α-quartz (SiO_2) phase accounting for the 14.9 wt.% of the total crystalline phase (see Figure 30). This large amount of crystalline silica/aluminosilicate phase is consistent with the amount of silica and alumina detected in the chemical composition performed by XRF spectroscopy (Table 4). The 14 wt.% of the iron oxide, reported in the chemical composition is ascribed to hematite (Fe_2O_3) evidenced in the XRD spectrum, whose weight contents was 0.7 wt.%. This value of the iron oxide content detected through XRD is controversial, giving the 14 wt.% of Fe_2O_3 detected through XRF spectroscopy (Table 4). The detected amount of crystalline iron oxide is not enough to justify the weight content detected in the XRF analysis (14 wt.%), suggesting that the rest of the iron oxide not detected in the XRD analysis, could be amorphous.

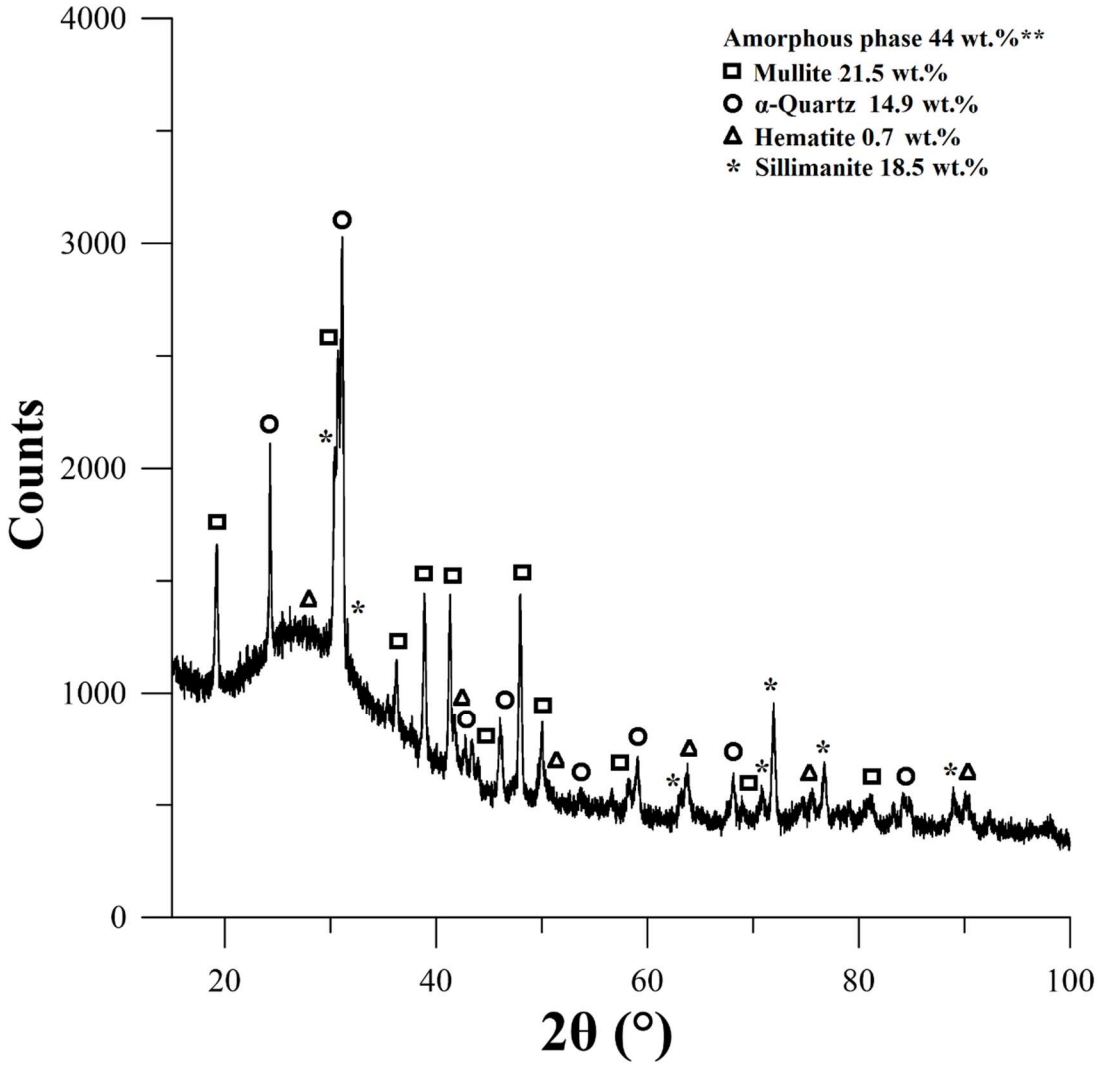

Figure 30: X-ray diffraction spectroscopic spectra of the fly ash. **Amorphous phase calculated through internal standard method [255]**.**

5.1.2 Morphology of the powders

The XRF spectroscopic analysis (Table 1) of the FA revealed a great diversity in the chemical composition and huge content of impurities, as this material is a derivative of natural fossil fuel. The large diversity in microstructure and the wide presence of impurities are also visible from the SEM micrographs reported in Figure 31 a-c, where a geometrical variety of the particles are appreciable from the overview image (Figure 31a), including shapeless particles and almost perfect spheres. The latter morphology is associated with aluminosilicate and silicate particles which form during the instant quenching of the ignited ash coming from the coal combustion following the high-temperature heat treatment in the combustion chambers. Figure 31b depicts a close up of one of these particles, whose surface looks perfectly smooth at the SEM, meaning that most of them have a glassy nature. Other important peculiarities are that, very often, they are also surrounded by smaller FA particles and that these spheres are mainly hollowed, and densely composed by a large deal of smaller FA sphere-like particles from inside

(Figure 31c). This morphology may help the reactivity of the FA during alkali activation, as once the outer shell is chemically attacked, the activator comes into contact with smaller particles with a higher specific surface, improving the dissolution of the FA. This mechanism will be evident when the morphology of GP samples will be investigated in details.

The microscopic appearance of the BSG powder (Figure 31d) is of random shape particles, typical of a brittle material processed through high energy ball milling (see Chapter 4.1). The high energy ball milling in alumina jar/balls is an efficient method to achieve micrometric grain size and suitable particles distribution. This characteristic will be treated in the upcoming sections, both for FA and BSG powders.

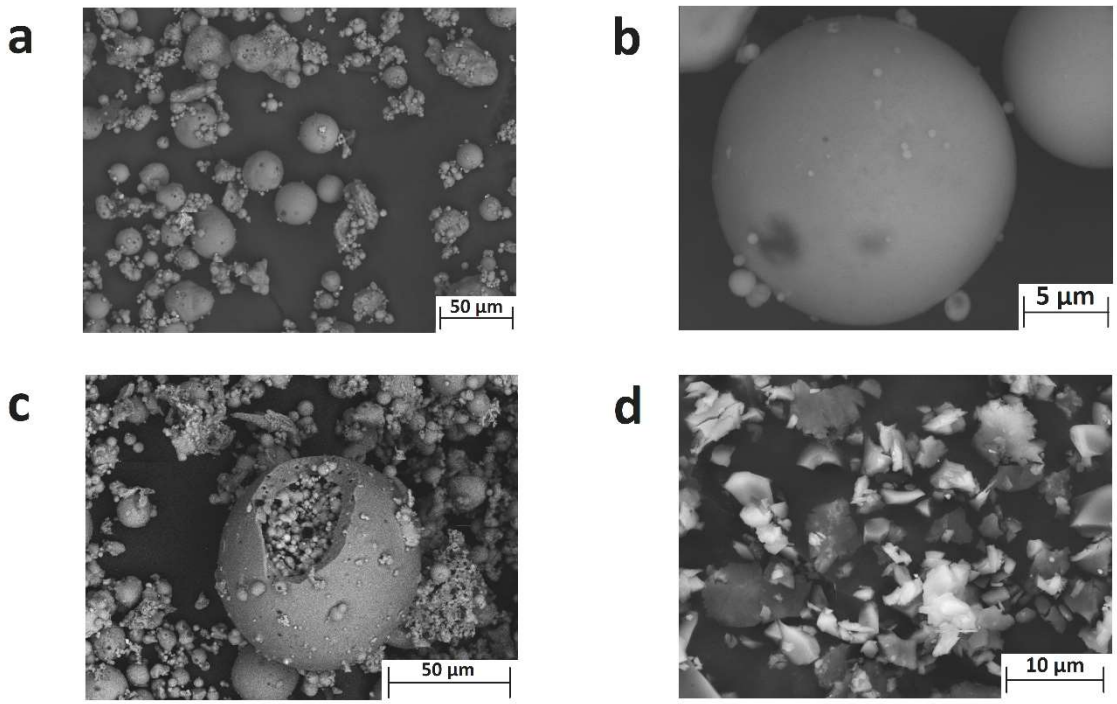

Figure 31: Scanning electron micrographs of the a) fly ash, b) fly ash particle, c) hollow fly ash particle and the d) borosilicate glass.

5.1.3 1-D Energy dispersive X-ray chemical analysis of the fly ash

The point EDS chemical analysis was conducted on different particles morphology in the attempt to couple the grain shape with the chemical nature of the material. The EDS analysis performed on several sphere-like particles evidenced that most of these particles are mainly aluminosilicate compounds, as depicted in the Spectrum 1 and 2 in Figure 32. Some of them are mainly silicate based particles, like the rounded grain analysed in Spectrum 3 in Figure 32. Figure 33, Spectrum 4, shows the presence of a rounded-like iron-based particle, in a content of about 14 wt.% (Table 4), while, Spectrum 5, shows a titanium-based particle, whose content was counted in the remainder site in XRF analysis (Table 4).

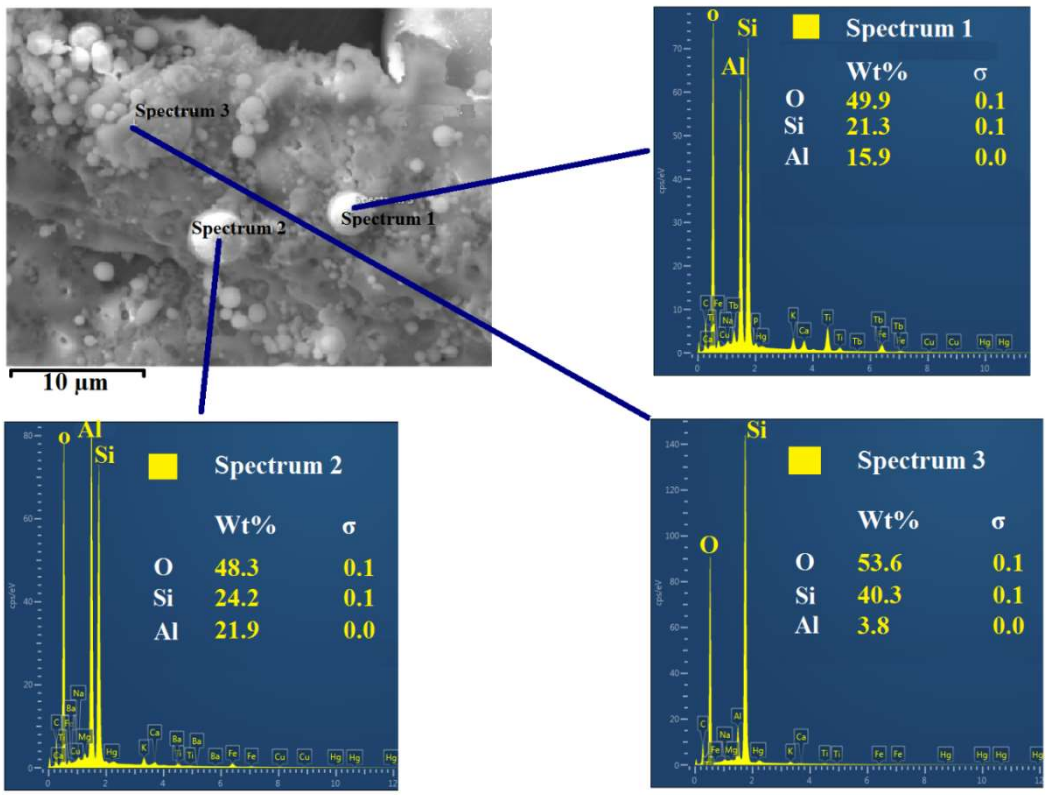

Figure 32: Energy dispersive X-ray chemical analysis of the sphere-like fly ash particles.

5.1.4 Density, specific surface and grain size of the powders

The evaluation of the density of a powder is a challenging calculation, especially if the powder is inhomogeneous and holding many impurities, like the FA. Smooth and quite precise results of the density can be provided by the pycnometer test, consisting of measuring the powder volume appropriately inserted in a chamber in which a gas is introduced. The precise measure of the powder weight is then coupled with the volume measure, so as to have an overall precise measure of the density. Both the FA and the BSG were measured through the pycnometer method, giving values of 2.35 g/cm^3 and 2.23 g/cm^3 respectively, as reported in Table 5.

As previously mentioned in Chapter 2.4, a characteristic of the powder which greatly influences the reactivity during the dissolution stage is the grain size: a finer particle, having a larger specific surface area is more easily attacked by the alkali activator [256]. Therefore, increasing the fineness of the powder improves the efficiency of the geopolymerization. This is always true when AAMs or GPs are produced using uniquely FA. The situation becomes more complicated when several raw sources are utilized, like in the case of the present thesis. The reactivity of the powders is not only affected by the fineness, but also by the chemical composition and the microstructure. This means that the two distinct powders may have different kinetics of dissolution: a focused study on the dissolution kinetics of the FA and BSG would widely facilitate the study of the geopolymerization of this system. The point is to have similar rates of dissolution of the

powders: this peculiarity may avoid inhomogeneous product of geopolymerization, incomplete reaction and preferential dissolution of the more reactive powder. The latter issue induces consumption of the Na^+ cations in favour of one compound, preventing the other to dissolve and react.

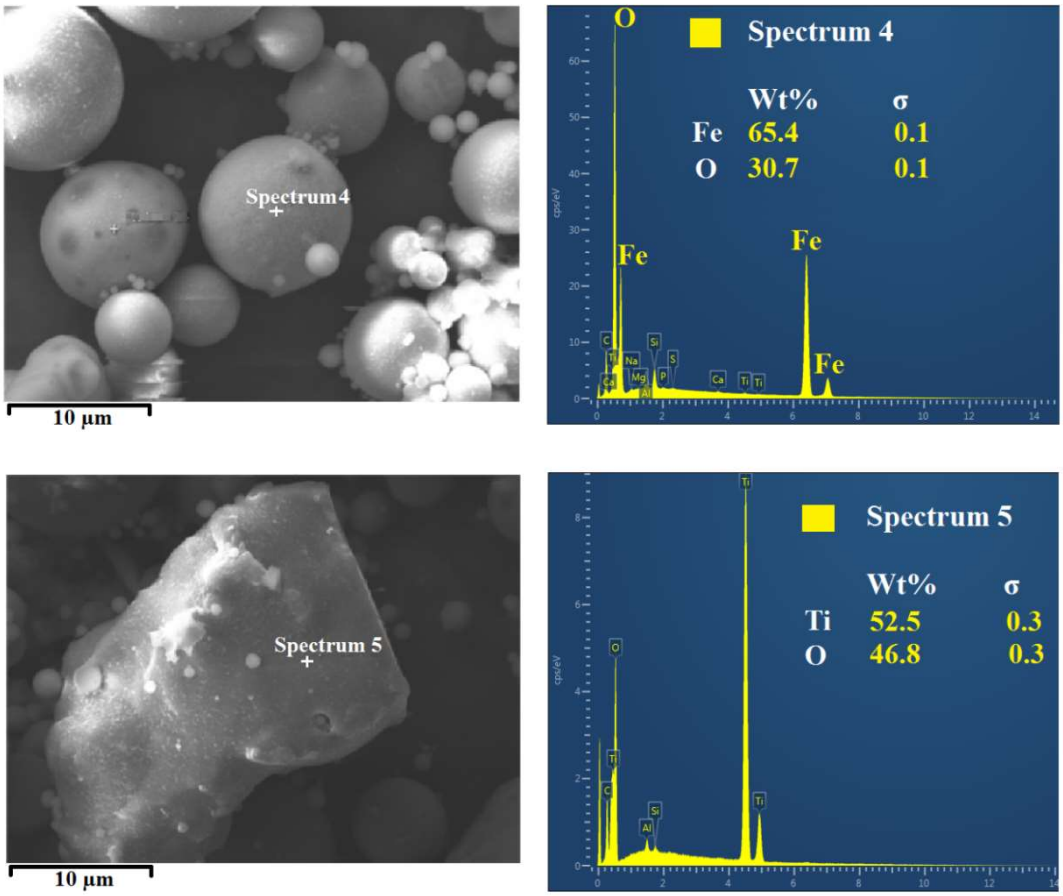

Figure 33: Energy dispersive X-ray chemical analysis of the impurities in fly ash.

Giving that, the BSG was ground using two velocities of rotation in milling (350 and 400 rpm), we came up with to two different grades of fineness. The specific surface area, i.e. the indicator of the available surface to alkali-attack, was measured using the Brunauer-Emmet-Teller (BET) theory, which is also based on the absorption of gas molecules on a solid surface. The values associated with these two milling energy are reported in Table 5: if lower energy was used (350 rpm), the available specific surface area was calculated to be 0.23 m^2/g, but this value considerably increases up to 0.71 m^2/g if the powder was milled at 40 rpm. The BET analysis was also carried out on FA, giving a value of 2.65 m^2/g, which is more than three times higher than the high energy ball-milled BSG value, and even 10 times larger than the low energy ball-milled BSG value. This result must be weighted with the kinetics of the reaction of each powder: being the BSG more reactive than FA, the latter must be finer in order to have homogeneity in dissolution. The experience gathered in the lab helped to have a better homogeneity in dissolution for the mix FA and 400 rpm ball-milled BSG: indeed, only this BSG batch was used in GP

manufacturing, and in the following paragraphs, the authors will only refer to the 400 rpm ball-milled BSG.

Table 5: Density, specific surface and grain size (50% of probability) of the fly ash and borosilicate glass milled according to two different rotating speeds (350 and 400 rpm).

Powder	**Density (g/cm^3)**	**BET* Specific Surface area (m^2/g)**	**Grain size d_{50} (μm)**
Fly ash	2.35	2.65	22.24
BSG (35 rpm)	2.23	0.23	/
BSG (400 rpm)	2.23	0.71	5.09

* Brunauer-Emmet-Teller method

The double check of the specific surface area measurements was accomplished through laser diffraction technique, for the assessment of the grain size distribution. Surprisingly, the average grain size (values associated with the d_{50}, i.e. 50% of probability of distribution) calculated for FA and BSG are discordant with the results related to the BET method. Table 5 reports 22.24 and 5.09 μm for FA and BSG respectively, suggesting that the BSG might be finer than FA. This misleading result has to be interpreted taking into account some constraints related to laser diffraction technique, being an approximated method of grain size measurement, since the size of each particle passing through the gas based He-Ne laser is measured by diffraction of the laser light, therefore the equipment approximates each particle as a spherical one [147]. The hollowed shape of the sphere particles, like those depicted in Figure 31c, is not treatable through this technique, as the smaller particles inside the hosting hollowed sphere are not detectable. In contrast, the absorption of the gas in the BET method is undergone by each particle, regardless of their arrangement, thus it is inferred that the BET method is more reliable for FA. Nevertheless, the distribution curves in Figure 34 indirectly confirms what uttered before: the FA distribution curve presents a smaller hump about 1 μm (highlighted in blue in Figure 34) beside the main one, comprehended between 5 and 800 μm. This hump is associated with the few particles set free in suspension during the sonication, although they are only a small part of the total, as the dispersion is very inefficient.

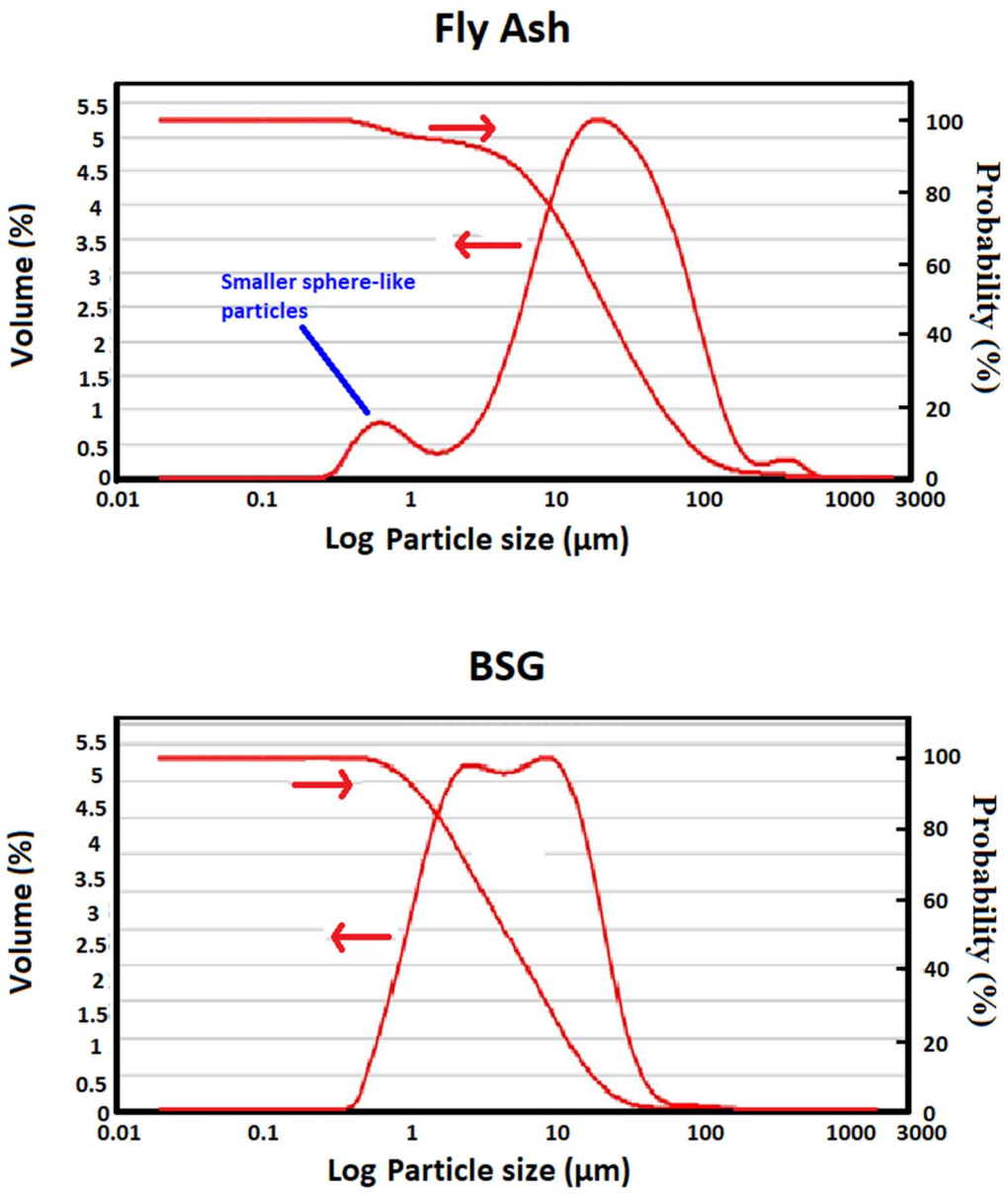

Figure 34: Grain size distribution of the fly ash and borosilicate glass powders.

The laser diffraction spectroscopy is rather more reliable for the BSG powder grain size distribution analysis, except for the particle shape approximation. Indeed, the second plot reported in Figure 34, related to the BSG, is continuous and smoother than the FA distribution, rendering the value (5.09 µm) in Table 5 a reliable one.

5.1.5 Characterization of the cellulose fibres

The cellulose fibres were used as given in the manufacturing of the GPs samples and dispersed appropriately to unravel the bundles and produce a homogenous composite material. What is playing a predominant role in the mechanical properties of the composite is a dispersion of the fibres, the fibres nature and the size of the fibres. Even dispersion of the fibres and the unraveling of the bundles is of paramount importance as they optimize

the fracture mechanisms associated with composite materials (crack bridging and pull out of the fibres) and homogenize the occurrence of them throughout the material. These restrictions are accomplished by high energy sonication in an aqueous suspension, as described in Chapter 4.1 (Figure 27).

The length and the nature of the fibres govern the efficiency of these mechanisms, as the extent of crack bridging is strictly dependent on the fibres nature and their average size on one hand, and the pull out mechanism efficiency is related to the interactions between the fibre surface and the composite matrix, and the size of the fibres too. The assessment of the average size of the cellulose fibres was carried out through direct measurement of the fibre length from SEM images observation. The minimum measurements were set to be 200. Figures 35a-b depict two examples of the SEM images collection at low (150 x) and higher (300 x) magnification of the cellulose fibres, in order to be accurate in the measurement of longer and shorter fibres. Indeed, Figure 35b depicts some short fibers with longer ones: this is indicative of a spread size distribution. By averaging the whole measurements, the calculated average length was found to be approximately 0.5 mm. The fibres diameter was not calculated using the same method due to lack of accuracy, therefore the mean diameter provided by the supplier and reported in Chapter 4.1 (i.e. 40 μm) was considered.

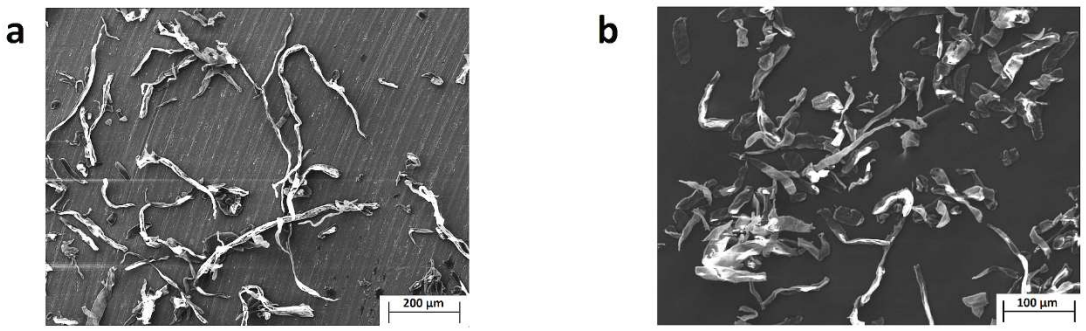

Figure 35: Scanning electron microscope micrographs of the cellulose fibres at a magnification of a) 150x and b) 300x.

5.2 Microstructural and chemical characterization of geopolymers

The first step to be taken in the accomplishment of the GPs and AAMs samples characterization is to define the microstructure, in terms of morphology and chemical composition. The SEM/EDS spectroscopy analyses of both the fracture surface and a polished surface of the GP sample help to define the morphology of the crystalline and amorphous phases, together with the degree of reaction (extent of the geopolymeric product), while they give some preliminary insight of the chemical composition of each phase. The nature of the crystalline phases is given by XRD diffraction spectroscopy.

In geopolymerization, what is really important, besides the degree of reaction, is the chemical connectivity of the semi-amorphous phase. Despite the overall idea of the microstructure and chemical composition provided by SEM/EDS and XRD spectroscopies, these analyses are not enough to determine the exact quantity of silica/alumina and how the silicon connects to other elements (aluminium and boron) through oxygen bridging bonds, i.e. the degree of connectivity [23,79,257]. This information is totally given by FTIR and ^{29}Si NMR spectroscopy, the former analyzing the type of bonds present in the microstructure and the latter investigating the chemical ambient surrounding a single silicon element. The nomenclature of each single silicon ambient is performed by a specific designation adopted for ^{29}Si NMR analysis, already described in details in Chapter 2.4.4. The degree of connectivity is, instead, determined for aluminium and boron through ^{27}Al NMR and ^{11}B NMR spectroscopy respectively.

In this chapter, a detailed investigation of the microstructure of the Mix-1 formulation GP sample is reported, aiming to highlight the type of connectivity and the ions participation in geopolyemrization. The role of boron in geopolymerization will also be demonstrated.

5.2.1 Microstructure

The semi-amorphous nature of the product of geopolymerization is deducible by observing the morphology of microstructure of each GP batch, reported in Figures 36a-f. Regardless of the adopted formulation, the microstructure of each sample evidences a typical morphology of the geopolymeric product, showing a poor presence of crystals, suggesting a high presence of amorphous phase. This deduction will be quantitatively demonstrated by XRD spectroscopy.

The production of crystals is associated with the process of geopolymerization, whose presence is associated with either pre-existent crystalline phase held by FA (as demonstrated by the FA XRD spectrum in Figure 30), or formation of new crystals during geopolymerization. The last option justifies the scientific community to define the product of geopolymerization as semi-amorphous phase [88]. The formation of new crystals will be analysed in details through XRD and EDS spectroscopy in the next paragraphs, as they are not easy to observe only from a large overview of the microstructure.

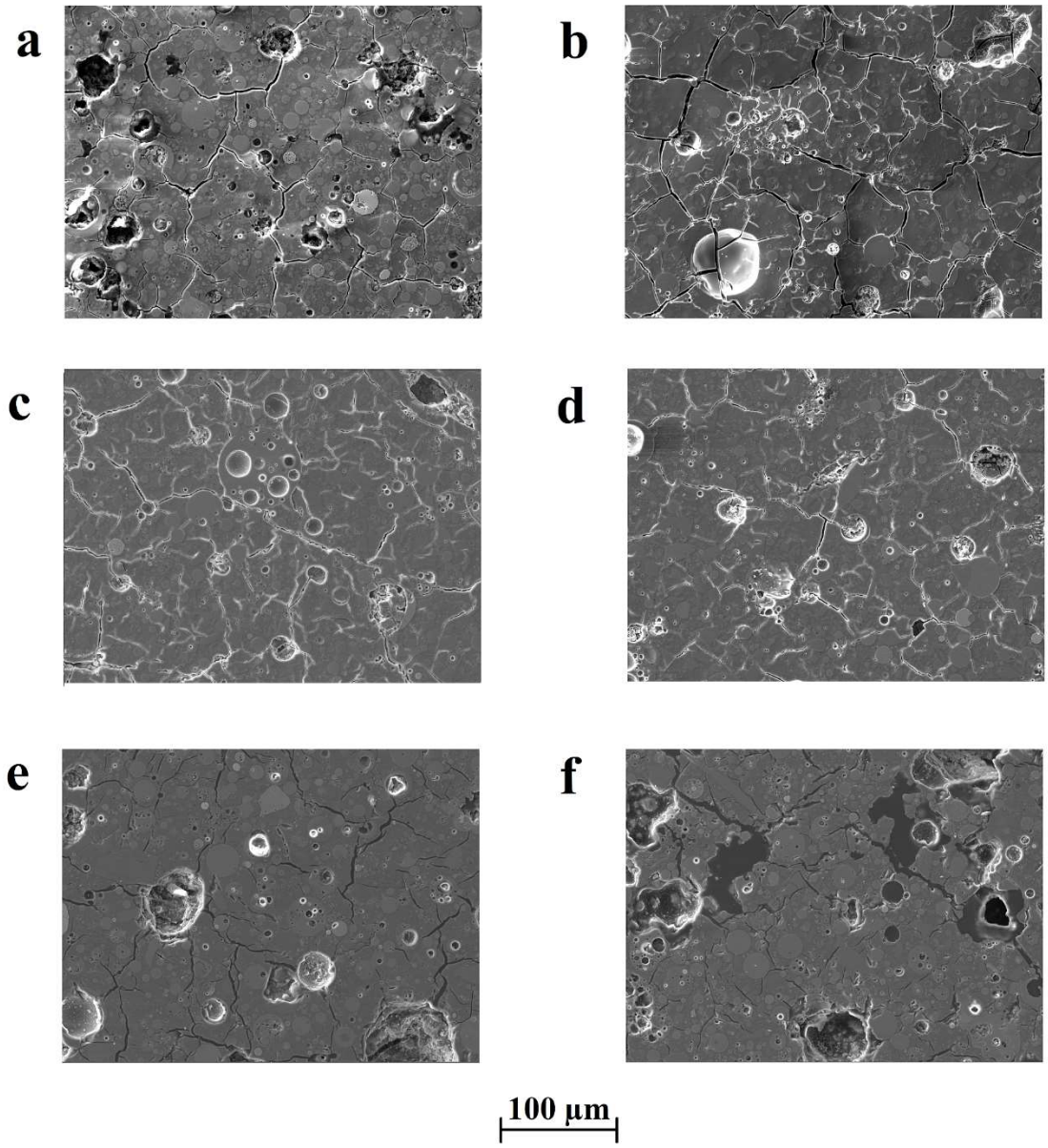

Figure 36: Secondary electron pictures of the polished surfaces of a) Mix-1, b) Mix-2, c) Mix-3, d) Mix-4, e) Mix-5 and f) Mix-6. All the images were reported with the same magnification (the marker applies for each picture).

The analysis of the microstructure of the GP samples (from Mix-1 to Mix-6) has not provided sufficient insights to be drawn from the observation of the image, since the microstructures look quite alike. However, few slight differences could be observed, such as the amount and the morphology of closed porosity and cracks. Mix-1 (Figure 36a), for instance, presents a regular amount of pores and cracks, but when the BSG content in the formulation is increased, as in Mix-2 in Figure 36b, the presence of cracks visibly increases, while the porosity seems to remain the same. In Mix-3 (Figure 36c), the BSG content was increased up to 60 wt.%, thus inducing an apparent increase of both the porosity and cracks, but the microstructure gets better if a Mix-4 formulation is adopted, as reported in Figure 36d. The increase of the curing time of the Mix-2 formulation, giving

rise to Mix-5 sample (Figure 36e) is accompanied by a formation of larger closed pores, a characteristic equally observed also in Mix-6 (Figure 36f).

One of the main issues of geopolymerization is to optimize the reaction as efficiently as possible. This would ensure the high provision of a geopolymeric product, which helps to obtain a continuous matrix and the least defects formation. Unfortunately, this is not totally possible to achieve, and the inefficiency of reaction, due to the inefficiency of the dissolution stage, is one of the factors, leading to a prominent presence of unreacted particles, like those sphere-like FA particles, especially depicted in Figure 36a. This detail is also observable in the other mixes, and the more the BSG content, the higher the number of unreacted BSG particles, and eventually entrapped in the geopolymeric matrix.

5.2.2 X-ray diffraction and energy dispersive spectroscopy

The geopolymerization process does not only yield an amorphous binder as a product of the rearrangement of the dissolved aluminosilicate species but also induces the formation of some crystalline phases, part of them as a side effect of the elevated alkalinity of the solvent.

To investigate the new phases formed during and after geopolymerization, the XRD spectra (Figure 37) were obtained also for the GP samples and put in comparison with that of the FA reported previously (Figure 30). A change of the crystallinity, both quantitatively and qualitatively, is evident from the analysis of the two spectra, where the most significant changes were observed for the mullite ($Al_6Si_2O_{13}$) phase, α-quartz (SiO_2) phase and sillimanite ($Al_2(SiO_4)O$) phase, all of them experiencing a clear decrease, irrespective of the type of mixture. In contrast, the amount of amorphous phase always increases, from the 44 wt.% detected in the FA XRD spectrum, depicted in Figure 30.

From this interpretation, two possible mechanisms happening in geopolymerization process:

1- The amorphous phase of the FA totally dissolves along with part of its crystalline portion;
2- The increase of the amorphous phase in GP samples is highly supplied by the presence of BSG in a different amount, contributing to the percent decrease of the crystalline phases in the microstructure (no dissolution of the crystalline phases).

To better understand these mechanisms, one might observe and compare the XRD spectra of the GP samples in Figure 37. If the mechanism 2 was to mainly occur, one would expect a linear proportional increase of the amorphous phase, and concurrently a decrease of the crystalline phases, with the increasing addition of BSG in the formulation. This is not clearly happening, as the amorphous phase amount decrease from Mix-1 (83.9 wt.%) to Mix-2 (78.5 wt.%), having a higher amount of BSG. The same could be uttered for the amorphous amount of Mix-3 and Mix-4 (87.1 wt.% and 85.0 wt.% respectively). From this observation, it is deduced that the crystalline phases of FA are active contributors in

geopolymerization. It is still questionable whether or not the new amount of crystalline phases is only a result of the dissolution or a combination of their dissolution and rearrangement after geopolymerization. However, the mullite and the sillimanite phases display no smooth trend of their content from Mix-1 to Mix-4 (Figure 37), especially showing depletion of sillimanite when the mullite is higher in percentage, like happening in Mix-2 (mullite 16.4 wt.% and sillimanite 0.1 wt.%). The trend of α-quartz content remains approximately constant through the spectra, suggesting very limited reformation of this phase after dissolution. The presence of other phases, including calcium-based oxides and hematite (Fe_2O_3), remains nearly the same, always below 1 wt.%.

Focusing on the formulation with longer curing time (Mix-5) and lower alkalinity (Mix-6), it was noticed that a higher amorphous content results in 10 M *NaOH* solvent, i.e. 88 wt.%, coinciding also with the larger amount of amorphous phase among all the mixtures. For a longer time of curing, a higher formation of crystallinity was detected (amorphous phase was calculated to be 80.1 wt.% through internal standards). Indeed, the Mix-5 holds a considerable percentage of mullite (13.2 wt.%), almost as high as the Mix-2 (6.4 wt.%, the highest), most likely part of that formed during geopolymerization. In Mix-5, the tendency to have almost depleted sillimanite (0.5 wt.%) higher content of mullite with respect to the average repeats. Low content of sillimanite was detected also for Mix-6, though the mullite content is moderate, suggesting that the extensive formation of the amorphous phase is followed by a limited formation of crystals. Also, in this case, the content of crystalline silica is approximately constant. On the contrary, in the Mix-5, the amount of secondary phases (other phases in Figure 37) is more prominent, suggesting a slightly more pronounced attitude to crystals formation if the curing stage is prolonged.

Regardless of the formation of crystals, it must be borne in mind that the main product of geopolymerization is the amorphous aluminosilicate matrix. The halo appearing in all the FA and GP samples spectra is a fingerprint of the amorphous phase. The shift in the halos of the GP samples spectra is merely a consequence of the geopolymerization reaction, having the characteristic to have a halo in the range of 25° and 45°, whereas the characteristic hump in FA spectrum falls between 20° and 40° [101].

Concerning the other crystalline contributions, the hematite does not involve any significant change, but new phases are formed from scratch after geopolymerization, that is calcium silicate ($Ca_2(SiO_4)$) about 4.3 wt.% and sodium carbonate ($Na_2(CO_3)\cdot H_2O$), whose content is as high as 19.1 wt.% after activation. The first phase is associated with the formation of crystalline C-(A)-S-H chains, quite common in Ca-based AAMs and cement (OPC), due to the presence of lime (*CaO*) both in FA (3.5 wt.%) and BSG (1 wt.%) (see Table 4). The second one is a product of the efflorescence process, that is the migration of sodium-carbon based salts to the surface of the sample. As previously mentioned in Chapter 2.3.6, this is a phenomenon ordinary happening in AAMs and GPs activated at a high level of alkalinity, which does not have any influence on the mechanical properties of the material, but its presence is only negatively taken due to aesthetic reasons.

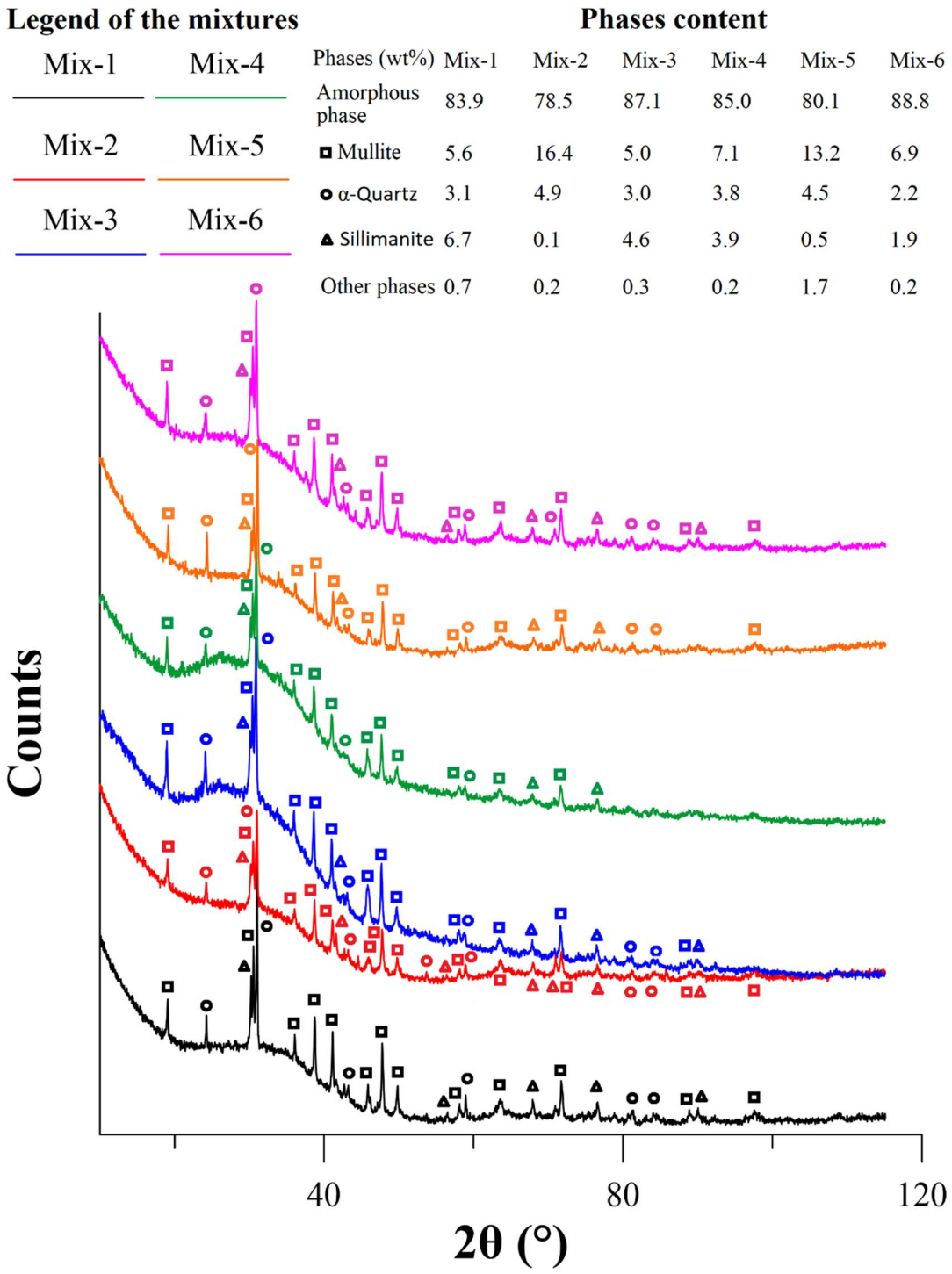

Figure 37: A comparison of the X-Ray diffraction spectra of the GP samples (from Mix-1 to Mix-6).

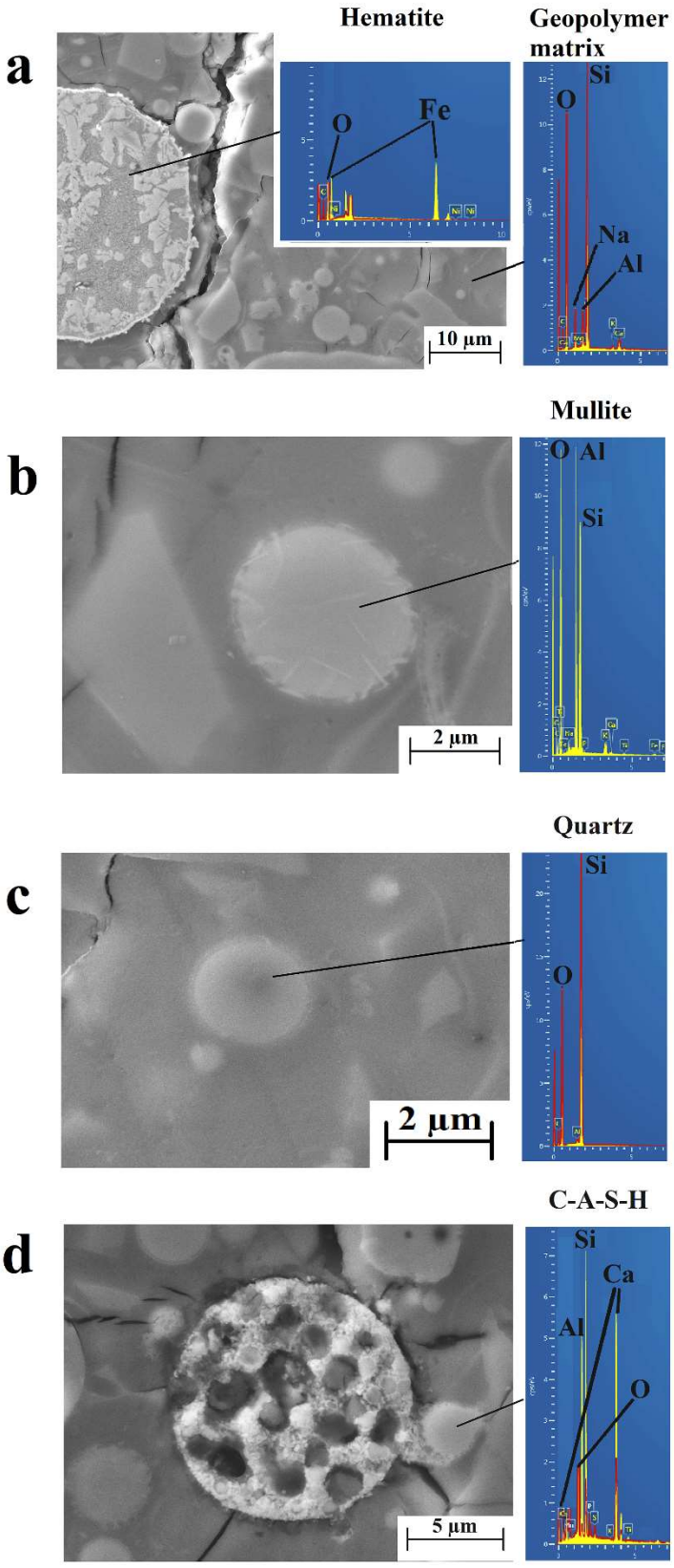

Figure 38: Energy dispersive analysis of a) hematite and Geopolymer matrix, b) mullite, c) quartz low and d) calcium silicate (C-S-H).

The detected phases were also sought at the SEM microscopy and their nature was deduced through EDS chemical composition. Figure 38a reports an example of hematite particle, which remained unchanged after geopolymerization, as observable from the grain boundary (there is no interaction with the matrix). In the same figure, the chemical composition of the geopolymeric product (vitreous phase) was also detected, showing that it is a sodium-aluminosilicate-based compound, richer in silicon. In the case of crystalline phases produced during geopolymerization, the mullite phase is the main product, like the one depicted in Figure 38b, whose chemical composition is an Al-rich aluminosilicate, with no Na^+ cations associated. The quartz low remained unchanged, except for a minimal dissolution during alkali attack, but being a silicon-based material, it is expected to produce a sort of chemical interaction with the matrix, as exposed in Figure 38c. Finally, C-S-H particle was observed and reported in Figure 38d (not to be confused with the bigger crystalline particle, which was seen to be hematite).

5.2.3 Fourier transform infrared analysis

The analysis of the chemical composition of the GP matrix performed through EDS is a qualitative tool to understand the nature of this compound, but it is not enough to define its chemical structure and the steps it took to get there. If some more insights are required concerning the type of chemical bonds and the way each element rearrange in the geopolymeric structure, FTIR and NMR spectroscopies are necessary.

FTIR spectroscopy uses the absorbed infrared radiation emitted by the machine to establish the type of chemical bonds in the microstructure, by coupling the quantity of absorbed light with the energy required by a single bond to excite. The type of chemical excitations are bending and stretching vibrations, the latter in turn can be symmetric or antisymmetric [258]. The comparison between the FA FTIR spectra with the one from GP sample may help to understand the dynamics of geopolymerization, by analyzing the newly formed chemical structure (in terms of bonds) after reaction [259]. The range of wavelengths was taken between 400 and 4000 cm^{-1}, as the main radiation absorption is comprehended in this frame for GP-like compounds [121].

In Figure 39 are depicted both the FA and the GP sample spectra, together with the detection of each absorption bands and their wavelength. Starting from the FA spectra, the most meaningful absorption picks are below the 1000 cm^{-1} wavelength. The portion of the FTIR spectrum underneath 700 cm^{-1} is also known as mid-infrared (mid-IR) spectra [104,136]. Sitarz et al. have done an extensive and clear study of the excited bonds in the mid-IR region for aluminosilicate-based materials and they have found that, in this region, only simple species can vibrate, like dimers, oligomers, single and double ring species [103,104,260,261]. In FA materials, most parts of the bond vibrations fall in this range, as depicted in Figure 39. According to Sitarz et al., the most sophisticated ring species absorb radiation at a lower wavelength, suggesting a weaker bond. Therefore, the 6-membered rings have a characteristic absorption band within 550 and 600 cm^{-1}, the 4-membered ring at about 640 cm^{-1} and the 3-membered ring within 720-700 cm^{-1} [104,262]. In the FA spectrum, an intense absorption band is evident at ca. 555 cm^{-1}, meaning that the FA holds

a sizeable amount of the 6-membered ring elements. The presence of other ring species is not prominent, except for a slight shoulder located at 720 cm^{-1} connected to the 3-membered ring elements. The band at 466 cm^{-1} is, instead, related to in-plane bending vibration of Al-O and Si-O oligomeric species [263,264].

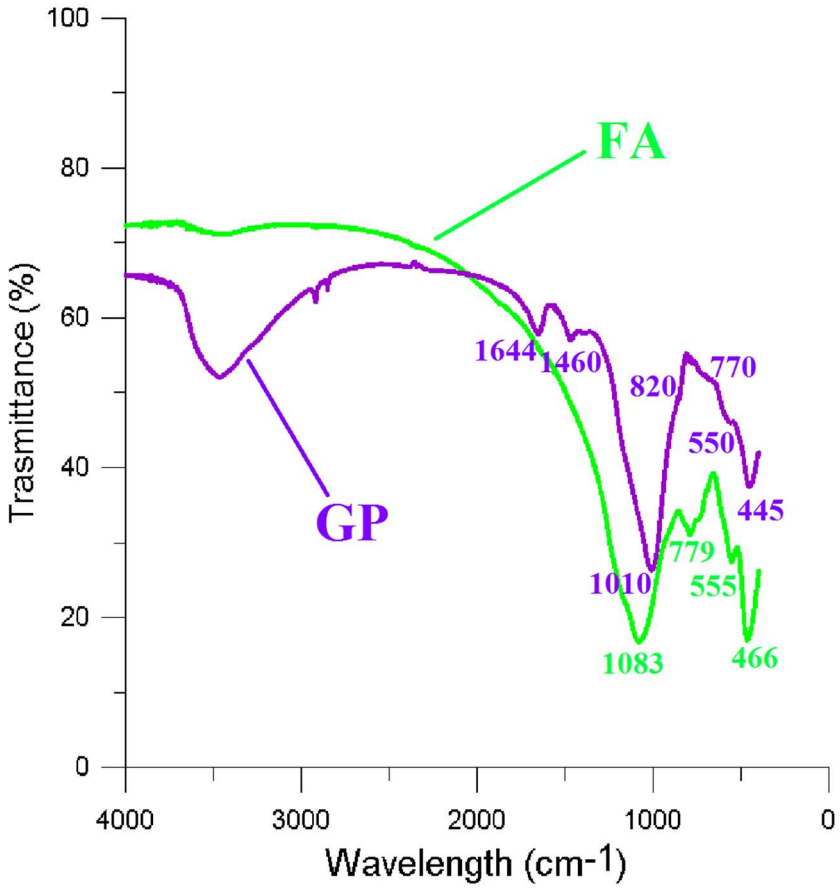

Figure 39: Fourier transform infra-red spectroscopy of the fly ash (FA-green solid line) and the Mix-1 geopolymer (GP-purple solid line).

Outside the mid-IR region, the most noticeable absorption bands vibrate at 779 cm^{-1} and 1083 cm^{-1}, both attributed to Si-O-Si(Al) stretching vibration, symmetric and asymmetric respectively [107,264–266]. Specifically, the second one is the characteristic band associated with aluminosilicate-based materials, and it incorporates several signals coming from silicon chemical ambient [107]. These signals are those detected by the ^{29}Si MAS NMR spectroscopy, and they will be analysed in details in the next paragraph (see also Chapter 2.4.4). Generally speaking, the more the band is shifted toward higher wavelengths, the more structured the aluminosilicate network is [107,265].

The GP spectrum presents more absorption bands than the FA spectrum at higher wavelengths, whereas it remains almost unchanged in the mid-IR region, except for the fact that the absorption bands are slightly shifted to the right (lower wavelength). The symmetric Si-O-Si(Al) stretching vibration is almost depleted, although a slight shoulder is

visible at 770 cm^{-1}. The characteristic band is, instead, shifted slightly towards lower wavelengths (1010 cm^{-1}), suggesting that the geopolymeric matrix might have a less intricate network, with a higher level of hydration (more Si-OH terminal bonds) [107]. This observation was confirmed by the broad band between 2066 cm^{-1} and 3400 cm^{-1} associated with stretching vibration of –OH group (silanol). The band at 1644 cm^{-1} is attributed to constitutional water, related to bending vibration of the H-O-H bonds [107,262,267,268]. The effect of the efflorescence reveals at the GP spectrum through the 1460 cm^{-1} absorption band, attributed to the bending vibration of O-C-O bonds (carbonation) [267,269]. Finally, a small shoulder was detected at 820 cm^{-1}, associated with the vibration of the B-OH tetrahedral boron species, whereas no signal was identified for the presence of the trigonal borate, whose characteristic bands usually are located at 1280 and 1420 cm^{-1}: the first band is of difficult identification due to the broad characteristic band at 1010 cm^{-1}, while the second does not appear at all [270–273]. This observation will turn out useful in the analysis of the ^{11}B MAS NMR spectra (next paragraph).

5.2.4 Nuclear magnetic resonance spectroscopy

For a better understanding of the chemical coordination and structural configuration of the single element, playing a predominant role in geopolymerization (Si and Al), the results from NMR spectroscopy are normally coupled with those from FTIR spectra.

Being the silicon (Si) the most plentiful and important element in the network formation, the chemical nature of the geopolymeric matrix structure is firstly defined by the ^{29}Si MAS NMR spectroscopy, whose spectra are reported in Figure 40. The comparison with the FA (Figure 40) says how the active aluminosiliciate compound evolves during geopolymerization, so as to identify the geopolymeric matrix. The spectra were also appositely deconvoluted through specific software (see Chapter 4.2.2) in order to identify the contribution of each signal. The silicon ambient was designated according to the $Q^n(mAl)$ notation, previously exposed in Chapter 2.4.4. Starting from the FA spectrum, one can notice that it holds several signals at high ppm and an intense one at -110 ppm. The resonance signals from -84 to -104 ppm are related to the different vitreous and crystalline structure of the Si in Q^2 and Q^3 configuration [4,87,99,268]. The -100 ppm peak is a $Q^4(0Al)$ amorphous ambient, whereas the shoulders produced by the -114 and -118 ppm are the crystalline configuration of the same ambient [4,87,99]. From the calculation of the relative content of each Si species, it was found that the most part of the spectra is composed by Q^3 and Q^4 species (more than 60%, see table beside the FA spectra) which is in accordance to the left-shifted characteristic band in FA FTIR spectrum in Figure 39.

The evaluation of the GP spectrum in Figure 40 is not trivial due to the contribution of many forms of silicon states, both in an amorphous and a crystalline phase. To simplify the deconvolution of the spectra, the crystalline contributions were ignored, as the geopolymeric product is mainly amorphous (see Chapter 5.2.2). From the literature, it was found that the resonances associated with low ppm signal (from -100 ppm to -115 ppm) are mainly $Q^4(0\text{-}1Al)$ species, whereas, at high ppm, the signals may be attributed to Al-

rich silicate species ($Q^4(2\text{-}4Al)$) [87,99]. These signals are listed in the table beside the GP spectra in Figure 40.

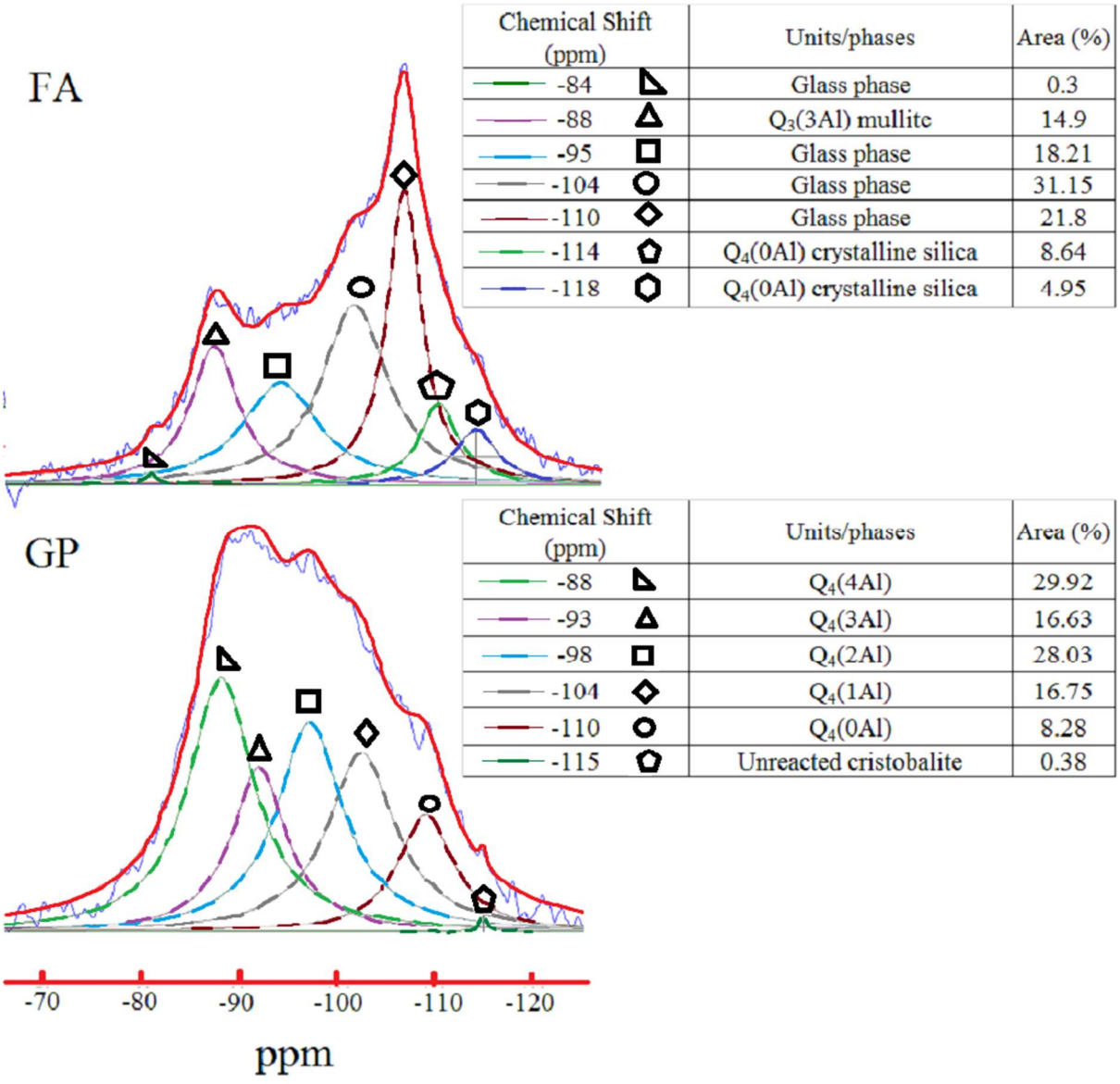

Chemical Shift (ppm)	Units/phases	Area (%)
-84	Glass phase	0.3
-88	$Q_3(3Al)$ mullite	14.9
-95	Glass phase	18.21
-104	Glass phase	31.15
-110	Glass phase	21.8
-114	$Q_4(0Al)$ crystalline silica	8.64
-118	$Q_4(0Al)$ crystalline silica	4.95

Chemical Shift (ppm)	Units/phases	Area (%)
-88	$Q_4(4Al)$	29.92
-93	$Q_4(3Al)$	16.63
-98	$Q_4(2Al)$	28.03
-104	$Q_4(1Al)$	16.75
-110	$Q_4(0Al)$	8.28
-115	Unreacted cristobalite	0.38

Figure 40: ^{29}Si magic angle spinning nuclear magnetic resonance spectra of fly ash and geopolymer sample Mix-1.

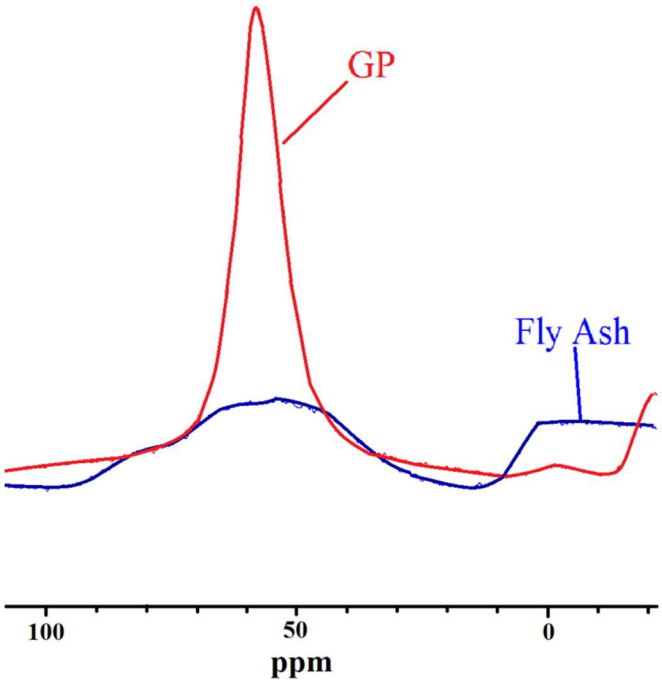

Figure 41: ^{27}Al magic angle spinning nuclear magnetic resonance spectroscopy of the fly ash and the Mix-1 geopolymer sample.

The key to understanding the efficiency of rearrangement of dissolved silicate and aluminate species during polycondensation is based on the determination of the coordination number of the elements – in case of the silicon, this analysis is meaningless as it holds only a tetrahedral configuration. The aluminum can, instead, have both octahedral (6-fold coordination) and tetrahedral configuration (4-fold coordination) – the first one is the base aluminum coordination of crystalline α-alumina, the second one is the coordination that the aluminum assumes when it combines with silicon to form crystalline phases (kaolinite, Na-feldspar, dickite) and/or an amorphous phase [274,275]. Therefore, ascertaining an excess of tetrahedral boron after geopolymerization is direct evidence of the chemical rearrangement of the aluminates during the polycondensation reaction. The way to detect this change is through ^{27}Al MAS NMR spectroscopy of the raw material (FA) and GP sample, whose spectra are reported in Figure 41. From the plot of the FA spectra, one can see two main resonance signals, one at +3 ppm, related to 6-fold coordination, and one at +53 ppm associated with 4-fold coordination [274,276,277]. The resonance associated with octahedral aluminium is cantered close to 0 ppm, since the α-alumina structure is taken as standard. After the geopolymerization reaction, the intensity of this signal decreases in favour of a more intense signal of the tetrahedral aluminium, meaning that the dissolved aluminate species totally rearrange in a tetrahedral configuration, to recombine with silicates during polycondensation process.

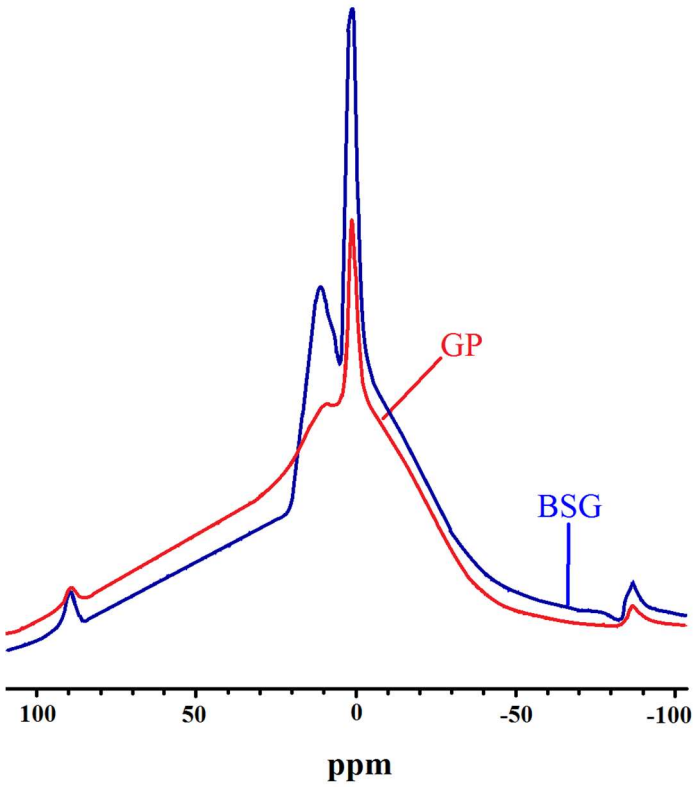

Figure 42: ^{11}B magic angle spinning nuclear magnetic resonance of the borosilicate glass and the Mix-1 geopolymer sample.

Until now, in the whole spectroscopic analysis, the contribution of the BSG was almost ignored, except for a small signal detected in the GP FTIR spectra in Figure 39. The choice to incorporate recycled BSG in the GP's formulation was not only dictated to the chemical adjustment of the silica to alumina (SiO_2/Al_2O_3) ratio but also to introduce in the network another possible player, i.e. the boron. Indeed, the BSG is rich in borate contents (12 wt.%, see Table 4), and giving the chemical affinity of this element with aluminium (same column in the periodic table), it is reasonable to believe that the boron could actively participate in geopolymerization in the same way the aluminium does. Based on this observation, the participation of the borates (BO_4^-) species was demonstrated according to the same rationale as before. For this purpose, the ^{11}B MAS NMR spectroscopy was performed on raw BSG and GP sample, whose plots are shown in Figure 42. The intense hump characterizing both spectra is a background noise due to the interference of the borosilicate-based rotor mounted in the NMR machine – being equally intense for both the analyses, it is easily ignored. The BSG spectra (blue solid line) evidences two main peaks – one at +10 ppm attributed to trigonal coordinated boron, and one more intense at 0 ppm related to the resonance of the tetrahedral coordinated boron [130,278–280]. The GP sample spectroscopy (red solid line Figure 42) leaded to a spectra almost nil in +10 ppm resonance signal in favour of a more intense 0 ppm signal, demonstrating for the first time that the boron is an active element in geopolymerization process, and the borates are building blocks of the inorganic polymeric network resulting from the polycondensation reaction [4].

5.3 The effect of the processing parameters on the geopolymerization process

5.3.1 The silica to alumina ratio and α coefficient

In the attempt to couple the mechanical properties of GP samples with the methodology of manufacturing and parameters influencing the geopolymerization reaction, different mixtures, chemistry, and curing conditions were adopted. The geopolymerization process was tuned by considering the influence of the SiO_2/Al_2O_3 ratio, the molarity of the alkali solution, and the soaking time and humidity during curing, although the parameters influencing the process also include the temperature of curing, nature of the alkali solution, silica-to-alkali ratio, liquid-to-solid ratio, and so forth. In this thesis work, the pressure was also accounted for the first time as an influencing parameter in geopolymeriation, as the application of pressure induces an enhancement of the solubility of the solution, thus an improvement of the dissolution stage [281]. In this chapter, the study is focused on the former parameters, while the influence of the hydraulic pressure will be considered in Chapter 5.6.

The calculation of the SiO_2/Al_2O_3 ratio was based on the chemical composition of the raw materials, that is, FA and BSG reported in Table 4. The SiO_2/Al_2O_3 ratio is associated with the chemistry of reaction determined by the reactive alumina and silica compounds supplied by raw materials (FA and BSG), and the proportion of these two compounds strongly influences the microstructure of the product of geopolymerization, as previously described in the introductory chapters (see Chapter 2.4.4). The effect of this parameter on the geopolymerization process was determined by tuning the formulation of the raw material, i.e. using different weight content of FA and BSG glass. The 4 adopted FA/BSG formulations (from Mix-1 to Mix-4) were already described in the methodology section (Table 4) and reported also in Table 6 for simplicity. The calculated SiO_2/Al_2O_3 ratio was 2.7, 3.3, 4.2 and 5.0 for Mix-1, Mix-2, Mix-3, and Mix-4 respectively (Table 6). Considering other ratios as well (silica-to-soda and water-to-soda), all the formulations fall in the chemical ranges giving a stoichiometric GP [26,93]. This detail was already discussed in the introductory chapters.

Table 6: Formulations (fly ash and borosilicate glass mixture) adopted in geopolymer samples manufacturing and relative parameters (silica-to-alumina 'SiO_2/Al_2O_3' ratio, 'α coefficient' and relative density 'ρ_{rel}').

Sample	FA–BSG (wt.%)	Molarity (M)	Curing Time (day)	SiO_2/Al_2O_3	α Coefficient	ρ_{rel} (%)
Mix-1	70–30	13	1	2.7	2.2	87.1
Mix-2	55–45	13	1	3.3	2.5	84.4
Mix-3	40–60	13	1	4.2	2.8	81.5
Mix-4	30–70	13	1	5.0	3.0	86.4
Mix-5	55–45	13	3	3.3	2.5	82.9
Mix-6	55–45	10	1	3.3	2.5	77.4

In this study, other factors were also included, such as molarity of the solvent, soaking time and relative humidity in curing. A 10 M *NaOH* solution was adopted for producing a Mix-6 mixture, whereas 3 days at 85 °C was utilized for manufacturing the Mix-5 sample

(Table 6). The influence of the relative humidity was assessed by employing two sealing methods, method-1 and method-2, previously exposed in Chapter 4.1.1.

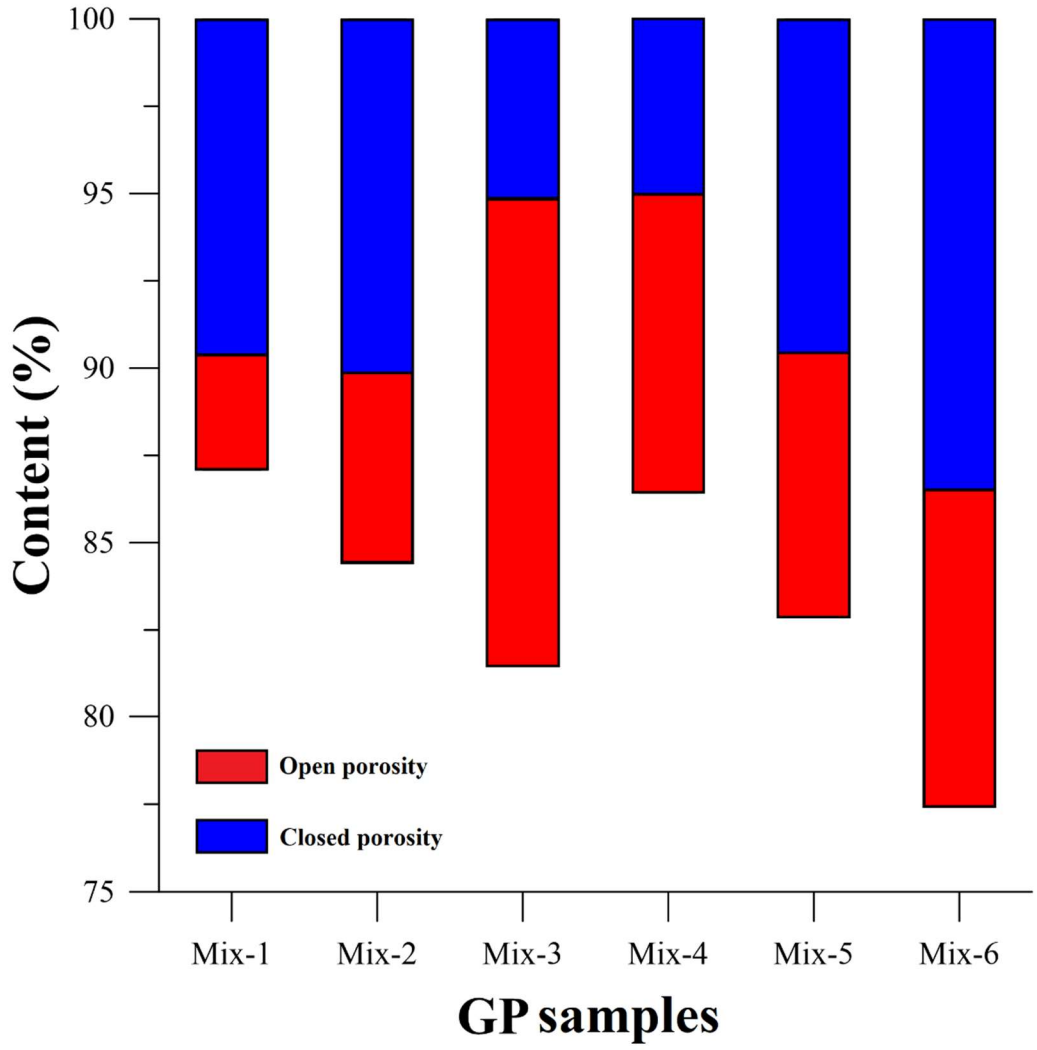

Figure 43: Open porosity (red) and closed porosity (blue) measured for the GP samples.

The SiO_2/Al_2O_3 ratio is one of the most important parameter influencing the GPs microstructure, and it is often adopted in systematic studies of GPs and geopolymerization [102,105,106]. One of the aims of this thesis work, as mentioned in section 3, is the utilization of silica-based recycled glass to tune the chemistry of reaction. The BSG is a totally amorphous rich-in-silica material, with a silica weight content up to 72 wt.% (Table 4): an increment of the BSG content from 30 wt.% (Mix-1) to 45 wt.% (Mix-2) has an enormous influence on the SiO_2/Al_2O_3 ratio (from 2.7 to 3.3). The utilization of BSG as GPs filler induces a supply of further elements during the dissolution stage, such as borates, whose content in BSG is up to 12 wt.% (see Table 4). These species were demonstrated to be active during the inorganic polymeric network formation, substituting alumina in its role (see the previous chapter). For the reason specified, it is legitimate to

include the contribution of the boron in the calculation of the abovementioned ratio by setting a more refined version of it, conventionally named α coefficient:

$$\alpha = \frac{\%SiO_2}{\%(Al_2O_3 + B_2O_3)} \quad (16)$$

As for the silica to alumina ratio, the calculation of Equation 16 was performed using the XRF results exposed in Table 4. The recalculated parameter for each formulation was then 2.2, 2.5, 2.8 and 3.0 for Mix-1, Mix-2, Mix-3, and Mix-4 respectively (Table 6). The relative content of each species is supposed to strongly influence the GP structure and in turn the mechanical properties of GPs [87].

A first clue of the effect of α coefficient is given by the relative density measured through the apparent density (volumetric assessment of the samples) and theoretical density calculation (Table 6). It was found that the relative density is the highest one (87.1%) when the mix contains a lower amount of BSG in formulation (Mix-1), and goes down as the BSG content is raised (Mix-2 and Mix-3), and again it raises (86.4% in Table 6) when the BSG content is as high as 70 wt.%. Therefore, the highest amount of porosity coincides with the Mix-3 batch (relative density of 81.5%), containing 60 wt.% of BSG. By means of the Archimedes method, the portion of open measured was deducted from the total porosity provided by the relative density value in Table 6, and the results were reported in Figure 43. It was observed that the amount of open porosity sensitively increases with the increase of the α coefficient value up to the Mix-3 formulation, and again decreases in a similar way as noticed for the total amount of porosity (relative density). It has to be noticed that the portion of open porosity is not only a direct consequence of the geopolymerization process (release and evaporation of water) but also of the shrinkage during setting of the material, causing the formation of random cracks. A more pronounced effect of the shrinkage would explain the increase of the relative density from Mix-3 to Mix-4, all attributed to a decrease of the open porosity (the amount of the closed porosity is merely the same). To define the individual contribution of these two effects, a specific micrographic study is required.

5.3.2 Influence of alkalinity and curing conditions

The measurement of the relative density and the open and closed porosity of the GP was also conducted on samples with longer curing stage (3 days Mix-5) and lower alkalinity (10 M Mix-6), as to give a basic notion regarding the influence of these essential parameters of the geopolymerization. Table 6 and Figure 43 report the results of the study. Longer exposure to curing stage of a Mix-2 formulation (designated as Mix-5) does not induce a significant difference in the relative density of the sample (82.9%), but the amount of open and closed porosity is differently distributed. In Figure 43, the Mix-5 sample evidences a higher amount of open porosity (or lower amount of closed porosity) as compared to Mix-2. If a lower concentrated solution is used, the change in the relative density is more remarkable (78.1% Table 6), with a large increase both of the amount of the open and closed porosity (Figure 43).

A large deterioration of the microstructure was observed if the GP samples are processed according to the sealing method-2, in which the samples were closed in an air-tightened jar with additional water inside (likely commensurate with a 99% of relative humidity). The method-2 sample presents a microstructure with less product of geopolymerization, as depicted in the comparative SEM analysis of the fracture surface of the samples (Figure 44). Therefore, the Mix-2 samples sealed through method-1 (Figure 44a) were tested, while the method-2 (Figure 44b) was not, as it was not possible to cut off the specimens to the desired geometry.

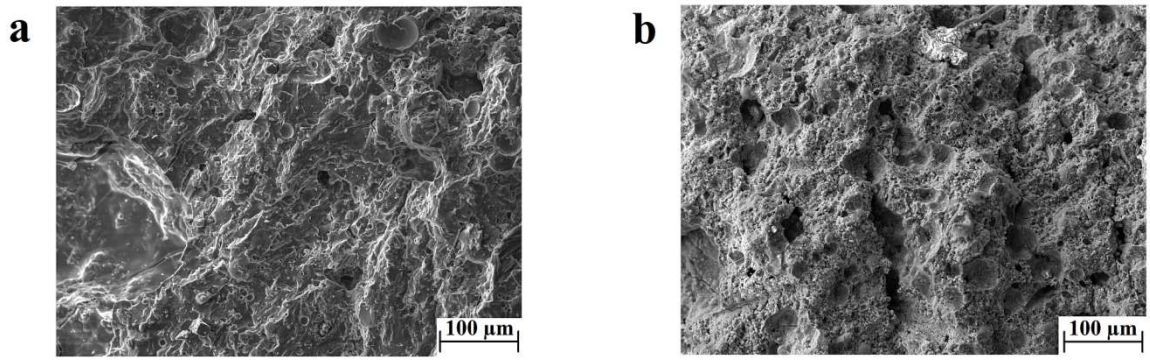

Figure 44: Scanning electron microscope images of the fracture surface of the 'Mix-2' sample sealed according to a) method 1 and b) method 2.

5.4 Mechanical properties of geopolymer samples

5.4.1 Compressive strength

The preliminary insight of mechanical performance related to materials devoted to construction and building applications is given by the compression test. The compressive strength is the main stress that a cementitious product should withstand under operation. The main goal of the thesis is to demonstrate also the suitability of GPs in structural applications. This insight is, instead, promptly hinted by flexural strength and fracture toughness (see next paragraph). Here, we only report a quick comparison between Mix-1 and Mix-2 samples, with the purpose to give a baseline of the performance of these materials in a compression test.

The compression test was conducted on a series of 10 on Mix-1 and Mix-2 GP samples, having a prismatic shape to avoid the influence of the local stress induced by the interference of the compressive cones [246]. The results of the compression test, reported in Table 7, evidence higher compressive strength (45 MPa) if higher content of BSG is used in formulation (Mix-2). The Mix-1 sample revealed a compression strength of about 10% lower than Mix-2 (39 MPa).

5.4.2 Vickers micro-hardness

A series of micro-indentations (10 micro-indentations) was also conducted on Mix-1 and Mix-2 GP samples to investigate the hardness of the geopolymeric compound. It must be pointed out that this test is highly sensitive to the dwelling time prior to testing, as the geopolymeric matrix undergoes a continuous and gradually abating process of hardening until it reaches a plateau. The most significant stint of the hardening process happens in the first week, becoming less intense in the upcoming weeks until it is almost nil after one month [87,101,115,282,283]. For this reason, a longer dwelling time prior testing was selected for micro-indentations (1 month).

The results of the micro-indentation test evidenced an average value of 78 HV out of 10 indentations for Mix-2 sample, slightly higher than Mix-1, which showed an indentation hardness of 73 HV (see Table 7).

Table 7: Compression strength and indentation hardness of geopolymer samples.

Sample	Compressive strength (MPa)	Hardness (HV)
Mix-1	39	73
Mix-2	45	78

5.4.3 Flexural strength and fracture toughness

The compression test exposed in the previous paragraph is usually sufficient to evaluate the reliability of material in construction application, and the compressive strength is the

main parameter considered in the design. The main drawback of any cementitious binder is the low resistance to bending stress and crack propagation [284,285], preventing them to be used in the structural application. For such purpose, the OPC was combined with highly resistance fibres and/or wires, to produce OPC-based composites [148,284,286,287]. Combining the OPC binder with other fillers is the most employed solution if the goal is to increase the fracture toughness of the cementitious material, attaining flexural strength and stress intensity factor values up to 3 times higher than the plain binder. Unfortunately, the durability of the binder dramatically decreases due to chemical degradation and, sometimes, oxidation at the binder-to-fibre interface [9,288].

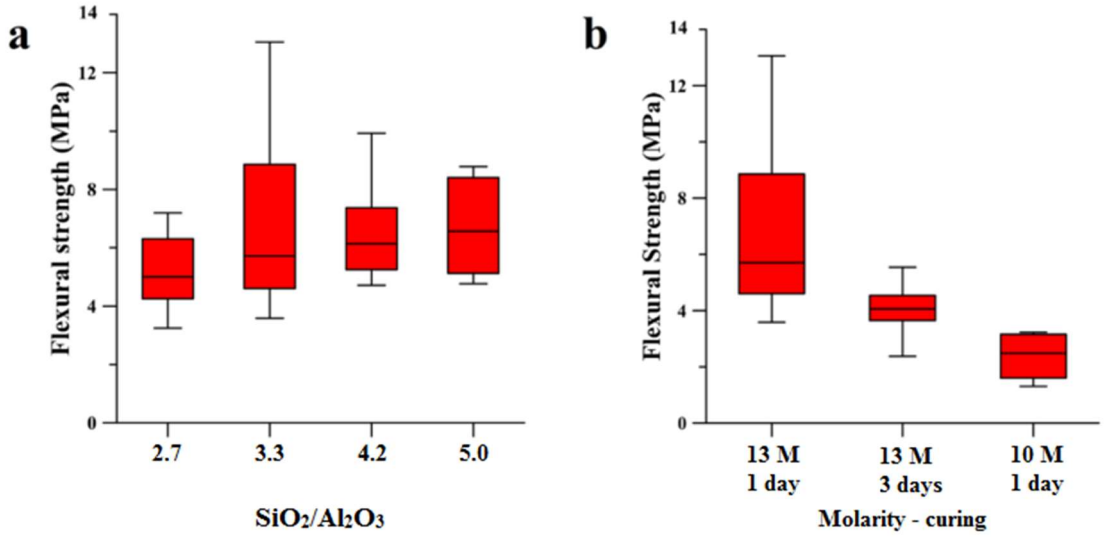

Figure 45: Flexural strength of geopolymer samples in terms of a) silica-to-alumina ratio of the mixtures from Mix-1 to Mix-4 (2.7, 3.3, 4.2, 5.0 respectively) and b) molarity of the activator and curing time used for Mix-2 (13 M for 1 day), Mix-5 (13 M for 3 days) and Mix-6 (10 M for 1 day).

Likewise, GPs and AAMs materials present low flexural strength and fracture toughness, especially due to high material heterogeneity, porosity, cracks formation (due to shrinkage during curing stage) and intrinsic brittleness of the product of alkali-activation [14,18,289,290]. The same restrictions were also expected for FA/BSG based GP samples, irrespective of the formulation and the reaction/curing parameters. Nevertheless, a study of the flexural strength and fracture toughness was conducted on all the mixtures reported in Table 3. The influence of the α coefficient (Equation 16) on the flexural strength is evidenced in Figure 45a, which reports the bending test results of the mixtures subjected to a different formulation (from Mix-1 to Mix-4). It was observed that the highest flexural strength (12 MPa) was obtained for Mix-2 formulation (FA-BSG 55-45 wt.%), but the largest data scatter as well (red boxes in Figure 45). This scattering, determined through IQR factor of 1.5 (see Chapter 4.3), could be explained by the lower relative density, or equally high porosity, that this mix presents as compared to Mix-1 (Table 6 and Figure 43). Nevertheless, the data dispersion seems to be narrower for Mix-3, which in turn exhibits the lowest density among the batches, as depicted in Figure 43, suggesting

that porosity is not the only reason for data dispersion. A unique characteristic possessed by the Mix-2 as compared to all the other mixtures is to have the lowest amount of amorphous phase (Figure 37): the presence of higher crystallinity could then induce also a larger inhomogeneity of the sample, leading to larger data scattering. In contrast to this observation, the average value of the flexural strength increase with the value of α coefficient, indicating a beneficial effect of the silica addition in the formulation.

The Mix-5 and Mix-6 in Figure 45b take in consideration the effect of the molarity of the alkali solution (10 M) and the curing time (3 days) respectively, and the results were put in comparison with the Mix-2. It was found that both the reduction of molarity of the solution and the longer curing time were detrimental for the flexural strength of the GP samples, displaying a bending resistance up to 2 times for Mix-5 and 3 times for Mix-6 lower than the Mix-2. Anyway, comparing the two batches, Mix-6 presents a lower flexural strength with a similar data scattering, proving again that the amount of porosity is not the only parameter influencing the resistance of GPs.

The morphology of the fracture surface is deducible from Figure 44a, which mainly presents an irregular shape, as the crack propagates along no preferential planes or grain boundaries. Although the fracture is clearly brittle, the crack propagation in FA-based GPs depends on many characteristics and variable, rendering the study of the failure quite complex. Indeed, the propagation of the main crack is altered substantially from defects (porosity), preexistent cracks (due to shrinkage), unreacted particles, and discontinuities of the geopolymeric matrix and inhomogeneity of the material. All these flaws are due to the high percentage of impurities held by the FA and BSG, inefficiency of the chemical reaction and effects of the curing conditions. A systematic study of each batch was not reported, as the dynamics of failure are almost the same irrespective of the formulation and so are the fracture surface morphologies.

The systematic study of the parameters in terms of the fracture toughness was tried alongside the bending test, but the results are not reported in this thesis work as they were all below 0.3 $MPa \cdot m^{1/2}$, thus not enough to draw a reliable evaluation of the resistance to crack propagation of the material. It will be seen in the next chapter that the incorporation of cellulose fibres will greatly increase the fracture toughness.

5.5 Cellulose fibres-based geopolymer composite

5.5.1 Flexural strength and fracture toughness

As mentioned in the previous chapter, the manufacture of composites from a cementitious matrix is a common practice to increase the flexural strength and fracture toughness of the material. Unfortunately, cement is highly subjected to corrosion and degradation, especially if it incorporates a filler [288]. The extreme chemical stability of the geopolymeric matrix renders this material more suitable for composite manufacturing. Indeed, the literature is plenty of scientific works concerning the production and the investigation of the geopolymeric composite, using several fibres, wires or fabrics of different natures [7,144,291–294]. Further details were provided in Chapter 2.7.

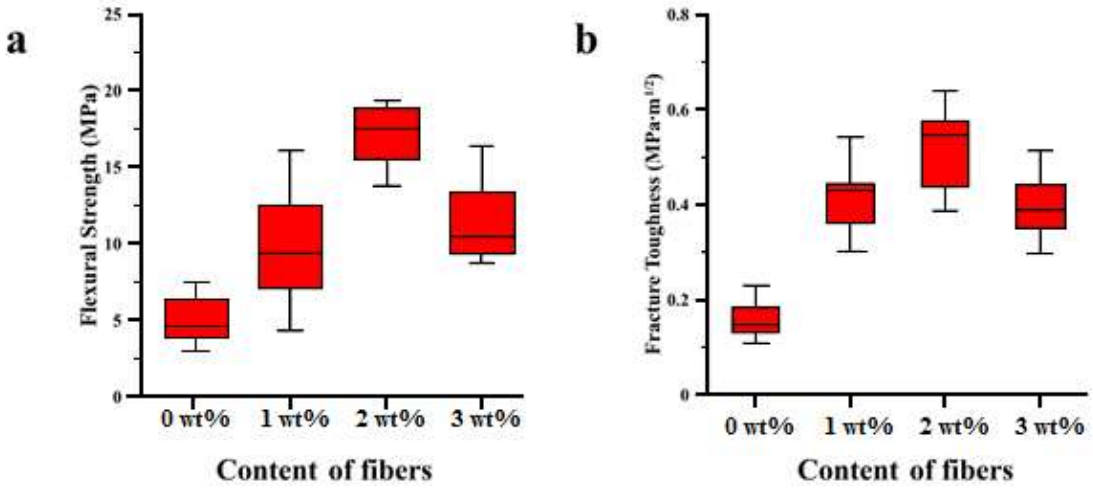

Figure 46: a) Flexural strength and b) fracture toughness of the geopolymer matrix composite.

The cellulose is one of the options to manufacture a geopolymeric matrix composite from the formulation exposed above, and it was expected to be promising, due to its unique properties and specific tensile strength. The matter in using this material resides on the Na^+ absorption, known as a mercerization process, which sucks alkali cations to the geopolymerization process, and the formation of cellulose fibres bundles, not easy to unravel. The first issue was partially solved increasing the liquid-to-solid ratio up to about 0.8, guaranteeing the same rheology of the slurry. This will be weighted to the exact content of fibres in the matrix. The second problem was faced by inserting a step more to the methodology of manufacture – preparation of an aqueous suspension including all raw materials and then sonication of the solution (as above described in the methodology section). Figures 47a-c show an overview of a polished surface of a GP matrix composite samples with 1 wt.%, 2 wt.% and 3 wt.% of cellulose respectively, evidencing a fine dispersion of the fibers. The amount of porosity is probably less pronounced in the 2 wt.% sample, explaining the saturation of the properties for cellulose content higher than 2 wt.% (Figure 46). This would be demonstrated by a study of the density, as previously done for

GP samples, but unfortunately, this was not effective since the presence of cellulose alters the Archimede's values. Besides, in all the cases a good dispersion of the cellulose fibres was achieved, due to the sonication stage prior activation.

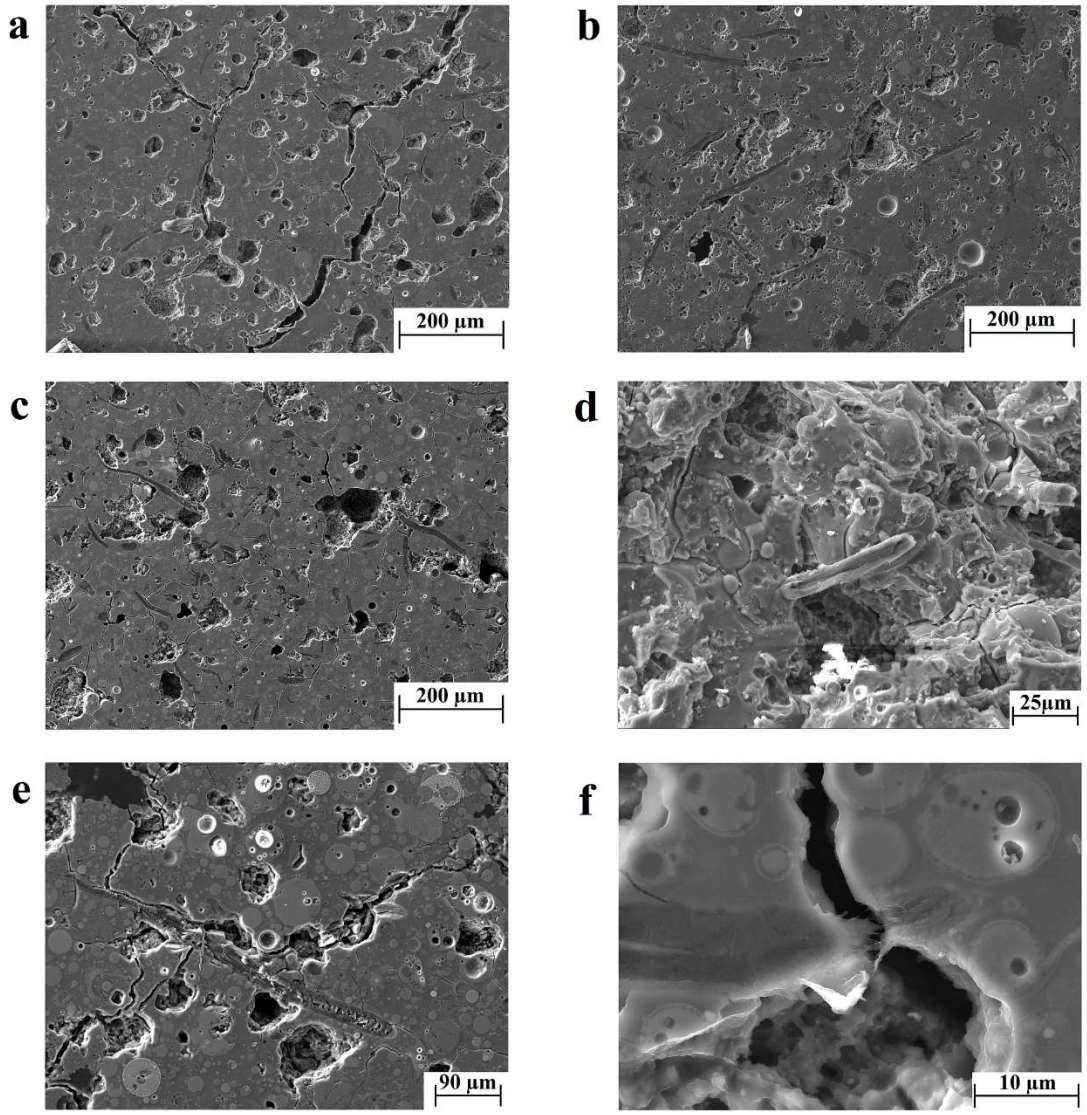

Figure 47: Geopolymeric matrix composite micrographs of the samples with a) 1 wt.%, b) 2 wt.%, c) 3 wt.% of cellulose (polished surface), d) pull out mechanism (fracture surface) in 2 wt.% of cellulose sample, e) bridging mechanism (polished surface) and f) fibre tearing mechanism (polished surface) in 3 wt.% of cellulose sample.

Also, in this case, a study of the flexural strength and fracture toughness was carried out on a set of three different batches, in which an increasing amount of cellulose fibers was dispersed, according to the methodology described in Chapter 4.1, and then put in comparison with the plain GP Mix-1 sample. The results of the 3PB test are reported in Figure 46a, showing that the highest flexural strength (20 MPa) is achieved when 2 wt.% of cellulose fibres are dispersed in the geopolymeric matrix. Comparing these results with those in Figure 45, it was observed that the GP composite attains a resistance to bending

stress almost double than the Mix-2 sample, and even 5 times higher than Mix-1 sample. The samples with 1 wt.% and 3 wt.% of cellulose displayed a similar flexural strength, but anyway lower than that with 2 wt.%. The explanation of this behaviour for the sample with 1 wt.% of cellulose is that the fibre content is not enough to reach higher performance. In case of the 3 wt.% of cellulose sample, the drop of the flexural strength is attributed to the depletion of Na^+ cations on geopolymerization, since to high content of fibres induces an excessive absorption of alkali ions due to mercerization of the cellulose.

The assessment of the fracture toughness of the samples from the chevron notch test provided similar results as the flexural strength (Figure 46b) – the higher fracture toughness is related to the sample with 2 wt.% of cellulose, having a critical stress intensity factor up to almost 0.7 $MPa \cdot m^{1/2}$. This value was found to be more than 3-fold higher than the fracture toughness measured on Mix-1 sample (see Figure 46b).

The analysis of the fracture surface of the GC samples evidenced the presence of mechanisms of fibre pull-out and crack-bridging, as depicted in Figure 47d and e. The crack bridging is the mechanisms, which increases the resistance to fracture propagation of the material by preventing the crack opening and deflecting its path, thus increasing the energy required to fracture. The fibre pull-out efficiency is dependent on the interaction of the fibre with the composite matrix, and a higher interaction means better mechanical performance of the composite [248,291,292,295,296]. Despite this, an excessively strong fibre-to-matrix interface could involve phenomena of fibre tearing, happening when the interface is stronger than the fibre. This event was found in microstructure and reported in Figure 47f.

5.1.2 Analysis of the fibre-to-matrix interface

The absorption of alkali cations (especially Na^+) by the cellulose fibres is a widely known process known as ‘mercerization’. The cellulose swells due to the interference of alkali cations between the polymeric chains, creating electrostatic layers of positively charged $Na+$ ions and negatively charged polymeric chains [146]. What is not equally reported is the absorption of other chemical elements, which creates, in cellulose-based composites, a sort of transitional interface between the inner part of the fibre and the matrix. Tonoli et al. [286] demonstrated the formation of a modified surface on cellulose fibres dispersed in the cement matrix, due to Ca^{2+} absorption from the C–S–H network of the cement. Previously, Merrill et al. [297] published a study reporting the sodium silicate sorption in cellulose fibres, in which it was proved that the cellulose can also absorb silicon ions from the water glass, although to a lower extent than sodium, involving a polycondensation with the polymeric chains.

In our GP matrix samples, irrespective of the weight amount of the dispersed fibres, cellulose was found to undertake a surface modification and a new phase formation at the interface with the geopolymeric matrix. Figure 48a shows the detail of a cellulose fibre, whose surface is clearly modified. It is evident from the figure that the affected polymeric fibrils at the fibre surface are rearranged in an orthogonal configuration to the GP interface

(see insert in Figure 48a), whereas, at the core, the fibrils are parallel to the interface line. An EDS analysis was conducted to detect the chemical species absorbed by the new phase, and the results are reported in Figure 48b. The chemical analysis was carried out in three different zones in order to draw a conclusion regarding the elements' absorption: zone 1- the cellulose fibre core, zone 2- the cellulose/GP interface, and zone 3- the geopolymeric matrix. In all zones, the amount of sodium was the same, whereas the silicon was observed to be more abundant in zone 3 than zone 2, as expected. Further spectroscopic analysis of the interface is required to measure the exact quantity of oxygen in the three zones and its connectivity with Si, in order to assume a polycondensation between the polymeric chains and the GP matrix.

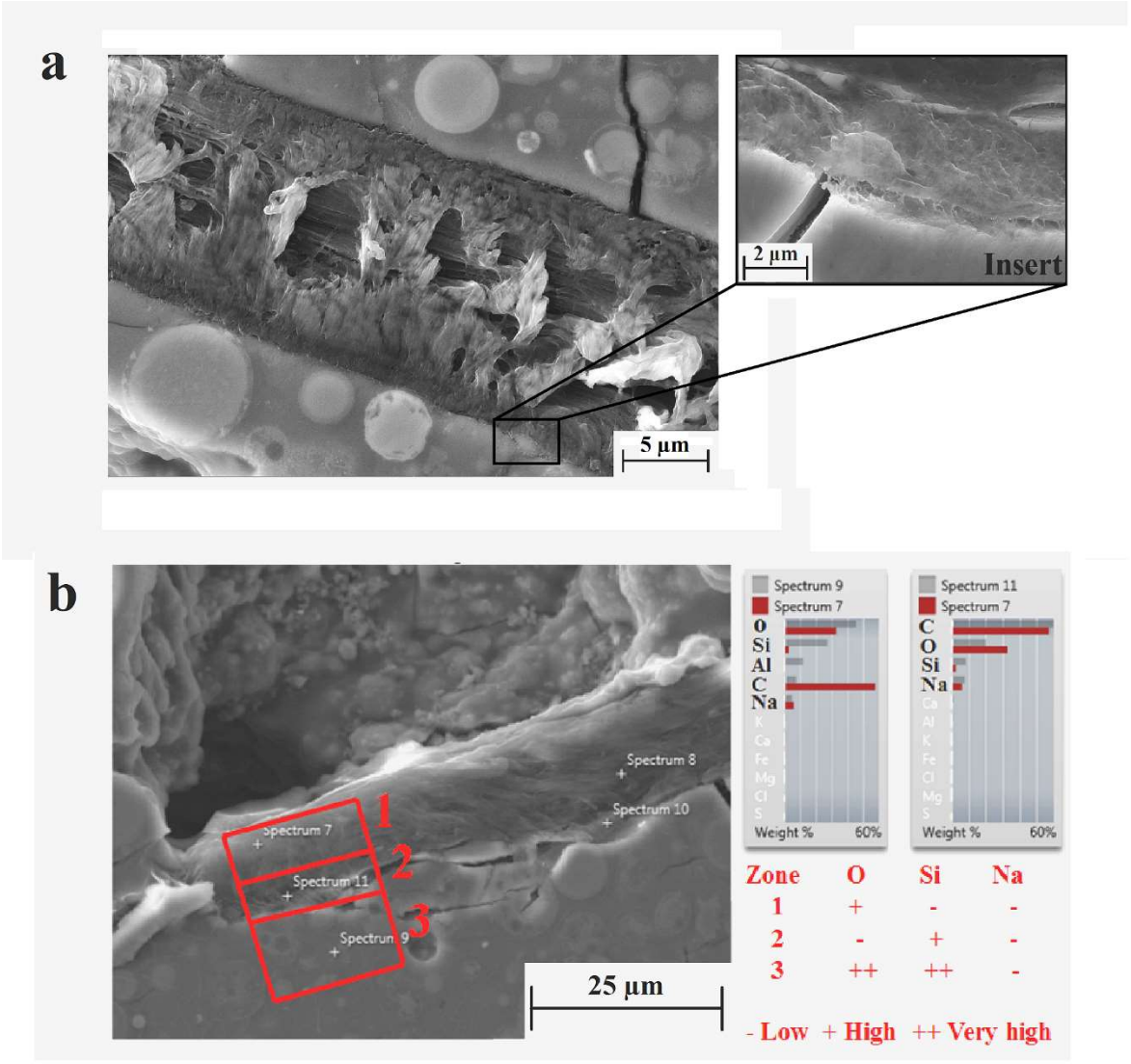

Figure 48: a) Scanning electron microscopy image of cellulose fibre and b) energy dispersive spectroscopy of the cellulose, cellulose-to-matrix and matrix zones.

5.6 Hydro-pressure sintering of fly ash

5.6.1 Overview

In the attempt to establish a synergy between geopolymerization reaction and physical effects induced by the application of pressure, an 'ad hoc' set up was prepared and installed on a compression testing configuration, as described in the methodology section (Chapter 4.4).

Remembering that the first stage of the geopolymerization (or alternatively alkali-activation) is the dissolution of the raw sources releasing aluminosilicate species in solution, the increment of the concentration of these species is a crucial step to optimize the reaction. Based on this purpose, the idea is to apply pressure to the slurry in order to increase the solubility limit of the solution and increment the release of aluminosilicate species. In the single case of silica compounds, the solubility limit of amorphous SiO_2 in water is 0.13 g/l [281], and it is strongly influenced by the pressure – Willey et al. [298] determined a linear increment of the dissolution of silica in sea-water at 0 °C with the increase of the pressure. The solubility is a property connected to the material and its crystallinity, indeed SiO_2 in the crystalline form of quartz was found to have a solubility limit in water four times lower than amorphous silica [299]. Generally speaking, the solubility of a material in a solution is connected to the chemical compatibility of the powder with the solvent (whether the solvent is polar or non-polar), and the ionic potential of the material. For a clear overview of the dissolution of materials and their ionic species, L. B. Railsback implemented a periodic table of the elements focused on the chemical properties of the ionic species [300].

Another physical mechanism induced by the application of pressure in a liquid phase is the preferential dissolution and the recrystallization of the dissolved species - a phenomenon known as Ostwald ripening [301–303]. First found by Wilhelm Ostwald in 1896, the Ostwald ripening is the observed phenomenon in which smaller particles (or crystals) in a liquid (or solid) solution dissolves in favor of a coarsening of bigger particles, by migration, rearrangement, and deposition of dissolved species onto the surface of big particles (see Figure A1 and Table A1 in Appendix A). The dynamics of the Ostwald ripening are driven by the minimization of the surface energy, a physical quantity often associated with the atomic diffusion in thermally triggered sintering. For this reason, observations of necking were expected, as the contact points of sphere-like particles are typical examples of the maximum of the surface energy [304,305]. To demonstrate all these dynamics, the Ostwald ripening mechanisms were tested on fused silica microbeads, and the results are reported in Appendix A.

The simultaneous effect of the hydrostatic pressure (due to the sealed setup) and the solvent on the raw material eventually led to a densification of the FA, up to 90% of relative density (the relative density was measured through the Archimedes method as the first degree of assessment) under 500 MPa for 5 minutes using either water or low concentrated $NaOH$ (3M and 5M) solutions. Therefore, this method of densification,

named hydro-pressure sintering (HyPS), allows to densify inorganic material without using aggressive and highly concentrated solution, usually required in the process of geopolymerization. The novel HyPS process is similar to a recent invention carried out in Pennstate University by Randall et al. [306–309], named cold sintering process (CSP), who successfully densified a series of inorganic thermoelectric materials under the simultaneous effect of a uniaxial pressure and relative low temperatures (300 °C) applied on a moisturized powder, achieving relative densities in some case higher than 90% [306]. For further details regarding the differences standing between CSP and HyPS processes, the attention of the reader is addressed to Appendix B (see Figure B1).

Hereafter, a brief description and discussion of the results relative to the densification of FA according to the HyPS process is reported, mostly dealing with spectroscopy and microstructural observation of the sample. A mechanical assessment of the HyPS samples is missing in this thesis work, which will be one of the topics of future developments.

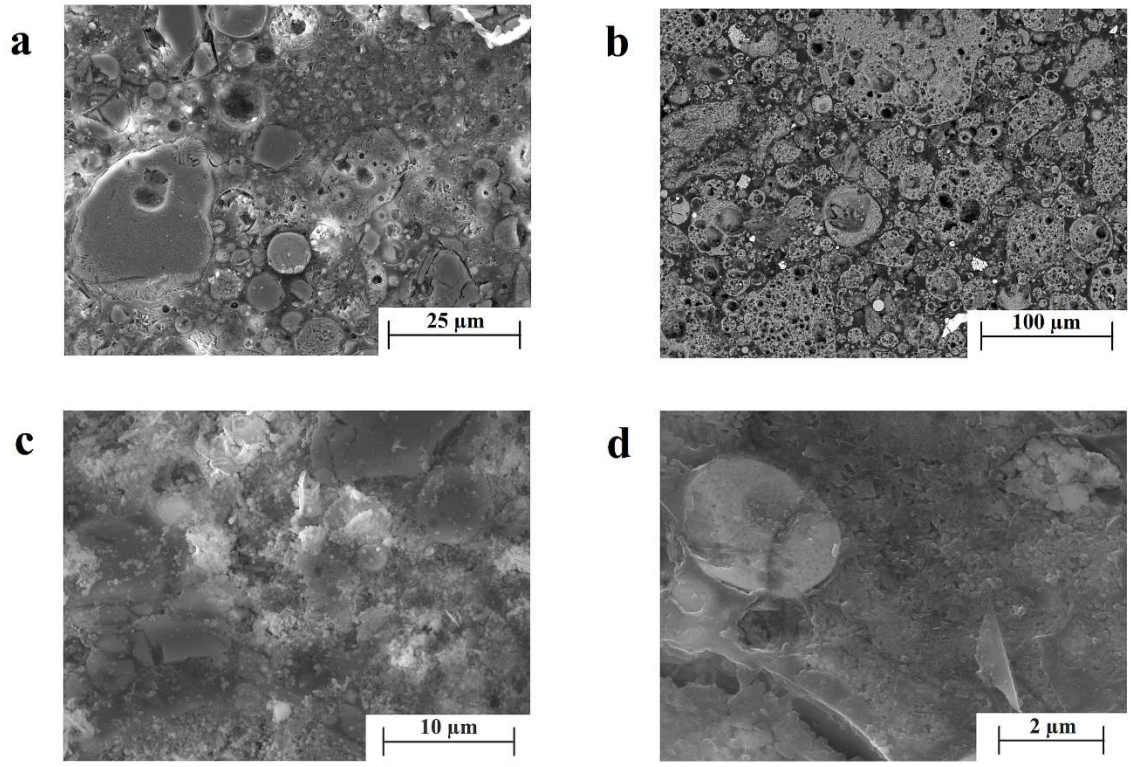

Figure 49: Scanning electron microscopy of fly ash densified in according to the hydro-pressure sintering process under 500 MPa for 5 minutes in a) water, b) 3M NaOH solution, c) 5M NaOH solution and d) a detail of the crystals of the sample processed in water.

5.6.2 Analysis of the microstructure

The microstructure of the FA based HyPS samples processed in water and *NaOH* solution (3M and 5M) under 500 MPa of hydrostatic pressure and kept in these conditions for 5 minutes was observed at the scanning electron microscope and reported in Figure 49. The

morphology of the polished surface of all the samples, at a first sight, seemed nicely densified, similarly to a normal geopolymerization, but some differences are rising from the microstructural observation. Among all, the product of geopolymerization holds a more crystalline morphology, with an extensive presence of needle-like and sponge-like crystals (see Figure 49c and d). This was particularly more evident in the *NaOH* 5M HyPS and water HyPS sample – especially the latter was surprising, as the formation of crystals in GPs was often connected to the presence of Na^+ cations, forming zeolitic crystalline precursors [92].

This observation is motivated by the effect of the Ostwald ripening mechanisms – the migration and reorganization of the species (recrystallization) onto bigger particles could involve the formation of more crystals. Nevertheless, the formation of crystals was an unexpected result, as the release of pressure and the fast drying of the sample should retain the metastable microstructure. Being the liquid phase a highly concentrated solution of aluminosilicate species, it was, instead, expected that the microstructure would have shown an amorphous aspect. From Figure 49, it was observed that this is not the case for FA-based samples, irrespective of the type of solvent.

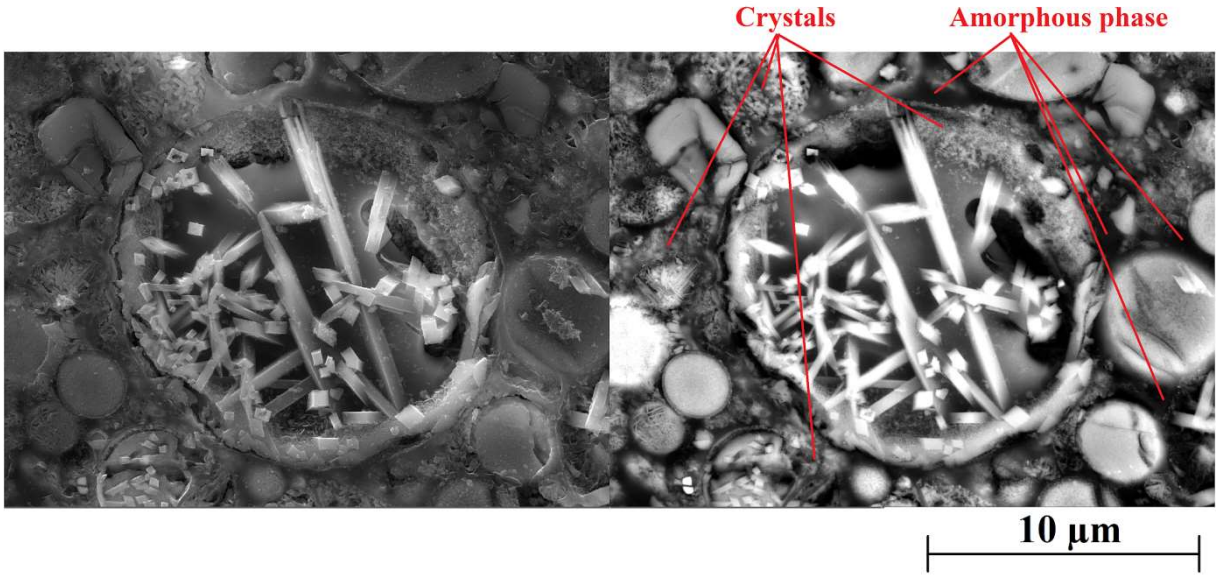

Figure 50: Secondary electrons image (left) and back-scattered electrons image (right) of consolidated fly ash by HyPS in water.

A better insight concerning the crystalline phases present in the microstructure is provided by the back-scattered electron (BSE) microscopy. Figure 50 reports a sample processed in water in secondary electrons (SE - left) and the view in back-scattered electrons (BSE - right). The crystals belonging to the geopolymerization product region are mostly needle-like shaped, and appearing lighter at the BSE image, while the amorphous part is darker. By cross-checking this microstructure with the one exposed in the EDS images provided in Figures 38, one can find out a much higher presence of crystals in the FA samples processed through HyPS. The recrystallization of the aluminosilicate species prevails on

the surface of the intact bigger spheres, as evidenced in Figure 50, in which preferential crystal growth is visible on the big particle contour.

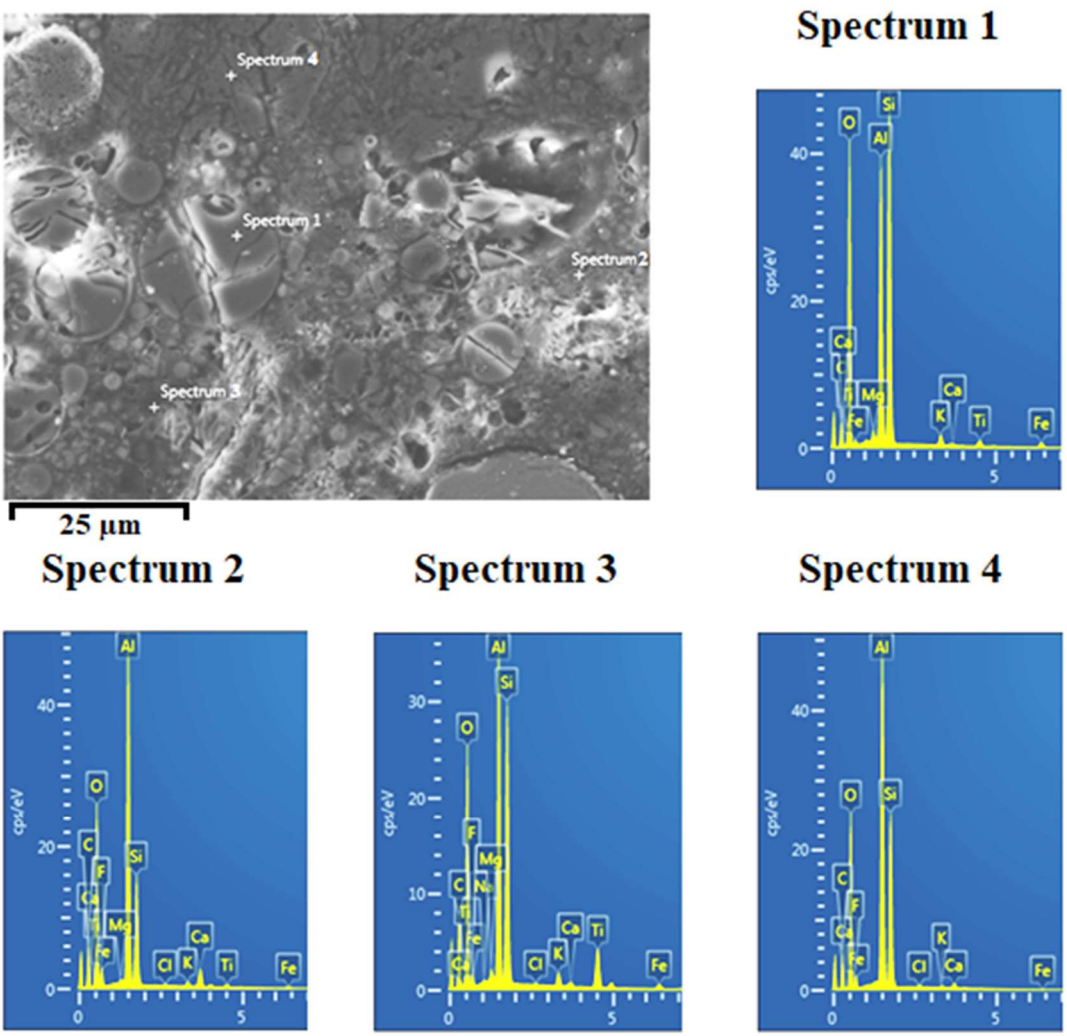

Figure 51: Energy dispersive spectroscopy analysis of the fly ash HyPS sample processed in water.

The spectroscopic analysis of the microstructure was further integrated with the chemical information provided by the energy dispersive microscopy (EDS) performed on the FA HyPS sample processed in water (Figure 51). A point EDS analysis was selected in order to get more precise information regarding the chemical composition of each phase. The spectrum 1, associated with an aluminosilicate undissolved particle, was put in comparison with the chemical composition of the product of geopolymerization in several points (spectrum 2, 3 and 4 in Figure 51), appropriately selected to investigate both the amorphous and the crystalline sites. The glassy phase of the geopolymeric product (spectrum 3 and 4) was found to have a higher content of aluminium if compared to the GP matrix (Figure 38), but this was expectable as the GP formulation comprehended both FA and BSG. Interestingly, the chemical composition of the crystalline site (spectrum 2) is

visibly richer in aluminium, even double than the silica content, conceivably attributable to the formation of sillimanite phases.

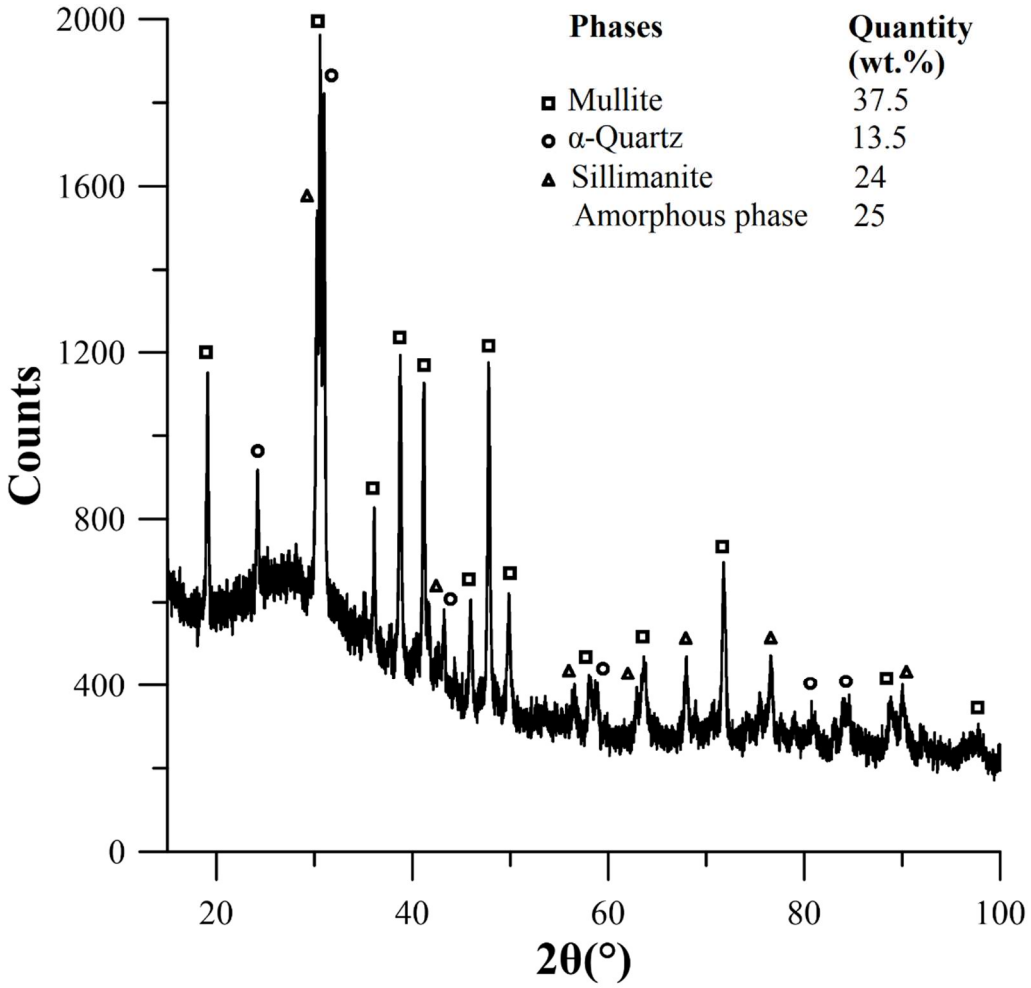

Figure 52: X-ray diffraction spectrum of the fly ash based HyPS sample.

To demonstrate this observation, the same sample was examined to the X-ray diffraction spectroscopy, in order to quantitatively and qualitatively define the crystalline phases produced after the process. The XRD spectrum of the FA based HyPS sample consolidated in water is reported in Figure 52. The fitting of the spectrum peaks evidenced a large presence of aluminosilicate crystalline phases, such as mullite ($Al_6Si_2O_{13}$) and sillimanite (Al_2SiO_5) (37.5 and 24 wt.% respectively), consistent with the EDS results.

Compared to the XRD spectrum of the FA sample (Figure 30), the level of the quartz phase is almost unvaried. The hematite was negligible, similarly to FA (the iron oxide is not expected to react irrespective of the process). The major difference between the two spectra resides on the sillimanite and mullite contents, which are 18.5 and 21.5 wt.% in the FA sample, as reported in Figure 30. This could suggest part of the amorphous phase contained in FA dissolves and recrystallizes in the form of mullite and sillimanite (a mechanism well explained by the Ostwald ripening). Indeed, one might observe that the

characteristic halo associated with the amorphous phase in the FA spectrum (Figure 30) hold a halo falling in the range of 25° and 40°. The FA-based HyPS sample spectrum characteristic hump not only is slightly shifted to the left (20° - 35° 2θ) but it is also associated with a less amount of glassy phase in microstructure (55 wt.% through internal standard method). This result also supports the SEM analysis of the HyPS sample, in which it was observed a more crystalline microstructure as compared to the SEM images of the GP sample.

6. Discussions

6.1 Raw materials

6.1.1 Fly ash

The chemical composition of the FA was assessed through XRF spectroscopy and the results were reported in Table 4. Being the content of calcium oxide (lime) way lower than 15 wt.%, FA is classifiable as class F, according to the international standards related to coal derivatives (see Chapter 2.6) [133,134]. While the concentration of alumina (either reactive or not) is in line with those found in the literature, the silica compound was found to be from 10 to 20 wt.% less in content than FAs already characterized in the state of the art [310–312]. This mismatch is justified by an excessive percentage of iron oxide (14 wt.% Table 4) [313–315].

The high content of iron oxide is, anyway, instrumental if the final goal is to produce an inorganic foam based on a GP formulation, since iron oxide is an effective foaming agent if fired up to 800 °C, as this compound reduces from Fe_2O_3 from to FeO_2 configuration, releasing oxygen [316]. This foaming method is quite effective especially if the inorganic polymer is based on activated glass, as the glassy phase undergoes a change of the rheology above 600 °C [317,318]. This could be a drawback when the fire resistance of GPs is considered. Figure 53a depicts a photo of a GP sample undergoing a foaming process through iron oxide reduction, Figure 53b illustrates a detail of the microstructure.

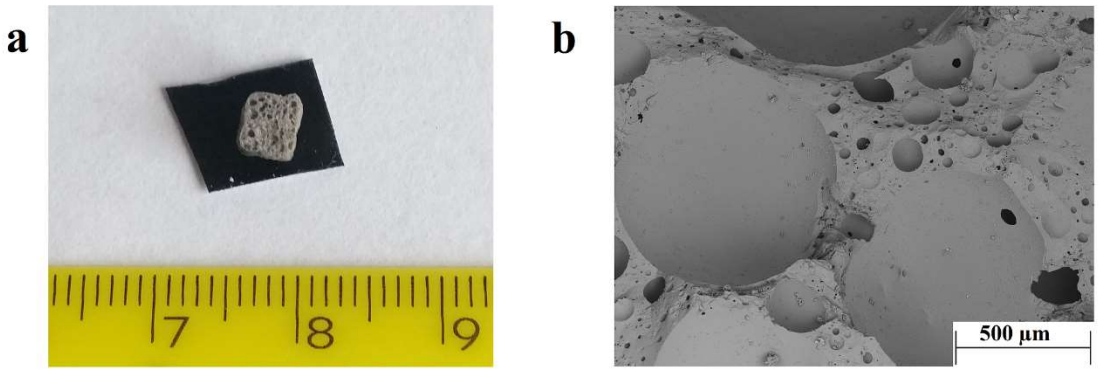

Figure 53: a) Photo of a foamed geopolymer sample and b) second electron image of the same sample.

The XRD spectroscopy analysis carried out on the FA (Figure 30) qualitatively and quantitatively defined the crystalline phases of the aluminosilicate powder, as well as led to the estimation of the amount of amorphous phase, connected to the hump of the XRD spectrum. The fitting of the spectrum peaks determined the presence of mullite, sillimanite, and quartz, while the internal standard method showed an amorphous content of 44 wt.%. By comparing the results from XRD spectroscopy with the literature [92,135,319], it was observed that these phases are contained in every type of FA. Specifically, this FA was

found to have a way less amount of glassy phase if compared with the literature and a higher percentage of crystalline phase in the microstructure [310,311], but in line as compared to other studies [312]. The quantity of amorphous phase contained in the FA is intimately related to the heat exposure which the coal undertakes in the combustion chamber of the power plant. These characteristics of the microstructure of the FA may influence its reactivity: a decisive lower presence of glassy aluminosilicate phase renders this type of FA definitely less efficient during the dissolution stage than other FA analysed in the literature, whereas the polycondensation stage is rather positively influenced by the high presence of silica source (irrespective of the phase nature).

The content of the hematite phase (iron III oxide) in the XRD spectrum was found to be 2.5 wt.%, not coinciding with the amount of iron oxide displayed in the XRF spectroscopy. In the EDS analysis of the FA, a spherical particle (attributed to an amorphous structure) was ascertained to be iron-based, meaning that the mismatch between XRF and XRD is attributed to the presence of amorphous iron oxide. The amorphous iron oxide particles are not uncommon, and it was found they have unique mechanical, electrical, thermal, magnetic, and capillary properties, and because of that largely studied and employed in several applications [320,321]. Due to these reasons, a specific utilization of the iron (III) oxide contained in the FA could be an intriguing solution for further applications related to this material. If such a solution is intended to be undertaken, the FA has to be beneficiated, as this material contains many impurities (up to 5.5 wt.%, see Table 4).

The SEM observation of the powder evidenced a spherical and hollowed morphology of the particles, as depicted in Figure 31. This is a basic characteristic of each FAs which renders this aluminosilicate powder highly reactive in a base-alkali ambient (especially in presence of sodium cations) [67,322,323].

One of the main factors influencing the degree of reaction of a powder is the grain size – the finer the particle the faster and higher the dissolution [256]. Table 5 reports the fineness of the FA, in average 22.64 μm, while the distribution curve (Figure 34) exhibits two humps, one micrometric and one sub-micrometric. This was considered to be why FA has a higher BET value than BSG (Table 5). This peculiarity related to FA grain size measurement was already partially evidenced in previous studies [324]. Table 5 also reports the density of the FA, which was calculated to be 2.35 g/cm^3, which is in accordance with the literature, as this value usually ranges between 2.20 and 2.60 g/cm^3, depending on the nature of the raw powder [135].

6.1.2 Borosilicate glass

The chemical composition of the BSG was provided by the XRF spectroscopy (Table 4), mostly composed of silica (72 wt.%), and displaying a presence of some significant network modifiers, i.e. alumina 7 wt.% and borate 12 wt.%. This composition is typical for a Pyrex glass, turning out to be the bottom-line for any type of borosilicate glass, being the borate content the minimal one [279,325]. The content of borates, in particular, determines

also the structure of the GP, as they replace the reactive alumina in its role during the geopolymerization [4].

The analysis at the pycnometer revealed a density of 2.23 g/cm^3, coincident with most of the borosilicate glass already existent in the market [325,326], and quite close to the FA, helping the dispersion and the homogenization of the two powders. Indeed, the segregation of the powder during curing is driven by the specific weight (density). Its grain size distribution (Figure 34) and the specific surface area (BET in Table 5) are merely related to the energy of ball-milling – the higher the round speed the finer the powder.

6.2 Geopolymer samples

6.2.1 Microstructure of the GP samples

The SEM observation of the GP samples (both the fracture and the polished surface) is depicted in Figure 35. It was noticed that the microstructure is characterized by a matrix, i.e. the product of geopolymerization, holding an amorphous morphology (Figure 35a and c). This glassy compound, initially in a liquid saturated state, spreads everywhere and somehow glues the remaining particles, usually composed by FA and BSG unreacted particles, organic and metal oxide grains. The hardening of the matrix freezes the microstructure in a pattern described in Figure 35d. If FA is present in the formulation, this is a typical microstructure of a GP sample, widely advertised in many studies, holding similar morphological characteristics [319]. The systematic study of the GP samples did not lead to any visible difference between each formulation, most likely because of the insufficient variations of the playing parameters (such as molarity of the solution). Indeed, in one of their studies, Palomo et al. evidenced a decay of the FA based AAMs setting (and so the microstructure) if the concentration of the *NaOH* solution is 8M [67]. A similar deterioration of the microstructure was observed if the curing stage is kept under sealed and humid conditions according to method 2, as exposed in Figure 44.

The nature of the geopolymeric product is based on an aluminosilicate compound, for the alkali solution dissolves and activates mainly the aluminosiliciate particles (both from FA and BSG). The EDS analysis of the GP matrix (Figure 38a) corroborates the aluminosilicate composition, more specifically with a surplus of the silicon over aluminium, sometimes in a weight percentage even double – the same results were already exposed in another study conducted by Palomo et al., focused on a microstructural identification of a FA-based AAMs, irrespective of the nature and concentration of the alkali solution [24].

One must bear in mind that the chemical composition of the AAMs has not necessarily to be different from a GP material, albeit the chemical modulus (SiO_2/Al_2O_3 *ratio*) are largely different. Indeed, the rearrangement of the aluminosilicate species must proceed in a way to respect the Lowenstein's restriction, in which Al-O-Al bond is not chemically consistent [45,76,87,183]. What really changes is the degree of connection of the Si-Al network, which is directly evidenced by the NMR spectroscopy. It was shown that the ambient of the silicon chemical ambient is dictated by the content of aluminium and boron in relation to the silicon content – specifically, a high silica to alumina ratio is supposed to give rise to a higher amount of Q^4 and $Q^4(0\text{-}1Al)$ species produced, i.e. higher structured network [62]. To determine the relationship between the silica to alumina ratio and the type of microstructure, it's sufficient to perform the ^{29}Si MAS NMR spectroscopy to samples with a variable formulation. Nevertheless, this work is quite long and time-consuming, but a future development could include this analysis.

The geopolymeric matrix is the main compounds rising from the geopolymerization, but not the only product of the reaction. Figures 38 gives examples of crystals formation after

the reaction, which is a typical outcome of an alkali activation [92]. The quantitative and qualitative study of this crystalline product was performed through concurrently XRD and EDS analysis of the GP samples (Figures 37 and 38). Based on the fitting of the GPs XRD spectra peaks, it was found that the main crystalline formation is defined by mullite and sillimanite, whereas a secondary crystals (other phases in Figure 37) could be ascribed to formation of C-S-H crystals, due to the presence of Ca in composition, and sodium carbonate, is the aftermath of an elevated alkalinity of the solution. These phases were identified in the EDS analysis in Figure 38. The extensive XRD study conducted on activated FA and reported in the literature by Criado et al., showed many crystalline phases formation, including Na-chabazite ($(Ca,Na_2,K_2,Mg)Al_2Si_4O_{12}\cdot 6H_2O$) and various forms of zeolite [92], which determines one of the main differences between AAMs and GPs. Williams et al. [254] detected a similar crystalline microstructure in FA based GP samples, except for the carbonates compounds. Torres-Carrasco et al. [87] processed GP samples based on a formulation including waste glass, and the XRD spectroscopy displayed the production of hydroxysodalite, often associated with an N-A-S-H gel of AAMs in many studies conducted by Palomo et al. [20,41,118]. This result is quite contradictory with what has been found in our XRD spectra, however one should bear in mind that the XRD spectroscopy is a powerful mean of crystalline investigation, but the procedure of peaks fitting is not trivial as the single signal may experience local shifts due to lattice distortions, thus the pattern of peaks could be confused for something else. Therefore, the analysis of the XRD data could be corrupted by a subjective evaluation of the operator, who usually fits the peaks in accordance with crystalline phases found in the literature.

6.2.2 FTIR and NMR spectroscopy

The FTIR spectroscopy gives important insight regarding the type of bonds established after geopolymerization, and mostly held by the amorphous aluminosilicate geopolymeric matrix. The comparative analysis of the FA and GP FTIR spectra (Figure 39) suggests some modifications, but the absorption band at 1000 cm^{-1} associated with a Si-O stretching vibration (typical of an aluminosilicate amorphous compound) remains still the prominent one in GP sample as well. The only change is a shift of the band centre towards higher wavelengths, generally attributed in the literature to an increase of the degree of the connectivity [87,107].

To understand the connectivity state of the silicon and aluminium in the amorphous network, the FITR spectrum should be integrated with the information given by the ^{29}Si NMR spectroscopy. In the interpretation of the NMR spectra, many authors agreed that the shift that the main resonance hump centre experienced after geopolymerization/alkali-activation is attributed to the formation of $Q^4(3\text{-}4Al)$ silicon ambient, and so did we in Chapter 5.2. These analyses are totally admissible, as these species are likely to exist into the structure. But a high percentage of these signals would shift the characteristic band of the FTIR towards the left in a higher extent. This is not the case as the band is cantered at 1010 cm^{-1} (see Figure 39). Thus, another interpretation of the NMR spectra is that some contribution at high ppm is given by Q^1 and Q^2 species, usually resonating approximately

at -92 and -94 ppm respectively [268,327–330]. The presence of these species explains the centration of the GP FTIR characteristic band at lower wavelengths. The ^{11}B MAS NMR spectra, reported in Figure 42, demonstrated for the first time the participation of borates in the microstructure. Nicholson et al. back to 2005 [130], carried out a work focused on the synthesis of GPs incorporating borates salts, analysing the boron interaction with the geopolymeric matrix through ^{11}B NMR, but such explicit conclusion was not drawn. The boron participation was parameterized in this thesis work through α coefficient (Equation 16), a total novelty in the determination of the GP chemistry.

6.2.3 Mechanical properties

In Chapter 2.8, dealing with the exploration of all the past and potential GPs and AAMs applications, it was understood that since the discovery of these materials, their characteristics and mechanical properties would fit in building and construction application. The basic requirements are chemical stability to endure environmental degradations [288,331–334] and structural properties, especially in compressive strength [335]. The first condition has always been the point of strength of GPs against OPC cement, as cement involves dehydration process of the hydroxide groups of the C-S-H chains, a condition less relevant for GPs and AAMs due to the lower hydration level of the microstructure [26,336]. The second condition is not uniquely defined, as the GPs and AAMs mechanical performances are strictly related to the raw materials, the chemistry of the reaction and the physical conditions adopted in the synthesis of the material. However, many works based on a comparative study of GPs and AAMs mechanical performance have found a smooth affinity with the compressive strength of OPC cement, having an average compressive strength in frame range of 40-80 MPa [337–339]. The compressive strength of FA/recycled glass based GPs were found to have a slightly lower value than reported for AAMs in the literature, most likely due to the inhomogeneity of the raw materials and the change of the chemistry, going more towards high silica content. One of the first work related to the incorporation of urban recycled glass in GPs synthesis was carried out by Torres-Carrasco et al. [19,87,122], who attained a compressive strength of 38 MPa for a FA based GPs incorporating 15 wt.% of recycled glass and activated with a 10 M *NaOH* solution, after 28 days of curing, which is 25% lower as compared to FA/BSG based GPs.The results of the micro-indentations evidenced an average value of 78 HV, which is in line with GPs and AAMs hardness value found in the literature [6,340].

The study of the GP production parameters was applied to the bending test reported in Figure 45a-b. Irrespective of the parameters, the highest flexural strength, i.e. 12 MPa, associated with the Mix-2 sample, is comparable with the flexural strength of FA-based GPs found in the literature (from 10 to 15 MPa in GPs incorporating fly ash and urban recycled glass) [18]. A similar study concerning the assessment of the fracture toughness through chevron notch test was conducted on the above-mentioned samples. The results coming displayed a stress intensity factor always lower than 0.3 $MPa \cdot m^{1/2}$. These results are not far from the typical values of the resistance to crack propagation of GPs reported in the literature [291].

6.3 Geopolymer matrix composites

6.3.1 Geopolymer matrix composite microstructure

Figures 46a and b depict the polished surface of a GP matrix composite. The SEM images evidence a homogenous dispersion of the cellulose fibres, corroborating the effectiveness of the method of dispersion reported in Chapter 4.1. GC incorporating cellulose derived fibres/fabrics were extensively studied in the literature, showing always an increment of the mechanical and fracture properties of the material [6,7,144,291,341]. All these works, however, have encountered serious issues in fibres bundles unraveling, which could be preferential spots of crack initiation and decreases the efficiency of matrix toughening.

Crack bridging and fibres pull-out mechanisms were demonstrated in Figures 46c-f, likely to happen quite often in this kind of composites. These mechanisms were found also in cotton fibres based GCs [6,7].

6.3.2 Flexural strength and fracture toughness

The systematic study of the flexural strength and the fracture toughness was also performed on GP matrix composites, incorporating various weight percentage of cellulose fibres (1, 2 and 3 wt.%) starting from a Mix-1 formulation. The sample with 2 wt.% of cellulose displayed the highest value of flexural strength, as high as 20 MPa on average as depicted in Figure 46a.

The fracture toughness deduced from the chevron notch test was calculated through Equation 14 in Chapter 4.2. The highest resistance to crack propagation was in average 0.7 $MPa \cdot m^{1/2}$, also in this case displayed by the 2 wt.% sample (Figure 46b). Increasing or decreasing the number of incorporated cellulose fibres in the GP matrix from the 2 wt.% concentration induces a decrease of the mechanical and fracture performance of the composite.

A similar study on the flexural strength and fracture toughness of GP matrix with dispersed cotton fibres was conducted by Alomayri et al. [7]. In their work, these authors found that the highest flexural strength and fracture toughness was achieved when 0.5 wt.% of cotton fibres were dispersed in the matrix. The value of the flexural strength in average 12 MPa which is almost half the one reported in this thesis work, whereas the fracture toughness measured according to the straight notch technique turns out to be higher (1.1 $MPa \cdot m^{1/2}$). These discrepancies are explained by the different nature of the filler, as the cotton is composed by 90 wt.% of cellulose, thus having a lower specific tensile strength, thus lower flexural strength of the composite. The higher fracture toughness could be simply attributed to the higher performance of the GP matrix.

6.3.3 Cellulose-to-matrix interface

A sort of chemical interaction was detected between the organic network of the cellulose fibres and the aluminosilicate based one of the GP matrix (Figure 48a). The EDS analysis

on the fibre-to-matrix interface evidences a synergy between the two networks, suggesting a poly-condensation reaction happening between the organic and inorganic chains [297]. In all the studies regarding cellulose fibres based GP composites, such interaction was never observed. Tonoli et al. [286] observed a surface modification of the cellulose fibres dispersed in OPC matrix, but no interaction with the C-S-H network was observed. This is anyway expectable, as the crystalline microstructure of the OPC cement does not easily interact, in the same way, a glassy phase does.

6.4 HyPS process

6.4.1 Crystals formation

The densification of the FA, exceeding 80% of relative density, was carried out on a HyPS setup according to the methodology reported in Chapter 4.4. Both from the SEM observation (Figure 50) and the XRD spectroscopic analysis (Figure 52) of the samples, it was evident an increment of the crystallinity of the microstructure, irrespective of the type of solvent and its alkali concentration. The HyPS process carried out on FA was found to produce a crystal phases in an amount even double than the FA/BSG based GP samples and any other FA based GPs and AAMs in the literature [319,342], as evidenced by a comparative study conducted with the XRD spectroscopy of the GP samples reported in Figure 37.

6.4.2 Geopolymer matrix

The remaining amorphous phase detected in the XRD spectrum of the FA HyPS samples was expected to be associated with the geopolymeric product, since, at high pressure, the glassy phase contained in the FA is readily dissolved in the solution. The EDS analysis in Figure 51 revealed that the amorphous sites of the geopolymeric product are richer in aluminium than the GP samples. This result is also discordant with the literature, reporting that the amorphous product of GPs and AAMs based on FA have a silica-rich composition [24]. This is likely due to the fast setting time – following the stages of geopolymerization described by Provis et al. [20,23,71], in which the liquid saturated phase forms initially a Gel-1 rich in aluminium, prior reorganizing into a silicon-rich compound. Therefore, the liquid phase freezes in an aluminium-rich composition after sample drying. From the EDS analysis (Figure 51), it was also deduced that being the aluminium in a higher amount in the amorphous phase than silicon, the Lowenstein's rule was clearly violated, a condition that was recently found to happen in some low silica zeolite phase synthesis [343].

The future work will include a basic understanding of the chemical dynamics happening during HyPS process, by integrating insights from FTIR and NMR spectroscopy, and a systematic study of the mechanical properties and the results will be compared to those coming from the GP and GP composite sample. Being merely a manufacturing process, the HyPS could also successfully densify any material (similarly to CSP process), and the heat-free process allows to include the densification of organic-based material, which easily degrades under the effect of a heat-flux. This would open a different and more interesting scenario in the processing of organic-inorganic hybrid materials. For further examples concerning the densification of inorganic materials according to the HyPS methodology, the attention of the reader is addressed to Appendix C.

7. Conclusions

7.1 Geopolymer

1. New geopolymer was designed by incorporation of fly ash and borosilicate recycled glass, evidencing an improvement in compressive strength of about 25% as compared to geopolymers based on fly ash and recycled glass (e.g. urban glass) reported in the literature.
2. The silica to alumina (SiO_2/Al_2O_3) ratio was tuned so as to find the best formulation. The bending test evidenced the highest flexural strength for a ratio of 3.3 (45 MPa - Mix-2). The chevron notch technique displayed a fracture toughness always below 0.3 $MPa \cdot m^{1/2}$ for all the examined geopolymer formulations. No improvements were observed as compared to the literature.
3. The alkalinity of the solvent and curing conditions were also inspected, revealing best performance in terms of flexural strength for a 13 M caustic soda solution, cured at 85 °C for 1 day in sealed condition for a given formulation.
4. The chemistry of the material was investigated through FTIR and NMR spectroscopy, showing a shift of the characteristic FTIR peak (~ 1000 cm^{-1}) towards higher wavelength and of the ^{29}Si NMR hump toward lower ppm as the silica to alumina ratio is increased. ^{11}B NMR spectra demonstrated that borates contained in the borosilicate glass play an active role in the geopolymerization similar to aluminates, pushing the authors to substitute the silica to alumina ratio with a more suitable coefficient (α coefficient) which takes into account the influence of boron in the reaction.

7.2 Geopolymer composites

1. Geopolymer matrix composites with dispersed cellulose fibres on the basis of the fly ash and borosilicate glass formulation and dispersing cellulose fibres by ultra-sonication were successfully produced. Improvements in flexural strength and fracture toughness of about 162% and 51% respectively as compared to plain geopolymer formulation were achieved, rendering this material more suitable for structural applications.
2. The toughening mechanisms of fibres pull-out and crack-bridging, as well as fibres tearing, were identified.
3. Cellulose fibres were superficially modified by the geopolymeric matrix, establishing an intermediate layer between the two materials. The formation of this affected zone suggests a sort of interaction between the organic polymer and the geopolymeric compound.

7.3 Hydro-Pressure sintering

1. A new room-temperature pressure-driven method of power densification, named hydro-pressure sintering, was developed using the simultaneous effect of the

dissolution from an aqueous solvent and the effect of the pressure (this method has been submitted in a patent application Nr. D18079023).

2. The dynamics of densification are characterized by the preferential dissolution, migration, and re-precipitation of dissolved aluminosilicate species driven by the mechanisms of the Ostwald ripening.
3. Fly ash was successfully densified up to 80% of relative density, under 500 MPa for 5 minutes in water and *NaOH* (3 M and 5 M) solutions, thus allowing the utilization of less aggressive solvents.
4. The observation of the microstructure through secondary electron microscope evidenced the formation of crystals, likely induced by the pressure. The XRD spectroscopy corroborated this observation, revealing the presence of aluminosilicate crystalline phases (mullite and sillimanite), and lower content of the glassy phases forming during conventional geopolymerization.

Appendix A – Ostwald ripening mechanisms under hydro-pressure sintering conditions

The Ostwald ripening mechanism [301–303] is the observed phenomenon driven by minimization of the surface energy in which smaller particles (or crystals) in a liquid (or solid) solution dissolves promoting the growth of bigger particles. Coarsening by migration, rearrangement, and deposition of dissolved species.

The Ostwald ripening mechanisms (Figure A1) were investigated through HyPS (450 MPa) applied to silica microbeads-water suspension in the condition of high liquid to solid ratio (1:100). The as-received microbeads particle size was falling in the range of 1-20 µm (Figure S1a). Once the hydraulic pressure was applied, the size distribution of beads visibly changed (Figure A1b), in favour of a size distribution bigger than 3 µm, as quantitatively demonstrated by the grain size analysis conducted using SEM, before and after application of HyPS (Table A1). This demonstrates a preferential dissolution of the particles. Figure A1c shows pieces of evidence of preferential precipitation of the dissolved species onto high surface energy spots (as dictated by the Ostwald ripening theory), i.e. the uniform deposition of the second-phase over undissolved particles and the formation of necks (necking).

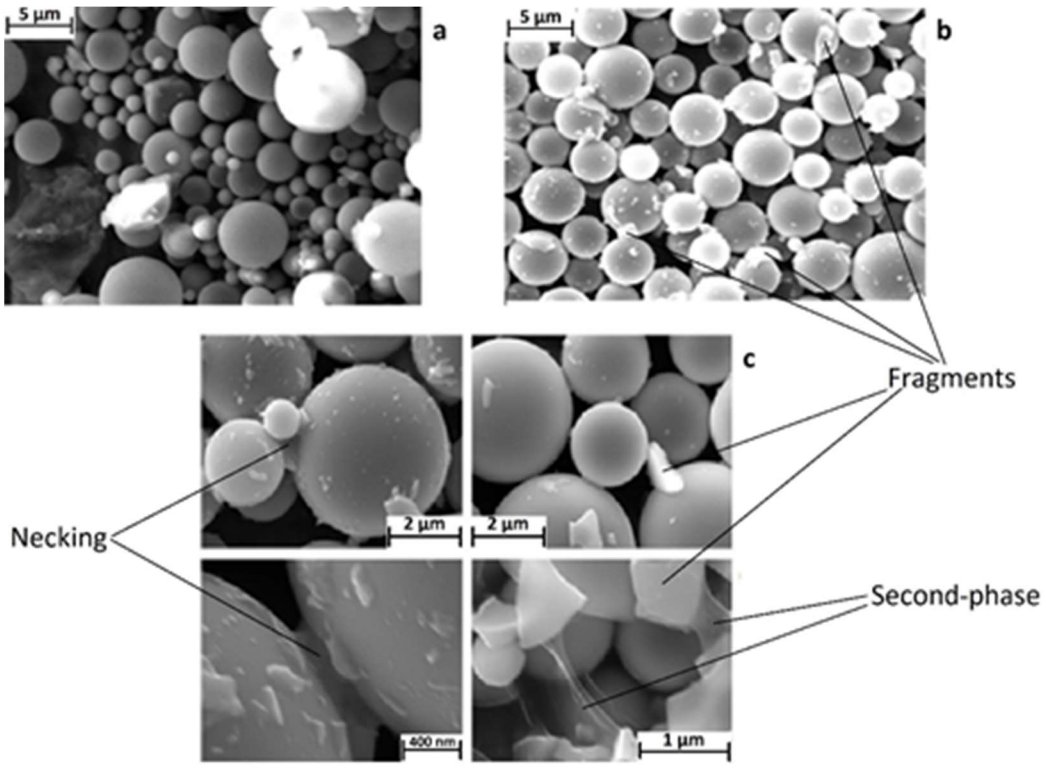

Figure A1: Second electrons image of silica microbeads a) as received and b) after hydraulic pressing in excess of water (liquid to solid ratio 100:1) at 450 MPa for 30 minutes and c) magnifications of Figure S1b.

Table A1: Grain size analysis of the microbeads as given and after applying hydro-pressure sintering (450 MPa, 30 minutes, in water).

		total	**Below 1µm**	**[1,2]µm**	**[2,3]µm**	**Above 3µm**
As received	**Counts**	234	5	31	53	145
	Percentage (%)		2.14	13.25	22.65	61.97
After HyPS	**Counts**	244	1	4	17	222
	Percentage (%)		0.41	1.64	6.97	90.98

Appendix B – Vickers micro-indentation hardness and indentation fracture toughness on nanosilica based hydro-pressure sintering and cold sintering samples

Amorphous silica nanoparticles were densified through HyPS process under 450 and 600 MPa using either water or *NaOH* solution (0.5M). The average relative densities of densified nano-silica samples, measured using SEM images and reported in Figure S2d, were 99.99%, 99.95% and 99.95% for samples processed at 600 MPa in water, 450 MPa in water and 450 MPa in *NaOH* (0.5 M) respectively, all of them for a total duration of 5 minutes. Differently, from silica microbeads samples, the pressure seems to be more effective than the type of solvent if the particle size is reduced to nanometric size. The relative density was also calculated through Archimede's technique, for nanosilica Cold Sintering (CSP) sample (200°C, 450 MPa, 2h) [308], giving an average value of 81%.

Surprisingly, HyPS samples (Figure B1d) also show translucency, which is related to low light scattering [344–347], and to relative densities close to 100% [348], in line with the values calculated for nanosilica HyPS samples. The translucency is a characteristic of pure silica compounds.

Assessments of the mechanical properties were conducted on nanosilica HyPS samples processed in water under 450 MPa (Figure B1a), and CSP samples (Figure B1b) by means of micro-indentation test for Vickers hardness and relative measurements of the median cracks for the indentation fracture toughness (IFT) assessment [349]. The cracks were ascertained to be median by multiple polishing of the sample surface. The average value of the Vickers micro-hardness (HV 0.2) among a set of 10 indentations was 155 for the HyPS samples and 32 for CSP samples, i.e. material compacted through the HyPS process is 5 fold harder than the same material processed according to CSP methodology, though it results 4 times softer than a silica-based sintered material [350].

The resulting IFT for HyPS samples was in average 0.69 $MPa \cdot m^{1/2}$, in line with the IFT values of silica-based glasses reported in the literature [245,351]. No cracks (neither Palmqvist's nor median) were observed in CSP samples, thus no IFT was related to these samples, meaning that CSP samples are not hard enough to induce the formation of cracks on the indentation corners. The discrepancy between HyPS and CSP samples is also demonstrated by the indentation plot in Figure B1c, showing a deeper indentation displacement for CSP samples [349,352,353].

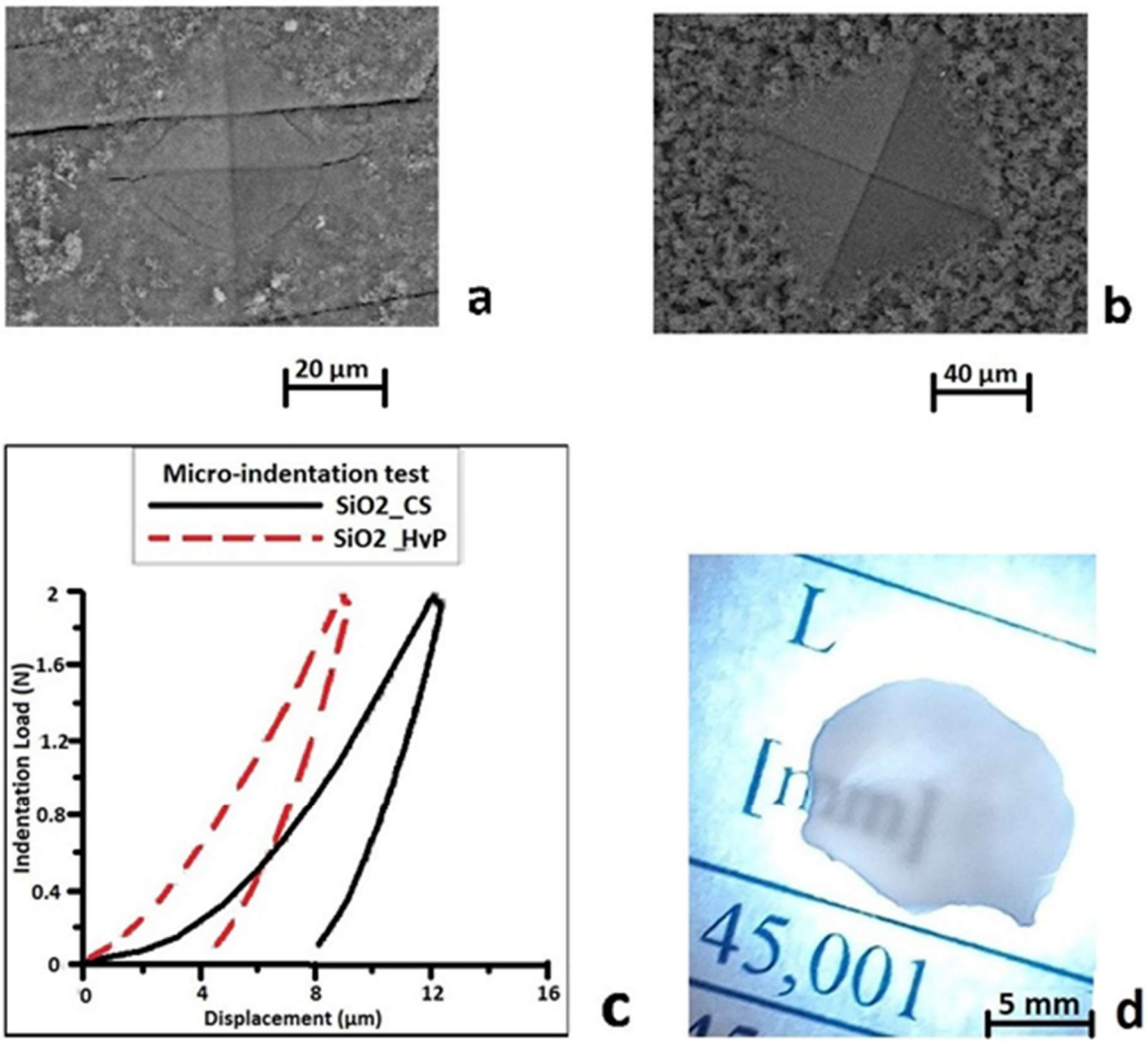

Figure B1: Vickers Hardness micro-indentations on a) nanosilica hydro-pressure sintering sample (450 MPa in water for 5 minutes) and b) nanosilica cold sintering sample (450 MPa in water for 2 h at 200 °C). c) Micro-hardness load plot of nanosilica cold sintering sample (black line) and nanosilica hydro-pressure sintering sample (red line). d) Macrograph of a translucent nanosilica hydro-pressure sintering sample (600 MPa in water for 5 minutes).

Appendix C – Hydro-pressure densification of borosilicate glass powder

The HyPS process was found to be also effective for the densification of the borosilicate glass powder in water under 500 MPa of pressure kept for 5 minutes. The BSG is highly soluble even in simple water [354], more than another silica-based glasses (e.g. soda-lime, sodium trisilicate, fused silica, etc.) due to the presence of borates and other network modifiers in the composition. This is why the HyPS process was found to not be effective if the *NaOH* solution was used as a solvent – in this condition BSG particles almost totally dissolve and no compaction of powder is possible.

Due to these reasons, BSG powder is highly densified through HyPS process, as deductible from Figure C1a-b, showing a relative density of about 90% (Archimedes method). The second-phase produced under pressure is mainly amorphous, a part from a presence of some cristobalite detected through XRD spectroscopy. Most interestingly, the quasi-amorphous second-phase seems to create by deposition of the borosilicate species in nanoparticles clusters around undissolved BSG microparticles, and conjugate each other through the formation of a network, as depicted in Figure C1c. This phenomenon is likely to be attributed to the Ostwald ripening mechanisms, like happens in the biosintering of diatoms and sea-sponges [82,84].

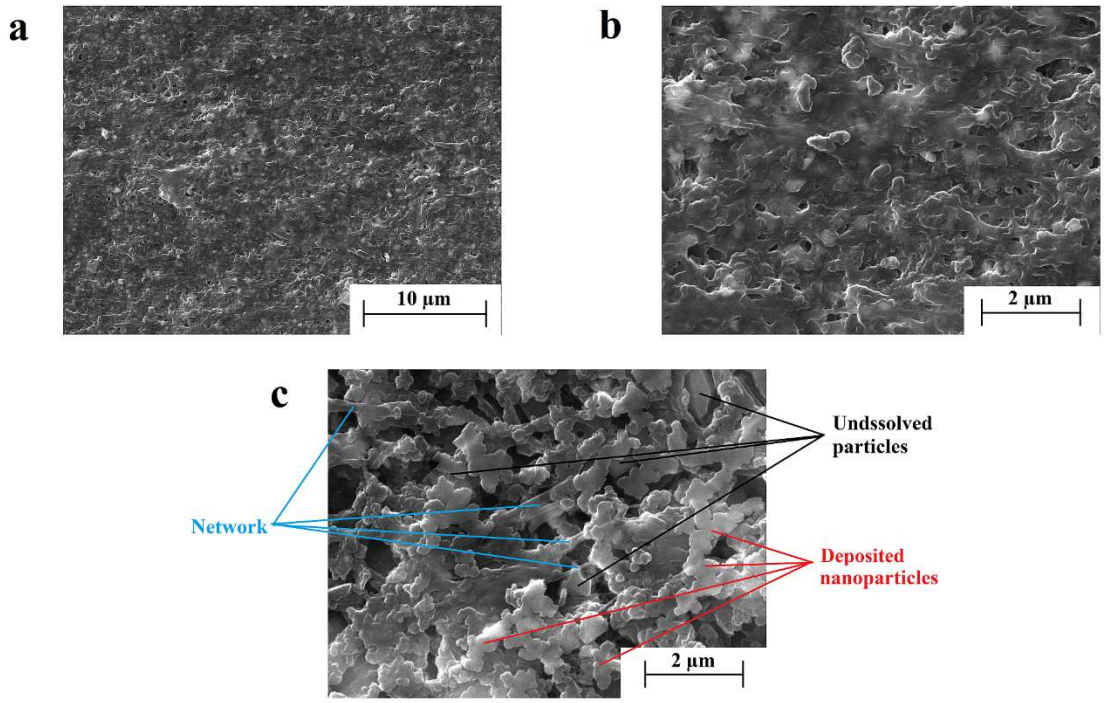

Figure C1: Scanning electron microscopy of a borosilicate hydro-pressure sintering sample in the water at 500 MPa for 5 minutes a) 5000, b) 20000x and c) 20000x less dense site.

8. References

[1] F. Pacheco-Torgal, J. Castro-Gomes, S. Jalali, Alkali-activated binders: A review. Part 1. Historical background, terminology, reaction mechanisms and hydration products, Constr. Build. Mater. 22 (2008) 1305–1314. doi:10.1016/j.conbuildmat.2007.10.015.

[2] B. Singh, G. Ishwarya, M. Gupta, S.K. Bhattacharyya, Geopolymer concrete: A review of some recent developments, Constr. Build. Mater. 85 (2015) 78–90. doi:10.1016/j.conbuildmat.2015.03.036.

[3] ECOBA, Torwards a thematic strategy on the prevention and recycling of waste, (2001) 5.

[4] G. Taveri, J. Tousek, E. Bernardo, N. Toniolo, A.R.R. Boccaccini, I. Dlouhy, Proving the role of boron in the structure of fly-ash / borosilicate glass based geopolymers, Mater. Lett. 200 (2017) 105–108. doi:10.1016/j.matlet.2017.04.107.

[5] D. Khale, R. Chaudhary, Mechanism of geopolymerization and factors influencing its development: A review, J. Mater. Sci. 42 (2007) 729–746. doi:10.1007/s10853-006-0401-4.

[6] T. Alomayri, I.M. Low, Synthesis and characterization of mechanical properties in cotton fiber-reinforced geopolymer composites, J. Asian Ceram. Soc. 1 (2013) 30–34. doi:10.1016/j.jascer.2013.01.002.

[7] T. Alomayri, F.U.A. Shaikh, I.M. Low, Characterisation of cotton fibre-reinforced geopolymer composites, Compos. Part B Eng. 50 (2013) 1–6. doi:10.1016/j.compositesb.2013.01.013.

[8] K.L. Pickering, M.G.A. Efendy, T.M. Le, A review of recent developments in natural fibre composites and their mechanical performance, Compos. Part A Appl. Sci. Manuf. 83 (2016) 98–112. doi:10.1016/j.compositesa.2015.08.038.

[9] S. Pavía, E. Condren, Study of the Durability of OPC versus GGBS Concrete on Exposure to Silage Effluent, J. Mater. Civ. Eng. 20 (2008) 313–320. doi:10.1061/(ASCE)0899-1561(2008)20:4(313).

[10] K.J.D. MacKenzie, M.E. Smith, A. Wong, J. V. Hanna, B. Barry, M.W. Barsoum, Were the casing stones of Senefru's Bent Pyramid in Dahshour cast or carved? Multinuclear NMR evidence, Mater. Lett. 65 (2011) 350–352. doi:10.1016/j.matlet.2010.10.035.

[11] M.W. Barsoum, A. Ganguly, G. Hug, Microstructural evidence of reconstituted limestone blocks in the Great Pyramids of Egypt, J. Am. Ceram. Soc. 89 (2006) 3788–3796. doi:10.1111/j.1551-2916.2006.01308.x.

[12] J.L. Provis, S.A. Bernal, Alkali Activated Materials: State of the Art Report, Taylor Fr. 13 (2014) 125–144. doi:10.1007/978-94-007-7672-2_5.

[13] E. Gotti, J.P. Oleson, L. Bottalico, C. Brandon, R. Cucitore, R.L. Hohlfelder, A comparison of the chemical and engineering characteristics of ancient roman hydraulic concrete with a modern reproduction of vitruvian hydraulic concrete,

Archaeometry. 50 (2008) 576–590. doi:10.1111/j.1475-4754.2007.00371.x.

[14] M.D. Jackson, E.N. Landis, P.F. Brune, M. Vitti, H. Chen, Q. Li, M. Kunz, Mechanical resilience and cementitious processes in Imperial Roman architectural mortar, Proceeding Natl. Acad. Sci. United State Am. 111 (2014) 1–6. doi:10.1073/pnas.1417456111.

[15] Industry Briefing, Europe energy Europe coal phase outs gather pace, Econ. Intell. Unit. (2017) 2017–2019. http://www.eiu.com/industry/article/556113839/europe-coal-phase-outs-gather-pace/2017-11-13#.

[16] M.D.A. Thomas, Optimizing the Use of Fly Ash in Concrete, Portl. Cem. Assoc. (2007) 24. doi:10.15680/IJIRSET.2015.0409047.

[17] Z.Z. Ismail, E.A. AL-Hashmi, Recycling of waste glass as a partial replacement for fine aggregate in concrete, Waste Manag. 29 (2009) 655–659. doi:10.1016/j.wasman.2008.08.012.

[18] N. Toniolo, G. Taveri, K. Hurle, J.A.A. Roether, P. Ercole, I. Dlouhý, A.R.R. Boccaccini, Fly-ash-based geopolymers: How the addition of recycled glass or red mud waste influences the structural and mechanical properties, J. Ceram. Sci. Technol. 8 (2017) 411–419. doi:10.4416/JCST2017-00053.

[19] F. Puertas, M. Torres-Carrasco, Use of glass waste as an activator in the preparation of alkali-activated slag. Mechanical strength and paste characterisation, Cem. Concr. Res. 57 (2014) 95–104. doi:10.1016/j.cemconres.2013.12.005.

[20] C. Shi, A.F. Jiménez, A. Palomo, New cements for the 21st century: The pursuit of an alternative to Portland cement, Cem. Concr. Res. 41 (2011) 750–763. doi:10.1016/j.cemconres.2011.03.016.

[21] J.A. Church, N.J. White, A 20th century acceleration in global sea-level rise, Geophys. Res. Lett. 33 (2006) n/a-n/a. doi:10.1029/2005GL024826.

[22] B. Salah, Portland cement, Conrete Technology, Course Hero, 1995.

[23] J.L. Provis, A. Palomo, C. Shi, Advances in understanding alkali-activated materials, Cem. Concr. Res. 78 (2015) 110–125. doi:10.1016/j.cemconres.2015.04.013.

[24] A. Palomo, A. Fernandez-Jimenez, M. Criado, “Geopolymers”: same basic chemistry, different microstructures, Mater. Constr. 54 (2003) 77–91. doi:10.3989/mc.2004.v54.i275.249.

[25] A.O. Purdon, The action of alkalis on blast-furnace slag, J. Soc. Chem. Ind. 59 (1940) 191–202. https://www.scopus.com/record/display.uri?eid=2-s2.0-0041769907&origin=inward (accessed September 4, 2018).

[26] J. Davidovits, Geopolymer: Chemistry & Applications, Institute Geopolymere, 2008.

[27] J. Davidovits, Synthetic Mineral Polymer Compound of the Silicoaluminates Family and Preparation, 1984.

[28] J. Davidovits, Mineral Polymer and Methods of Making Them, United States Pat. (1982) 1–6.

[29] J. Davidovits, J.L. Sawyer, Early high-strength mineral polymer, United States Pat. (1985) 1–12. https://www.google.com/patents/US4509985.

[30] P.D. Krivenko, Alkaline cements: terminology, classification, aspects of durability, in: Proc. 10th Int. Congr. Chem. Cem., Amarkai AB and Congrex, Gothenburg, Sweden, 1997. https://openlibrary.org/works/OL13353671W/Proceedings_of_the_10th_International_Congress_on_the_Chemistry_of_Cement_Gothenburg_Sweden_June_2-6 (accessed June 25, 2018).

[31] A. Palomo, P. Krivenko, I. Garcia-Lodeiro, E. Kavalerova, O. Maltseva, A. Fernandez-Jimenez, A review on alkaline activation: new analytical perspectives, Mater. Construcción. 64 (2014) 1–23. doi:10.3989/mc.2014.00314.

[32] H. Kuhl, Slag cement and process of making the same. US Patent 900,939, 1930. https://patentimages.storage.googleapis.com/01/6d/9c/e419a866806506/US900939.pdf.

[33] C. Shi, D. Roy, P. Krivenko, D. Roy, P. Krivenko, Alkali-Activated Cements and Concretes, 1st Editio, Taylor & Francis, Lodon, 2003. doi:10.1201/9781482266900.

[34] R.D. Hooton, Bridging the gap between research and standards, Cem. Concr. Res. 38 (2008) 247–258. doi:10.1016/j.cemconres.2007.09.012.

[35] J.S.J. van Deventer, D.G. Brice, S.A. Bernal, J.L. Provis, S. Bernal, S. Bernal, J. Provis, J. Provis, Development, Standardization, and Applications of Alkali-activated Concretes, in: ASTM Symp. Geopolymers, San Diego, CA, ASTM International, 100 Barr Harbor Drive, PO Box C700, West Conshohocken, PA 19428-2959, 2013: pp. 196–212. doi:10.1520/STP156620120083.

[36] J.S.J. Van Deventer, J.L. Provis, P. Duxson, Technical and commercial progress in the adoption of geopolymer cement, Miner. Eng. 29 (2012) 89–104. doi:10.1016/j.mineng.2011.09.009.

[37] F. Pacheco-Torgal, Z. Abdollahnejad, A.F. Camões, M. Jamshidi, Y. Ding, Durability of alkali-activated binders: A clear advantage over Portland cement or an unproven issue?, Constr. Build. Mater. 30 (2012) 400–405. doi:10.1016/j.conbuildmat.2011.12.017.

[38] A. Palomo, M.T. Blanco-Varela, M.L. Granizo, F. Puertas, T. Vazquez, M.W. Grutzeck, Chemical stability of cementitious materials based on metakaolin, Cem. Concr. Res. 29 (1999) 997–1004. doi:10.1016/S0008-8846(99)00074-5.

[39] P.-T. Fernando, C.-G. João, Jalali Said, Durability and Environmental Performance of alkali-activated Tunsten Mine waste mortars, J. Mater. Civ. Eng. 22 (2010) 897–905. doi:10.1061/?ASCE?MT.1943-5533.0000092 CE.

[40] T. Bakharev, J.G. Sanjayan, Y.B. Cheng, Resistance of alkali-activated slag concrete to acid attack, Cem. Concr. Res. 33 (2003) 1607–1611. doi:10.1016/S0008-8846(03)00125-X.

[41] A. Fernandez-Jimenez, I. Garcia-Lodeiro, A. Palomo, Durability of alkali-activated fly ash cementitious materials, J. Mater. Sci. 42 (2007) 3055–3065. doi:10.1007/s10853-006-0584-8.

[42] U. Diederichs, U.-M. Jumppanen, V. Penttala, Behavior of high strength concrete at high temperatures, Rep. 1992. (1989).

[43] J. Davidovits, Geopolymers, J. Therm. Anal. 37 (1991) 1633–1656. doi:10.1007/BF01912193.

[44] R.E. Lyon, P.N. Balaguru, A. Foden, U. Sorathia, J. Davidovits, M. Davidovics, Fire resistant alumosilicate composites, Fire Mater. 21 (1997) 67–73.

[45] J.L. Provis, J.S.J. van Deventer, Geopolymers. Structures, Processing, Properties and Industrial Applications, 2009. doi:10.1533/9781845696382.

[46] H. Xu, J.S.J. van Deventer, Geopolymerisation of alumino-silicate minerals, Int. J. Miner. Process. 59 (2000) 247–266. doi:10.1016/S0301-7516(99)00074-5.

[47] A. Fernandez-Jimenez, A. Palomo, Alkali Activated Fly Ashes: Properties and Characteristics, in: 11th, Int. Congr. Chem. Cem., PCA, Durban, South Africa, 2003: p. 137. https://www.tib.eu/en/search/id/BLCP%3ACN056953423/Alkali-Activated-Fly-Ashes-Properties-and-Characteristics/ (accessed June 19, 2018).

[48] D.W. Breck, Zeolite molecular sieves: structure, chemistry, and use, Wilej, New York. (1973) 589.

[49] F. Puertas, T. Amat, A. Fernández-Jiménez, T. Vázquez, Mechanical and durable behaviour of alkaline cement mortars reinforced with polypropylene fibres, Cem. Concr. Res. 33 (2003) 2031–2036. doi:10.1016/S0008-8846(03)00222-9.

[50] R. Brooks, M. Bahadory, F. Tovia, H. Rostami, Properties of alkali-activated fly ash: High performance to lightweight, Int. J. Sustain. Eng. 3 (2010) 211–218. doi:10.1080/19397038.2010.487162.

[51] Y. Fu, L. Cai, W. Yonggen, Freeze-thaw cycle test and damage mechanics models of alkali-activated slag concrete, Constr. Build. Mater. 25 (2011) 3144–3148. doi:10.1016/j.conbuildmat.2010.12.006.

[52] F. Škvára, L. Kopecký, V. Šmilauer, Z. Bittnar, Material and structural characterization of alkali activated low-calcium brown coal fly ash, J. Hazard. Mater. 168 (2009) 711–720. doi:10.1016/j.jhazmat.2009.02.089.

[53] E.N. Kani, A. Allahverdi, J.L. Provis, Composites Efflorescence control in geopolymer binders based on natural pozzolan, Cem. Concr. Compos. 34 (2012) 25–33. doi:10.1016/j.cemconcomp.2011.07.007.

[54] F. Škvára, L. Kopecký, L. Myšková, V. Šmilauer, L. Alberovská, L. Vinšová, Aluminosilicate polymers - Influence of elevated temperatures, efflorescence, Ceram. - Silikaty. 53 (2009) 276–282.

[55] J. Temuujin, A. van Riessen, R. Williams, Influence of calcium compounds on the mechanical properties of fly ash geopolymer pastes, J. Hazard. Mater. 167 (2009) 82–88. doi:10.1016/j.jhazmat.2008.12.121.

[56] N. Tenn, F. Allou, C. Petit, J. Absi, S. Rossignol, Formulation of new materials based on geopolymer binders and different road aggregates, Ceram. Int. 41 (2015) 5812–5820. doi:10.1016/j.ceramint.2015.01.010.

[57] J. Davidovits, Method for Eliminating the Akali Aggregate Reaction in Concretes and Cement Thereby Obtained, 1994. doi:US005485919A.

[58] J. Davidovits, Process for Obtaining a Geopolymeric Alumino-Silicate and Products Thus Obtained, 1994.

[59] J. Davidovits, Properties of Geopolymer Cements, First Int. Conf. Alkaline Cem. Concr. (1994) 131–149.

[60] J. Davidovits, Geopolymers, J. Therm. Anal. 37 (1991) 1633–1656. doi:10.1007/BF01912193.

[61] F. Pacheco-Torgal, J. Castro-Gomes, S. Jalali, Alkali-activated binders: A review. Part 2. About materials and binders manufacture, Constr. Build. Mater. 22 (2008) 1315–1322. doi:10.1016/j.conbuildmat.2007.03.019.

[62] V.F.F. Barbosa, K.J.D. MacKenzie, C. Thaumaturgo, Synthesis and characterisation of materials based on inorganic polymers of alumina and silica: Sodium polysialate polymers, Int. J. Inorg. Mater. 2 (2000) 309–317. doi:10.1016/S1466-6049(00)00041-6.

[63] H. Rahier, B. Van Mele, M. Biesemans, J. Wastiels, X. Wu, Low-temperature synthesized aluminosilicate glasses: Part I. Low-temperature reaction stoichiometry and structure of a model compound, J. Mater. Sci. 31 (1996) 71–79. doi:10.1007/BF00355128.

[64] H. Rahier, B. Van Mele, J. Wastiels, Low-temperature synthesized aluminosilicate glasses: Part II. Rheological transformations during low-temperature cure and high-temperature properties of a model compound, J. Mater. Sci. 31 (1996) 80–85. doi:10.1007/BF00355129.

[65] H. Rahier, W. Simons, B. Van Mele, M. Biesemans, Low-temperature synthesized aluminosilicate glasses: Part III Influence of the composition of the silicate solution on production, structure and properties, J. Mater. Sci. 32 (1997) 2237–2247. doi:10.1023/A:1018563914630.

[66] M. Criado, A. Palomo, A. Fernández-Jiménez, Alkali activation of fly ashes. Part 1: Effect of curing conditions on the carbonation of the reaction products, Fuel. 84 (2005) 2048–2054. doi:10.1016/j.fuel.2005.03.030.

[67] A. Fernández-Jiménez, A. Palomo, M. Criado, Microstructure development of alkali-activated fly ash cement: A descriptive model, Cem. Concr. Res. 35 (2005) 1204–1209. doi:10.1016/j.cemconres.2004.08.021.

[68] A. Palomo, S. Alonso, A. Fernandez-Jiménez, Alkaline Activation of Fly Ashes : NMR Study of the Reaction Products, J. Am. Ceram. Soc. 87 (2004) 1141–1145. doi:10.1111/j.1551-2916.2004.01141.x.

[69] A. Fernández-Jiménez, A. Palomo, Mid-infrared spectroscopic studies of alkali-activated fly ash structure, Microporous Mesoporous Mater. 86 (2005) 207–214.

doi:10.1016/j.micromeso.2005.05.057.

[70] P. Duxson, J.L. Provis, G.C. Lukey, S.W. Mallicoat, W.M. Kriven, J.S.J. Van Deventer, Understanding the relationship between geopolymer composition, microstructure and mechanical properties, Colloids Surfaces A Physicochem. Eng. Asp. 269 (2005) 47–58. doi:10.1016/j.colsurfa.2005.06.060.

[71] P. Duxson, A. Fernandez-Jimenez, J.L. Provis, G.C. Lukey, A. Palomo, J.S.J. Van Deventer, Geopolymer technology: The current state of the art, J. Mater. Sci. 42 (2007) 2917–2933. doi:10.1007/s10853-006-0637-z.

[72] J. Davidovits, Process for the fabrication of sintered panels and panels resulting from the application of this process, 1975. doi:10.1016/j.(73).

[73] H. Rahier, J. Wastiels, M. Biesemans, R. Willlem, G. Van Assche, B. Van Mele, Reaction mechanism, kinetics and high temperature transformations of geopolymers, J. Mater. Sci. 42 (2007) 2982–2996. doi:10.1007/s10853-006-0568-8.

[74] L. Weng, K. Sagoe-Crentsil, T. Brown, S. Song, Effects of aluminates on the formation of geopolymers, Mater. Sci. Eng. B Solid-State Mater. Adv. Technol. 117 (2005) 163–168. doi:10.1016/j.mseb.2004.11.008.

[75] L. Weng, K. Sagoe-Crentsil, Dissolution processes, hydrolysis and condensation reactions during geopolymer synthesis: Part I-Low Si/Al ratio systems, J. Mater. Sci. 42 (2007) 2997–3006. doi:10.1007/s10853-006-0820-2.

[76] L. Weng, K. Sagoe-Crentsil, Dissolution processes, hydrolysis and condensation reactions during geopolymer synthesis: Part II-High Si/Al ratio systems, J. Mater. Sci. 42 (2007) 3007–3014. doi:10.1007/s10853-006-0818-9.

[77] T.W. Swaddle, J. Salerno, P.A. Tregloan, Aqueous, Aluminates, Silicates, and Aluminosilicates, J. Phys. D Appl. Phys. 28 (1995) 2554.

[78] J.L. Provis, Alkali-activated materials, Cem. Concr. Res. (2016). doi:10.1016/j.cemconres.2017.02.009.

[79] J.L. Provis, S.A. Bernal, Geopolymers and Related Alkali-Activated Materials, Annu. Rev. Mater. Res. 44 (2014) 299–327. doi:10.1146/annurev-matsci-070813-113515.

[80] B.L. Deopura, R. Alagirusamy, M. Joshi, B. Gupta, Polyesters and Polyamides, 2008. doi:10.1533/9781845694609.

[81] V.B. Gupta, Manufactured Fibre Technology, 1997. doi:10.1007/978-94-011-5854-1_16.

[82] D.J. Belton, O. Deschaume, C.C. Perry, An overview of the fundamentals of the chemistry of silica with relevance to biosilicification and technological advances, FEBS J. 279 (2012) 1710–1720. doi:10.1111/j.1742-4658.2012.08531.x.

[83] V.V. Annenkov, E.N. Danilovtseva, V.A. Pal'shin, O.N. Verkhozina, S.N. Zelinskiy, U.M. Krishnan, Silicic acid condensation under the influence of water-soluble polymers: from biology to new materials, RSC Adv. 7 (2017) 20995–21027. doi:10.1039/c7ra01310h.

[84] X. Wang, U. Schloßmacher, M. Wiens, R. Batel, H.C. Schröder, W.E.G. Müller, Silicateins, silicatein interactors and cellular interplay in sponge skeletogenesis: Formation of glass fiber-like spicules, FEBS J. 279 (2012) 1721–1736. doi:10.1111/j.1742-4658.2012.08533.x.

[85] A.K. Davis, M. Hildebrand, Molecular Processes of Biosilicification in Diatoms, 2010. doi:10.1002/9780470986325.ch8.

[86] D. Otzen, The Role of Proteins in Biosilicification, Scientifica (Cairo). 2012 (2012) 22.

[87] M. Torres-Carrasco, F. Puertas, Waste glass in the geopolymer preparation. Mechanical and microstructural characterisation, J. Clean. Prod. 90 (2015) 397–408. doi:10.1016/j.jclepro.2014.11.074.

[88] A. Fernández-Jiménez, A. Palomo, Composition and microstructure of alkali activated fly ash binder: Effect of the activator, Cem. Concr. Res. 35 (2005) 1984–1992. doi:10.1016/j.cemconres.2005.03.003.

[89] J.L. Provis, G.C. Lukey, J.S.J. Van Deventer, Do geopolymers actually contain nanocrystalline zeolites? a reexamination of existing results, Chem. Mater. 17 (2005) 3075–3085. doi:10.1021/cm050230i.

[90] R. Iler, Colloidal components in solutions of sodium silicate, Soluble Silic. (ACS Symp. Ser. 194). (1982) 95–114. doi:10.1021/bk-1982-0194.ch007.

[91] S.K. Young, Sol-Gel Science for Ceramic Materials, Mater. Matters. 1.3 (2006) 1–5.

[92] M. Criado, A. Fernandez-Jimenez, a G. de la Torre, M. a G. Aranda, A. Palomo, An XRD study of the effect of the SiO2/Na2O ratio on the alkali activation of fly ash, Cem. Concr. Res. 37 (2007) 671–679. doi:10.1016/j.cemconres.2007.01.013.

[93] J. Klinowski, Nuclear magnetic resonance studies of zeolites, Prog. Nucl. Magn. Reson. Spectrosc. 16 (1984) 237–309. doi:10.1016/0079-6565(84)80007-2.

[94] A. Fernández-Jiménez, A. Palomo, M. Criado, Alkali activated fly ash binders. A comparative study between sodium and potassium activators, Mater. Construcción. 56 (2006) 51–65. doi:10.3989/mc.2006.v56.i281.92.

[95] R.M. Hamidi, Z. Man, K.A. Azizli, Concentration of NaOH and the Effect on the Properties of Fly Ash Based Geopolymer, Procedia Eng. 148 (2016) 189–193. doi:10.1016/j.proeng.2016.06.568.

[96] J.G.S. Van Jaarsveld, J.S.J. Van Deventer, The Effect of metal contaminants on the formation and properties of waste-based geopolymers, Cem. Concr. Res. 29 (1999) 1189–1200. doi:10.1016/S0008-8846(99)00032-0.

[97] G.M. Nasab, F. Golestanifard, K.J.D. MacKenzie, The effect of the SiO2/Na2O ratio in the structural modification of metakaolin-based geopolymers studied by XRD, FTIR and MAS-NMR, J. Ceram. Sci. Technol. 5 (2014). doi:10.4416/JCST2014-00007.

[98] K.J.D. MacKenzie, M.E. Smith, Multinuclear Solid-State Nuclear Magnetic

Resonance of Inorganic Materials - Kenneth J.D. MacKenzie, M.E. Smith - Google Books, I, Elsevier, 2002. https://books.google.cz/books?hl=en&lr=&id=_nDsTC1wQOwC&oi=fnd&pg=PP1&ots=xGh5ziikCg&sig=0QRQzbMoMmmXfiJWv5iRuJiuFFA&redir_esc=y#v=onepage&q=notation &f=false (accessed August 16, 2018).

[99] J.E. Oh, Y. Jun, Y. Jeong, P.J.M. Monteiro, The importance of the network-modifying element content in fly ash as a simple measure to predict its strength potential for alkali-activation, Cem. Concr. Compos. 57 (2014) 44–54. doi:10.1016/j.cemconcomp.2014.12.001.

[100] A.W. Chester, E.G. Derouane, Zeolite characterization and catalysis: A tutorial, 2010. doi:10.1007/978-1-4020-9678-5.

[101] M. Criado, A. Fernández-Jiménez, A. Palomo, I. Sobrados, J. Sanz, Effect of the SiO2/Na2O ratio on the alkali activation of fly ash. Part II: 29Si MAS-NMR Survey, Microporous Mesoporous Mater. 109 (2008) 525–534. doi:10.1016/j.micromeso.2007.05.062.

[102] J.J. Trochez, R.M. De Gutiérrez, J. Rivera, S.A. Bernal, Synthesis of Geopolymer from Spent FCC : Effect of SiO2/Al2O3 and Na2O/SiO2 Molar Ratios, Mater. Constr. 65 (2015) 1–11. doi:10.3989/mc.2015.00814.

[103] M. Sitarz, M. Handke, W. Mozgawa, E. Galuskin, I. Galuskina, The non-ring cations influence on silicooxygen ring vibrations, J. Mol. Struct. 555 (2000) 357–362. doi:10.1016/S0022-2860(00)00621-9.

[104] M. Sitarz, W. Mozgawa, M. Handke, Rings in the structure of silicate glasses, J. Mol. Struct. 511–512 (1999) 281–285. doi:10.1016/S0022-2860(99)00169-6.

[105] P. Timakul, K. Thanaphatwetphisit, P. Aungkavattana, Effect of silica to alumina ratio on the compressive strength of class C fly ash-based geopolymers, Key Eng. Mater. 659 (2015) 80–84. doi:10.4028/www.scientific.net/KEM.659.80.

[106] P. Chindaprasirt, P. De Silva, K. Sagoe-Crentsil, S. Hanjitsuwan, Effect of SiO2 and Al2O3 on the setting and hardening of high calcium fly ash-based geopolymer systems, J. Mater. Sci. 47 (2012) 4876–4883. doi:10.1007/s10853-012-6353-y.

[107] M. Criado, A. Fernández-Jiménez, A. Palomo, Alkali activation of fly ash: Effect of the SiO2/Na2O ratio. Part I: FTIR study, Microporous Mesoporous Mater. 106 (2007) 180–191. doi:10.1016/j.micromeso.2007.02.055.

[108] K. Gao, K.-L. Lin, D. Wang, C.-L. Hwang, H.-S. Shiu, Y.-M. Chang, T.-W. Cheng, Effects SiO2/Na2O molar ratio on mechanical properties and the microstructure of nano-SiO2 metakaolin-based geopolymers, Constr. Build. Mater. 53 (2014) 503–510. doi:10.1016/j.conbuildmat.2013.12.003.

[109] R. Zejak, I. Nikoli, D. Đurović, B.P. Mugo, D. Ble, V. Radmilovi, Influence of Na2O / Al2O3 and SiO2 / Al2O3 ratios on the immobilization of Pb from electric arc furnace into the fly ash based geopolymers, in: E3S Web Conf., 2013: pp. 2–4. doi:10.1051/e3sconf/20130131007.

[110] V. Bocullo, D. Vaičiukynienė, V. Vaitkevičius, A. Kantautas, The influence of the silica/sodium ratio on the fly ash geopolymer binder, Chem. Technol. 68 (2017) 23–

28. doi:10.5755/j01.ct.68.1.18873.

[111] H. Cheng, K. Lin, R. Cui, C. Hwang, Y. Chang, T. Cheng, The effects of SiO2 / Na2O molar ratio on the characteristics of alkali-activated waste catalyst – metakaolin based geopolymers, Constr. Build. Mater. 95 (2015) 710–720. doi:10.1016/j.conbuildmat.2015.07.028.

[112] T.A. García-Mejía, M. de Lourdes Chávez-García, Compressive Strength of Metakaolin-Based Geopolymers: Influence of KOH Concentration, Temperature, Time and Relative Humidity, Mater. Sci. Appl. 7 (2016) 772–791. doi:10.4236/msa.2016.711060.

[113] M.S. Muñiz-Villarreal, A. Manzano-Ramírez, S. Sampieri-Bulbarela, J.R. Gasca-Tirado, J.L. Reyes-Araiza, J.C. Rubio-Ávalos, J.J. Pérez-Bueno, L.M. Apatiga, A. Zaldivar-Cadena, V. Amigó-Borrás, The effect of temperature on the geopolymerization process of a metakaolin-based geopolymer, Mater. Lett. 65 (2011) 995–998. doi:10.1016/j.matlet.2010.12.049.

[114] B.H. Mo, H. Zhu, X.M. Cui, Y. He, S.Y. Gong, Effect of curing temperature on geopolymerization of metakaolin-based geopolymers, Appl. Clay Sci. 99 (2014) 144–148. doi:10.1016/j.clay.2014.06.024.

[115] A.A. Adam, Horianto, The effect of temperature and duration of curing on the strength of fly ash based geopolymer mortar, in: Procedia Eng., Elsevier B.V., 2014: pp. 410–414. doi:10.1016/j.proeng.2014.12.199.

[116] S.Y. Oderji, B. Chen, S. Taseer, A. Jaffar, Effects of relative humidity on the properties of fly ash-based geopolymers, Constr. Build. Mater. 153 (2017) 268–273.

[117] G. Kovalchuk, A. Fernandez-Jimenez, A. Palomo, Alkali-activated fly ash: Effect of thermal curing conditions on mechanical and microstructural development - Part II, Fuel. 86 (2007) 315–322. doi:10.1016/j.fuel.2006.07.010.

[118] M. Criado, A. Fernández-Jiménez, A. Palomo, Alkali activation of fly ash. Part III: Effect of curing conditions on reaction and its graphical description, Fuel. 89 (2010) 3185–3192. doi:10.1016/j.fuel.2010.03.051.

[119] M. Delle Selve, J.P. Judson, Press Release European Container Glass Industry Welcomes, Eur. Contain. Glas. Fed. (2015) 1–2.

[120] V. Corinaldesi, G. Gnappi, G. Moriconi, A. Montenero, Reuse of ground waste glass as aggregate for mortars, Waste Manag. 25 (2005) 197–201. doi:10.1016/j.wasman.2004.12.009.

[121] A. Rincón, G. Giacomello, M. Pasetto, E. Bernardo, Novel “ inorganic gel casting ” process for the manufacturing of glass foams, J. Eur. Ceram. Soc. 37 (2017) 2227–2234. doi:10.1016/j.jeurceramsoc.2017.01.012.

[122] M. Torres-Carrasco, F. Puertas, M.. Blanco-Varela, Preparación de cementos alcalinos a partir de residuos vítreos. Solubilidad de residuos vítreos en medios fuertemente básicos, XII Congr. Nac. Mater. (2012) 113. doi:10.1016/j.jclepro.2014.03.018.

[123] F. Puertas Maroto, J.J. Torres Castanos, V. Fernández, Procedimiento Para la

Fabricacion de Cementos Alcalinos a Partir de Residuos Vitreos Urbanos e Industriales., 2013. https://worldwide.espacenet.com/searchResults?search=ES2394979 A1&DB=EPODOC&submitted=true&locale=en_EP&ST=singleline&compact=false&DB=EPODOC&query=ES2394979 A1.

[124] J.J. Torres, M. Palacios, M. Hellouin, F. Puertas, Alkaline Chemical Activation of Urban Glass Wastes to Produce Cementitious Materials, 1st Spanish Natl. Conf. Adv. Mater. Recycl. Eco – Energy Madrid, 12-13 Novemb. 2009. (2009) 12–13.

[125] M. Torres-Carrasco, C. Rodríguez-Puertas, M. Del Mar Alonso, F. Puertas, Alkali activated slag cements using waste glass as alternative activators. Rheological behaviour, Bol. La Soc. Esp. Ceram. Y Vidr. 54 (2015) 45–57. doi:10.1016/j.bsecv.2015.03.004.

[126] M. Torres-carrasco, J.G. Palomo, F. Puertas, Sodium silicate solutions from dissolution of glass wastes . Statistical analysis, Mater. Construcción. 64 (2014) 1–14. doi:10.3989/mc.2014.05213.

[127] R.K. Chinnam, E. Bernardo, J. Will, A.R. Boccaccini, A.R.B. Processing, Processing of porous glass ceramics from highly crystallisable industrial wastes, Adv. Appl. Ceram. 6753 (2015). doi:10.1179/1743676115Y.0000000053.

[128] R.K. Chinnam, A.R. Boccaccini, E. Bernardo, H. Epstein, Glass-Ceramic Composites from Borosilicate Glass and Alumina-Rich Residues, Int. J. Appl. Ceram. Technol. 12 (2015) E19–E27. doi:10.1111/ijac.12197.

[129] A.A. Francis, R.D. Rawlings, R. Sweeney, A.R. Boccaccini, Processing of coal ash into glass ceramic products by powder technology and sintering, Soc. Glas. Technol. 43 (2002) 58–62. http://www.ingentaconnect.com/content/sgt/gt/2002/00000043/00000002/art00001?crawler=true (accessed August 28, 2018).

[130] C. Nicholson, B. Murray, R.A. Fletcher, D.R.M. Brew, K.J.D. MacKenzie, M. Schmuker, Novel geopolymer materials containing borate structural units, in: Geopolymergreen Chem. Sustain. Dev. Solut., Saint-Quentin (France), 2005.

[131] A. Palomo, M.W. Grutzeck, M.T. Blanco, Alkali-activated fly ashes: A cement for the future, Cem. Concr. Res. 29 (1999) 1323–1329. doi:10.1016/S0008-8846(98)00243-9.

[132] N. Gamage, Overview of Different Types of Fly Ash and Their Use as a Building and Construction Material, in: Conf. Proceeding, n.d.

[133] R.C. Joshi, R.P. Lohtia, Types and Properties of Fly Ash, Prog. Cem. Concr. (1985) 118–157.

[134] N. Gamage, K. Liyanage, S. Fragomeni, S. Setunge, Overview of different types of fly ash and their use as a building and construction material, in: Int. Conf. Struct. Eng. Constr. Manag., 2013. http://dl.lib.mrt.ac.lk/handle/123/9367.

[135] A. Fernández-Jiménez, A. Palomo, Characterisation of fly ashes. Potential reactivity as alkaline cements, Fuel. 82 (2003) 2259–2265. doi:10.1016/S0016-2361(03)00194-7.

[136] M. Criado, A. Fernández Jiménez, I. Sobrados, A. Palomo, J. Sanz, Effect of relative humidity on the reaction products of alkali activated fly ash, J. Eur. Ceram. Soc. 32 (2012) 2799–2807. doi:10.1016/j.jeurceramsoc.2011.11.036.

[137] P.J.G. Puertas F., Varga C., Torres M., Torres J.J., Moreno E., Reuse of Urban and Industrial Glass Wastes to Prepare Alkaline Cements, 4th Int. Conf. Eng. Waste Biomass Valoris. (2012) 65–70.

[138] Y. Hu, D. Luo, P. Li, Q. Li, G. Sun, Fracture toughness enhancement of cement paste with multi-walled carbon nanotubes, Constr. Build. Mater. 70 (2014) 332–338. doi:10.1016/j.conbuildmat.2014.07.077.

[139] K.C. Marc Meyers, Mechanical behavior of materials - Second edition, 2009. doi:10.1017/CBO9780511807756.003.

[140] T.L. Anderson, Fracture mechanics. Fundamentals and applications - Third edition, Third, 2005.

[141] S. Yan, P. He, D. Jia, Z. Yang, X. Duan, S. Wang, Y. Zhou, In situ fabrication and characterization of graphene/geopolymer composites, Ceram. Int. 41 (2015) 11242–11250. doi:10.1016/j.ceramint.2015.05.075.

[142] S. Yan, P. He, D. Jia, Z. Yang, X. Duan, S. Wang, Y. Zhou, Effect of fiber content on the microstructure and mechanical properties of carbon fiber felt reinforced geopolymer composites, Ceram. Int. 42 (2016) 7837–7843. doi:10.1016/j.ceramint.2016.01.197.

[143] D.P. Dias, C. Thaumaturgo, Fracture toughness of geopolymeric concretes reinforced with basalt fibers, Cem. Concr. Compos. 27 (2005) 49–54. doi:10.1016/j.cemconcomp.2004.02.044.

[144] T. Alomayri, F.U.A. Shaikh, I.M. Low, Effect of fabric orientation on mechanical properties of cotton fabric reinforced geopolymer composites, Mater. Des. 57 (2014) 360–365. doi:10.1016/j.matdes.2014.01.036.

[145] T. Alomayri, F.U.A. Shaikh, I.M. Low, Thermal and mechanical properties of cotton fabric-reinforced geopolymer composites, J. Mater. Sci. 48 (2013) 6746–6752. doi:10.1007/s10853-013-7479-2.

[146] Y. Wang, Cellulose Fiber Dissolution in Sodium Hydroxide Solution at Low Temperature : Dissolution Kinetics and Solubility Improvement, 2008.

[147] J. Wei, Impact of Cement Hydration on Durability of Cellulosic Fiber-Reinforced Cementitious Composites in the Presence of Metakaolin, Adv. Eng. Mater. 20 (2018) 1–12. doi:10.1002/adem.201700642.

[148] R.D. Tolêdo Filho, K. Joseph, K. Ghavami, G.L. England, The Use of Sisal Fibre As Reinforcement in Cement Based Composites, Rev. Bras. Eng. Agrícola E Ambient. 3 (1999) 245–256. doi:10.1590/1807-1929/agriambi.v3n2p245-256.

[149] J. Deja, Carbonation aspects of alkali activated slag mortars and concretes, Silic. Ind. 67 (2002) 37–42. https://www.tib.eu/en/search/id/tema%3ATEMA20030704768/Carbonation-aspects-of-alkali-activated-slag-mortars/ (accessed August 31, 2018).

[150] N. De Belie, H.J. Verselder, B. De Blaere, D. Van Nieuwenburg, R. Verschoore, Influence of the cement type on the resistance of concrete to feed acids, Cem. Concr. Res. 26 (1996) 1717–1725. doi:10.1016/S0008-8846(96)00155-X.

[151] J. Davidovits, 30 Years of Successes and Failures in Geopolymer Applications . Market Trends and Potential Breakthroughs ., in: Geopolymer 2002 Conf., Melbourne, Austrialia, 2002: pp. 1–16. doi:10.1017/CBO9781107415324.004.

[152] H.T. Yu, J. Mallela, M.I. Darter, Highway Concrete Pavement Technology Development and Testing : Volume IV — Field Evaluation of Strategic Highway Research Program (SHRP) C-206 Test Sites (Early Opening of Full-Depth Pavement Repairs), U.S. Dep. Transp. IV (2006).

[153] K. Jones, Special Cements for Fast Track Concrete, Iowa Dep. Transp. (1988).

[154] P.G. Malone, Ch.A. Randall, Potential applications of alkali-silicate binders in military operations, Geotech. Lab. (1985) 1–39.

[155] C. Ozyildirim, A Field Investigation of Concrete Patches Containing Pyramet Blended Cement. Final Report, Virginia Dep. Transp. (1994). https://trid.trb.org/view/405198 (accessed September 3, 2018).

[156] P. Zia, M.L. Leming, S.H. Ahmad, J.J. Schemmel, R.P. Elliott, Mechanical Behavior of Production of High Performance Concrete, 1993.

[157] J. Davidovits, PYRAMENT cement good for heavy traffic after 25 years – Geopolymer Institute, (n.d.). https://www.geopolymer.org/news/pyrament-cement-good-for-heavy-traffic-after-25-years/ (accessed September 3, 2018).

[158] M. Vanooteghem, uit de jaren 50 - Het Purdocement Woord vooraf, 2011.

[159] B. Talling, Effect of Curing Conditions on Alkali-Activated Slags, in: 3rd Int. Conf. Fly Ash, Silica Fume, Slag Nat. Pozzolans Concr., Trondheim, Norway, 1989. https://trid.trb.org/view/921246 (accessed September 4, 2018).

[160] B. Forss, Process for producing a binder for slurry, mortar, and concrete. U.S. Patent 4,306,912, 1982. doi:10.1016/j.(73).

[161] J.J.J.M. Goumans, H.A. van der. Sloot, T.G. Aalbers, Waste materials in construction : proceedings of the International Conference on Environmental Implications of Construction with Waste Materials, Maastricht, the Netherlands, 10-14 November 1991, Elsevier, 1991.

[162] D. Wimpenny, P. Duxson, J. Provis, Fibre reinforced geopolymer concrete products for underground infrastructure, in: Concr. 2011, Perth, Aust., 2011: p. 64.

[163] VicRoads, VicRoads: Standard Specification - Section 703 - General Concrete Paving, (2010).

[164] VicRoads, VicRoads: Standard Specification - Section 620 - Precast Concrete Uunits, 620 (2009) 1–3.

[165] M. Uehara, New Concrete with Low Environmental Load Using the Geopolymer Method, Q. Rep. RTRI. 51 (2010) 1–7. doi:10.2219/rtriqr.51.1.

[166] A. Fernández-Jiménez, A. Palomo, D. Revuelta, Alkali activation of industrial by-products to develop new Earth-friendly cements, in: Proceeding 11th Int. Conf. Non-Conventional Mater. Technol. (NOMAT 2009), 2009: pp. 1–15.

[167] Á. Palomo, A. Fernández-Jiménez, C. López-Hombrados, J.L. Lleyda, Railway sleepers made of alkali activated fly ash concrete, Rev. Ing. Constr. 22 (2007) 75–80. doi:10.4067/S0718-50732007000200001.

[168] M. Grutzeck, S. Kwan, M. DiCola, Zeolite formation in alkali-activated cementitious systems, Cem. Concr. Res. 34 (2004) 949–955. doi:10.1016/j.cemconres.2003.11.003.

[169] P. Krivenko, G.Y. Kovalchuk, Directed synthesis of alkaline aluminosilicate minerals in a geocement matrix, J. Mater. Sci. 42 (2007) 2944–2952. doi:10.1007/s10853-006-0528-3.

[170] R. Arellano Aguilar, O. Burciaga Díaz, J.I. Escalante García, Lightweight concretes of activated metakaolin-fly ash binders, with blast furnace slag aggregates, Constr. Build. Mater. 24 (2010) 1166–1175. doi:10.1016/j.conbuildmat.2009.12.024.

[171] R.L. Helferich, Ligthweight Hydrogel-Bound Aaggregate Shapes and Process for Producing Same - US 4963515A, 1990.

[172] J.L. Bell, W.M. Kriven, Developments in Strategic Materials, 2009.

[173] E. Prud'Homme, P. Michaud, E. Joussein, J.M. Clacens, S. Rossignol, Role of alkaline cations and water content on geomaterial foams: Monitoring during formation, J. Non. Cryst. Solids. 357 (2011) 1270–1278. doi:10.1016/j.jnoncrysol.2010.12.030.

[174] E. Prud'homme, P. Michaud, E. Joussein, C. Peyratout, A. Smith, S. Arrii-Clacens, J.M. Clacens, S. Rossignol, Silica fume as porogent agent in geo-materials at low temperature, J. Eur. Ceram. Soc. 30 (2010) 1641–1648. doi:10.1016/j.jeurceramsoc.2010.01.014.

[175] E. Prud'homme, P. Michaud, E. Joussein, C. Peyratout, A. Smith, S. Rossignol, In situ inorganic foams prepared from various clays at low temperature, Appl. Clay Sci. 51 (2011) 15–22. doi:10.1016/j.clay.2010.10.016.

[176] J. Henon, A. Alzina, J. Absi, D.S. Smith, S. Rossignol, Porosity control of cold consolidated geomaterial foam: Temperature effect, Ceram. Int. 38 (2012) 77–84. doi:10.1016/j.ceramint.2011.06.040.

[177] V. Vaou, D. Panias, Thermal insulating foamy geopolymers from perlite, Miner. Eng. 23 (2010) 1146–1151. doi:10.1016/j.mineng.2010.07.015.

[178] D.L. Bell, P.G. Malone, Alkali-Aactivated Glassy Silicate Foamed Concrete - US 5605570, 1997. doi:10.1007/s00253-005-1916-3.

[179] G.D. Birch, Cellular Cementitious Composition - US 8167994B2, 2012. doi:10.1016/S0141.

[180] Y. Zhao, J. Ye, X. Lu, M. Liu, Y. Lin, W. Gong, G. Ning, Preparation of sintered foam materials by alkali-activated coal fly ash, J. Hazard. Mater. 174 (2010) 108–

112. doi:10.1016/j.jhazmat.2009.09.023.

[181] B.E. Laney, T.E. Williams, R.L. Rutherford, D.T. Bailey, Advanced geopolymer composites - US 5244726A, 1993. https://patents.google.com/patent/US5244726A/en.

[182] A. Buchwald, R. Oesterheld, H. Hilbig, Incorporation of aluminate into silicate gels and its effect on the foamability and water resistance, J. Am. Ceram. Soc. 93 (2010) 3370–3376. doi:10.1111/j.1551-2916.2010.03842.x.

[183] R.A. Fletcher, K.J.D. MacKenzie, C.L. Nicholson, S. Shimada, The composition range of aluminosilicate geopolymers, J. Eur. Ceram. Soc. 25 (2005) 1471–1477. doi:10.1016/j.catcom.2006.11.029.

[184] M. V. Sukhanevich, S.G. Guzii, The effect of technological factors on properties of alkali aluminosilicate systems used for preparation of fireproof coatings, Refract. Ind. Ceram. 45 (2004) 217–219. doi:10.1023/B:REFR.0000036733.85631.f1.

[185] J. Temuujin, A. Minjigmaa, W. Rickard, M. Lee, I. Williams, A. van Riessen, Fly ash based geopolymer thin coatings on metal substrates and its thermal evaluation, J. Hazard. Mater. 180 (2010) 748–752. doi:10.1016/j.jhazmat.2010.04.121.

[186] W. Brylicki, J. Malolepszy, S. Stryczek, Industrial scale application of the alkali activated slag cementitious materials in the injection sealing works, Stud. Environ. Sci. 60 (1994) 841–849.

[187] M.C.M. Nasvi, P.G. Ranjith, J. Sanjayan, The permeability of geopolymer at down-hole stress conditions: Application for carbon dioxide sequestration wells, Appl. Energy. 102 (2013) 1391–1398. doi:10.1016/j.apenergy.2012.09.004.

[188] K. Javanmardi, K.D. Flodberg, Mud to Cement Technology Proven in Offshore Drilling Project, Oil Gas J. 91 (1993) 49–57. https://www.ogj.com/articles/print/volume-91/issue-7/in-this-issue/general-interest/mud-to-cement-technology-proven-in-offshore-drilling-project.html (accessed November 5, 2018).

[189] J.J. Nahm, K. Javanmardi, K.M. Cowan, A.H. Hale, Slag mix mud conversion cementing technology: Reduction of mud disposal volumes and management of rig-site drilling wastes, J. Pet. Sci. Eng. 11 (1994) 3–12. doi:10.1016/0920-4105(94)90058-2.

[190] A. Ruiz-Santaquiteria, C., Fernandez-Jimenez, A. Palomo, Reological Properties of Alkali Activated Cement for Oil Well Linings., in: Second Int. Symp. Des. Perform. Use Self-Consolidating Concr. SCC'2009-China, June 5-7 2009, Beijing,China, 2009: pp. 878–891.

[191] A.H. Hale, K.M. Cowan, J.J.W. Nahm, Universal fluid for drilling and cementing wells - US 5464060, 1995.

[192] D. Wu, B. Huang, Slag / mud mixtures improve cementing operations in China, Oil Gas J. 94 (1996) 95–100.

[193] M.G.P. Silva, C.R. Miranda, A.R.D. Almeida, G. Campos, M.T.A. Bezerra, Slag Cementing Versus Conventional Cementing : Comparative Bond Results, in: 5th

Lat. Am. Caribb. Pet. Eng. Conf. Exhib. Rio Janeiro, Brazil., 1997. doi:10.2118/39005-MS.

[194] O.G. Benge, W.W. Webster, Blast Furnace Slag Slurries May Have Limits for Oil Field Use, Oil Gas J. 92 (1994) 41–49.

[195] V. Balet-Gouedard, O. Porcherie, E. Pershikova, Pumpable geopolymer formulation for oilfield application - EP2093200A1, 2009. doi:10.1371/joumal.pone.0010853.

[196] V. Barlet-Gouedard, B. Zustatz-Ayache, O. Porcherie, Geopolymer Composition and Application for Carbon Dioxide Storage - US 7846250 B2, 2010. doi:10.1038/incomms1464.

[197] J.R. Conner, S.L. Hoeffner, Critical Reviews in Environmental Science and Technology, Crit. Rev. Environ. Sci. Technol. 28 (2010) 267–276. doi:10.1080/10643389.2011.647788.

[198] F.P. Glasser, Fundamental aspects of cement solidification and stabilisation, J. H. 52 (1997) 151–1701. doi:Doi 10.1016/S0304-3894(96)01805-5.

[199] R. Malviya, R. Chaudhary, Factors affecting hazardous waste solidification/stabilization: A review, J. Hazard. Mater. 137 (2006) 267–276. doi:10.1016/j.jhazmat.2006.01.065.

[200] F.P. Glasser, Progress in the immobilization of radioactive wastes in cement, Cem. Concr. Res. 22 (1992) 201–216. doi:10.1016/0008-8846(92)90058-4.

[201] F.P. Glasser, Mineralogical aspects of cement in radioactive waste disposal, October. 65 (2001) 621–633. doi:10.1180/002646101317018442.

[202] N.B. Milestone, Reactions in cement encapsulated nuclear wastes: need for toolbox of different cement types, Adv. Appl. Ceram. 105 (2006) 13–20. doi:10.1179/174367606X81678.

[203] C. Shi, A. Fernández-Jiménez, Stabilization/solidification of hazardous and radioactive wastes with alkali-activated cements, J. Hazard. Mater. 137 (2006) 1656–1663. doi:10.1016/j.jhazmat.2006.05.008.

[204] J.G.S. Van Jaarsveld, J.S.J. Van Deventer, The Potential Use of Geopolymeric Materials to Immobilise Toxic Metals Part I . Theory and Applications, Miner. Eng. 10 (1997) 1–10.

[205] J.G.S.V.A.N. Jaarsveld, J.S.J.V.A.N. Deventer, A. Schwartzman, The potential use of geopolymeric materials to immobilise toxic metals- part II. Material and leaching characteristics, Miner. Eng. 12 (1999) 75–91.

[206] E. Hermann, C. Kunze, R. Gatzweiler, G. Kießig, J. Davidovits, Solidification of Various Radioactive Residues by Geopolymere® with Special Emphasis on Long-Term-Stability Solidification, in: Geopolymer ’99 Proceeding, 1999.

[207] J. Deja, Immobilization of Cr6+,Cd2+,Zn2+ and Pb2+ in alkali-activated slag binders Jan, Cem. Concr. Res. 32 (2002) 1971–1979. doi:10.1002/(SICI)1096-9861(19960805)371:4<567::AID-CNE6>3.3.CO;2-M.

[208] J.W. Cho, K. Ioku, S. Goto, Effect of PBII and CrVI ions on the hydration of slag alkaline cement and the immobilization of these heavy metal ions, Adv. Cem. Res. 11 (1999) 11–118. doi:10.1680/adcr.1999.11.3.111.

[209] Y.H. Ahmed, N.R. Buenfeld, An Investigation of Ground Granulated Blastfurnace Slag as a Toxic Waste Solidification/Stabilization Reagent, Environ. Eng. Sci. 14 (1997) 113–132. doi:10.1089/ees.1997.14.113.

[210] C. Shi, J. Stegemann, R. Caldwell, An Examination of Interference in Waste Solidification Through Measurement of Heat Signature, Waste Manag. 17 (1998) 249–255.

[211] R.J. Caldwell, J.A. Stegemann, C. Shi, Effect of curing on field-solidified waste properties . Part 2: Chemical properties, Waste Manag. Res. 17 (1999) 44–49.

[212] R.J. Caldwell, J.A. Stegemann, C. Shi, Effect of curing on field-solidified waste properties. Part 1: physical properties., Waste Manag. Res. 17 (1999) 37–43.

[213] J.G.S. Van Jaarsveld, J.S.J. Van Deventer, L. Lorenzen, Factors affecting the immobilization of metals in geopolymerized flyash, Metall. Mater. Trans. B. 29 (1998) 283–291. doi:10.1007/s11663-998-0032-z.

[214] A. Palomo, M. Palacios, Alkali-activated cementitious materials: Alternative matrices for the immobilisation of hazardous wastes - Part II. Stabilisation of chromium and lead, Cem. Concr. Res. 33 (2003) 289–295. doi:10.1016/S0008-8846(02)00964-X.

[215] M. Palacios, A. Palomo, Alkali-activated fly ash matrices for lead immobilisation: a comparison of different leaching tests, Adv. Cem. Res. 16 (2004) 137–144. doi:10.1680/adcr.16.4.137.46661.

[216] J. Zhang, J.L. Provis, D. Feng, J.S.J. van Deventer, Geopolymers for immobilization of Cr6+, Cd2+, and Pb2+, J. Hazard. Mater. 157 (2008) 587–598. doi:10.1016/j.jhazmat.2008.01.053.

[217] K.R. Henke, Waste Treatment and Remediation Technologies for Arsenic, 2009. doi:10.1002/9780470741122.ch7.

[218] P. Bankowski, L. Zou, R. Hodges, Using inorganic polymer to reduce leach rates of metals from brown coal fly ash, Miner. Eng. 17 (2004) 159–166. doi:10.1016/j.mineng.2003.10.024.

[219] E. Álvarez-Ayuso, X. Querol, F. Plana, A. Alastuey, N. Moreno, M. Izquierdo, O. Font, T. Moreno, S. Diez, E. Vázquez, M. Barra, Environmental, physical and structural characterisation of geopolymer matrixes synthesised from coal (co-)combustion fly ashes, J. Hazard. Mater. 154 (2008) 175–183. doi:10.1016/j.jhazmat.2007.10.008.

[220] A.M. Fernandez-Jiminez, E.E. Lachowski, A. Palomo, D.E. Macphee, Microstructural characterisation of alkali-activated PFA matrices for waste immobilisation, Cem. Concr. Compos. 26 (2004) 1001–1006. doi:10.1016/j.cemconcomp.2004.02.034.

[221] A. Fernández-Jiménez, A. Palomo, D.E. Macphee, E.E. Lachowski, Fixing arsenic

in alkali-activated cementitious matrices, J. Am. Ceram. Soc. 88 (2005) 1122–1126. doi:10.1111/j.1551-2916.2005.00224.x.

[222] D.M. Sherman, S.R. Randall, Surface complexation of arsenic(V) to iron(III) (hydr)oxides: Structural mechanism from ab initio molecular geometries and EXAFS spectroscopy, Geochim. Cosmochim. Acta. 67 (2003) 4223–4230. doi:10.1016/S0016-7037(03)00237-0.

[223] J.Z. Xu, Y.L. Zhou, Q. Chang, H.Q. Qu, Study on the factors of affecting the immobilization of heavy metals in fly ash-based geopolymers, Mater. Lett. 60 (2006) 820–822. doi:10.1016/j.matlet.2005.10.019.

[224] J.M. Diez, J. Madrid, A. Macias, Characterization of Cement-Stabilized Cd Wastes, Cem. Concr. Res. 27 (1997) 337–343.

[225] M.P. Pomiès, N. Lequeux, P. Boch, Speciation of cadmium in cement- Part I. Cd2+uptake by C-S-H, Cem. Concr. Res. 31 (2001) 563–569. doi:10.1016/S0008-8846(00)00480-4.

[226] J. Tits, E. Wieland, C.J. Müller, C. Landesman, M.H. Bradbury, Strontium binding by calcium silicate hydrates, J. Colloid Interface Sci. 300 (2006) 78–87. doi:10.1016/j.jcis.2006.03.043.

[227] W. Xuequan, Y. Sheng, S. Xiaodong, T. Mingshu, Y. Liji, Alkali-activated slag cement based radioactive waste forms, Cem. Concr. Res. 21 (1991) 16–20. doi:10.1016/0008-8846(91)90026-E.

[228] C. Shi, R. Day, Alkali-Slag Cements For the Immobilization Of Radioactive Wastes, in: Stab. Solidif. Hazardous, Radioact. Mix. Wastes 3rd Vol., ASTM International, 100 Barr Harbor Drive, PO Box C700, West Conshohocken, PA 19428-2959, 1996: pp. 163-163–11. doi:10.1520/STP14111S.

[229] Z. Aly, E.R. Vance, D.S. Perera, J. V. Hanna, C.S. Griffith, J. Davis, D. Durce, Aqueous leachability of metakaolin-based geopolymers with molar ratios of Si/Al = 1.5-4, J. Nucl. Mater. 378 (2008) 172–179. doi:10.1016/j.jnucmat.2008.06.015.

[230] M.G. Blackford, J. V. Hanna, K.J. Pike, E.R. Vance, D.S. Perera, Transmission electron microscopy and nuclear magnetic resonance studies of geopolymers for radioactive waste immobilization, J. Am. Ceram. Soc. 90 (2007) 1193–1199. doi:10.1111/j.1551-2916.2007.01532.x.

[231] M.Y. Khalil, E. Merz, Immobilization of Intermediate-Level Wastes in Geopolymers, J. Nucelar Mater. 211 (1994) 141–148. doi:10.1002/art.1780271110.

[232] S. Berger, F. Frizon, C. Joussot-Dubien, Formulation of caesium based and caesium containing geopolymers, Adv. Appl. Ceram. 108 (2009) 412–417. doi:10.1179/174367609X422072.

[233] S. Chen, M. Wu, S. Zhang, Mineral phases and properties of alkali-activated metakaolin-slag hydroceramics for a disposal of simulated highly-alkaline wastes, J. Nucl. Mater. 402 (2010) 173–178. doi:10.1016/j.jnucmat.2010.05.015.

[234] G.E. Fryxell, J. Liu, S. V Mattigod, L.Q. Wang, M. Gong, T.A. Hauser, Y. Lin, K.F. Ferris, X. Feng, Environmental Issues and Waste Management Technologies in the

Ceramic and Nuclear Industries, Environmental Applications of Interfacially Modified Mesoporous Ceramics, 2000.

[235] A.D. Chervonnyi, N.A. Chervonnaya, Geopolymeric agent for immobilization of radioactive ashes after biomass burning, Radiochemistry. 45 (2003) 182–188. doi:10.1023/A:1023845628670.

[236] D. Strlezcki, Geopolymer succeeds at Chernobyl field test, Pollut. Eng. 33 (2001) 36. http://connection.ebscohost.com/c/articles/5595906/geopolymer-succeeds-chernobyl-field-test (accessed November 6, 2018).

[237] P. Childress, The use of EKOR TM to stabilize fuel-containing material at Chernobyl., in: WM Symp. | WM2019, Tucson, AZ, 2001. http://wmsym.org/archives/2001/4/4-1.pdf (accessed November 6, 2018).

[238] R. Zhao, J.G. Sanjayan, Geopolymer and Portland cement concretes in simulated fire, Concr. Res. 63 (2011) 163–173. doi:10.1680/macr.9.00110.

[239] J. Giancaspro, P.N. Balaguru, R.E. Lyon, Use of Inorganic Polymer to Improve the Fire Response of Balsa Sandwich Structures, J. Mater. Civ. Eng. 18 (2006) 390–397. doi:10.1061/(ASCE)0899-1561(2006)18:3(390).

[240] G. Taveri, E. Bernardo, I. Dlouhy, Mechanical Performance of Glass-Based Geopolymer Matrix Composites Reinforced with Cellulose Fibers, Materials (Basel). 11 (2018) 2395. doi:10.3390/ma11122395.

[241] M. Todd, E. Janelle, HR-MAS NMR Spectroscopy in Material Science, in: Adv. Asp. Spectrosc., 2012: pp. 279–306. doi:10.5772/48340.

[242] G. Hofecker, Solid-state NMR spectroscopy - An introduction, Aktuelle Gerontol. 6 (1976) 103–110.

[243] Schurko, Introduction to Solid-State NMR, (n.d.).

[244] K. Pelzer, Principles of solid state NMR and applications in catalysis applications, Inorg. Chem. Dpt. - Fritz-Haber Inst. Der Max-Planck Gesellschaft. (2015).

[245] L. Bertolla, I. Dlouhý, P. Tatarko, A. Viani, A. Mahajan, Z. Chlup, M.J. Reece, A.R. Boccaccini, Pressureless spark plasma–sintered Bioglass® 45S5 with enhanced mechanical properties and stress–induced new phase formation, J. Eur. Ceram. Soc. 37 (2017) 2727–2736. doi:10.1016/j.jeurceramsoc.2017.02.003.

[246] D.J. Oehlers, P. Visintin, T. Zhang, Y. Chen, D. Knight, Flexural rigidity of reinforced concrete members using a deformation based analysis Flexural Rigidity of Reinforced Concrete Members Using a Deformation Based Analysis, in: Concr. Aust., 2012: pp. 50–56.

[247] ASTM International, ASTM D790 - 17 Standard Test Methods for Flexural Properties of Unreinforced and Reinforced Plastics and Electrical Insulating Materials, ASTM Stand. (2018). https://www.astm.org/Standards/D790.htm (accessed January 8, 2019).

[248] A.R. Boccaccini, H. Kern, I. Dlouhy, Determining the fracture resistance of fibre-reinforced glass matrix composites by means of the chevron-notch flexural

technique, Mater. Sci. Eng. A. 308 (2001) 111–117. doi:10.1016/S0921-5093(00)01984-5.

[249] ASTM E92 Standard test methods for Vickers hardness of metallic materials, in: Am. Soc. Test. Mater., 2017.

[250] G.R. Anstis, A Critical Evaluation of Indentation Techniques for Measuring Fracture Toughness: I, Direct Crack Measurements, J. Am. Ceram. Soc. 46 (1981) 533–538. http://onlinelibrary.wiley.com/doi/10.1111/j.1151-2916.1981.tb10320.x/abstract.

[251] D. Ma, O.C. Wo, J. Liu, J. He, Determination of Young's modulus by nanoindentation, Sci. China Ser. E. 47 (2004) 398. doi:10.1360/03ye0590.

[252] W.C. Oliver, G.M. Pharr, An improved technique for determining hardness and elastic modulus using load and displacement sensing indentation experiments, J. Mater. Res. 6 (1992).

[253] A. Fernandez-Jimenez, A.G. De La Torre, A. Palomo, G. Lopez-Olmo, M.M. Alonso, M.A.G. Aranda, Quantitative determination of phases in the alkali activation of fly ash. Part I. Potential ash reactivity, Fuel. 85 (2006) 625–634. doi:10.1016/j.fuel.2005.08.014.

[254] R.P. Williams, A. Van Riessen, Determination of the reactive component of fly ashes for geopolymer production using XRF and XRD, Fuel. 89 (2010) 3683–3692. doi:10.1016/j.fuel.2010.07.031.

[255] A. Monshi, Quantitative Phase Analysis in Industrial Research, in: ACXRI 1996, 1996: pp. 1–4. doi:10.1007/978-94-007-5580-2.

[256] L.N. Assi, E. Eddie Deaver, P. Ziehl, Effect of source and particle size distribution on the mechanical and microstructural properties of fly Ash-Based geopolymer concrete, Constr. Build. Mater. 167 (2018) 372–380. doi:10.1016/j.conbuildmat.2018.01.193.

[257] N. Toniolo, A.R. Boccaccini, Fly ash-based geopolymers containing added silicate waste. A review, Ceram. Int. 43 (2017) 14545–14551. doi:10.1016/j.ceramint.2017.07.221.

[258] MEE (Materials Evaluation and Engineering), Handbook of Analytical Methods for Materials, 2014.

[259] M. Cerruti, G. Magnacca, V. Bolis, C. Morterra, Characterization of sol–gel bioglasses with the use of simple model systems: a surface-chemistry approach, J. Mater. Chem. 13 (2003) 1279–1286. doi:10.1039/B300961K.

[260] W. Mozgawa, M. Sitarz, M. Rokita, Spectroscopic studies of different aluminosilicate structures, J. Mol. Struct. 511–512 (1999) 251–257. doi:10.1016/S0022-2860(99)00165-9.

[261] M. Sitarz, M. Handke, W. Mozgawa, Identification of silicooxygen rings in SiO2 based on IR spectra, Spectrochim. Acta - Part A Mol. Biomol. Spectrosc. 56 (2000) 1819–1823. doi:10.1016/S1386-1425(00)00241-9.

[262] I. Lecomte, C. Henrist, M. Liégeois, F. Maseri, A. Rulmont, R. Cloots, (Micro)-structural comparison between geopolymers, alkali-activated slag cement and Portland cement, J. Eur. Ceram. Soc. 26 (2006) 3789–3797. doi:10.1016/j.jeurceramsoc.2005.12.021.

[263] J.W. Phair, J.S.J. Van Deventer, Effect of Silicate Aactivator pH on the Leaching and Material Characteristics of Waste-Based Inorganic Polymers, Int. J. Miner. Process. 66 (2002) 121–143. doi:http://dx.doi.org/10.1016/S0301-7516(02)00013-3.

[264] E. Arioz, Ö. Arioz, Ö.M. Koç, The Effect of Curing Conditions on the Properties of Geopolymer Samples, Int. J. Chem. Eng. Appl. 4 (2013) 4–7. doi:10.7763/IJCEA.2013.V4.339.

[265] S. Alonso, A. Palomo, Calorimetric study of alkaline activation of calcium hydroxide-metakaolin solid mixtures, Cem. Concr. Res. 31 (2001) 25–30. doi:10.1016/S0008-8846(00)00435-X.

[266] H. Jansson, D. Bernin, K. Ramser, Silicate species of water glass and insights for alkali-activated green cement, AIP Adv. 5 (2015) 1–9. doi:10.1063/1.4923371.

[267] S.M. Bobrowski A., Stypula B., Hutera B., Drozynski D., Ftir Spectroscopy of Water Glass - The Binder Moulding Modified by ZnO Nanoparticles, 51 (2012) 477–480.

[268] G.Taveri, S.Grasso, Bio-Inspired Hydro-Pressure Consolidation of Silica, Adv. Funct. Mater. 1805794 (2018) 1–22. doi:10.1002/adfm.201805794.

[269] S.A. Bernal, J.L. Provis, V. Rose, R. Mejía De Gutierrez, Evolution of binder structure in sodium silicate-activated slag-metakaolin blends, Cem. Concr. Compos. 33 (2011) 46–54. doi:10.1016/j.cemconcomp.2010.09.004.

[270] C. Su, D.L. Suarez, Coordination of Adsorbed Boron: A FTIR Spectroscopic Study., Environ. Sci. Technol. 29 (1995) 302–11. doi:10.1021/es00002a005.

[271] C. Gautam, A.K. Yadav, A.K. Singh, A Review on Infrared Spectroscopy of Borate Glasses with Effects of Different Additives, ISRN Ceram. 2012 (2012) 1–17. doi:10.5402/2012/428497.

[272] M. Nolan, T.S. Perova, R.A. Moore, C.E. Beitia, J.F. McGilp, H.S. Gamble, Spectroscopic Investigations of Borosilicate Glass and Its Application as a Dopant Source for Shallow Junctions, J. Electrochem. Soc. 147 (2000) 3100. doi:10.1149/1.1393863.

[273] T.S. Perova, M. Nolan-Jones, J. McGilp, H.S. Gamble, Borosilicate glass nanolayer as a spin-on dopant source: FTIR and spectroscopic ellipsometry investigations, J. Mater. Sci. Mater. Electron. 27 (2016) 6292–6304. doi:10.1007/s10854-016-4561-y.

[274] A. Fernández-Jiménez, A. Palomo, I. Sobrados, J. Sanz, The role played by the reactive alumina content in the alkaline activation of fly ashes, Microporous Mesoporous Mater. 91 (2006) 111–119. doi:10.1016/j.micromeso.2005.11.015.

[275] M. Yamane, M. Okuyama, Coordination Number of Aluminum Ions in Alkali-free Alumino-Silicate Glasses, J. Non. Cryst. Solids. 52 (1982) 217–226.

[276] P.S. Singh, M. Trigg, I. Burgar, T. Bastow, Geopolymer formation processes at room temperature studied by 29Si and 27Al MAS-NMR, Mater. Sci. Eng. A. 396 (2005) 392–402. doi:10.1016/j.msea.2005.02.002.

[277] P.S. Singh, T. Bastow, M. Trigg, Structural studies of geopolymers by 29Si and 27Al MAS-NMR, J. Mater. Sci. 40 (2005) 3951–3961. doi:10.1007/s10853-005-1915-x.

[278] L. van Wullen, W. Muller-Warmuth, 11B MAS NMR spectroscopy for characterizing the structure of glasses, Solid State Nucl. Magn. Reson. 2 (1993) 279–284. doi:10.1016/0926-2040(93)90009-C.

[279] A. Grandjean, M. Malki, V. Montouillout, F. Debruycker, D. Massiot, Electrical conductivity and 11B NMR studies of sodium borosilicate glasses, J. Non. Cryst. Solids. 354 (2008) 1664–1670. doi:10.1016/j.jnoncrysol.2007.10.007.

[280] S. Sen, Z. Xu, J.. Stebbins, Temperature dependent structural changes in borate, borosilicate and boroaluminate liquids: high-resolution 11B, ^{29}Si and ^{27}Al NMR studies, J. Non. Cryst. Solids. 226 (1998) 29–40. doi:10.1016/S0022-3093(97)00491-2.

[281] H.B. Merrili, The Solubility of Silica, J. Am. Chem. Soc. (1917) 2630–2638.

[282] M.P. Gunasekara, D.W. Law, S. Setunge, Effect of synthesizing parameters on workability and compressive strength of Fly ash based Geopolymer mortar, in: 23rd Aust. Conf. Mech. Struct. Mater., 2014: pp. 168–177. doi:10.6088/ijcser.201203013016.

[283] M.S. Jansen, M.U. Christiansen, Effect of Water-Solids Ratio on the Compressive Strength and Morphology of Fly Ash-Waste Glass Geopolymer Mortars, in: World Coal Ash Conf. Coal Ash Conf., Nashville, TN (USA), 2015.

[284] H. Toutanji, B. Xu, J. Gilbert, T. Lavin, Properties of poly(vinyl alcohol) fiber reinforced high-performance organic aggregate cementitious material: Converting brittle to plastic, Constr. Build. Mater. 24 (2010) 1–10. doi:10.1016/j.conbuildmat.2009.08.023.

[285] W. Li, S. Ma, Y. Hu, X. Shen, The mechanochemical process and properties of Portland cement with the addition of new alkanolamines, Powder Technol. 286 (2015) 750–756. doi:10.1016/j.powtec.2015.09.024.

[286] G.H.D. Tonoli, U.P. Rodrigues Filho, H. Savastano, J. Bras, M.N. Belgacem, F.A. Rocco Lahr, Cellulose modified fibres in cement based composites, Compos. Part A Appl. Sci. Manuf. 40 (2009) 2046–2053. doi:10.1016/j.compositesa.2009.09.016.

[287] L. Bodnarova, J. Hroudova, J. Brozovsky, J. Zach, J. Valek, Behaviour of Cement Composites with Lightweight and Heavyweight Aggregates at High Temperatures, Priodica Polytech. 61 (2017) 272–281.

[288] P.C. Association, Types and Causes of Concrete Deterioration, 2002.

[289] X.Y. Zhuang, L. Chen, S. Komarneni, C.H. Zhou, D.S. Tong, H.M. Yang, W.H. Yu, H. Wang, Fly ash-based geopolymer: Clean production, properties and applications, J. Clean. Prod. 125 (2016) 253–267. doi:10.1016/j.jclepro.2016.03.019.

[290] E.F. Côrtes Pires, C.M. Campinho de Azevedo, A.R. Pimenta, F.J. da Silva, F.A.I. Darwish, Fracture Properties of Geopolymer Concrete Based on Metakaolin, Fly Ash and Rice Rusk Ash, Mater. Res. 20 (2017) 630–636. doi:10.1590/1980-5373-MR-2016-0974.

[291] H. Assaedi, T. Alomayri, A. Shaikh, I. Low, Characterisation of mechanical and thermal properties in flax fabric reinforced geopolymer composites, J. Adv. Cermics. 4 (2015) 272–281. doi:10.1007/s40145-015-0161-1.

[292] A. Natali, S. Manzi, M.C. Bignozzi, Novel fiber-reinforced composite materials based on sustainable geopolymer matrix, Procedia Eng. 21 (2011) 1124–1131. doi:10.1016/j.proeng.2011.11.2120.

[293] P. Timakul, W. Rattanaprasit, P. Aungkavattana, Improving compressive strength of fly ash-based geopolymer composites by basalt fibers addition, Ceram. Int. 42 (2015) 6288–6295. doi:10.1016/j.ceramint.2016.01.014.

[294] M. Alzeer, K. MacKenzie, Synthesis and mechanical properties of novel composites of inorganic polymers (geopolymers) with unidirectional natural flax fibres (phormium tenax), Appl. Clay Sci. 75–76 (2013) 148–152. doi:10.1016/j.clay.2013.03.010.

[295] I. Dlouhý, A.R. Boccaccini, Reliability of the chevron notch technique for fracture toughness determination in glass composites reinforced by continuous fibres, Scr. Mater. 44 (2001) 531–537. doi:10.1016/S1359-6462(00)00601-1.

[296] T. Alomayri, H. Assaedi, F.U.A. Shaikh, I.M. Low, Effect of water absorption on the mechanical properties of glass/polyester composites, Mater. Des. 28 (2007) 1647–1650. doi:10.1016/j.matdes.2006.03.014.

[297] R. Merrill, R. Spencer, Sorption of Sodium Silicates and Silica Sols by Cellulose Fibers, Ind. Eng. Chem. 42 (1950) 744–747. http://pubs.acs.org/doi/abs/10.1021/ie50484a046.

[298] J.O.A.N.D. Willey, The Effect of Pressure on the Solubility of Amorphous Silica in Seawater at 0 ° C, Mar. Chem. 2 (1974) 239–250.

[299] G.M. Anderson, C.W. Burnham, The solubility of quartz in super-critical water, Am. J. Sci. 263 (1965) 494–511. doi:10.2475/ajs.263.6.494.

[300] L. Bruce Railsback, An earth scientist's periodic table of the elements and their ions, Geol. Soc. Am. 31 (2003) 737–740.

[301] S.B. Kang, J. Bin Lim, D. Jo, I.S. Nam, B.K. Cho, S.B. Hong, C.H. Kim, S.H. Oh, Ostwald-ripening sintering kinetics of Pd-based three-way catalyst: Importance of initial particle size of Pd, Chem. Eng. J. 316 (2017) 631–644. doi:10.1016/j.cej.2017.01.136.

[302] Q. Zheng, W.X. Yao, L.C. Lim, Ostwald ripening and grain growth in Ti(C,N)-based cermets during liquid phase sintering, Int. J. Refract. Met. Hard Mater. 58 (2016) 1–7. doi:10.1016/j.ijrmhm.2016.03.008.

[303] R. Anderson, R. Buscall, R. Eldridge, P. Mulvaney, P.J. Scales, Ostwald ripening of comb polymer stabilised Ag salt nanoparticles, Colloids Surfaces A Physicochem.

Eng. Asp. 459 (2014) 58–64. doi:10.1016/j.colsurfa.2014.06.033.

[304] R.L. Coble, Sintering crystalline solids. I. intermediate and final state diffusion models, J. Appl. Phys. 32 (1961) 787–792. doi:10.1063/1.1736107.

[305] R.L. Coble, Sintering crystalline solids. II. experimental test of diffusion models in powder compacts, J. Appl. Phys. 32 (1961) 793–799. doi:10.1063/1.1736108.

[306] J.-P. Maria, X. Kang, R.D. Floyd, E.C. Dickey, H. Guo, J. Guo, A. Baker, S. Funihashi, C.A. Randall, Cold sintering: Current status and prospects, J. Mater. Res. (2017) 1–14. doi:10.1557/jmr.2017.262.

[307] J. Guo, H. Guo, A.L. Baker, M.T. Lanagan, E.R. Kupp, G.L. Messing, C.A. Randall, Cold Sintering: A Paradigm Shift for Processing and Integration of Ceramics, Angew. Chemie - Int. Ed. 55 (2016) 11457–11461. doi:10.1002/anie.201605443.

[308] H. Guo, A. Baker, J. Guo, C.A. Randall, Cold Sintering Process: A Novel Technique for Low-Temperature Ceramic Processing of Ferroelectrics, J. Am. Ceram. Soc. 3507 (2016) 3489–3507. doi:10.1111/jace.14554.

[309] J. Guo, S.S. Berbano, H. Guo, A.L. Baker, M.T. Lanagan, C.A. Randall, Cold Sintering Process of Composites: Bridging the Processing Temperature Gap of Ceramic and Polymer Materials, Adv. Funct. Mater. 26 (2016) 7115–7121. doi:10.1002/adfm.201602489.

[310] A. Fernandez-Jimenez, A.G. de la Torre, A. Palomo, G. Lopez-Olmo, M.M. Alonso, M.A.G. Aranda, Quantitative determination of phases in the alkaline activation of fly ash. Part II: Degree of reaction, Fuel. 85 (2006) 1960–1969. doi:10.1016/j.fuel.2006.04.006.

[311] J.E. Oh, Y. Jun, Y. Jeong, Characterization of geopolymers from compositionally and physically different Class F fly ashes, Cem. Concr. Compos. 50 (2014) 16–26. doi:10.1016/j.cemconcomp.2013.10.019.

[312] W.D.A. Rickard, R. Williams, J. Temuujin, A. van Riessen, Assessing the suitability of three Australian fly ashes as an aluminosilicate source for geopolymers in high temperature applications, Mater. Sci. Eng. A. 528 (2011) 3390–3397. doi:10.1016/j.msea.2011.01.005.

[313] K. Sobolev, S.P. Shah, Nanotechnology in Construction & Civil Engineering, Springer, 2014.

[314] R. Singh, L. Singh, S.V. Singh, Beneficiation of iron and aluminium oxides from fly ash at lab scale, Int. J. Miner. Process. 145 (2015) 32–37. doi:10.1016/j.minpro.2015.08.001.

[315] M.J. Murtha, G. Burnet, The Magnetic Fraction of Coal Fly Ash : Its Separation, Properties, and Utilization, Proc. Iowa Acad. Sci. 85 (1978).

[316] M. Caldirola, E. Bernardo, M. Ferraris, Heat-insulating porous glass-ceramic material in slabs and process for producing such material - Patent WO 2015/011737 A2, 2015.

[317] A. Rincón, D. Desideri, E. Bernardo, Functional glass-ceramic foams from "inorganic gel casting" and sintering of glass/slag mixtures, J. Clean. Prod. 187 (2018) 250–256. doi:10.1016/j.jclepro.2018.03.065.

[318] H. Elsayed, A.R. Romero, G. Molino, C.V. Brovarone, E. Bernardo, Bioactive glass-ceramic foam scaffolds from "inorganic gel casting" and sinter-crystallization, Materials (Basel). 11 (2018) 1–12. doi:10.3390/ma11030349.

[319] A. Van Riessen, N. Chen-Tan, Beneficiation of Collie fly ash for synthesis of geopolymer Part 2 - Geopolymers, Fuel. 111 (2013) 829–835. doi:10.1016/j.fuel.2013.04.015.

[320] S.M. Yusuf, M.D. Mukadam, J.M. De Teresa, M.R. Ibarra, J. Kohlbrecher, A. Heinemann, A. Wiedenmann, Structural and magnetic properties of amorphous iron oxide, Phys. B Condens. Matter. 405 (2010) 1202–1206. doi:10.1016/j.physb.2009.11.040.

[321] L. Machala, R. Zboril, A. Gedanken, Amorphous iron(III) oxide - A review, J. Phys. Chem. B. 111 (2007) 4003–4018. doi:10.1021/jp064992s.

[322] R. Terzano, M. Spagnuolo, L. Medici, F. Tateo, R. Pacifico, Characterization of Different Coal Fly Ashes for Their Application in the Synthesis of Zeolite X as Cation Exchanger for Soil Remediation, Fresenius Environ. Bull. 14 (2005) 263–267.

[323] N. Garg, Raman spectroscopy for characterizing and determining the pozzolanic reactivity of fly ashes, Iowa University, 2016.

[324] A. Polyakovs, A. Shishkin, J. Baronins, Preparation of Coal-Water Slurry Uusing a High-Speed Mixer Disperser, in: 4th Int. Conf. Civ. Eng. - Environ. Environ. Eff., 2013: pp. 77–81.

[325] Corning company, PYREX 7740 Glass_Data sheet, 2018. http://www.quartz.com/pxprop.pdf.

[326] S.K. Lee, C.B. Musgrave, P. Zhao, J.F. Stebbins, Topological Disorder and Reactivity of Borosilicate Glasses: Quantum Chemical Calculations and ^{17}O and ^{11}B NMR Study, J. Phys. Chem. B. 105 (2001) 12583–12595. doi:10.1021/jp012119f.

[327] D.W. Sindorf, G.E. Maciel, Silicon-29 CP/MAS NMR studies of methylchlorosilane reactions on silica gel, J. Am. Chem. Soc. 103 (1981) 4263–4265. doi:10.1021/ja00404a055.

[328] D. Sindorf, G. Maciel, Cross-polarization magic-angle-spinning silicon-29 nuclear magnetic resonance study of silica gel using trimethylsilane bonding as a probe of surface geometry and, J. Phys. Chem. 86 (1982) 5208–5219. doi:10.1021/j100223a029.

[329] A.J. Vega, G.W. Scherer, Study of structural evolution of silica gel using 1H and 29Si NMR, J. Non. Cryst. Solids. 111 (1989) 153–166. doi:10.1093/qjmed/hct085.

[330] P.W.J.G. Wijnen, T.P.M. Beelen, J.W. de Haan, C.P.J. Rummens, L.J.M. van de Ven, R.A. van Santen, Silica gel dissolution in aqueous alkali metal hydroxides studied by 29SiNMR, J. Non. Cryst. Solids. 109 (1989) 85–94. doi:10.1016/0022-

3093(89)90446-8.

[331] M. Jedidi, O. Benjeddou, Chemical Causes of Concrete Degradation, MOJ Civ. Eng. 4 (2018). doi:10.15406/mojce.2018.04.00095.

[332] H.M. Saleh, M.E. Tawfik, T.A. Bayoumi, Chemical stability of seven years aged cement-PET composite waste form containing radioactive borate waste simulates, J. Nucl. Mater. 411 (2011) 185–192. doi:10.1016/j.jnucmat.2011.01.126.

[333] M.G. Sohail, R. Kahraman, N.G. Ozerkan, N.A. Alnuaimi, B. Gencturk, M. Dawood, A. Belarbi, Reinforced Concrete Degradation in the Harsh Climates of the Arabian Gulf: Field Study on 30-to-50-Year-Old Structures, J. Perform. Constr. Facil. 32 (2018) 4018059. doi:10.1061/(ASCE)CF.1943-5509.0001204.

[334] T. Kim, H.K. Lee, G.D. Kim, S.W. Lee, G.T. Chae, B.W. Yum, Analysis on the chemical and mechanical stability of the grouting cement for CO2 injection well, Energy Procedia. 37 (2013) 5702–5709. doi:10.1016/j.egypro.2013.06.492.

[335] ASTM D1633 - 17 Standard Test Methods for Compressive Strength of Molded Soil-Cement Cylinders, in: n.d. https://www.astm.org/Standards/D1633.htm (accessed December 16, 2018).

[336] Q. Zhang, G. Ye, Dehydration kinetics of Portland cement paste at high temperature, J. Therm. Anal. Calorim. 110 (2012) 153–158. doi:10.1007/s10973-012-2303-9.

[337] J.B.M. Dassekpo, X. Zha, J. Zhan, Compressive strength performance of geopolymer paste derived from Completely Decomposed Granite (CDG) and partial fly ash replacement, Constr. Build. Mater. 138 (2017) 195–203. doi:10.1016/j.conbuildmat.2017.01.133.

[338] P.R. Vora, U. V. Dave, Parametric studies on compressive strength of geopolymer concrete, Procedia Eng. 51 (2013) 210–219. doi:10.1016/j.proeng.2013.01.030.

[339] K. Neupane, P. Kidd, D. Chalmers, D. Baweja, R. Shrestha, Investigation on compressive strength development and drying shrinkage of ambient cured powder-activated geopolymer concretes, Aust. J. Civ. Eng. 14 (2016) 72–83. doi:10.1080/14488353.2016.1163765.

[340] Subaer, J.J. Ekaputri, H. Fansuri, M.A.B. Abdullah, The relationship between vickers microhardness and compressive strength of functional surface geopolymers, AIP Conf. Proc. 1885 (2017). doi:10.1063/1.5002364.

[341] T. Alomayri, F.U.A. Shaikh, I.M. Low, Synthesis and mechanical properties of cotton fabric reinforced geopolymer composites, Compos. Part B Eng. 60 (2014) 36–42. doi:10.1016/j.compositesb.2013.12.036.

[342] J. Ibanez, O. Font, N. Moreno, J.J. Elvira, S. Alvarez, X. Querol, Quantitative Rietveld analysis of the crystalline and amorphous phases in coal fly ashes, Fuel. 105 (2013) 314–317. doi:10.1016/j.fuel.2012.06.090.

[343] R.E. Fletcher, S. Ling, B. Slater, Violations of Löwenstein's rule in zeolites, Chem. Sci. 8 (2017) 7483–7491. doi:10.1039/c7sc02531a.

[344] S.F. Wang, J. Zhang, D.W. Luo, F. Gu, D.Y. Tang, Z.L. Dong, G.E.B. Tan, W.X. Que, T.S. Zhang, S. Li, L.B. Kong, Transparent ceramics: Processing, materials and applications, Prog. Solid State Chem. 41 (2013) 20–54. doi:10.1016/j.progsolidstchem.2012.12.002.

[345] S. Grasso, H. Yoshida, H. Porwal, Y. Sakka, M. Reece, Highly transparent alumina obtained by low cost high pressure SPS, Ceram. Int. 39 (2013) 3243–3248. doi:10.1016/j.ceramint.2012.10.012.

[346] S. Ma, W.Q. Quek, Q.F. Li, Y.F. Zhang, J.Y.H. Fuh, L. Lu, Sintering of translucent alumina, J. Mater. Process. Technol. 209 (2009) 4711–4715. doi:10.1016/j.jmatprotec.2008.10.056.

[347] M. Carrabba, A.J. Keeling, A. Aziz, A. Vichi, R. Fabian Fonzar, D. Wood, M. Ferrari, Translucent zirconia in the ceramic scenario for monolithic restorations: A flexural strength and translucency comparison test, J. Dent. 60 (2016) 70–76. doi:10.1016/j.jdent.2017.03.002.

[348] J. Petit, P. Dethare, A. Sergent, R. Marino, M.H. Ritti, S. Landais, J.L. Lunel, S. Trombert, Sintering of α-alumina for highly transparent ceramic applications, J. Eur. Ceram. Soc. 31 (2011) 1957–1963. doi:10.1016/j.jeurceramsoc.2011.04.034.

[349] G.R. Anstis, P. Chantikul, B.R. Lawn, D.B. Marshall, A Critical Evaluation of Indentation Techniques for Measuring Fracture Toughness: I, Direct Crack Measurements, J. Am. Ceram. Soc. 64 (1981) 533–538. doi:10.1111/j.1151-2916.1981.tb10320.x.

[350] J. Zhang, R. Tu, T. Goto, Densification, microstructure and mechanical properties of SiO2-cBN composites by spark plasma sintering, Ceram. Int. 38 (2012) 351–356. doi:10.1016/j.ceramint.2011.07.013.

[351] K.K. Ray, A.K. Dutta, Comparative study on indentation fracture toughness evaluations of soda–lime–silica glass, Br. Ceram. Trans. 98 (1999) 165–171. doi:10.1179/096797899680381.

[352] G.R. Anstis, P. Chantikul, B.R. Lawn, D.B. Marshall, A Critical Evaluation of Indentation Techniques for Measuring Fracture Toughness: II, Strength Method, J. Am. Ceram. Soc. 64 (1981) 539–543. doi:10.1111/j.1151-2916.1981.tb10321.x.

[353] Z. Li, A. Ghosh, A.S. Kobayashi, R.C. Bradt, Indentation Fracture Toughness of Sintered Silicon Carbide in the Palmqvist Crack Regime, J. Am. Ceram. Soc. 72 (1989) 904–911. doi:10.1111/j.1151-2916.1989.tb06242.x.

[354] G. Perera, R.H. Doremus, W. Lanford, Dissolution Rates of Silicate Glasses in Water at pH 7, J. Am. Ceram. Soc. 74 (1991) 1269–1274. doi:10.1111/j.1151-2916.1991.tb04096.x.

9. List of abbreviations

FA – Fly Ash

BFS – Blast Furnaces Slags

EAF – Electric Arc Furnace (dust)

S/S – Stabilization/Solidification

OPC – Ordinary Portland Cement

AAMs – Alkali-Activated Materials

BSG – Borosilicate Glass

GP – Geopolymer

GC – Geopolymer Composite

FTIR – Fourier Transform Infra-Red

NMR – Nuclear Magnetic Resonance

PCM – Partial Charge Model

XRD – X-Ray Diffraction

EDS/EDX – Energy Dispersive Spectroscopy

XRF – X-Ray Fluorescence Analysis

BET – Brunauer-Emmet-Teller method

3PB – 3 Point Bending

HyPS – Hydro-Pressure Sintering Process

CSP – Cold Sintering Process

IFT – Indentation Fracture Toughness

IQR – Inter-Quartile range

10. Outreach related to thesis

International conferences

- 'Mechanical characterization of fly-ash/borosilicate based geopolymers'. World of Coal Ash Conference (WOCA), May 9th – 11th 2017, Lexington (USA). Oral presentation.
- 'Properties of geopolymers incorporating wastes'. 12th Pacific Rim conference (PACRIM), May 21st – 27th 2017, Waikoloa, Hawaii (USA). Oral presentation.
- 'The importance to use borosilicate in geopolymers incorporating wastes'. 15th Conference & Exhibition of the European Ceramics Society, July 9th – 13th 2017, Budapest (H). Oral presentation.
- 'Geopolymer incorporating wastes and composites processing'. 12th International Conference on Ceramic Materials and Components for Energy Environmental Applications (CMCEE18), July 22nd – 27th 2018, Singapore. Oral Presentation.
- 'Mechanical and Fracture Performance of Cellulose Fibers Based Geopolymeric Composites Incorporating Wastes'. Technical Meeting and Exhibition on Materials Science & Technology (MS&T18), October 14th – 18th 2018, Columbus, Ohio (USA). Oral Presentation.

Publications

- **G. Taveri**, J. Tousek, E. Bernardo, N. Toniolo, A.R. Boccaccini, I. Dlouhy, Proving the role of boron in the structure of fly-ash / borosilicate glass based geopolymers, Mater. Lett. 200 (2017) 105–108. doi:10.1016/j.matlet.2017.04.107 (**Impact factor**: 2.687).
- N. Toniolo, **G. Taveri**, K. Hurle, J.A. Roether, P. Ercole, I. Dlouhy, A.R. Boccaccini, Fly-Ash-Based Geopolymers: How the Addition of Recycled Glass or Red Mud Waste Influences the Structural and Mechanical Properties, J. Ceram. Sci. Technol., 08 [3] 411-420 (2017). doi: 10.4416/JCST2017-00053 (**Impact factor**: 1.220).
- **G. Taveri**, S. Grasso, F. Gucci, J. Tousek and I. Dlouhy, Bio-Inspired Hydro-Pressure Consolidation of Silica, Adv. Func. Mat. 2018, 1805794. DOI: 10.1002/adfm.201805794 (**Impact factor**: 13.325).
- **G. Taveri**, E. Bernardo and I. Dlouhy, Mechanical Performance of Glass-Based Geopolymer Matrix Composites Reinforced with Cellulose Fibers, Materials 2018, 11, 2395. DOI: 10.3390/ma11122395 (**Impact factor**: 2.467).
- A. Rincon Romero, S. Tamburini, **G. Taveri**, J. Tousek, I. Dlouhy and E. Bernardo, Extension of the 'Inorganic Gel Casting' Process to the Manufacturing of Boro-Alumino-Silicate Glass Foams, Materials 2018, 11, 2545. DOI: 10.3390/ma11122545 (**Impact factor**: 2.467).
- Czech patent application Nr. D18079023, file Nr. PV 2018-420, Inventor: **G. Taveri**, co-authors: S. Grasso, I. Dlouhy. Title: Proces zhutňování anorganických prášků za působení hydrostatického tlaku a zařízení k tomuto.